C-1

Utilization of NMR Surface Coil Techniques to Study Muscle Fatigue

by

JONATHAN WAI KUA LEE

B.Sc.(Hons.), The University of British Columbia, 1981.

M.Sc., The University of British Columbia, 1986.

A THESIS SUBMITTED IN PARTIAL FULFILMENT OF THE

REQUIREMENTS FOR THE DEGREE OF

DOCTOR OF PHILOSOPHY

in

THE FACULTY OF GRADUATE STUDIES

Department of Chemistry

We accept this thesis as conforming to the required standard

THE UNIVERSITY OF BRITISH COLUMBIA

October, 1991.

In presenting this thesis in partial fulfilment of the requirements for an advanced degree at the University of British Columbia, I agree that the Library shall make it freely available for reference and study. I further agree that permission for extensive copying of this thesis for scholarly purposes may be granted by the head of my department or by his or her representatives. It is understood that copying or publication of this thesis for financial gain shall not be allowed without my written permission.

Department of Chemistry

The University of British Columbia
Vancouver, Canada

Date Oct. 11, 1991.

DE-6 (2/88)

ABSTRACT

Skeletal muscle has a greater biochemical dynamic range than any other tissue. Upon strenuous exercise its oxidative demands may increase a hundredfold, and its glycolytic rate, a thousandfold. It is particularly for this tissue that the distinction between conditioning and disease becomes blurred, since poor conditioning may produce more functional compromise in muscle than many diseases produce in other target organs. Muscle, which amounts to about 40% of the body mass, is thus a prime candidate for functional or metabolic diseases. Therefore, muscle provides a convenient biochemical "window" for early detection of potentially life-threatening diseases.

In this thesis a modified Chance/Radda method was used to investigate the use of P-31 NMR Spectroscopy (NMRS or MRS) to monitor patients with muscle diseases. The work described is divided into two parts: (a) design and evaluation of NMR surface coils of various configurations, and assessment of a preliminary clinical protocol, (b) optimization of the technique by normalizing the results with respect to the cross-sectional area of the human upper arm, and to the various parameters which influence the mechanical output of the appropriate muscles.

The highlight of the work presented in this thesis has involved the development, improvement, characterization, and experimental implementation of a novel design of surface coil, namely the spiral resonator surface coil gantry, as well as the delineation, refinement, and clinical execution of a tractable protocol to study muscle fatigue. Assessment of the role of P-31 NMRS as a screening and diagnostic modality indicates that it can serve as an adjunctive tool. The P-31 NMR spectrum can provide information regarding the composition and level of the phosphate metabolites and thus can characterize cellular energetic state. It can also be used to determine the intracellular pH.

The specific exercise protocol outlined in this thesis improves both the sensitivity and the selectivity of the diagnosis of mitochondrial disease, even when little or no muscle symptoms are present. It is also a useful technique to monitor drug therapy of patients with mitochondrial myopathy. The most important feature of the spiral resonator surface coil, developed during the course of our clinical investigation, is its flexibility with respect to the location where it can operate. Its stability and improved sensitivity are added advantages.

Potential extension of the spiral resonator surface coil design to observe other nuclei of biological interest, such as C-13, as well as the adaptation of our clinical protocol to study the effect on muscular function of patients with Acquired Immune Deficiency Syndrome (AIDS) during anti-HIV drug therapy (AZT or DDI) have been explored and experimentally demonstrated.

At the time when this work was initiated, only the research groups of Britton Chance in Philadelphia, George Radda in Oxford, plus a few others were active in the use of P-31 NMRS to study intact muscle weakness. Since then, worldwide interest has increased; it is our hope that the technique developed at UBC with limited resources will be easily implemented in many other NMR facilities.

TABLE OF CONTENTS

LIST OF FIGURES

LIST OF TABLES

Acknowledgements

I am extremely thankful to my supervisor, *Prof. Laurance Hall,* for providing support and encouragement thoughout this thesis. It has been a unique and rewarding experience working under his guidance. Special thanks are also extended to my collaborator and friend, *Dr. Andrew Penn* (Division of Neurology, Department of Medicine, Walter Mackenzie Health Sciences Center, University of Alberta, Edmonton, Alberta, Canada), whose consistent support and encouragement during this project has been invaluable and much appreciated.

I wish to express my deepest gratitude to *Mr. Tom Markus* and *Mr. Cedric Neale* of the Electronic and Mechanical Shops, whose expert technical support, dedication, and enthusiasm are notably indispensable throughout the course of this project.

In a multi-disciplinary study such as that described in this thesis, the work could not have been completed without the assistance of the many scientists and clinicians I have collaborated with. It is my pleasure to give special thanks to *Dr. Michael Menard, Dr. Laurie Dusik,* (Division of Physical Medicine and Rehabilitation, St. Paul's Hospital), *Dr. Andrew Eisen, Dr. Andrew Travlos,* (Neuromuscular Disease Unit, VGH), *Dr. Donald McKenzie, Mr. Andrew Dawson* (School of Physical Education and Recreation, UBC), and *Dr. L. S. Weiler* (Department of Chemistry, UBC), for their assistance and support for the project as a whole.

I would also like to thank *Dr. Nick Burlinson, Dr. L. D. Burtnick, Dr. F. G. Herring, Dr. E. E. Burnell* (Department of Chemistry, UBC), *Dr. Lalith Talagala* (Pittsburgh NMR Institute, Pittsburgh, Pennsylvania), and *Dr. Vasanthan Rajanayagam* (Huntington Medical Research Institute, Pasadena, California) for

their helpful discussions, as well as for proof reading this Thesis. Finally, many thanks to the past and present members of Dr. Hall's group for their friendship and valuable intellectual support over the years

Chapter 1

1. INTRODUCTION

1.1 Historical Perspective

The first successful demonstrations of nuclear magnetic resonance (NMR) in bulk matter were published in 1946 by research teams led by Edward Purcell at Harvard University (1) and Felix Bloch at Stanford University (2); in 1952, both investigators won the Nobel Prize in physics for their work. The impact of their work was immediate and the applications of NMR have progressively widened from physics and chemistry to a surprising range of disciplines from archeology to medicine. NMR is an analytic tool that used non-destructive, radio-frequency (RF) energy as a physical probe for identifying the chemical content of materials and molecular structure. As applied to living tissues, NMR has become a powerful, non-invasive method for analyzing tissue and monitoring biochemical reactions.

Soon after the first successful NMR experiments at Stanford(3), Bloch obtained a strong proton NMR signal when he inserted his finger into the RF coil of his spectrometer. In 1948 Purcell and Ramsey in turn inserted their heads into the 2-Tesla field of the Harvard cyclotron; around their heads was a coil connected to a powerful RF generator tuned to the proton NMR frequency. Subsequently, occasional NMR experiments were reported on materials of

biological interest (4-5), but substantial advances awaited the development of high-field, high-resolution, Fourier-transform spectrometers in the late 1960s. In one type of application, high-resolution NMR spectra have been obtained from enzymes and from other proteins and biomolecules in solution (6), yielding structural and dynamical information of importance in biochemistry and biology. This NMR contribution to molecular biology continues to be an active area at the frontier of research.

In a second type of application, NMR spectroscopy has been applied to living systems. First, Moon & Richards (7) reported high-resolution P-31 NMR studies of intact red blood cells and they could assign individual lines to specific metabolites. That work was followed by the recording of a P-31 NMR spectrum from intact, freshly-excised muscle from a rat's leg by Hoult *et al* (8); it was found possible to maintain muscles in good physiological condition in the spectrometer and to record the effects of electrical stimulation. The 5cm diameter bore of the then available superconducting NMR magnet was nevertheless a severe restriction. However, magnets with a 10cm diameter bore were soon available and a wide range of studies on perfused animal-hearts, -kidneys, -livers and other organs (9-11) were pursued, mainly using P-31 NMR, but also H-1 and C-13 NMR spectroscopy.

It was then a natural step to examine whole intact living organisms, ranging from bacteria to mice, rats and rabbits. With animals it is of course important to know from what anatomical part, or organ, the NMR spectrum originates. In some cases this could be achieved by winding the RF coil around the part concerned; in other cases a small RF coil was placed on the surface of the animal to record the NMR signal from the region immediately below it.

From animals, logically it is just one further step to man; however, a prerequisite to the extension of high-resolution NMR spectroscopy to human beings was the provision of magnets with a very much larger access. In 1980 the

Oxford Instrument Company in England, who had previously pioneered many NMR magnet developments, produced superconducting solenoid magnets operating at a field strength of 1.89 Tesla, with a 30cm diameter horizontal bore, and a high-resolution NMR capability over a region 2-4cm in diameter.

With such magnets, it was possible to accommodate the human hand and arm, or foot and leg, and many high-resolution NMR spectra have been recorded of P-31, and also C-13 and H-1 nuclei. The first studies of intact human muscle were performed by Chance *et al* (12), Cresshull *et al* (13), and Ross *et al* (14). In this way it was possible to monitor the metabolism of both normal and diseased human limbs. The effects of exercise, or of restricting blood flow using a tourniquet, could be followed; diseased muscles could be diagnosed and their treatment followed in biochemical detail. Magnets of this same size have also been used to study clinical problems in the heads of babies (15).

In all such studies, it is of course important to gather the NMR spectra from a clearly defined region of the human anatomy. Two main methods have been developed for such spatial localization. One is by the use of a surface coil (16), which limits the region of interest to parts of the anatomy near the surface of the body. The other method, topical magnetic resonance spectroscopy (17-18), involves careful profiling of the magnetic field so that only a small, well-defined volume has the necessary uniformity to yield a high-resolution NMR spectrum.

With such technology, and access to 1.5T superconducting magnets with 1m diameter bore and high-resolution capability which have been available since 1983, the whole human body can be studied and the high-resolution NMR spectrum can be obtained from any desired part of the anatomy.

In the investigation of patients with muscle disease there have been in the past only three avenues of interrogation; the clinical examination, electromyography (EMG), and biopsy. Where muscle damage is prominent in

disease these have usually been sufficient. Where symptoms are due to biochemical dysfunction, however, there may not be electrical or morphological correlates and therefore no clear evidence available for "disease". This is particularly true of mitochondrial disease in which conventional detection rates are probably less than 50%. Given the peculiarities of mitochondrial genetics there is a real possibility that mitochondrial dysfunction and cellular energy failure could be much more important mechanisms in neurological disease than anticipated. In recent years, many neurological techniques have become available but none have reached a state of general usage. Nevertheless, P-31 Nuclear Magnetic Resonance spectroscopy has been shown to have considerable potential in the clinical and experimental investigation of muscle diseases and has been applied to muscle disease since the early 1980's particularly by the groups of Britton-Chance in Philadelphia and George Radda in Oxford (12,14). P-31 NMRS allows a view of muscle metabolism *in-vivo* that EMG and biopsy cannot provide, and does so non-invasively. The latter point is particular significance in the diagnosis for metabolic myopathies and the monitoring of new therapies, where repeated measurements may be required over an extended period along with studies of siblings or parents who are non-symptomatic.

1.2 Scope and Contents of the Thesis

Skeletal muscle has a greater biochemical dynamic range than any other tissue. Upon strenuous exercise its oxidative demands may increase a hundredfold, and its glycolytic rate, a thousandfold (19-21). Moreover, it is the inherent paradox of the muscle contractile machinery that attainment of maximal force by the recruitment of all fiber groups, with the greatest demand for oxidative energy provision, simultaneously produces the greatest blockade of capillary blood flow and hence the most anoxic state. It is particularly for this

tissue that the distinction between conditioning and disease becomes blurred, since poor conditioning may produce more functional compromise in muscle than many diseases produce in other target organs. Muscle, which amounts to about 40% of the body mass, is thus a prime candidate for functional or metabolic diseases, that is, enzyme or carrier defects that limit maximal performance, but may be unaccompanied by anatomic pathology. Thus, muscle provides a convenient biochemical "window" for early detection of potentially life-threatening diseases.

In this thesis we used a modified Chance/Radda method to investigate the use of P-31 NMR Spectroscopy to monitor patients with muscle diseases. Ideally, the perfect protocol for studies of the metabolism of intact muscle should be a comprehensively tractable technique that is applicable to patients of all ages and of various degrees of physical fitness; and, further, the technique should be able to be tailored to the capability of each patient. Although such a technique does not yet exist, and even the prospect may sound somewhat utopic, the works presented in this thesis are , for the most part, directed towards the development of such a technique to study muscle diseases, and to monitor drug therapies thereof. There are three primary reasons which motivated this approach; first, its potential and versatile prospect; second, the need to improve several aspects of current techniques; finally, as part of the author's own efforts to gain expertise in the biochemical field and to search for techniques which could improve the conventional detection rates of muscle diseases from 50%, to 85% or better.

The work described in this thesis is divided into two parts: (a) design and evaluation of NMR surface coils of various configurations, and evaluation of the preliminary clinical protocol, (b) optimization of the technique by normalizing the results with respect to the cross-sectional area of the human upper arm, and to the various parameters which influence the mechanical output of the appropriate muscles.

The format of the thesis is as follows: Chapter 2 reviews the basic concepts of Nuclear Magnetic Resonance Spectroscopy, the biochemistry of muscle metabolism, and the merit of the techniques which were available in 1985 to examine patients with complaints of muscle weakness and muscle-pain. Chapter 3 discusses the constraints of the UBC laboratory and the efforts made to overcome the associated difficulties by surface coils of various configurations, and eventually by a new design of gantry housing a novel resonator surface coil. Chapters 4 and 5 introduce the reader to a preliminary clinical exercise protocol which we have tested and modified during the past four years in dealing with over 200 subjects; the selectivity and sensitivity of our technique is discussed; and as part of our attempt to improve our clinical protocol, the effort devoted to study certain parameters which influence the mechanical output of muscle. Finally, in Chapter 6, a brief review of the work presented in this thesis as well as a discussion of future extension with the existing techniques are given.

At the time when this work was initiated, only the research groups of Britton Chance in Philadelphia , George Radda in Oxford, plus a few others were active in the use of P-31 NMRS to study intact muscle weakness. Since then, worldwide interest has increased; coupled with recent published reports which have linked mitochondrial failure to ageing (22), Parkinson's disease (23-24), Huntington's disease (25), Alzheimer's disease (26), as well as to mitochondrial myopathy caused by long-term Zidovudine (AZT) therapy (27), it is our hope that the technique developed at UBC with limited resources will be easily implemented in many other NMR facilities. In recognition of the multi-disciplinary nature of this work, a glossary of terms is provided at the end of this thesis; in addition, where possible, the terms are defined briefly as they appear in the text of this thesis.

References

1. F. Bloch, W. W. Hanson, and M. E. Packard, Phys. Rev. 70:460, 1946.

2. E. M. Purcell, H.C. Torrey, and R. V. Pound, Phys. Rev. 69:37, 1946.

3. F. Bloch, W. W. Hanson, and M. E. Packard, Phys. Rev. 69:127, 1946.

4. T. M. Shaw, and R. L. Elsken, J. Chem. Phys. 18:1113-1114, 1950.

5. B. Jacobson, W. A. Anderson, and J. T. Arnold, Nature 173:772-773, 1954.

6. P. F. Knowles, D. Marsh, and H. W. E. Rattle, Magnetic Resonance of Biomolecules, John Wily, London, 1976.

7. R. N. Moon, and J. H. Richards, J. Biol. Chem. 248:7276-7278, 1973.

8. D. I. Hoult, S. J. W. Busby, D. G. Gadian, G. K. Radda, R. E. Richards, and P. J. Seeley, Nature 252:285-287, 1974.

9. W. E. Jacobus, G. J. Taylor, D. P. Hollis, and R. L. Nunnally, Nature 265:756-768, 1977.

10. P. A. Sehr, G. K. Radda, P. J. Bore, and R. A. Sells, Biochem. Biophys. Res. Commun. 77:195-202, 1977.

11. S. M. Cohen, R. G. Shulman, and A. C. McLaughlin, Proc. Natl. Acad. Sci. U.S.A. 76:4840, 1979.

12. B. Chance, S. Eleff, and J. S. Leigh, Proc. Natl. Acad. Sci. U.S.A. 77:7430-7434, 1980.

13. I. Cresshul, M. J. Dawson, R. H. T. Edwards, *et. al.*, J. Physiol. 317:18p, 1981.

14. B. D. Ross, G. K. Radda, D. G. Gadian, G. Rocker, M. Esiri, and J. Falconer-Smith, N. Engl. J. Med. 304:1338-1342, 1981.

15. E. B. Cady *et. al.*, Lancet 1059-1062, 1983.

16. J. J. H. Ackerman, T. H. Grove, G. G. Wong, D. G. Gadian, G. K. Radda, Nature 283:167-170, 1980.

17. R. E. Gordon, P. E. Hanley, D. Shaw, *et. al.*, Nature 287:367-368, 1980.

18. R. E. Gordon, P. E. Hanley, and D. Shaw, Progress in NMR Spectroscopy 15:1, 1982.

19. P. Banks, W. Bartley, L. M. Birt, the Biochemistry of the Tissues, 2nd ed., Wiley Ltd., New York, pp. 93-158, 1976.

20. L. D. Peachey, and R. H. Adrian, eds., Handbook of Physiology, section 10, Skeletal Muscle, American Physiological Society, Bethesda, MD., 1983.

21. P. O. Astrand, and K. Rodahl, Textbook of Work Physiology, 2nd ed., McGraw-Hill Publishing Co., New York, 1977.

22. I. Trounce, E. Byrne, and S. Marzuki, Lancet 637-639, Mar. 25, 1989.

23. W. D. Parker, S. J. Boyson, and J. K. Parks, Ann. Neuro. 26:719-723, 1989.

24. A. H. V. Schapira, J. M. Cooper, D. Dexter, P. Jenner, J. N. Clark, and C. D. Marsden, Lancet 1:1296, 1989.

25. W. D. Parker, S. J. Boyson, A. S. Luder, and J. K. Parks, Neurology 40:1231-1234, 1990.

26. W. D. Parker, C. M. Filley, and J. K. Parks, Neurology 40:1302-1303, 1990.

27. M. C. Dalakas, I. Illa, G. H. Pezeshkpour, J. P. Laukaitis, B. Cohen, and J. L. Griffin, New England J. of Medicine 332(16):1098-1105, 1990.

Chapter 2

2 BASIC METHODS

2.1 Physical Concepts of NMR

Biological tissue is relatively transparent to radiation at very short wavelengths of the electromagnetic spectrum (e.g. X-rays) but becomes opaque at intermediate and longer wavelengths such as ultraviolet, infrared, and microwave. Surprisingly, the body is permeable to longer wavelengths such as radiowaves, the radiation used for Nuclear Magnetic Resonance (NMR). The benefits derived from the use of low-energy radiation and the unprecedented level of information available from NMR signals are what combine to make NMR such a valuable biochemical modality.

The core of atoms that accommodates most of the elemental mass is called the nucleus; it consists of neutrons and protons, each possessing a mass of approximately 1 on an atomic scale where the lighter isotope of carbon has been assigned a mass of 12. Certain nuclear species possess angular momentum, or spin, a property first suggested by Wolfgang Pauli in 1924. Thus, a nucleus with a non-zero spin quantum number produces a magnetic moment μ, which expresses the strength and direction of the surrounding magnetic field.

The phenomenon of NMR can be induced in atomic nuclei that possess an odd number of either protons or neutrons. At present the isotopes of greatest

interest for NMR spectroscopy in biochemical research and clinical studies are those whose properties are summarized in Table 2-1.

Table 2-1: NMR Active Isotopes for Biochemical Studies

Isotope	Natural Abundance	Basic Resonance Frequency (MHz/Tesla)	Relative Sensitivity
H-1	99.98%	42.58	100
C-13	1.1%	10.74	1.6×10^{-2}
P-31	100%	17.24	6.6
Na-23	100%	11.27	9.3
F-19	100%	40.06	83

Relative sensitivity is the product of NMR sensitivity of an equal number of protons, multiplied by the natural abundance.

In principle, each nucleus of a particular isotope in a different chemical environment gives rise to a separate NMR signal, whose intensity is proportional to the concentration at that site, and whose chemical shift can be related to electronic structure.

In this Chapter we will begin with a brief discussion of some of the physical basis for NMR spectroscopy. A discussion of some of the experimental and operational aspects of *in-vivo* spectroscopy will follow.

Atomic nuclei can be described in terms of their behavior under specified conditions. Nuclei with either an odd number of protons or neutrons have the property of precession (analogous to the rotational motion of a gyroscope in a gravitational field) when placed in a magnetic field. This precessional motion is characterized by two quantities: the frequency, or speed, of rotation; and the

sensitivity of the nucleus to the effect. When such nuclei are bathed in radiowaves of the appropriate frequency they can be induced to undergo magnetic resonance transitions between the available energy levels. The frequency at which a specific nucleus resonates is proportional to the strength of the static magnetic field (B_o).

For the proton (the principal isotope of hydrogen nucleus), which has spin quantum number I = 1/2, when subjected to a static magnetic field, there are two allowable basic states with orientations "parallel" (or spin up) and "antiparallel" (or spin down) to the field direction corresponding to magnetic quantum number m = +1/2 and -1/2, pertaining to a low- and high-energy state, respectively. These two orientations have slightly different energies; and the energy required to induce transitions between them, and thereby to obtain an NMR signal, is the energy difference, ΔE, between the two nuclear orientations; this is dependent on the strength of the magnetic field B_o in which the nucleus is placed (Fig. 2-1):

$$\Delta E = \gamma h B_o / 2\pi \qquad (2\text{-}1)$$

where h is Planck's constant (6.63×10^{-34} Joule-second). The Bohr condition ($\Delta E = h\upsilon$) enables the frequency υ_o of the nuclear transition to be written as the Larmor resonance equation:

$$\upsilon_o = \omega_o / 2\pi = \gamma B_o / 2\pi \qquad (2\text{-}2)$$

where υ_o is the resonance frequency in Hz, ω_o is the angular frequency in radians per second, B_o is the static magnetic field, and γ is the magnetogyric ratio, which is a nuclear constant characteristic of every isotope. Consequently, the NMR signal from a particular element can be observed without interference from any other.

It can also be shown that m can assume 2I+1 different states. I can be integral (e.g. H-2, N-14) or half integral (e.g. H-1, C-13, P-31, Na-23). Sodium-23,

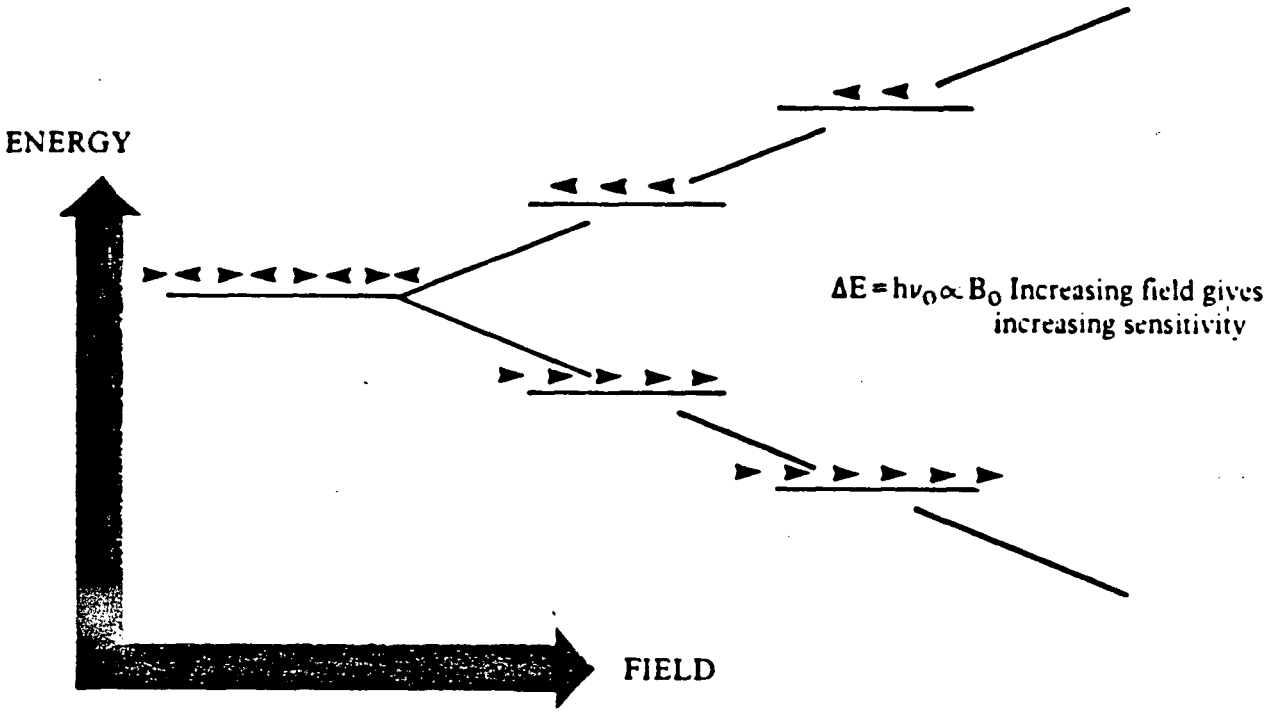

Figure 2-1 In the presence of a steady magnetic field, B_0, some nuclei (e.g. H-1, C-13, P-31) behave like tiny bar magnets and align themselves parallel or antiparallel to the direction of B_0. The two orientations, or spin states, have differing energies and transitions between these states can be introduced by a radiofrequency magnetic field oscillating at a frequency, ν_0.

for example, has I= 3/2 and thus m can assume values of -3/2, -1/2, +1/2, and +3/2. The allowable orientations are determined by quantum mechanics (Fig. 2-2). The orientation angle of the spin vectors in the magnetic field is given as:

$$\theta = \arccos m/\sqrt{I(I+1)} \qquad (2\text{-}3)$$

The phases of a large or "ensemble" of precessing magnetic moments are random, that is, the tips of the magnetic moment vectors have different locations on the precessional orbit (Fig. 2-3). Their combined alignment creates a macroscopic magnetic moment, M or magnetization, which can be calculated on the basis of Boltzmann statistics:

$$M = N(\gamma h/2\pi)^2 I(I+1)B_o/3kT \qquad (2\text{-}4)$$

where N is the number of individual identical nuclear spins per unit volume in thermal equilibrium with the surroundings at temperature T and subjected to a magnetic field B_o. In fact, the two states for a spin = 1/2 nucleus like the proton are almost equally probable (due to the small energy difference between them). For example, in a magnetic field of 1.89 T, the fractional excess population in the lower level is approximately 1.26×10^{-5} for proton and 5.10×10^{-6} for phosphorus. To enhance the difference in the population density, the Boltzmann formula states that we may either increase the strength of the applied magnetic field, or lower the temperature of the specimen, or both.

However, if the resonance frequency of a nucleus were only directly proportional to the external magnetic field, then all protons for example would absorb energy at the same frequency, and NMR would be a relatively uninteresting and uninformative technique incapable of distinguishing between protons from different atoms or molecules. Fortunately, the applied field also induces electronic currents in atoms and molecules, and those induced currents each produces a small magnetic field which is opposed to the applied field and acts to partially cancel it, thereby "shielding" the nucleus (Fig. 2-4). In general, the

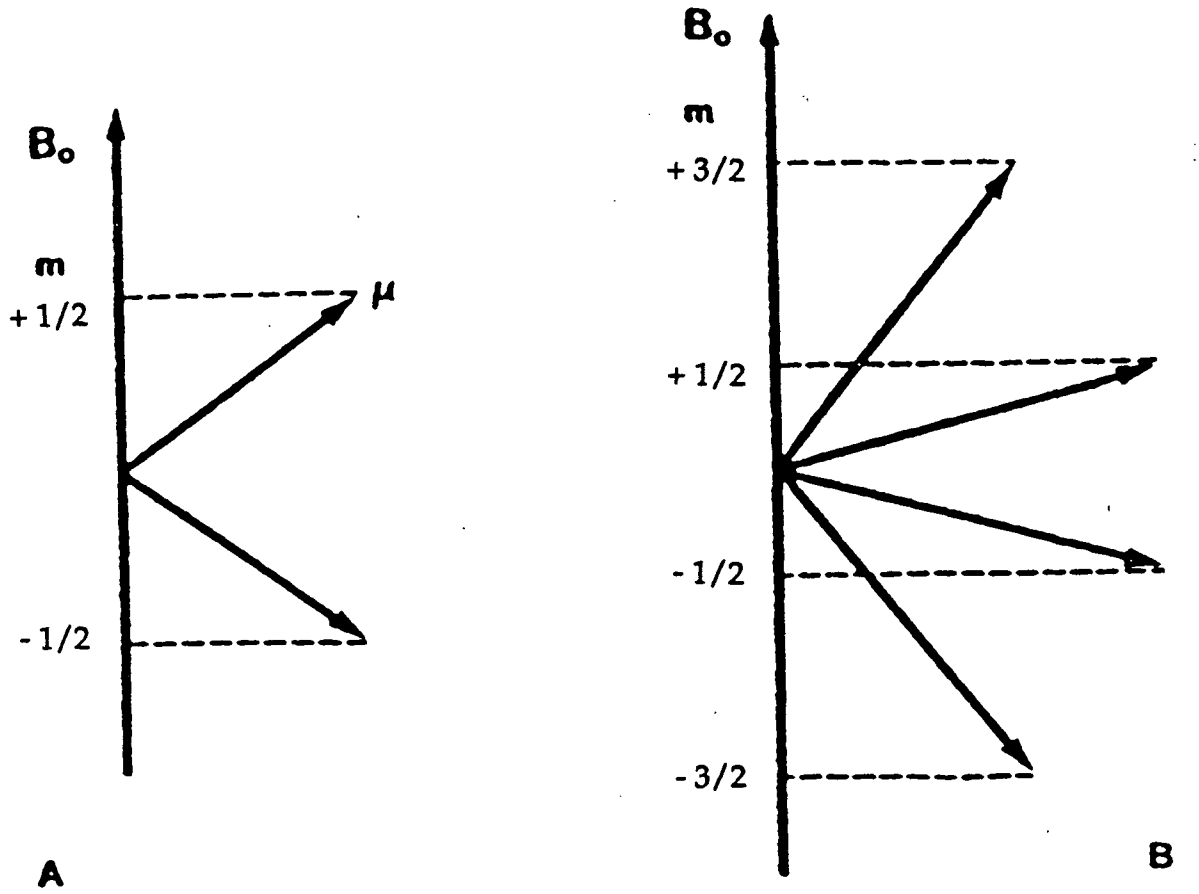

Figure 2-2 Quantization of nuclear spins in the magnetic field (B_{xy}) for spin quantum numbers (a) I = 1/2 and (b) I = 3/2. The measurable component of the spin angular momentum (z component) is expressed by the magnetic quantum number (m).

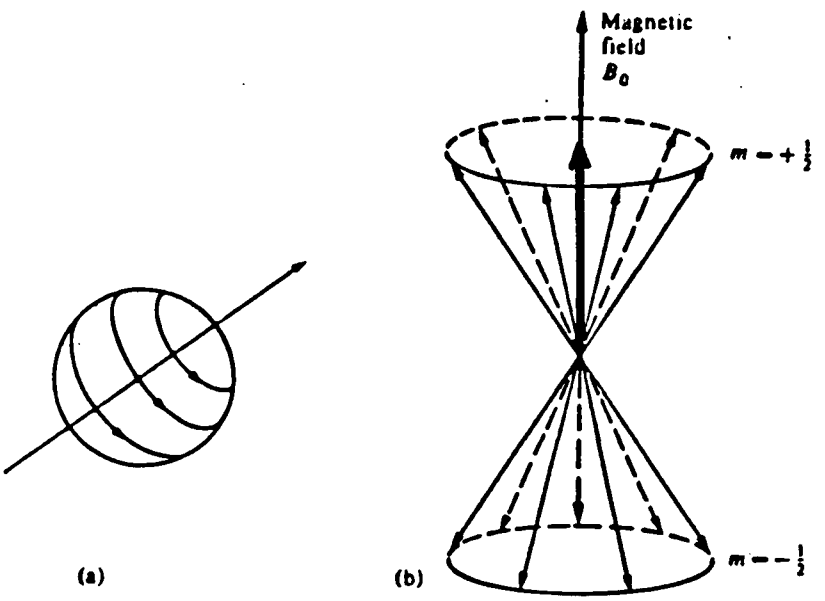

Figure 2-3 (a) A nucleus can be visualized as spinning about its own axis which is the axis of its magnetic moment. (b) Orientations that can be taken up in an applied field B_0 by the magnetic moment of a nucleus of a spin 1/2. The orientations are specified by the quantum number m and describe two cones.

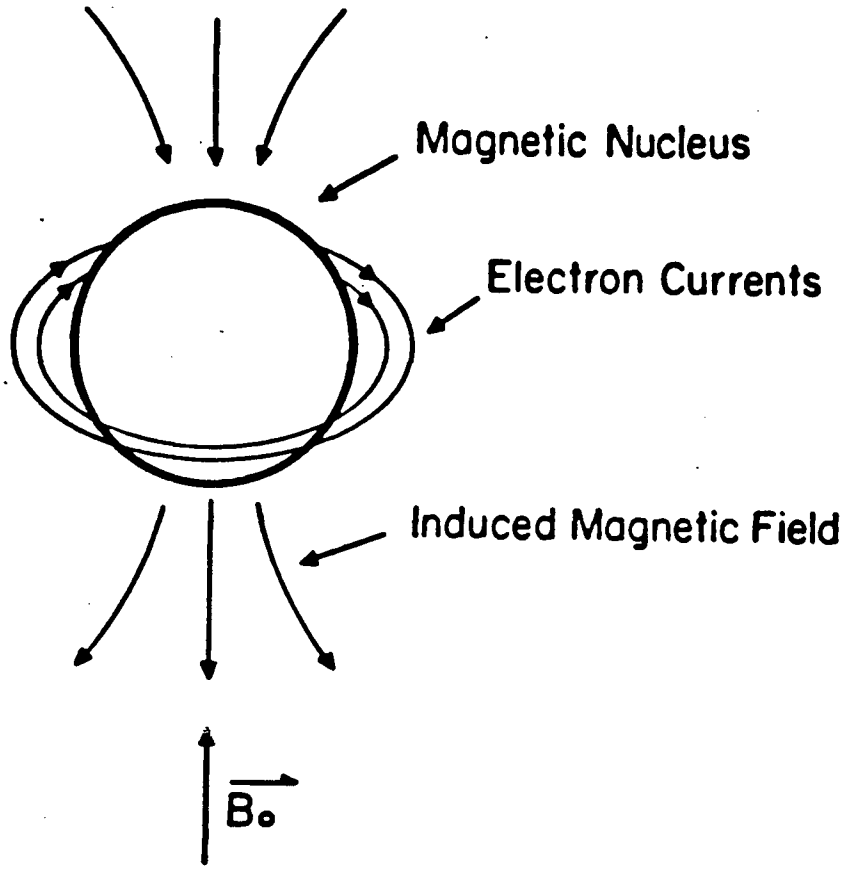

Figure 2-4 Electron currents around a nucleus are induced by placing the molecule in a magnetic field B_0. These electron currents, in turn, induce a small magnetic field opposed to the applied magnetic field B_0.

induced opposing field is about a million times smaller than the applied field. Consequently, the magnetic field perceived by the nucleus will be very slightly altered from the applied field, so the resonance condition of equation 2-2 will need to be modified to:

$$\upsilon_o = \omega_o/2\pi = \gamma B_{eff}/2\pi = \gamma B_o (1-\sigma)/2\pi \qquad (2\text{-}5)$$

where B_{eff} is the local field experienced by the nucleus and σ is a nondimensional screening, or shielding, constant, and has values typically in the region 10^{-6} to 10^{-3}.

These small local magnetic effects shift the resonance frequency of a particular nucleus by an amount called the chemical shift (δ). The chemical shift is measured with respect to the resonance frequency (ω_R) of a particular nucleus in a reference compound, and is expressed in the dimensionless units of parts per million (ppm) (Fig. 2-5):

$$\text{Chemical shift, } \delta(\text{ppm}) = (\omega_S - \omega_R) \times 10^6/\omega_R \qquad (2\text{-}6)$$

where ω_s is the resonance frequency of a particular nucleus in the sample, and ω_R is the resonance frequency of the reference nucleus. Expressing chemical shift in this way is useful because it allows direct comparison of spectra that may have been obtained at different field strengths.

The above description of nuclear magnetization was essentially based on quantum mechanics. However, many features of NMR can be comprehended more easily by a classical vector approach.

In an NMR experiment, the nonequilibrium magnetization is created by irradiating the nuclear spins with a small rotating magnetic field B_1, at a frequency near the Larmor frequency of spins, applied perpendicular to the field B_o, i.e. in a plane transverse to B_o (Fig. 2-6). In a rotating frame, the angle θ by which the magnetic moment vector is changed or flipped depends on the

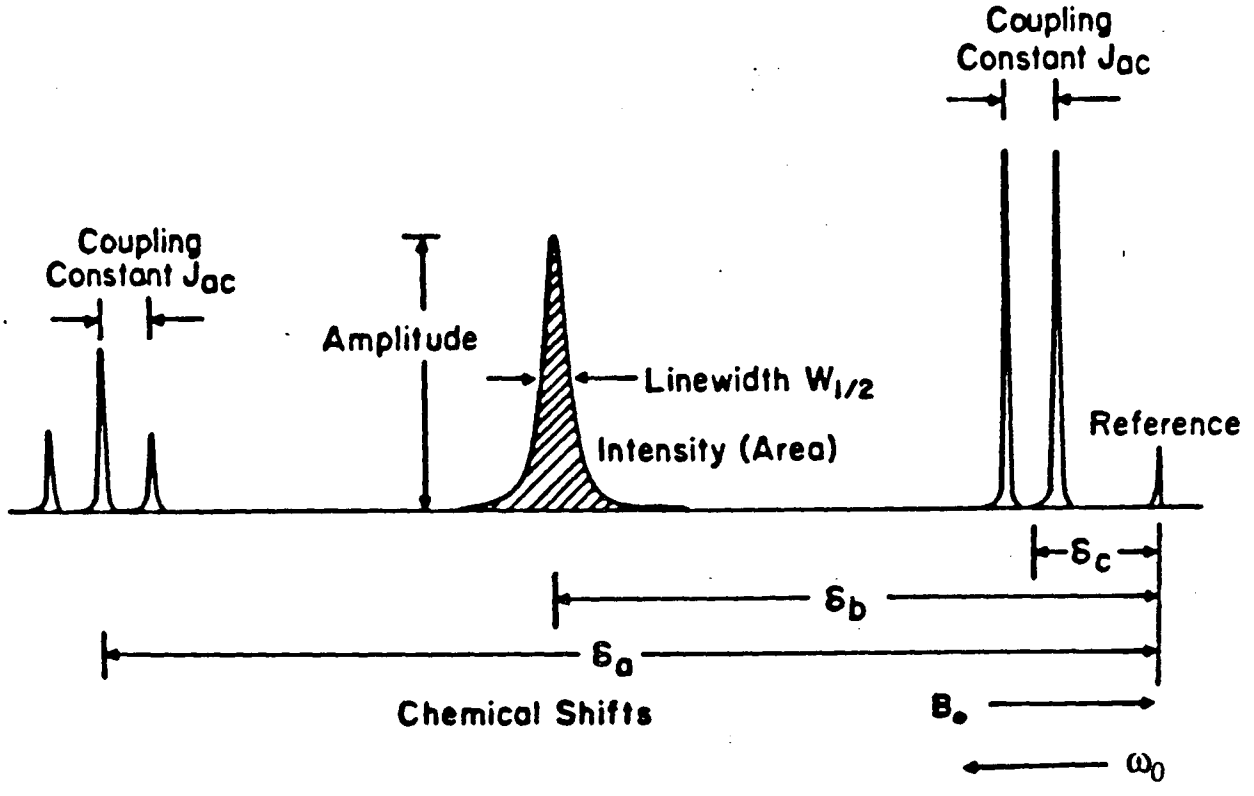

Figure 2-5 Nuclear magnetic resonance spectral parameters.

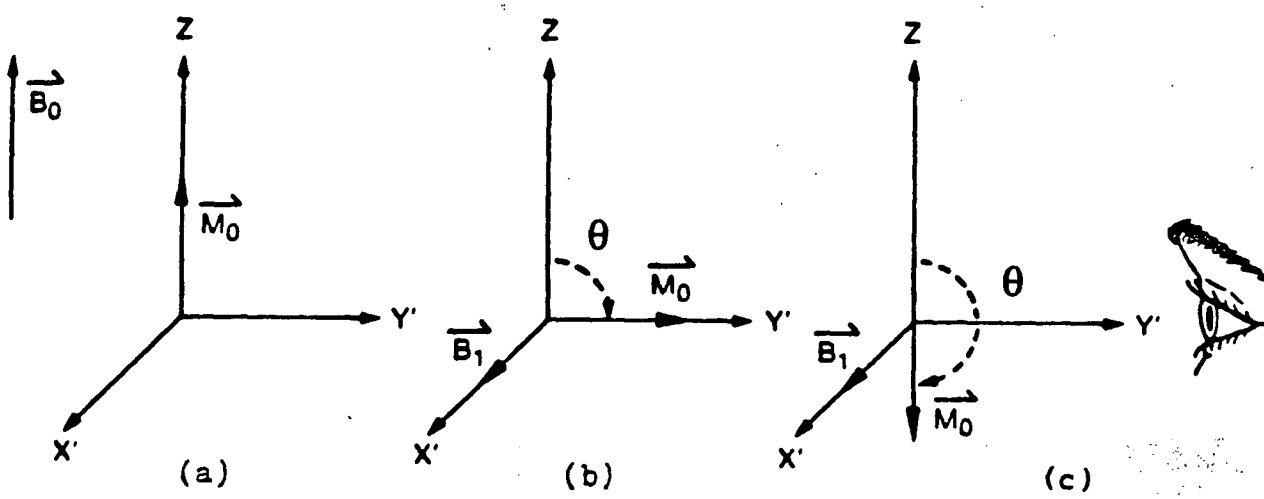

Figure 2-6 Rotation of the magnetization M_0 in the rotating coordinate system that rotates about the Z axis at the nuclear magnetic resonance instrument's operating frequency. (a) spin system at equilibrium in B_0 magnetic field; (b) application of a 90 (or $\pi/2$) B_1 pulse; and (c) application of a 180 (or π) B_1 pulse.

gyromagnetic ratio γ of the nucleus, the amplitude B_1 of the RF pulse, and the length of time t_ω the RF pulse is applied:

$$\theta = \gamma B_1 t_\omega \qquad (2\text{-}7)$$

Figure 2-6b illustrates the rotation of M_o by application of the RF pulse for sufficient time to rotate M_o by 90^o ($\theta = \pi/2$ radians). That pulse is called a 90^o or $\pi/2$ pulse. Application of the B_1 field for twice as long ($\theta = \pi$ radians) will result in inversion of M_o (Figure 2-6c).

The quantum mechanical analogs of 90^o and 180^o pulses of spin 1/2 nucleus are as follows: the 90^o pulse produces an equalization of populations in the two energy states; and the 180^o pulse produces an inversion of populations so that the high energy state has a larger number of nuclear spins.

Experimentally, the NMR signal is detected by a tuned RF coil with axis perpendicular to B_o. The oscillating NMR magnetization induces a voltage in the coil, analogous to the principle of an electric generator. The induced signal immediately following an RF pulse is termed a free induction decay (FID), reflecting the decay in the signal as nuclei dephase and eventually relax back to thermal equilibrium. This return to equilibrium is characterized by two relaxation times, T_1 and T_2.

The relaxation processes occur by interaction of the nuclear spin with fluctuating magnetic fields produced by magnetic dipoles (e.g. other nuclei, paramagnetic ions) which are fluctuating due to random molecular motions, both rotational and translational. In the vector model, T_1 characterizes the exponential growth of the longitudinal magnetization M_z to its equilibrium value M_o, while, T_2 denotes the decay constant of the transverse magnetization components M_x and M_y to their equilibrium values (zero).

The transverse magnetization components, M_x and M_y, in the rotating frame after the pulse can be expressed as:

$$M_{x'}(t) = M_o \, Sin\theta \, Sin\Delta\omega t \, exp(-t/T_2) \qquad (2\text{-}8)$$

and

$$M_{y'}(t) = M_o \, Sin\theta \, Cos\Delta\omega t \, exp(-t/T_2) \qquad (2\text{-}9)$$

where M_o is the equilibrium magnetization, $\Delta\omega$ is the resonance offset (the difference between the frequency of B_1 and the Larmor frequency), $M_{x'}$ and $M_{y'}$ are the transverse magnetizations along X' and Y' at time t and T_2 is the transverse relaxation time.

The induced signal (FID), which is initially in the radio-frequency range, is demodulated to an audio-frequency signal by a phase sensitive detector. In quadrature detection, both components $M_{x'}$ and $M_{y'}$ are detected and a convenient way to express this signal is to write it in a complex form:

$$S(t) = K[iM_{x'}(t) + M_{y'}(t)] \qquad (2\text{-}10)$$

and hence

$$S(t) = KM_o exp(-i\Delta\omega t) exp(-t/T_2) \qquad (2\text{-}11)$$

where $i = (-1)^{1/2}$ and $\Delta\omega$ is the resonance offset. K is time-independent constant of proportionally between the transverse magnetization and the signal it induces.

Fourier transformation of the time domain signal S(t) yields the frequency domain spectrum S(ω) given by:

$$S(\omega) = K[A(\omega)+iD(\omega)] \qquad (2\text{-}12)$$

this is composed of a real part A(ω) known as the Absorption spectrum (also known as a Lorentzian absorption line) and of an imaginary part D(ω) known as the Dispersion spectrum:

$$A(\omega) = M_o T_2/[1+T_2^2(\Delta\omega-\omega)^2] \quad (2\text{-}13)$$

$$D(\omega) = M_o T_2^2(\Delta\omega-\omega)/[1+T_2^2(\Delta\omega-\omega)^2] \quad (2\text{-}14)$$

In general, an organic molecule exhibits a range of resonance frequencies (different $\Delta\omega$ values) due to chemical shift effects. Thus the free induction decay consists of a superposition of a series of signals of different frequencies.

Radio-frequency stimulation causes the nuclei to absorb energy, lifting them to the excited state. In their excited state, the nuclei can return to the ground state only by dissipating their excess energy to their surroundings, the so-called lattice. This process is termed T_1, (spin-lattice relaxation). In liquids, the fluctuations in the lattice field are caused by random thermal motions of molecules (Brownian motion), which can either be rotational or translational. In the T_2 relaxation process ("spin-spin relaxation"), the nuclei in the excited and ground state exchange energy with each other, that is, while one nucleus absorbs energy its neighbor releases energy. It is the rate of loss of the transverse magnetization that determines the T_2 relaxation time. The transverse magnetization decays because the nuclear magnetic moments get out of phase due to their mutual interaction.

Both the nature and the rate of the molecular motions affect the T_1 and T_2 relaxation times. Molecular motions that occur at a rate comparable to the resonance frequency ν_o for the nucleus are most effective in promoting spin-lattice relaxation, i.e. yield the lowest values for T_1; T_2 values can be decreased even further as the molecular motion becomes slower than ν_o, but T_1 values will begin to increase (Fig. 2-7). These relationships for dipole-dipole interactions, for spin 1/2 nuclei (e.g. H-1, C-13, P-31), can be expressed as follows:

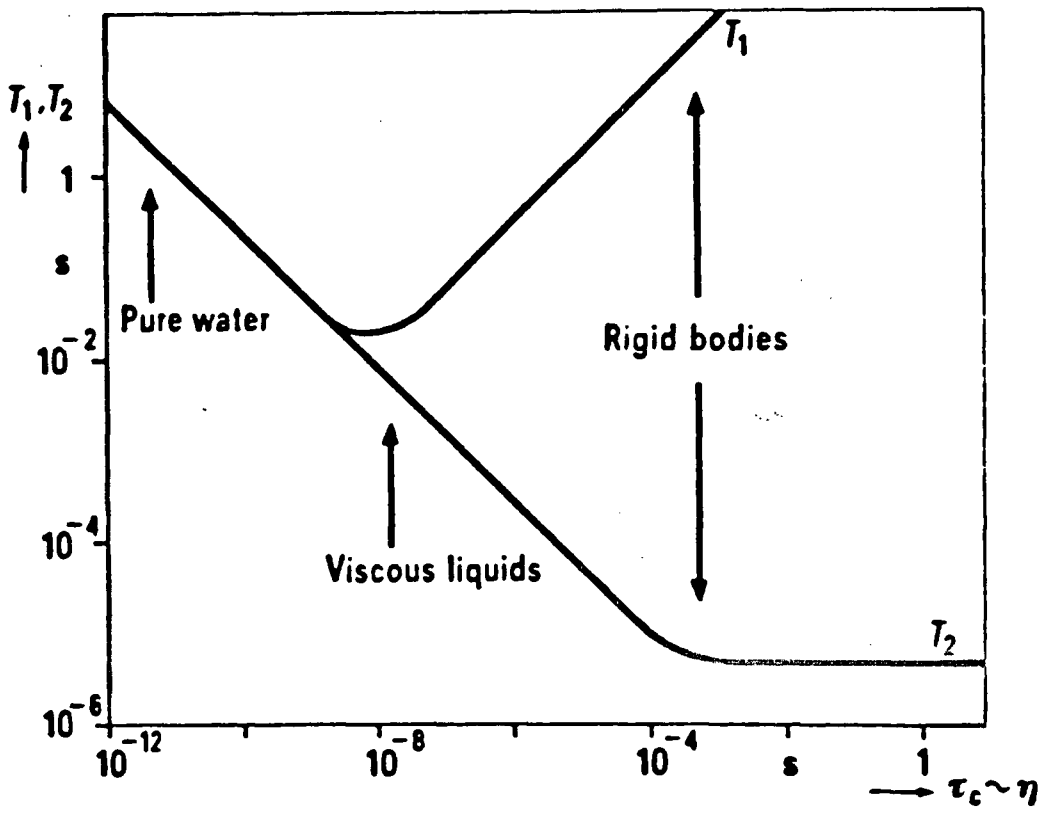

Figure 2-7 Dependence of T_1 and T_2 relaxation times of protons in water on the viscosity η of the solution. The correlation time τ_c is proportional to the viscosity η. Relaxation is dominated by intramolecular magnetic dipole-dipole interactions, between the two protons on the water molecule, that change with the reorientation of the molecule. (After Beall *et. al.*, Data Handbook for Biomedical Applications, Pergamon, New York, 1984)

$$1/T_1=(3/10)(\gamma^4/r^6)(h/2\pi)^2\{[\tau_c/(1+(2\pi\nu_o\tau_c)^2)]+[4\tau_c/(1+4(2\pi\nu_o\tau_c)^2)]\} \quad (2\text{-}15)$$

$$1/T_2=(3/20)(\gamma^4/r^6)(h/2\pi)^2\{3\tau_c+[5\tau_c/(1+(2\pi\nu_o\tau_c)^2)]+[2\tau_c/(1+4(2\pi\nu_o\tau_c)^2)]\} \quad (2\text{-}16)$$

where h is the Planck constant, r is the distance between interacting nuclei, and τ_c is the correlation time. The correlation time is a quantitative measure of the rate of a molecular motion; for rotational motion it is the length of time required to rotate through an angle of 33^o; for translational motion, the correlation time is the time required for a molecule to move through a distance equal to its diameter. Typically, the correlation time, either rotational or translational, is 10^{-12} to 10^{-11} second for small molecules, 10^{-9} to 10^{-6} second for macromolecules (or small molecules bound to macromolecules), and 10^{-6} to 10^{-3} second for some motions in biological membranes. Clearly from Fig. 2-7, we expect T_1 and T_2 to be equal for small molecules, and to diverge for macromolecules (or small molecules bound to them). Faster internal motions can exist in a macromolecule or membrane in addition to overall rotational and translational motions, that can make the situation more complicated.

Several different pulse sequences have been utilized to measure T_1 and T_2 (1-3). The most common (probably the best) technique for determining T_1 is to employ the "inversion recovery" sequence (180^o-τ-90^o). After an initial 180^o pulse which inverts the spin populations, the spin system begins relaxing toward thermal equilibrium. After time τ, a 90^o pulse is applied, and the FID following the pulse is acquired. As τ becomes longer, the magnetization more closely approaches the equilibrium situation rather than the inverted magnetization. A 90^o pulse must be applied to be able to detect any magnetization because detection is possible only in the transverse plane. The value of T_1 may be determined by measuring the magnitude M of the FID as a function of τ using the following expression:

for perfect 180^0 pulse: $M_Z(\tau) = M_\infty[1-2\exp(-\tau/T_1)]$ (2-17a)

for imperfect 180^0 pulse: $[M_Z(\tau)-M_\infty]/[M_0-M_\infty] = \exp(-\tau/T_1)$ (2-17b)

where M_0 is the magnitude of FID when τ=0, and M_∞ is the magnitude of FID when τ=infinity (i.e. at thermal equilibrium). A simple way to calculate T_1 from the measure $M_Z(\tau)$ values is to observe the value for which the signal after the 90° pulse becomes zero. This is referred to as τ_{null}. T_1 can be obtained from:

$$\tau_{null} = 0.693T_1 \quad (2\text{-}18)$$

while this is a very quick way of determining T_1, it is not usually recommended if an accurate T_1 is desired. Nevertheless, a determination of T_1 from τ_{null} helps the operator to determine the correct period to be used between M_Z excursions (Fig. 2-8).

The data, $M_Z(\tau)$ determined for different τ values can be plotted on a semilogarithmic plot of $[1-M_Z(\tau)/M_\infty]/2$ versus τ (Fig. 2-9). T_1 is obtained from the slope of the straight line according to a rearranged equation 2-17:

$$\ln\{[1-M_Z(\tau)/M_\infty]/2\} = -\tau/T_1 \quad (2\text{-}19)$$

Determination of T_2 is best carried out using a Carr-Purcell pulse sequence with the Meiboom-Gill modification (1-3). Figure 2-10 illustrates the Carr-Purcell process in the rotation coordinate frame. An initial 90° pulse rotates the magnetization into the Y' direction. Because the B_0 magnetic field is not generally perfectly homogeneous, the individual magnetic spins will have slightly different precessional frequencies. Consequently, the individual spins will fan out in the X'Y' plane with a loss of phase coherence. After a time $\tau/2$, a 180° pulse is applied. Because the precessional frequencies of the individual spins are unchanged, they will then achieve phase coherence at time τ along the

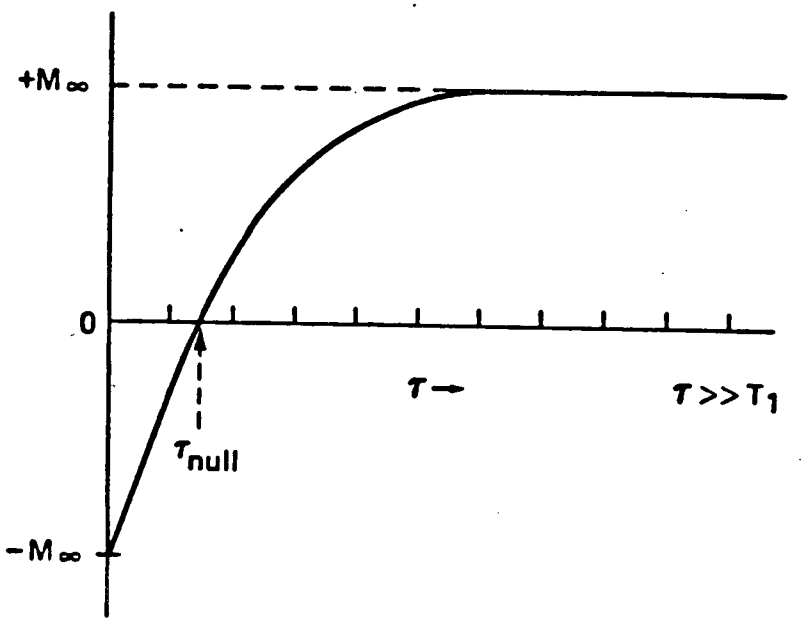

Figure 2-8 Build-up of magnetization as a function of τ in inversion recovery sequence.

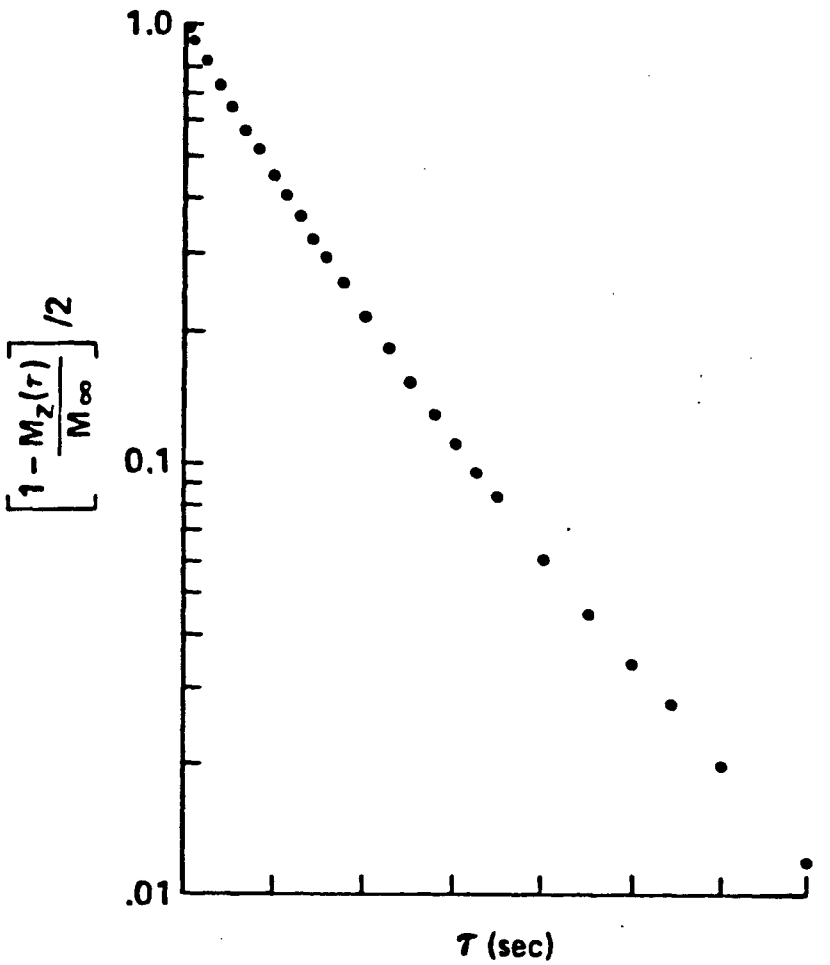

Figure 2-9 Typical semilog plot of $[1-M_Z(\tau)/M\infty]/2$ versus τ for determination of T_1 according to the $180^0 - \tau - 90^0$ method for water in tissues cells. Notice the slightly nonexponential nature of the plot. For pure water, such a plot would be a single straight line. The plot shown is for an arbitrary biological system. (After P.T. Beall, *et. al.*, Data Handbook for Biochemical Applications, Pergamon Press, New York, 1984)

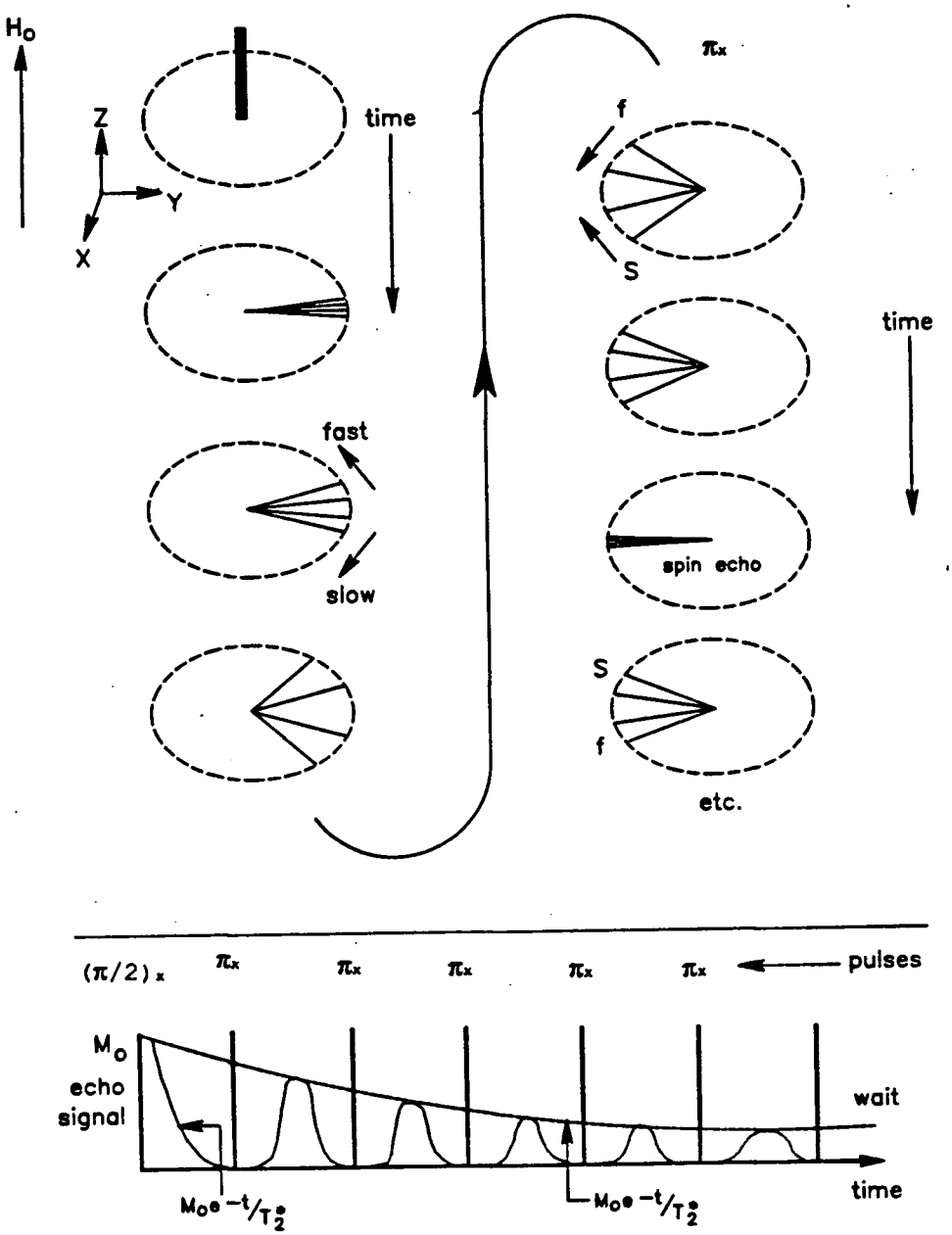

Figure 2-10 The behaviour of the magnetization during the Carr-Purcell (CP) spin-echo sequence $[90^0 - \tau/2 - (180^0 - \tau/2)_n]$. These echoes will be alternatively positive and negative if phase-sensitive detection is used. In diode detection, all echoes will have a positive sign.

negative Y' axis. This will result in a signal, called a spin-echo, being detected. The Carr-Purcell (CP) sequence is initiated with a 90^o pulse followed by a series of 180^o pulses, The Carr-Purcell-Meiboom-Gill (CPMG) sequence is essentially the same as the CP sequence, except that a phase shift of 90^o is introduced in all the 180^o pulses to eliminate effects due to imperfection of the π pulses. The magnitude of the echo decays exponentially as τ increases, so that the echo magnitude can be expressed as:

$$M(\tau) = M_0[\exp(-\tau/T_2)] \qquad (2\text{-}20)$$

where τ is the length of time from the 90^o pulse to the top of the echo. T_2 can be determined from the slope of a semilog plot of $M(\tau)/M_0$ (i.e. $\ln[M(\tau)/M_0]$) versus τ (Fig. 2-11) according to the following rearrangement of equation 2-20:

$$\ln[M(\tau)/M_0] = -\tau/T_2 \qquad (2\text{-}21)$$

Two kinds of references or standards are used in NMR spectroscopy, "internal" and "external". A reference compound that is added directly to the sample is termed an internal reference. If it is not possible to add a reference compound directly to the sample, it may be necessary to place a small amount of reference compound in a separate container close to the sample; this is called an external reference. It is preferable to use an internal reference, but it is not always possible to add an internal reference compound to a biological system, especially if the "system" is a human patient! However, it is still possible to use chemical shift measurements relative to a convenient alternative internal reference. For example, in P-31 in-vivo spectroscopy, the phosphocreatine (PCr) peak is a commonly accepted internal reference, since its resonance frequency is relatively insensitive to pH changes within a normal physiologic range.

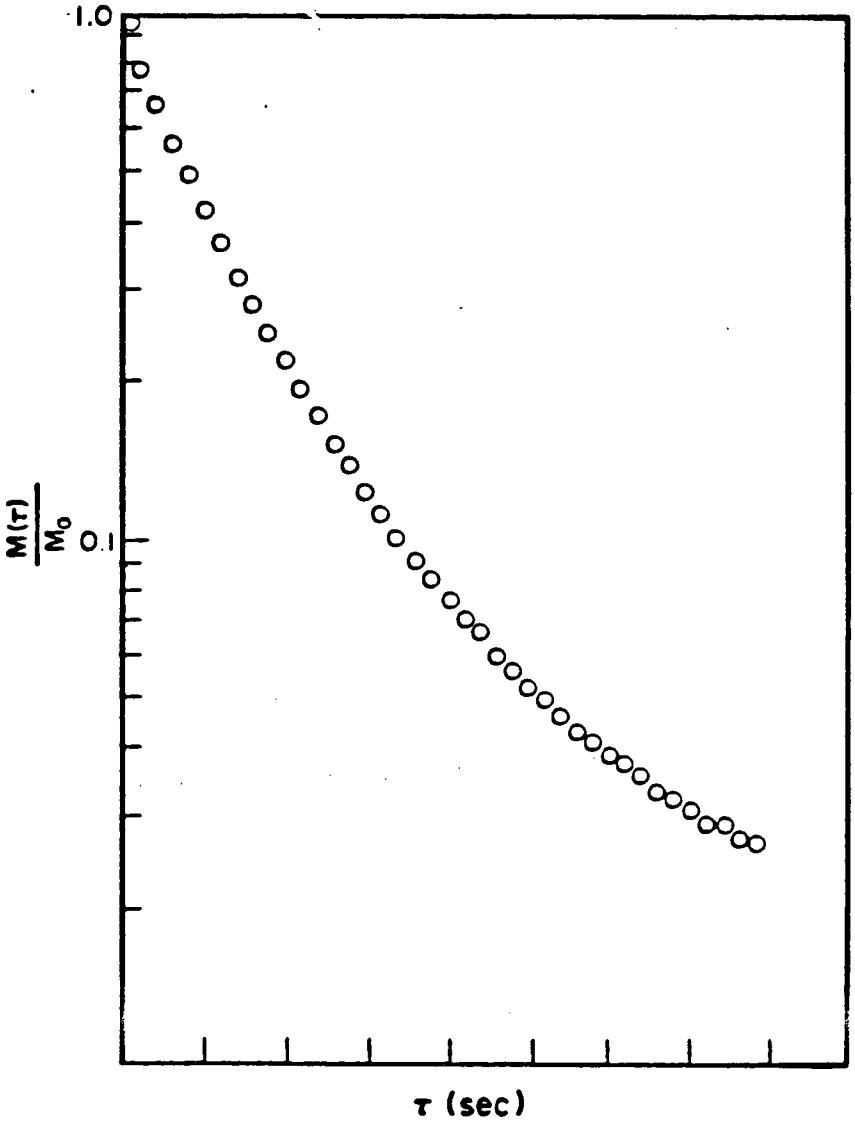

Figure 2-11 Typical semilog plot of $M\tau/M_\circ$ versus τ for the Hahn spin-echo or Carr-Purcell-Meiboom-Gill sequence for a biological system. Notice the nonexponential nature of the plot; for pure water, such a plot would be a single straight line. (After P.T. Beall, *et. al.*, Data Handbook for Biochemical Applications, Pergamon Press, New York, 1984)

The range of chemical shifts of different species varies widely. For example, as shown in Figure 2-12, the chemical shift range of different chemical states of C-13 may vary as much as 200 ppm, and those of P-31 by 25 ppm, whereas there is a range of less than 10 ppm for H-1 in the various functional groups of biological systems. The narrower the range of chemical shift, the more difficult it is to resolve and assign individual peaks.

In addition to the chemical shift range, the resolution in the NMR spectrum is strongly affected by the size of the molecule containing the nucleus of interest, the magnetogyric ratio (the resonance frequency in MHz/Tesla) of the nucleus, the natural background NMR spectrum of the biological system, and the effect of nuclear spin-spin coupling. Thus, the NMR line widths for complex biological systems will be in the following order: H-1 >> P-31 > C-13.

Quantitative information is also available from an NMR spectrum because the integrated signal intensity is proportional to the number of nuclei that contribute to that portion of the NMR spectrum. Unfortunately, the intensity of the peak is also dependent on a number of other factors, some of which are not easily quantifiable. However, the relative areas of the peaks within a spectrum will be equal to the relative numbers of nuclei and, thereby, to the relative concentrations of the nuclei that contribute to the individual peaks. This may or may not be representative of the exact concentrations of a specific nucleus in a biologic system.

Thus, all the nuclei of a particular species may not be "visible" in an NMR spectrum. For example, some nuclei may be so tightly bound to cell membranes or macromolecules with long correlation times that they contribute little or nothing to the observed NMR signal. It is important to understand then that the NMR determination of the amounts of specific chemical compounds present in a

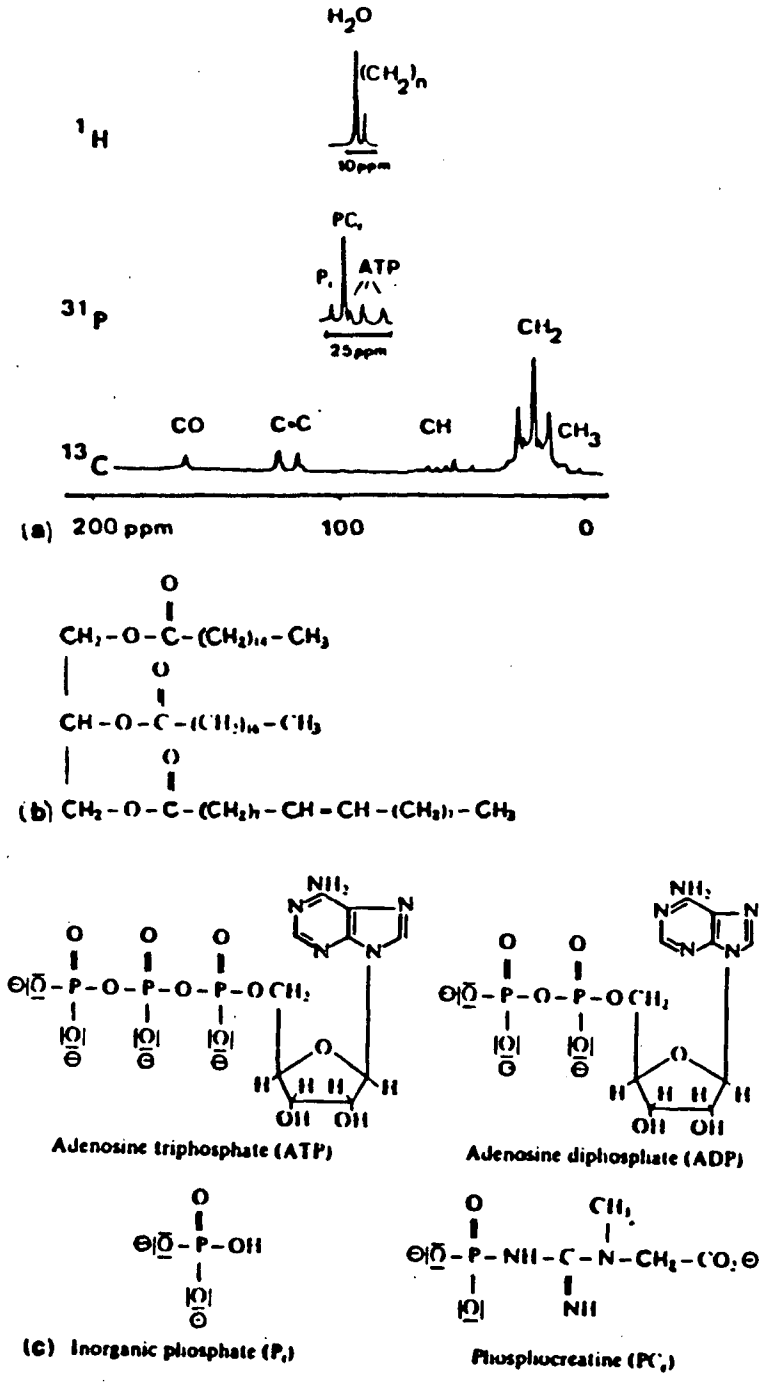

Figure 2-12 (a) NMR spectra from the forearm of a live human subject. The peaks in the H-1 NMR spectrum arise from the protons in water and in the methylene of tissue fat. The P-31 NMR spectrum contains signals for inorganic phosphate (Pi), phosphocreatine (PCr) and the three different phosphate atoms in adenosine triphosphate (ATP). In the C-13 NMR spectrum, all signals are produced by the various types of carbon atom occurring in fat (from documents published by Oxford Research Systems). (b) Glycerin ($HOCH_2$-CHOH-CH_2OH) esterified with palmitic, linoleic, and oleic acid (top to bottom), a typical constituent of fat. (c) ATP, ADP, PCr, and Pi.

sample represent the relative concentrations of only those compounds that are in a chemical state that allows NMR observation.

Saturation and relaxation phenomena are important characteristics of NMR experiments, and can affect the appearance of an NMR spectrum. Since the NMR experiment is inherently a low-sensitivity technique, one method of enhancing the NMR signal is by summing or averaging the results of many experimental observations. The ability to acquire many signals and average them quickly through fast Fourier transformation results in a significant improvement in the signal-to-noise ratio.

Saturation effects in part determine how rapidly signals can be acquired. If the successive excitation radiofrequency (RF) pulses are administered too rapidly, the population of the two energy levels will become more nearly equal, and subsequent RF pulses will then stimulate a decreased population of low-energy or equilibrium nuclei; this will result in an overall decrease in signal intensity. Lengthening the time between successive RF irradiations (increase of the repetition time, TR) allows a greater proportion of the excited nuclei to return to the low-energy equilibrium state so that subsequent RF irradiations always excite the thermal equilibrium population of the low energy state nuclei, to a high energy state; the end result of that is an increase in signal intensity.

The mechanism by which the excited or high energy nuclei return to the equilibrium state is called nuclear relaxation. This relaxation phenomenon can be described by two time constants, T_1 (spin-lattice relaxation time) and T_2 (spin-spin) relaxation time. The T_1 and T_2 parameters of specific nuclei and chemical states of the same nucleus are of practical importance in designing in-vivo spectroscopic experiments.

Saturation effects must always be considered when quantitatively assessing NMR spectra. As previously mentioned, if there is partial saturation or

incomplete relaxation of a particular nucleus in between pulses, then the overall signal intensity will be reduced. It is generally held that time between pulses (TR) should be at least 4 to 5 T_1 of the species with the longest T_1 to eliminate saturation effects.

It is important to note that the T_1 values for the metabolites in aqueous solution are not necessarily representative of the T_1 values of the metabolites in tissue. The shortening of T_1 values in tissue with respect to aqueous solutions can be due to a number of factors including the effect of paramagnetic ions, binding to macromolecules, and a slightly enhanced viscosity of the intracellular fluid. A further complication that should be noted is that the metabolite T_1values will be magnetic field dependent.

2.2 Experimental Aspects

Although its application in biomedical research is of rather recent origin, NMR spectroscopy has been used as an analytical and structural tool in chemistry and physics for over 40 years. A number of technical and conceptual hurdles had to be crossed before this powerful methodology could be exploited in the noninvasive study of animal models and humans. Three major technical developments in the late 1960s were critical in advancing the state of the art for high-resolution NMR spectroscopic studies of solutions and these same innovations were essential in the later development of NMR spectroscopy in medicine.

One was Fourier transform pulse NMR spectroscopy, which allowed facile discrimination of signal from background by rapid noise averaging, a technique that increased by orders of magnitude the sensitivity of an inherently insensitive method. A second, interrelated advance was the use of dedicated

computers to record data and control the spectrometers. Finally, the introduction of high-field superconducting magnets with wider and wider bores led, in the mid- to late 1970s, to study of perfused organs and small animal models. Today, magnets with 1-meter bore sizes and field strengths of 2 Tesla are widely available for human studies.

To optimize instrumentation for *in-vivo* spectroscopic studies, the signal-to-noise ratio must be increased either by increased sensitivity, decreasing noise, or both. One can increase sensitivity by increasing the field strength, improving the sensitivity of the RF coils, and increasing the efficiency of data acquisition. One can reduce noise by optimizing the receiver electronics, maximizing the RF shielding, or increasing the extent of signal averaging. As is invariably the case, there are trade-offs in trying to accomplish these goals.

Increasing the strength of the static magnetic field is especially important for detecting nuclei that may be present in low concentrations. Higher field strengths also increase the chemical shift dispersion and allow improved resolution of individual spectral peaks. The homogeneity for *in-vivo* spectroscopy ideally should be on the order of 0.1 to 0.5 ppm in the center of the magnet; moreover, the change in the static magnetic field over the observed volume of tissue must be less than the chemical shifts of the observed nuclear species. At some level, the patient or animal being studied affects the homogeneity of the static magnetic field. This involves local changes in magnetic permeability inside and outside cells, bulk changes in magnetic permeability secondary to different magnetic properties of bone, air, and soft tissue interfaces, and local eddy currents from gradient switching and from the effects of flow and diffusion of nuclei into and out of the sample volume.

As the operational frequency increases with higher field strength, the RF pulses become more efficiently absorbed by the tissues, and penetration into the

body decreases; thus at higher field strengths, eddy currents are induced in the body by the RF fields, that create phase shifts and result in radiofrequency (RF) attenuation (4). Consequently, an increased level of RF power will be necessary to penetrate deeper areas of the body, and certain pulse sequences will almost certainly result in RF power deposition that exceeds the current guidelines of 0.4W/kg as averaged over the whole body, or 2W/kg as averaged over any 1 gram of tissue. The above difficulties can be partially alleviated with the use of surface coils (5-6). Surface coils, due to a better filling factor, have improved sensitivity over standard imaging coils and also serve as a means of localization.

In addition to improving RF sensitivity, it is necessary to minimize the amount of RF noise reaching the receiver coil, and hence radiofrequency shielding is an important factor for reducing noise introduced through extraneous RF signals. Two approaches are currently in use; either the part of the person, or animal, being studied within the operating bore of the magnet can be shielded, or the entire room in which the magnet sits can be shielded. It seems, at this time, that the greatest degree of RF shielding can be obtained with the whole room concept. However, the latter can be very expensive and in the next chapter, we will detail an inexpensive, but effective, means of shielding the experimental subject without shielding the whole room.

Sensitivity can also be improved by increasing the efficiency of data acquisition; thus novel pulse sequences and signal processing techniques can effect overall system sensitivity. Improved efficiency of data collection can also occur with quadrature detection, which is a phase-sensitive method of radiofrequency signal detection that reduces noise by a factor of the square root of two (7-8). Quadrature detection also results in less RF power requirements. Homonuclear "decoupling" sequences and saturation pulses can also improve the ability to observe low-concentration metabolites (9). However, increasing the

number of overall signal averages acquired during data acquisition reduces the overall effective noise resulting in an overall signal improvement which is proportional to the square root of the number of scans acquired:

$$\Psi \propto N^{1/2} \tag{2-22}$$

and

$$N = t_{total}/t_1 \tag{2-23}$$

where Ψ is the signal to noise ratio, N is the number of scans, t_{total} is the total time taken to acquire the data and t_1 is the time taken for one scan.

The signal from a given sample volume is more or less constant; but the noise sources in a NMR instrument are numerous. Ψ has been shown to be mutually dependent on several instrumental and experimental conditions. One important expression which is noteworthy is given below (10):

$$\Psi = [K\omega^{7/4}V_s]/[T_s^{1/2}\Delta f^{1/2}] \tag{2-24}$$

where Δf is the bandwidth (in Hertz) of the receiver, ω is the resonance frequency, V_s is the sample volume, T_s is the sample temperature and K is a function of several parameters (e.g. coil Q factor, coil temperature, filling factor).

We began this chapter with a brief discussion of some of the physical basis for NMR spectroscopy, followed by discussion of some of the experimental and technical factors that affect the application of *in-vivo* spectroscopy. In the next section, we will explore the methodology in assessment of disease in intact muscle of humans.

2.3 Clinical Aspects

Clinical utilization of *in-vivo* human NMR is still in its infancy. The method has potential in diagnosing disease, monitoring therapy, and, more importantly, in gaining insight into human biochemistry and physiology. It provides a fundamental link between physiology, biochemistry, and human

disease. A significant amount of our past information has come from tissue extracts, isolated perfused organs, and invasive *in vitro* studies of animal models-morphologically and physiologically consistent with humans. Although model studies enhance our knowledge of physiology and biochemistry of diseased tissues/organs, they still do not necessarily reflect the actual living states of the metabolites in intact human tissues, as does *in vivo* NMR (11).

Diseases of skeletal muscle are uncommon but of grave importance for the sufferers and their families since, for most of them, no effective therapy is as yet available. Nevertheless, the past decade has seen an increasing number of reports of severe metabolic diseases caused by abnormalities of mitochondrial function. The defects have been discovered in the following functional areas:

(a) defects in the transport of biochemical-molecules which constitute the basic energy source for cellular function, such as pyruvate, fatty acids, and amino acids, from the cytosol into the mitochondrial matrix,

(b) defects of substrate utilization (e.g. fats or carbohydrates),

(c) defects of the tricarboxylic acid cycle,

(d) defects of oxidation-phosphorylation coupling,

(e) defects of the respiratory chain.

The clinical manifestation of these biochemical disorders are numerous and varied. Impaired muscle function of varying degree is the most common. Many patients have had evidence of multi-system involvement, particularly of the central nervous system (encephalopathy), myocardium (cardiomyopathy), retina (retinopathy), as well as skeletal muscle. These disorders may be inherited through defects in the maternal mitochondria. Unfortunately, there may be no symptoms or signs, and the clinical abnormality may be restricted , for example, to the extraocular muscles; alternatively there may be a severe proximal myopathy with fatigability and exercise intolerance. Diagnosis is usually based

on a muscle biopsy; the presence of ragged red fibers, which are now known to have this appearance as the result of subsarcolemmal accumulation of abnormal mitochondria, is the clearest indication.

The biochemical lesion in patients with mitochondrial myopathy may be located at any one of many different steps in the oxidation of substrates. Abnormalities have been reported involving the cytochromes, the iron-sulfur centers, the adenine nucleotide translocator, the adenosine triphosphate(ATP) synthetase itself, and various components of the carnitine transport system (12). The nature of the link between these lesions and the clinical manifestations of disease remains to be defined. Because mitochondria are the major source of energy for muscle cells, impaired energy metabolism is a logical candidate for being the final common pathway leading to cell injury.

ATP has been referred to as the "universal currency of free energy" in human body, mainly because of its widespread use as a carrier of freely available energy within a cell. Consequently, most of the energy required by muscle cells at rest is also supplied in the form of ATP, itself generated by mitochondrial oxidative phosphorylation. During exercise, there is an increased demand for ATP that is largely met by an increase in the rate of mitochondrial oxidative metabolism. This is augmented by phosphoryl transfer to adenosine diphosphate(ADP) from phosphocreatine(PCr) in the reaction catalyzed by creatine kinase and by an acceleration of anaerobic glycolysis.

Phosphorus Nuclear Magnetic Resonance Spectroscopy (P-31 NMRS) is useful in the noninvasive diagnosis of mitochondrial myopathies and in defining the pathophysiological basis of these disorders, and has been described for the study of metabolic disease of muscle in various publications from the research groups of George Radda and Britton Chance, who have pioneered the application of P-31 NMR Spectroscopy to study of mitochondrial disease (13-14).

The work of this thesis extends that theme, by describing how the study of muscle may also provide evidence for metabolic dysfunction in brain, even in the absence of clinical signs of myopathy. Various modifications of the Chance-Radda techniques have been used in this work in an attempt to design a protocol for study of contracting muscle which better accounts for mechanical and physiological considerations. The technique described in this thesis is also sensitive enough to be used for the assessment of therapy; perhaps most importantly, it is sufficiently tractable for routine clinical use.

Muscle, which may increase its energy turnover more than 100-fold during exercise, is ideal for metabolic assay by P-31 Magnetic resonance spectroscopy(NMRS) in vivo, as it is accessible and can be driven metabolically over a wide range of measurable mechanical outputs. P-31 NMRS not only identifies which phosphorus-containing compounds are present in high (millimolar) concentration, namely ATP, ADP, P*i* and PCr, but also provides information about their chemical environment including pH and intracellular distribution. The method is quantitative, non-destructive and permits repetitive measurements of intact functioning organs and systems.

The muscle chemistry which can be monitored by P-31 NMRS is briefly summarized below, using the structures and abbreviations as defined in Figure 2-12.

$$ATP \Longleftrightarrow ADP + Pi + Energy \qquad (2\text{-}25)$$

$$PCr + ADP \Longleftrightarrow Cr + ATP \qquad (2\text{-}26)$$

Aerobic Oxidation(Krebs Cycle\Electron Transport Chain):

$$Acetate + ADP + Pi \Longleftrightarrow ATP + CO_2 + H_2O \qquad (2\text{-}27)$$

O_2

Anaerobic Glycolysis:

$$\text{Glycogen} + P_i \longrightarrow \text{Glucose-1-phosphate}$$

$$\longrightarrow \text{Glucose-6-phosphate} + \text{ADP} + P_i$$

$$\longrightarrow \text{Lactic Acid} + \text{ATP} + H_2O \qquad (2\text{-}28)$$

$$HPO_4^{2-} + H^+(\text{from Lactic Acid}) \underset{(pK = 7.2)}{\Longleftrightarrow} H_2PO_4^- \qquad (2\text{-}29)$$

Forearm muscle normally contains the following approximate quantities of adenosine triphosphate (ATP), adenosine diphosphate (ADP), phosphocreatine (PCr), and inorganic phosphate (P*i*): 5mM; 20 nM; 20 mM; and 1 mM, respectively. The immediate source of energy to maintain exercise is the scission of ATP (equation 2-25), whose tissue levels are restored in the short term by the transfer of high-energy phosphate from the "fast energy" buffer PCr to ADP (equation 2-26). The ultimate long-term source of energy is the oxidation of acetate in the Kreb's cycle (equation 2-27) under aerobic conditions, with anaerobic glycolysis providing an emergency route to ATP under conditions of limited oxygen supply (for example, ischemia or hypoxia).

Under aerobic conditions, generation of ATP in the Kreb's cycle nearly matches exercise requirements: there is only a slight fall in PCr, a slight increase in P*i*, and no significant change in the tissue pH. On the other hand, anaerobic generation of ATP by glycolysis under ischemic conditions fails to meet the exercise requirements: there is a large decrease in PCr, a large increase in P*i*, and a large fall in pH due to lactic acidosis. Tissue pH can be monitored via the chemical shift of the inorganic phosphate peak, P*i*, which is a composite of those of the HPO_4^{2-} and $H_2PO_4^-$ ions that are in rapid chemical equilibrium (equation 2-29). The latter two ions have significantly different chemical shift, and the chemical shift of observed P*i* is a weighed average of the two populations.

Changes in pH alter the balance between monobasic and dibasic phosphate, thus producing a change in the chemical shift of the P*i* peak. Acidosis shifts the P*i* peak to the right (high field), whereas alkalosis shifts the peak to the left (low field).

Biochemical energy is provided to the living cell by two primary biochemical pathways: glycolysis and oxidative phosphorylation. An important step towards studies of these processes in intact human muscle was made just 15 years ago, when it was shown that it is possible to record high resolution P-31 NMR spectra from an excised rat muscle that was placed in a tube 8 mm in diameter (15). The compounds observed and identified from the spectra were phosphocreatine (PCr), adenosine triphosphate (ATP), inorganic phosphorus (P*i*), and sugar phosphate. Also, following the suggestion of Moon and Richards (16) based on their studies of red blood cells, intracellular pH was measured from the position of the P*i* resonance. Decreases in PCr concentration and the accompanying increase in P*i* and acidosis were followed as the metabolic capability of the muscle diminished.

The central role of ATP in providing the biochemical energy for contraction and "ion pumping" during contraction is well established. Adenosine triphosphate is mainly supplied by oxidative phosphorylation, that in turn requires adequate substrate and oxygen delivery. The conversion of PCr to ATP, catalyzed by creatine kinase, has been proposed to provide the "energy reserve" for some tissues to meet rapid demands for ATP. However, if phosphocreatine stores are depleted and ATP is not resynthesized, ATP concentration will fall to a point at which muscular contraction and ion transport can no longer occur. Further, it has been demonstrated that different forms of creatine kinase are present in muscle cells (e.g. cytoplasmic, or bound to the mitochondrial membrane) led to the hypothesis that PCr acts as the "energy shuttle" between

the mitochondrial and cytoplasmic compartments (17). This two-compartment hypothesis can be used to explain the different rates of recovery after exercise between pH and P*i*.

The integration of the biochemical events in the living body depends on the various control processes and for this reason metabolic control and its mechanism is best studied in the intact system. Thus, because it is non-invasive, one of the main advantages of NMR spectroscopy is that it can be used to study control processes in both normal and pathologic states.

As indicated in the beginning of this chapter, one of the major limitations of NMR spectroscopy is the poor sensitivity of the method. It is, therefore, essential that the instrument used has an optimal primary signal-to-noise(S/N) sensitivity; this is achieved by using adequate radiofrequency(RF) shielding, low noise preamplifiers, and sufficient isolation of RF amplifier and receiver. Effective grounding of the experimental subject is also very important since the body acts as an antenna, radiating noise into the spectrometer receiver coil. Beyond this primary sensitivity, spectroscopy requires further S/N improvements. The first of these improvements is offered by signal averaging; in general the S/N ratio improves with the square root of the time used to collect data. However, when examining patients there is a practical upper limit to the total amount of time that can be used for data collection. Thus, the total data acquisition time may be up to one hour, when obtaining a static spectrum from a particular tissue; however, in a dynamic experiment, such as in muscle exercise, changes may occur in the spectrum on a time scale less than a minute. Fortunately, for skeletal muscle, it is possible to obtain satisfactory P-31 NMR spectra at 2 Tesla in one minute, when using a surface coil of 4 cm. diameter. One can optimize the sensitivity for a given area of interest by use of an appropriate RF receiver coil. If the area of interest is relatively close to the surface it is

advantageous to use an appropriately placed surface coil, and coils of different size and geometry are therefore needed to meet the specific requirements for the particular area of interest. Although use of surface coils may complicate patient examination, surface coils are considered to be indispensable for spectroscopic application because of both S/N considerations and the simplicity with which they provide crude, yet effective spatial localization.

2.4 Diversity and Invariance

Most biochemical investigations of cellular systems, or animals, are carried out under well-defined conditions, often using animals of a given strain, so that the metabolic measurements can be more easily reproduced. However, when human subjects are used it becomes immediately evident that there is an enormous variety, diversity and polymorphism. Some individuals may begin the work too slowly and continue that way so that their final performance score reflects inappropriate pacing or motivation rather than physiologic and metabolic capacity. Even for healthy subjects, in principle, muscle metabolism of individuals doing the same form of exercise could vary from being almost entirely an aerobic-type response, to one where most of the energy is supplied through glycolysis, which could be observed by a very significant acidification (pH drop) in the muscle cells. These differences can arise because many factors such as glycolytic flux, oxidative ATP synthesis, blood flow, and muscle fiber types all contribute to the final response. However, since NMR spectroscopy is a quantitative method, it is essential to decide the range of diversity between healthy individuals before meaningfully using the method to study human disease. For example, Chance and coworkers have used P-31 NMRS very successfully to investigate athletic performance and response to training. Thus,

within each series of studies on disease, it will be important to devise tests first to determine the extent of variation, and second to emphasize the invariance of biochemistry within that human diversity.

2.5 Pre-1985 Techniques for Studying Human Muscle (Appendix B)

Before the commencement of the work of this Thesis in 1985, analysis of human muscle function, metabolism, and fatigue in both health and disease, a variety of techniques were employed. The most fundamental approach was the measurement of force, generated by either voluntary, or electrically-stimulated, contractions. More detailed information concerning the mechanisms of both weakness and fatigue was obtained when the electromyogram was recorded simultaneously with the force. The needle biopsy technique was recommended for the histological and histochemical examination of skeletal muscle; it has the advantage of being rapid and repeatable and has proved suitable for both diagnostic and follow-up purposes.

Neuromuscular disorders are illnesses that develop when the voluntary muscles of the body, or the nerves that control those muscles, are injured and thus work improperly. Any of the muscles of the body can be affected, although most commonly they are located in the arms and legs. However, eye movements, speaking, chewing, swallowing, and even breathing--activities controlled by muscles--can also become weak. However, no damage or deterioration occurs to that part of the brain that controls thinking or the sense of smell, sight, hearing, or taste (the latter are known as neurologic diseases).

Nerve cells that control movement (called neuronal cell bodies) begin in the spinal cord and brainstem. Nerve (motor axons) emerge from openings (foraminae) in the skull or spine and travel variable distance to reach particular

muscles (Fig. 2-13). If there is disease anywhere along the nerve, electrical impulses from the brain are not able to travel the full length of the nerve to the muscle. The muscle then gets smaller (atrophies) and does not contract normally. In some cases the nerves are normal, but there is disease in the muscles and so the nerve impulses cannot produce normal contraction of those muscles. Although the most common symptoms of neuromuscular diseases is weakness, other symptoms include muscle cramps, wasting (atrophy), and arm and leg aches. Prolonged weakness of an extremity can lead to secondary complications that include a loss of the full range of motion at joints, swelling of the legs, pressure sores, and in some cases even permanent deformities.

Although each neuromuscular disease has a characteristic course and progression, these is considerable variability between individuals with the same disease. With some disorders, symptoms often come and go in a relapsing-remitting fashion. Moreover, medication may reverse these symptoms, so a person's strength returns completely to normal, although the propensity to have a recurrence of symptoms may persist.

After a patient has been examined by a physician familiar with the clinical manifestations of neuromuscular diseases, a wide variety of test may be ordered to help establish an accurate diagnosis.

2.5.1 Nerve and Muscle Biopsy

A nerve may also be biopsied under local anesthesia. Most frequently, a sensory nerve is used, because motor nerve is not ordinarily removed as removal will result in permanent paralysis. However, in nerve diseases that affect only muscular nerves, a biopsy of the sensory nerve can be normal despite profound abnormalities in the motor nerve.

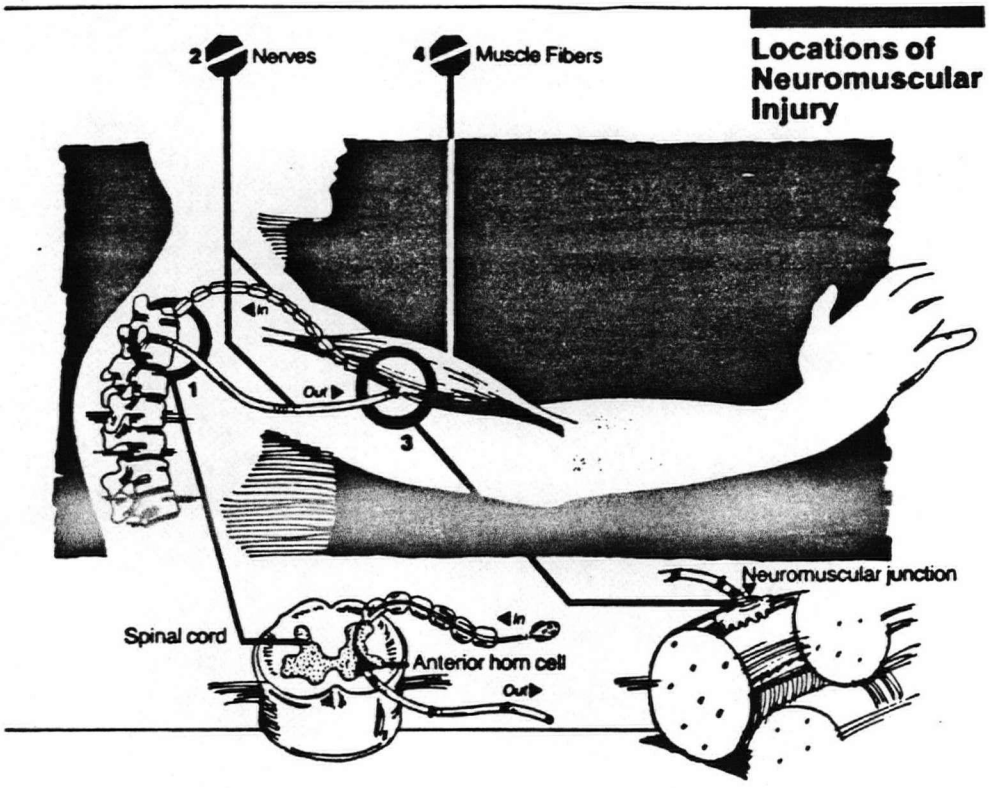

Figure 2-13 Anatomy of the neuromuscular system. Nerve impulses for movement begin in (1) the anterior horn cell (motor neuron) in the spinal cord and travel down (2) a motor nerve (axon) to (3) the nerve-muscle junction. A chemical (acetylcholine) released by the nerve terminal at the junction causes (4) the muscle to become activated and contract. Neuromuscular disorders result from injury to any of these four locations. (After S.P. Ringel, Neuromuscular Disorders-A Guide for Patient and Family, Raven Press, New York, 1986)

Direct examination of diseased tissue is particularly useful. With muscle diseases, a muscle biopsy (Fig. 2-14) is easily performed using local anesthesia. A weak muscle is selected for biopsy to ensure that if an abnormality is present it will be found. A small cylinder of muscle, approximately half a centimeter in diameter, is removed for study. The healed incision (scar) is usually about 1 inch long. Most modern diagnostic laboratories freeze the excised muscle sample, slice it into extremely thin sections, and stain it with certain chemicals to allow detailed interpretation of muscle abnormality.

There are limitations to the needle biopsy techniques. Since it is a "blind" procedure, there is a sampling problem, especially in neuropathies where fiber type grouping may be present and fiber type may vary at different depths within the muscle. Besides, there is always a delay, however slight, in freezing the specimen, which can lead to inaccuracy in the estimation of inorganic phosphate and phosphocreatine.

2.5.2 Electrodiagnostic Studies

More than 200 years ago Galvani discovered that a recording could be made of electrical impulses that travel along nerves and across the juncture where the nerve joints and activates the muscle (nerve-muscle junction). If a nerve, neuromuscular junction, or muscle is injured, the characteristic electrical impulses can be analyzed to determine where the injury occurred and its extent. Such studies require the active participation and cooperation of the patient. The procedures are sometimes associated with discomfort. To make an accurate diagnosis, physicians need to know how quickly an electric impulse travels down a nerve and into the muscle. Measuring nerve conduction velocities provides this information (Fig. 2-15). The speed (velocity) is calculated by

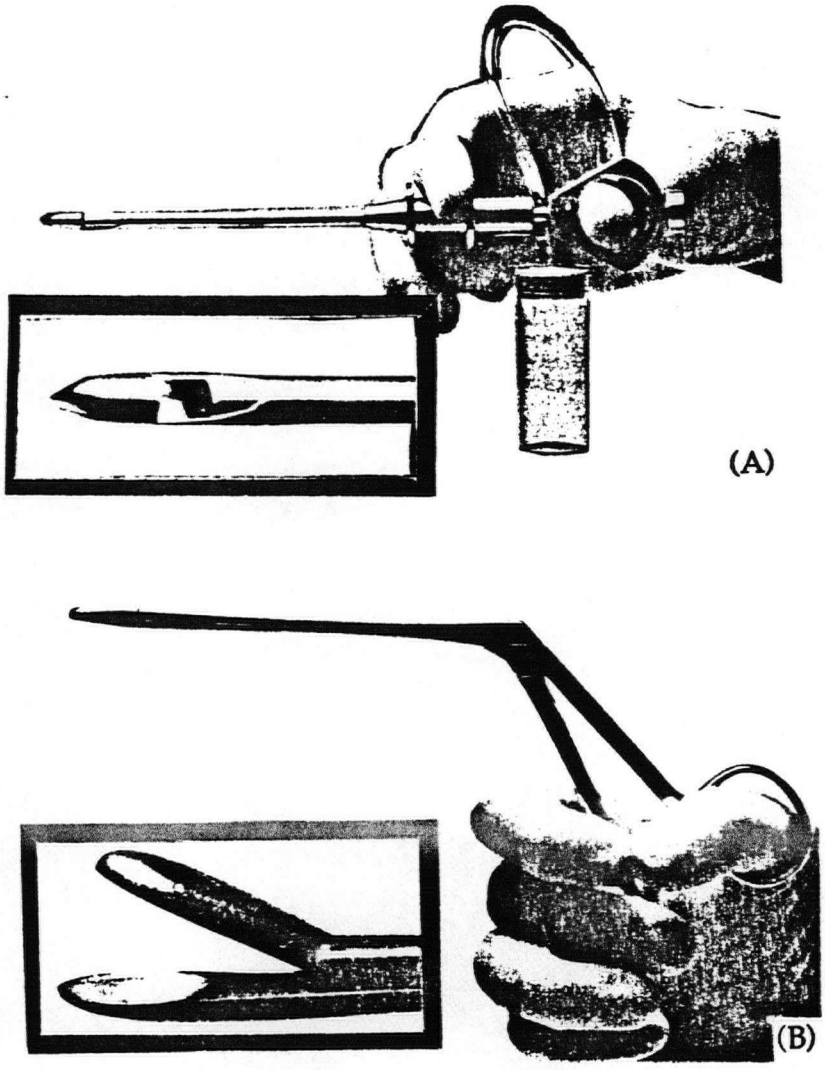

Figure 2-14 Muscle biopsy needle and forceps.

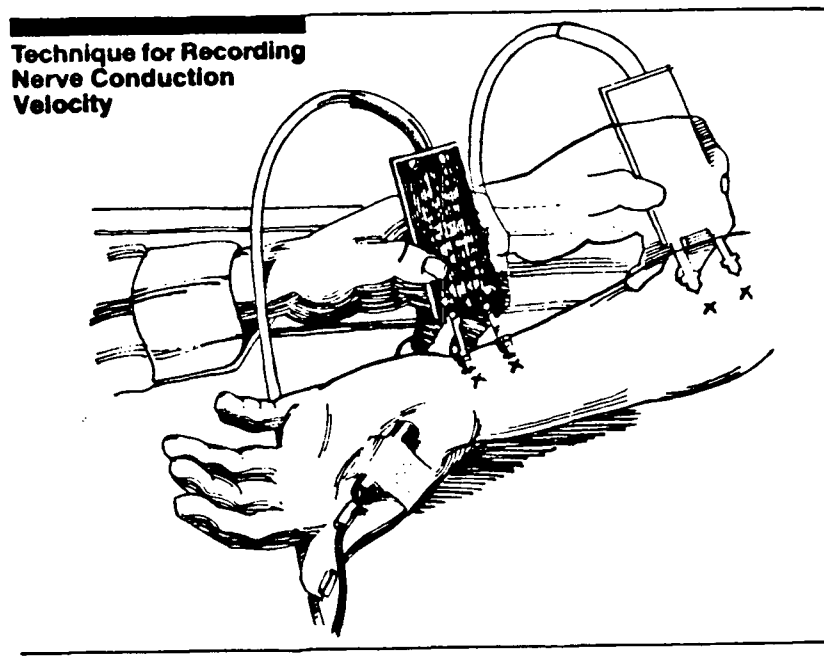

Figure 2-15 Technique for recording nerve conduction velocity. An electrode taped over the muscle records the time required for the stimulus to travel along the nerve from the wrist and from the forearm. The patient feels a mild shock sensation and muscle twitch with each direct-current stimulus. (After S.P. Ringel, Neuromuscular Disorders-A Guide for Patient and Family, Raven Press, New York, 1986)

stimulating the nerve and recording the time the impulse takes to arrive in the muscle. With an injury to the nerve, conduction is characteristically slowed.

When a disease of the nerve-muscle junction is suspected, a special test is used in which a series of electrical stimuli are applied to a nerve at a slow rate (repetitive stimulation). With myasthenia gravis, each response of the muscle following repetitive stimulation gets smaller because a partial block prevents complete transmission of electrical information from the nerve to the muscle. Thus, nerve conduction studies provide quantifiable data on nerve function, and can help to define the distribution, extent and degree of nerve damage, and the presence of axonal degeneration or demyelination.

Electromyography (EMG) measures electrical activity directly within a muscle. A thin, sharp needle is inserted through the skin and into the muscle. Insertion of a needle into the muscle is momentarily painful to most patients and can be quite frightening to a child. Once the needle is inserted no additional pain occurs, and most patients tolerate the procedure well. Muscle activity, which is both visually recorded on screen and heard by the examiner, is examined with the muscle resting and contraction. With disease of the muscle, abnormal electrical activity is recorded. By sampling a number of muscles, the extent and distribution of muscle disease can be determined.

The diagnostic yield of quantified EMG and muscle biopsy was examined by Buchthal and Kamieniecka in 1982 (18). They found that electromyography agreed with the clinical classification in 81% of their patients with myopathy (biopsy agreed in 79%). In neurogenic disease the EMG agreed with the clinical classification in 91% (biopsy 92%).

2.5.3 Blood Tests

When skeletal muscle is damaged, the muscle cells lose proteins such as creatine kinase (CK) in large amounts into the blood. CK is therefore a convenient marker of muscle cell breakdown. Other blood tests that are ordinarily helpful in the diagnosis of neuromuscular disorders include an erythrocyte sedimentation rate and assays for antinuclear antibody and rheumatoid factor. It is also useful to evaluate the function of the endocrine glands (pituitary, thyroid, adrenal, parathyroid) as disturbance of any of these glands can also cause weakness.

2.5.4 Electrocardiogram

An electrocardiogram (ECG) is often obtained in patients with neuromuscular disorder because abnormalities of the heart muscles may also be present. Irregular and potentially life-threatening heart rhythms most commonly are noted in patients with myotonic dystrophy.

2.5.5 Tests of Pulmonary and Swallowing Function

Tests of breathing capacity (pulmonary function tests) help identify the cause and severity of breathing problems in neuromuscular patients who notice shortness of breath either at rest or with exertion. For patients who have difficulty swallowing, X-ray films are obtained while the individual swallows barium mixed with a reasonably good-tasting liquid. These studies allow the physician to pinpoint the swallowing difficulty and prescribe appropriate therapy.

2.5.6 Miscellaneous Tests

Specialized biochemical tests can be performed using either blood samples or samples from a muscle biopsy if a patient is suspected of having one

of the uncommon metabolic neuromuscular disorders. Ordinarily, these tests (e.g. blood urea nitrogen, and urine porphobilinogen values, serologic tests for collagen-vascular disease, and measurement of vitamins B_{12} and E levels) are scheduled well in advance, and the specimens are forwarded to laboratories equipped to perform the desired test.

2.5.7 Conclusion

Thus far we have considered most of the techniques used to study neuromuscular diseases. Some techniques are very invasive and cannot be routinely prescribed, especially to children; whereas others cannot be repeated frequently enough. So there is a need for new techniques capable of continuously and noninvasively monitoring human muscle function, metabolism, fatigue, as well as muscle diseases.

In recent years, P-31 NMRS has been shown to have considerable potential in the clinical and experimental investigation of muscle disorders; and NMRS has already been considered as a complementary technique that may play an important role in monitoring disease progress or treatment strategies. Besides, the particular advantage of NMRS is that the volume of tissue sampled is 30 to 40 ml, far greater than any possible biopsy and therefore representing a broader sample of content from heterogeneous myopathic tissue.

The work that is presented in this Thesis represents our particular contribution to a worldwide effort to make NMRS a tractable technique for the routine testing of mitochondrial myopathy and fatigue in patients, regardless of their age, fitness, or size. In the next chapter, we will consider the surface coil technology that make such techniques possible.

References

1. A. Abragam, Principles of Nuclear Magnetism, Oxford University Press, London, 1961.

2. C. P. Slichter, Principles of Magnetic Resonance, 2nd ed., Springer-Verlad Ltd., Berlin, 1978.

3. T. L. James, Nuclear Magnetic Resonance in Biochemistry: Principles and Applications, Academic Press, New York, 1975.

4. H. R. Hart, P. A. Bottomley, W. A. Edelstein, *et. al.*, AM. J. Radiology, 141:1195, 1983.

5. J. J. H. Ackerman, T. H. Grove, G. G. Wong, *et. al.*, Nature 283:167, 1980.

6. O. C. Morse, and J. R. Springer, Science 170:440, 1970

7. D. I. Hoult, and R. E. Richards, Proc. Royal Soc. London 344:311, 1975.

8. E. O. Stejskal, and J. Schaeffer, J. Magn. Reson. 14:160, 1974.

9. M. J. Hetherington, T. Aurson, D. C. Jue, *et. al.*, Soc. of Magn. Reson. Med., pp.313-314, Berkeley, CA., 1984.

10. D. I. Hoult, and R. E. Richards, J. Magn. Reson. 24:71, 1976.

11. R. S. Balaban, Invest. Radiol. 24:948, 1989.

12. H. Przyrembel, J. Inher. Metab. Dis. 10:129-146, 1987.

13. B. Chance, S. Eleff, W. Bank, J. S. Leigh, and R. Warnell, Proc. Natl. Acad. Sci. USA 79:7714-7718, 1980.

14. G. K. Radda, P. J. Bore, D. G. Gadian, *et. al.*, Nature 294:608-609, 1982.

15. D. I. Hoult, S. J. W. Busby, D. G. Gadian, G. K. Radda, R. E. Richards, and P. J. Seeley, Nature 252:285-287, 1974.

16. R. B. Moon, and J. H. Richards, J. Biol. Chem. 248:7276-7278, 1973.

17. M J. Dawson, D. G. Gadian, and D. R. Wilkie, Nature 274:861-866, 1978.

18. F. Buchthal, and Z. Kamieniecka, Muscle and Nerve 5:265-280, 1982.

Chapter 3

3. TECHNICAL CONSIDERATIONS FOR SPATIALLY LOCALIZED NMRS

3.1 Introduction

At the beginning of this project, before routine clinical P-31 NMRS studies were possible with our Nicolet-Oxford 80 MHz NMR spectrometer, we had to overcome several almost insurmountable obstacles. As with all the other NMR spectrometers in the UBC Chemistry Department, our homebuilt unit was installed in 1983 without any RF shielding. For two years, the spectrometer had worked very well because we were mostly producing proton spectra and proton images. Subsequent efforts in our laboratory produced limited successes when P-31 NMRS was used to study animals (1-2), this was possible because the samples could still be enclosed inside the magnet and shielded from the surroundings by grounded cables and end caps. Afterwards, when attempts were made to study human patients, the author found himself cornered by a very challenging situation. Since our 30 cm. horizontal bore magnet was only large enough to accommodate human limbs, the remainder of the body was outside the magnet, acting as an efficient RF antenna gathering noises from the environment, especially from the Nicolet computer. The objective of this chapter is to outline the author's efforts, in collaboration with Dr. Andrew Penn, to upgrade the spectrometer to a stage where routine P-31 NMR spectra with acceptable signal-

to-noise ratio could be obtained in 1 minute, and to lay the ground work to make possible subsequent clinical studies presented in Chapters 4 and 5 of this Thesis. A novel design of spiral resonator surface coil housed in a moveable gantry will be presented as a highlight at the end of this chapter; but, before all those can be discussed, a basic knowledge of NMR spectrometer and RF surface coil, which has charted the course of the author's learning experience during the past five years, is essential and will be reviewed.

3.2 The NMR Spectrometer

The conventional NMR spectrometer consists of a computer, transmitter, RF power amplifier, RF coil, preamplifier, and receiver. The computer performs the various data processing tasks: Fourier Transform, data filtering, and storage. In the transmitter, the RF voltage is gated with the pulse envelopes from the computer interface to generate RF pulses that excite the resonance. These pulses are amplified to levels varying from 100 W to several KW, depending on the spectroscopic method and coil configuration, and are fed to the transmitter coil. The higher power levels are necessary for the large sample volumes encountered in whole-body experiments and where short-duration, closely spaced RF pulses are required.

Usually an electromagnetic shield is installed to protect the environment from the interfering effects of the exciting pulse during the transmit phase, and to prevent high frequency interference of the environment from reaching the sensitive measuring instrument of the NMR spectrometer during the receive phase, which measures the induced signals resulting from nuclear spin. RF shielding of the NMR probe is usually accomplished either with an electrically conducting screened room completely enclosing the magnet, a complete

conducting screen around the NMR coils restricted to the bore of the magnet, or some room/magnet bore combination. All cables entering the shield must be grounded to it and all conducting cables not directly used for NMR transmission or reception must pass through an RF filter at the shield with RF attenuation factors comparable to that of the shield. Since our spectrometer was installed with minimal cost as the main objective, we did not have the financial resources to spend on a RF-tight shielding room, but instead we had to resort to insulating the surface coil by a conducting screen restricted to the magnet. This conducting screen is in the form of electrically conductive end caps and a copper cylinder fitted horizontally inside the bore of the magnet, with the cable connecting the surface coil probe and the preamplifier grounded to the cylinder. When an experiment is conducted on human subjects, one end cap has to be removed and the patient's exercised upper arm is grounded by means of a copper foil connected to the conductive cylinder. Of course, this setup is by no means perfect and is also the main reason that the author has to resort to the resonator type of surface coil to improve the overall signal-to-noise, by further isolating the surface coil through an inductive coupling mechanism.

The RF coils can be either a single coil serving as both transmitter and receiver, or two separate coils that are electrically orthogonal. The latter configuration has the advantage of reduced pulse breakthrough into the receiver during the pulse and has an improved S/N advantage. In both cases, all coils generate RF fields orthogonal to the direction of the main magnetic field. The NMR coils are tuned to the desired frequency of operation with the aid of a capacitor, and the resonance frequency (f_r) of the circuit is given by:

$$f_r = 1/[2\pi(LC)^{1/2}] \qquad (3\text{-}1)$$

where L (inductance) = $(N^2\mu A_L)/h$ and C (capacitance) = $(\varepsilon A_C)/d$, N represents the number of turns in the coil, μ the permeability of the sample (i.e. μ measures

the ease with which magnetic flux lines can be established in the sample), A_L the cross-sectional area of the coil, h the height of the coil, ε the permittivity of the dielectric (i.e. ε is a measure of how easily the dielectric will permit the establishment of electric flux lines), A_C the area of the capacitor plate, d is the distance between the plate.

The NMR signal from the receiver coil is preamplified in a low-noise preamplifier that is protected from the high-power RF either by active gating or by passive filtering during the pulse. Feedback circuity in the preamplifier can be used to damp the ring down caused by high Q coils (3-4). Following preamplification the NMR signal is further amplified in the receiver, phase sensitive detected (usually quadrature detection), filtered, and then converted to digital signals for averaging and computer processing.

Spectral processing is the procedure by which raw NMR data is transformed into useful results and quantitative measurements. Processing typically involves four stages: (a) Pre-processing: DC voltage offsets and initial RF spikes are removed from data, followed by zero filling to improve spectral resolution, and exponential multiplication to enhance signal-to-noise ratio; (b) Fourier transformation to convert signal from time domain to frequency domain; (c) Phase corrections are applied to spectra to transform all resonances into the absorption mode; (d) Quantitative spectral measurement of chemical shifts and relative metabolite concentrations by either directly measuring peak height, by integrating the area under each resonance, or by first fitting each resonance to Lorentzian or Gaussian shapes which are then integrated.

There were two main obstacles relating to human studies. The first is that the region of interest has to fit within the bore of the magnet. The second problem is associated with signal detection. In conventional NMR experiments, the signals are obtained by placing the sample within a radio frequency coil that

transmits radiation into the sample and detects the free induction decay. For studies of human, however, it is neither very practical nor particularly useful to surround the subject by the coil; it is rather useless to obtain a composite signal originating from all of the various heterogeneous tissues within the human body. Clearly it is necessary to devise a method of localization that enables signals to be detected from a specific, well-defined region within the human body. Many such methods have been developed during the last ten years. All localization techniques fall into three general categories: those that localize by means of static spatial gradients in the main magnetic field, as in topical nuclear magnetic resonance method (TNMR or TMR); those that use pulsed or time-dependent spatial gradients, as exemplified by the depth-resolved surface coil spectroscopy (DRESS), slice interleaved DRESS (SLIT DRESS), imaged-selected *in vivo* spectroscopy (ISIS), outer volume suppressed ISIS (OSIRIS), volume selective excitation (VSE), spatially resolved spectroscopy (SPARS), discrete isolation from gradient-governed elimination of resonances (DIGGER), spatial and chemical-shift-encoded excitation (SPACE), and one to three dimensional (1-3D) phase/time encoding gradient or spectroscopic imaging techniques (2-4 DFT methods); and those that achieve localization using only B_1 magnetic gradients in the radio frequency excitation or detection fields, as in simple surface coil acquisition and rotating frame zeugmatography approach (RFZ). A detailed account of all the localization techniques is beyond the scope of this Thesis, but we will outline the advantages and disadvantages of selected techniques and come to a conclusion as to what is the best approach for clinical studies of muscle fatigue in our laboratory.

3.3 Localization Techniques

The first method of localization is topical nuclear magnetic resonance (5). The magnetic field is profiled in such a way that it is very homogeneous over a central, approximately spherical volume, but elsewhere is very inhomogeneous. As a result, narrow signals are observed only from the central region; the signals from outside this region are very broad and make very little effective contribution to the final spectrum. TMR has the advantage of localizing on internal organs without the need of surgery. Although the combination of TMR and surface coils does improve spatial localization, the sensitive volume is still quite poorly defined, and cannot be easily repositioned within the subject. Besides, the very high continuous power requirements of the TMR profiling coils is also another major drawback.

The DRESS method (6) and its derivative SLIT DRESS (7) utilize either a conventional volume RF coil or a large surface coil for providing a uniform RF excitation field over the sensitive volume and a smaller diameter surface coil which is used for detection only. The selective excitation pulse is applied during the presence of a magnetic field gradient pulse whose direction is coaxial with the surface coil. The combination of narrow-bandwidth selective excitation pulse and the applied field gradient excites a flat plane of nuclei parallel to the plane of the surface coil. The thickness and location of the selected plane is precisely defined by the RF excitation frequency and bandwidth and the magnitude of the gradient field. While the DRESS and SLIT DRESS approaches require only single selective $\pi/2$ excitation pulses, they suffer the disadvantage that localization in two of the dimensions is relatively poor, uncontrolled, and depth-dependent, it being defined by the broad sensitivity profile of a surface detection coil (8).

The alternative VSE method (9) and it derivatives SPARS (10), DIGGER (11), and SPACE (12) are based upon a combination of selective and nonselective RF pulses, such that nuclear magnetization is dephased in the transversal plane, except for the volume of interest where it is retained along the magnetic field direction. A subsequent 90^0 observation pulse then generates a signal arising from this volume of interest. The SPARS technique is not suitable for the examination of NMR signals with a short T_2. The VSE sequence and its modifications do provide gradient-controlled localization in all three dimensions, but can suffer from a loss of spatial discrimination due to T_1 relaxation between the preparation of the localized volume and the readout of the signal with a nonselective $\pi/2$ NMR pulse. For this reason, it is often necessary to cycle the VSE sequence (10,13). In addition, high-power RF is required to generate nonselective pulses, which must produce accurate nutation angles over the whole sample, in the presence of magnetic field gradients.

In ISIS (14) the method relies on the principle of selective inversion of the spin population. The width of the selected volume along any axis may be varied either by adjustment of the selective RF pulse length, or by adjustment of the size of the respective field gradient. The achievement of complete three-dimensional gradient-controlled localization necessitates the application of an eight-cycle sequence and the addition and subtraction of signal contributions that are orders of magnitude larger than those emanating from the selected voxel. This technique is thus highly susceptible to artifacts produced by irregular physiological motions that may occur during the sequence cycle.

The OSIRIS method (15) offers an improvement by the introduction of noise-modulated selective prepulses to achieve suppression of signals from volume before applying ISIS. Such prepulses have the dual advantage of modest RF power requirements and insensitivity to RF power level. Thus, while

retaining the advantages of the ISIS technique (no T_2 weighting, image-defined volume positioning, good volume definition due to the use of complex hyperbolic secant inversion pulses, and applicability using surface coils), OSIRIS minimizes the subtraction errors and enhances the signal-to-noise ratio by reducing the dynamic range. The technique can be combined readily with solvent suppression or editing sequences to enable the *in vivo* detection of the proton spectra of metabolites.

Another approach, proposed by Bottomley and Hardy (8), resulted in the point-resolved rotating gradient surface coil spectroscopy (PROGRESS) sequence. The two-dimensional spatially selective NMR inversion pulses, called ρ pulses for rotating pulses, consist of single π NMR pulses that are applied in the presence of two orthogonal time-dependent magnetic field gradients such that the net applied gradient field reorients through two dimensions within the duration of the NMR pulse. For complete three-dimensional localized P-31 NMR spectroscopy applications, it is necessary to use a surface coil to further attenuate the integrated contribution of Z magnetization from the central lobe and to use a slice-selective π/2 DRESS pulse for localization in the third dimension. Advantages of the PROGRESS technique are a fourfold reduction in the total sequence cycle time and a reduction by several orders of magnitude of the effect of any localization artifacts since only the magnetization from a small fraction of the sample is ever in the transverse plane. However, the principal disadvantage of the PROGRESS technique is the need for surface-coil attenuation of ρ-pulse side lobes. Because of the use of π inversion pulses, saturation effect is also a problem during signal-averaging and interleaving volume excitations.

Chemical-shift selective (CHESS) imaging techniques (16-17) including three- or four-dimensional Fourier imaging use pulsed phase-encoding gradient pulses for spatial resolution and acquire the signal without any gradient to retain

spectral information (18); whereas as multipoint echo-time-encoding (19) and its derivative spectroscopic fast low angle shot (SPLASH) imaging (20) use a stepwise increase of the time integral of the read-gradient defocusing pulse. The magnetic field gradients which in the standard configuration of superconducting magnets generate sufficiently large eddy currents upon gradient removal to temporarily degrade the field homogeneity. The field homogeneity is recovered after a time delay of approximately 10 ms; therefore most chemical-shift imaging experiments utilize a spin echo to refocus magnetization, and consequently the observed spectrum has a T_2 weighting factor for each resonance. This is one of the reasons why the implementation of high-resolution spectroscopy by most chemical-shift imaging methods is difficult and time consuming.

Another approach employed in spectral spatial localization has been the utilization of the inhomogeneous B_1 field generated by a surface coil probe. Depth pulses (21-23) and the Fourier series window (FSW) modification (24-27) of the rotating frame zeugmatography experiment (28) are among such techniques. With either method, there are at least three problems: the sensitivity loss accompanying application of variable RF pulse lengths during a sequence of addition and subtraction experiments, the presence of high flux signals, and the localization of spectra in regions defined by the curved B_1 isocontours which extend beyond the tissue or organ of interest.

However, an alternating method may easily be used if the region of interest is restricted to the skeletal muscle on the extremity. This method involves the use of an unusual type of radio frequency coil, which has been termed a surface coil (29). In its simplest form, it consisted of a flat, circular loop of wire containing one or more turns. If such a coil is placed adjacent to a sample, it will, under normal circumstances, detect signal from an approximately disk-shaped region of sample immediately in front of the coil, of radius and thickness

approximately equal to the radius of the coil. A surface coil therefore provides a very simple method of localizing on a selected region that is close to the surface of a sample. Besides, for P-31 NMR applications, localization techniques which involve Hahn spin-echoes are not suitable because the spin-spin relaxation times of the adenosine triphosphate (ATP) P-31 NMR resonances appear to be about 10 ms. Spectra acquired from echoes delayed beyond this will thus exhibit vanishingly small ATP resonances. Not only is ATP an important metabolite, its presence in P-31 spectra provides a valuable frame of reference for identifying the other resonances and measuring metabolite ratios. It is also desirable that spatial localization be accomplished with a minimum of excitation pulses. Schemes which require the addition and subtraction of signals from large numbers of excitation pulses are highly susceptible to instrumental instabilities and variations arising from physiological motions.

Finally, there is a valid reason for using minimal or no localization technique for many diseases. These include global or relatively unlocalized disorders such as muscular metabolic diseases of the limbs, global trauma in the brain, and large tumors that occupy all or most of the sensitive volume of an NMR surface coil. The substantial sensitivity advantage of acquiring spectra from whole volumes compared with much smaller localized volumes could easily outweigh any value in the spatial distribution of spectral information in such disorders, rendering sophisticated localization techniques unnecessary. In other cases, methods that simply eliminate surface tissue contributions may be all that is required.

3.4 Surface Coils

The currently accepted surface coil is the workhorse of remote sensing NMR (in which the sample is not contained within the NMR coil as in traditional NMR). It is a planar coil consisting of one or more circular turns of wire. Common variations include spiral winding with the wire still in one plane, noncircular turns, and winding combinations slightly out of the plane.

Unlike conventional radiofrequency coils which generate relatively uniform B_1 fields across the sample, surface coil generated B_1 fields are inhomogeneous and are strongly dependent on spatial coordinates. The B_1 field strength decreases with increasing axial distance where the B_1 magnitude (the component of magnetization produced by the RF pulse which is perpendicular to the direction of the B_0 field) is governed by the strength of the RF pulse and the surface coil geometry. For a single-turn flat circular coil orientated as in Figure 3-1, the magnetic field generated at any point q by unit current flowing in the coil is given by the Smythe's equations (30), which are modified versions of the Biot-Savard law:

$$B_\rho = \mu\xi/\{2\pi\rho[(a+\rho)^2+x^2]^{1/2}\{-K+[E(a^2+\rho^2+x^2)/(a-\rho)^2+x^2]\}\} \quad (3\text{-}2)$$

$$B_a = \mu/\{2\pi[(a+\rho)^2+x^2]^{1/2}\{-K+[E(a^2-\rho^2-x^2)/(a-\rho)^2+x^2]\}\} \quad (3\text{-}3)$$

where B_a and B_ρ are the axial (x) and radial (ρ) components of the field at point q, a is the coil radius, μ is the permeability of the sample about the coil and K and E are complete elliptic integrals of the first and second kind.

From Figure 3-1, the direction of B_a is always perpendicular to that of the static field B_0, while the perpendicular component of B_ρ, $(B_\rho)_{xy}$, is given by:

$$(B_\rho)_{xy} = B_\rho \sin\theta \quad (3\text{-}4)$$

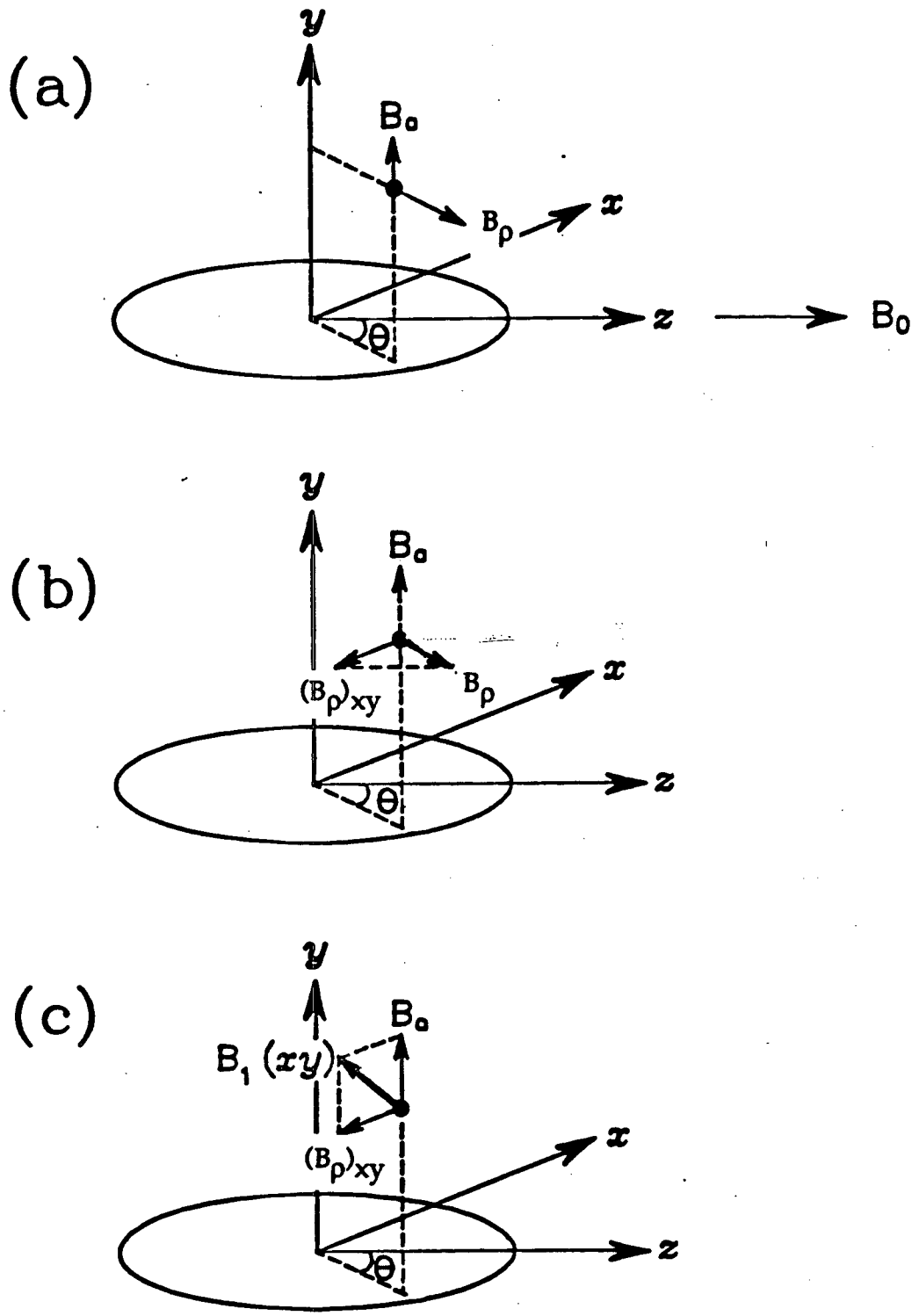

Figure 3-1 Schematic representation of a single turn surface coil showing RF magnetic field component vectors.

where θ is the angle between the directions of B_p and B_0. The magnetic field $(B_1)_{xy}$ generated at any point *q* therefore depends on θ and is given by:

$$(B_1)_{xy} = [B_a^2 + (B_p)_{xy}^2]^{1/2} \qquad (3\text{-}5)$$

$(B_1)_{xy}$ is localized in a volume about the centre of the coil roughly defined by the coil radius. It should therefore be possible to observe high resolution NMR signals from selected regions adjacent to the surface of the samples. As Hoult and Richards have suggested (31) and later confirmed by Ackerman *et. al.*(29), variation in the phase of $(B_1)_{xy}$ should not affect this type of single coil experiment because phase changes induced at transmission are mirrored at reception, and thus cancel.

Surface coils are important tools for in-vivo NMR spectroscopy as well as for imaging. The impetus for using surface coils stems from their two potential advantages: (a) improved signal-to-noise (S/N) ratio; (b) controlled region of sensitivity. In general, the use of surface coils gives a considerable improvement in spatial resolution, made possible by the increase in the signal-to-noise ratio. This increase results from the closeness of the surface coil to the body (increasing the signal strength because of a higher filling factor), and from the localized sensitivity-characteristic of the surface coil (i.e. a much smaller reception field), which reduces the detected Johnson noise contribution from adjacent regions. (RF noise arises from Brownian movement of electrolytes and other charge carriers in the body.)

Methods to increase the coil sensitivity are of critical importance in the future development of *in-vivo* P-31 NMR. The quality factor, Q, of a RF coil is a function of the coil's inductance, L, and intrinsic resistance, R:

$$Q = (L\omega)/R \qquad (3\text{-}6)$$

where ω is the resonant frequency of the circuit. Since the signal intensity varies as $Q^{1/2}$ (32-33), and Q in turn depends on coil geometry, our efforts have been

to improve P-31 NMR sensitivity through improved coil geometry, thereby achieving a higher value of Q.

The radiofrequency magnetic field B_1 interacts with the sample by two mechanisms: first, by inducing signals from the nuclei of interest within the sample; and second, by giving rise to resistive losses within the sample. The field distribution of B_1 is critical, and homogeneous fields are desired. A rapid decrease in the magnitude of B_1 outside the volume of interest is desired for accurate localization to tissue of interest.

The second mechanism of interaction between the magnetic field B_1 and the sample is a result of the conductivity of the sample. The alternating field B_1 from the RF coil induces eddy currents that result in resistive losses within the sample. Hoult and Lauterbur (34) expressed the power dissipated in a spherical sample as:

$$W = [\pi(2\pi f_0)B_1^2 b^5]/[15\rho] \qquad (3\text{-}7)$$

where ρ is the resistivity of the medium, and b is the radius of the sphere. Alternatively, the power dissipation can be expressed as an effective resistance R_m in series with the receiving coil *(note: $W = R_m/2$)*, and for a spherical sample placed inside a solenoidal coil of radius a, length $2g$, and n (>>1) turns

$$R_m = [\pi\omega_0^2\mu_0^2 n^2 b^5\sigma]/[30(a^2+g^2)] \qquad (3\text{-}8)$$

The quantity ω_0 is the resonant frequency, μ_0 is the permeability of free space, b is the sample radius, and σ is the specific conductivity of the sample. In case of a cylindrical sample of length $2g$, and radius b, it may also be shown that:

$$R_m = [\pi\omega_0^2\mu_0^2 n^2 b^5 g\sigma]/[16(a^2+g^2)] \qquad (3\text{-}9)$$

The power dissipated lowers the Q of the coil and decreases the overall signal-to-noise ratio.

The electric lines of force interact with the sample to cause a resonant frequency shift and "dielectric losses". These losses arise from the dielectric

properties of mobile molecules and from charge transport in the ionic and conductive medium. The losses (ε") are proportional to the conductivity of the medium (35):

$$\varepsilon'' = \varepsilon''_{dielectric} + [\sigma/(720\pi^2 f_0)] \quad (3\text{-}10)$$

where $\varepsilon''_{dielectric}$ is the imaginary part of the dielectric constant that is associated with loss in the nonconducting medium (i.e. pure H_2O), σ is the tissue conductivity (mho cm^{-1}), and f_0 the frequency. The electric lines of force pass through the sample because they are associated with the distributed capacitance of the coil. This capacitance exists for all coils, but its distribution is dependent upon coil geometry (36). Alternatively, the equivalent series resistance R_e resulting from dielectric losses can be expressed as:

$$R_e = \tau\omega_0{}^3 L^2 C_d \quad (3\text{-}11)$$

where τ is the loss factor of the sample, L is the coil inductance, and C_d is the distributed capacitance.

Thus, there are three main types of losses which could contribute noise, namely, the resistance of the coil, the magnetically induced eddy current losses in the sample, and the dielectric or conductive losses due to stray electric fields in the sample. Since the sample losses due to inductive and dielectric effects can be expressed as R_m and R_e in series with the coil, then effective Q($Q_{effective}$) or loaded Q (Q_L), the Q of the probe circuit in the presence of the sample, is:

$$Q_L = (\omega_0 L)/(R_{coil}+R_{magnetic}+R_{electric}) \quad (3\text{-}12)$$

or alternatively the effective Q of a coil can be written as following:

$$1/Q_L = (1/Q_{coil}) + (1/Q_{magnetic}) + (1/Q_{electric}) \quad (3\text{-}13)$$

where Q_{coil} is the energy lost due to Joulean heating of the coil, $Q_{magnetic}$ is the energy lost resulting from magnetic interactions in sample, and $Q_{electric}$ is the energy lost because of electric interactions in sample. Improved coil design can reduce Q_{coil} and $Q_{electric}$; whereas, introduction of RF shield can prevent

electric lines of force associated with distributed capacitance from passing through the sample, and therefore reduces the dielectric losses.

An estimate of the electric field penetration into the sample can be obtained by measuring the shift of the surface coil resonance frequency (Δf_0) upon introduction of the sample (37-38). The differing dielectric properties of the sample compared to air alter the distributed capacitance of the coil and hence its resonance frequency according to equation 3-1.

Earlier work in our laboratory (1), using copper wire surfaces coils with and without silverplating only showed marginal improvement in the Q factor and in the signal-to-noise ratio (Table 3-1). Since it was well known that radiofrequency travelled over the surface of any conductor, one way to increase the Q factor was to reduce the resistance in the RF coil, so we initially decided to construct flat surface coils out of copper tubing (Figure 3-2). The different configurations that we examined included circular, square, and rectangular in shape of various diameters. Table 3-1 provided a survey of our results revealing borderline improvement in signal-to-noise ratio. Subsequently, during the time of our renewal search for a better surface coil configuration, Hyde *et. al.* (38) published a paper about the use of resonators for *in vivo* P-31 NMR at 1.5 Tesla.

3.5 Resonator Surface Coils

Loop-gap resonator (LGR) (4.0 cm. in diameter, 5.0 cm. in height) designed in accordance with the prinicples developed for electron spin resonance (ESR) spectroscopy (39-40) but scaled to dimensions for NMR of P-31 at 1.89 T (32.5 MHz) were fabricated from copper foil (0.25 mm thick, 101 grade, OFHC) and formed on a Plexiglas coil former with two flaps which project normally from the circumference of the cylinder. 0.7 mm. thick sheet of teflon or

Table 3-1 Evaluation of Different Coil Configurations (H-1 NMRS, 80 MHz)

Coil Configuration	90° Pulse[a]	Max. S/N Ratio[b]
Loop Gap Generator type circular resonator surface coil (4.5 cm in diameter, 5 cm in length)	30 μSec	2280 +/- 53
Single turn circular surface coil (8.5 cm in diameter, copper tubing)	60 μSec	454 +/- 31
Single turn rectangular surface coil (8.75 cm x 7 cm, copper tubing)	70 μSec	277 +/- 8
Single turn square surface coil (4.5 cm each size, copper tubing)	35 μSec	621 +/- 14
Single turn circular surface coil (4 cm in diameter, copper tubing)	50 μSec	615 +/- 14
Double turn circular surface coil (2 cm in diameter, copper tubing)	20 μSec	697 +/- 51
Single turn circular surface coil[c] (2 cm in diameter, silver plated copper wire)	19 μSec	391 +/- 29
Double turn circular surface coil[c] (2 cm in diameter, silver plated copper wire)	22 μSec	462 +/- 35
0.9 double turn circular surface[c] (2 cm in diameter, silver plated copper wire)	11 μSec	846 +/- 67

a. Measurements were made with spherical phantom (1.2 cm in diameter) filled with copper sulfate solution located at the centre of all surface coils used.

b. Measurements were made with a beaker (16.5 cm in diameter, 6 cm in height) filled with copper sulfate solution situated at the top of all surface coils used.

c. Data taken from J. Schachter's M. Sc. Thesis, UBC, 1985.

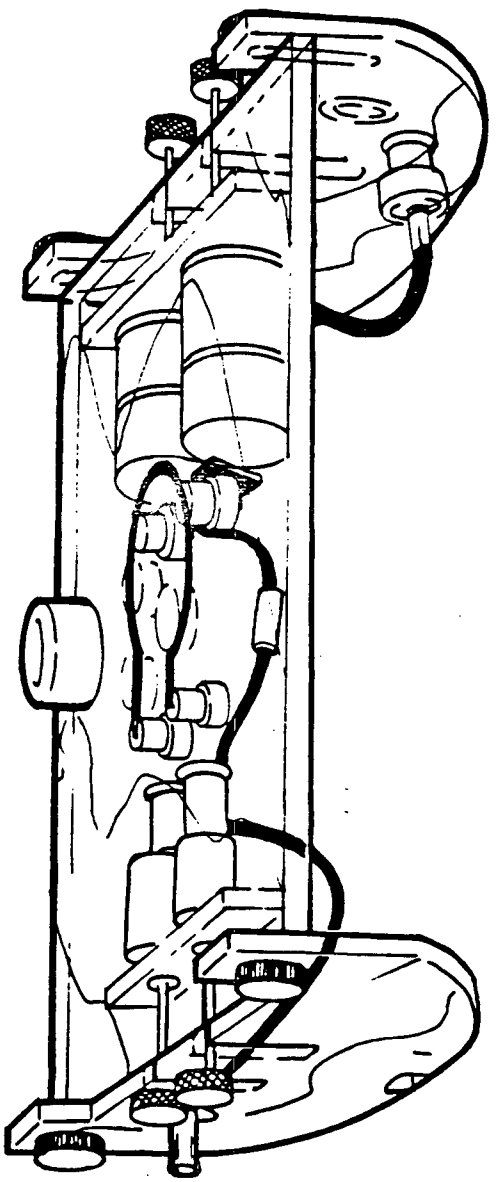

Figure 3-2 Schematic diagram (side view) of the NMR single turn circular copper tubing surface coil probe. The coil diameter is 4 cm., and the resonant frequency is 32.5 MHz. Copper tubing, with a thickness of 0.5 mm., is 4 mm. in diameter.

polyethylene dielectric films were inserted into the gap to form the capacitance, and the structure was secured by sandwiching the copper foils and dielectric between two Plexiglas plates. The capacitance was varied by fine adjustment of the distance across the dielectric with the aid of Teflon screws. In addition, the copper foils were made slightly longer than necessary and the extra length was bent sideway to provide the extra capacitance needed for tuning. Such construction methodology completely eliminated the need for high-cost commercial capacitors and resulted in easily fabricated and low-cost NMR surface coil probe. With inductive coupling, the only interaction between the transmission line and the coil was through space, with no direct connection by wires. The coupling efficiency is altered by changing the distance between the coupling loop and the resonator. Maximum power transfer occurs when the resonator is both tuned and matched.

The higher Q of the loop-gap resonance is attributed to (a) lower intrinsic resistance of the loop, (b) higher transmit and receive efficiency, and (c) elimination of losses in the transmission line that connects the surface coil and its resonating capacitor network. Besides, the resonator coil is intrinsically free-floating, thereby reducing differences in electric potential between the coil and the ground, resulting in higher $Q_{electric}$. In addition, coils made with copper foil rather than wire have a lower inductance and hence must have higher capacity to achieve resonance. It follows that voltage across the capacitors tends to be lower, resulting in an additional decrease in dielectric losses. The presence of infinite numbers of lumped capacitors within the spiral resonance surface coil further helps to lower the dielectric losses in the patient considerably.

From the preceding discussion it is evident that the resonator surface coil is very much superior, and this has prompted the current research interest in alternative surface coil designs. Figure 3-3 was the result of such initiative and

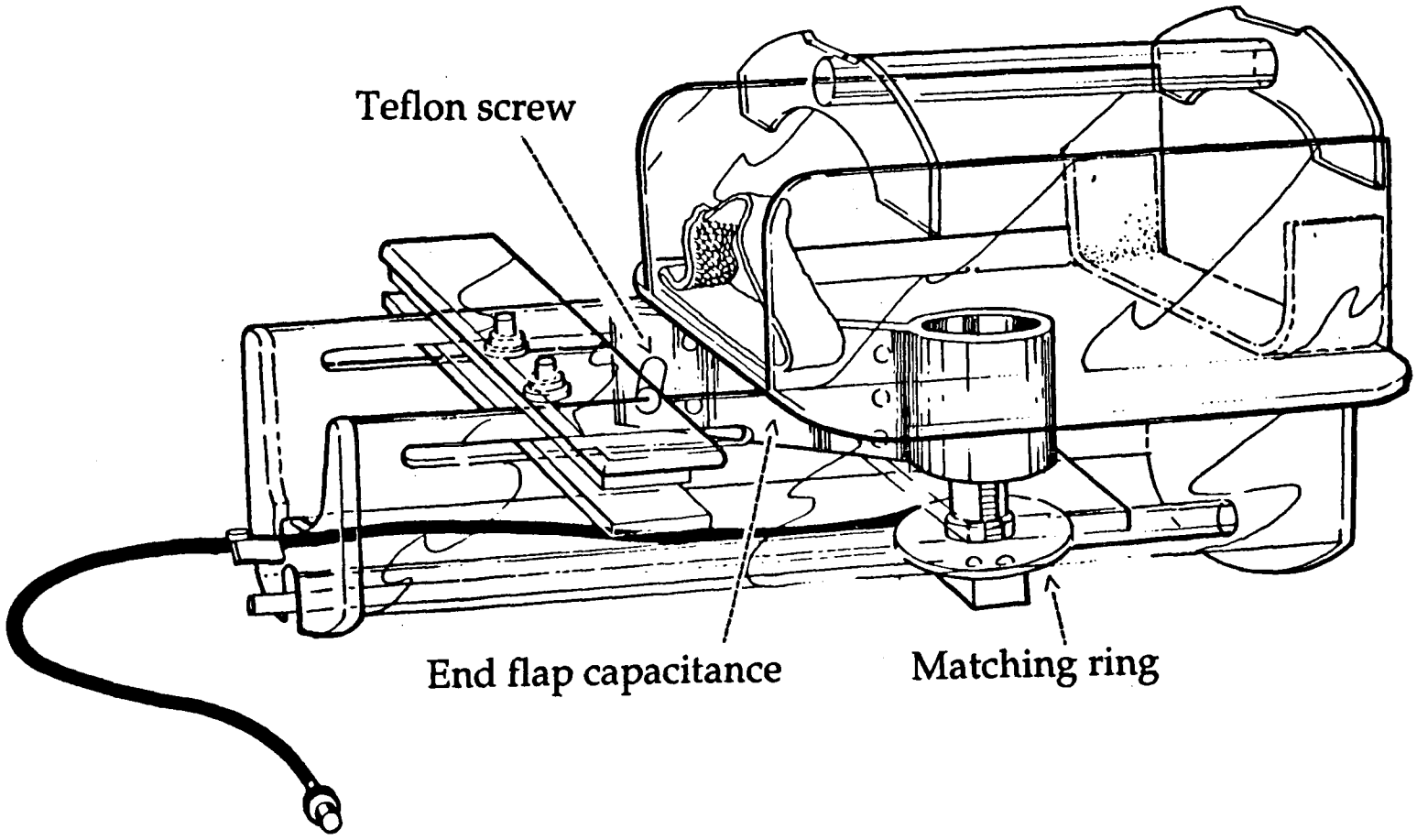

Figure 3-3 Schematic diagram (side view) of the NMR Loop-gap resonantor surface coil probe. The coil is 4 cm. in diameter and 5 cm. in length, and the resonant frequency is 32.5 MHz. The loop-gap resonator was fabricated from copper foil (0.25 mm. thick) and formed on a Plexiglas coil former with two flaps (12 cm. in length) which project normally from the circumference of the cylinder. 0.7 mm. thick sheet of teflon was inserted into the gap to form the capacitance, and the structure was secured by sandwiching the copper foils and the dielectric between two Plexiglas plates. The capacitance was varied by fine adjustment of the distance across the dielectric with the aid of a Teflon screw. In addition, the copper foils were made slightly longer than necessary and the extra length was bent sideway to provide the extra capacitance needed for tuning.

our result (Table 3-1) indicated a four fold increase in H-1 proton signal-to-noise ratio. A subsequent effort to extend this idea to P-31 however was not trivial. Equation 3-1 dictated that if the resonant frequency was to reduce from 80 MHz. to 32.5 MHz., the product of inductance and capacitance had to be increased by at least four times. Thus, in order to have our 4.0 cm. resonator surface coil resonated at 32.5 Hz (i.e. 1.89 Tesla), we had to make the capacitor end flap 12 cm. in length. Most of our preliminary clinical studies presented in the next chapter of this Thesis were carried out using the loop-gap resonator surface coil. During that one and half years, we gradually came to realize that although the loop-gap resonator surface coil dramatically improved the signal-to-noise of our spectrometer, because of its long end flap it was unstable during RF pulsing. The tuning and matching of the coil also tended to be temperature sensitive, i.e. the coil would required 5 to 10 minutes of continuous pulsing to warm up and tuning had to be readjusted afterwards.

As part of our continuous efforts to improve our clinical protocol, the spiral resonator surface coil (Figures 3-4 and 3-5) was constructed. Instead of having long capacitor end flap, the copper foil was wrapped around a Plexiglas coil former and then around itself. Successive layers of copper foil were separated by teflon dielectric films (thickness. 0.03 mm). The RF transmitter/receiver is inductively coupled via a copper ring to the spiral resonator, and fine tuning of the surface coil is achieved by using a second unattached copper ring located on the same side of the probe. The maximum coupling is accomplished by moving the two copper rings in or out the magnetic flux lines of the spiral resonator. This movement of the tuning and matching rings with respect to the surface coil alters the resonance frequency by changing the total effective inductance of the spiral resonator. The coil was housed in a gantry which allowed it to be moved in 3 dimensions to provide an iteritive

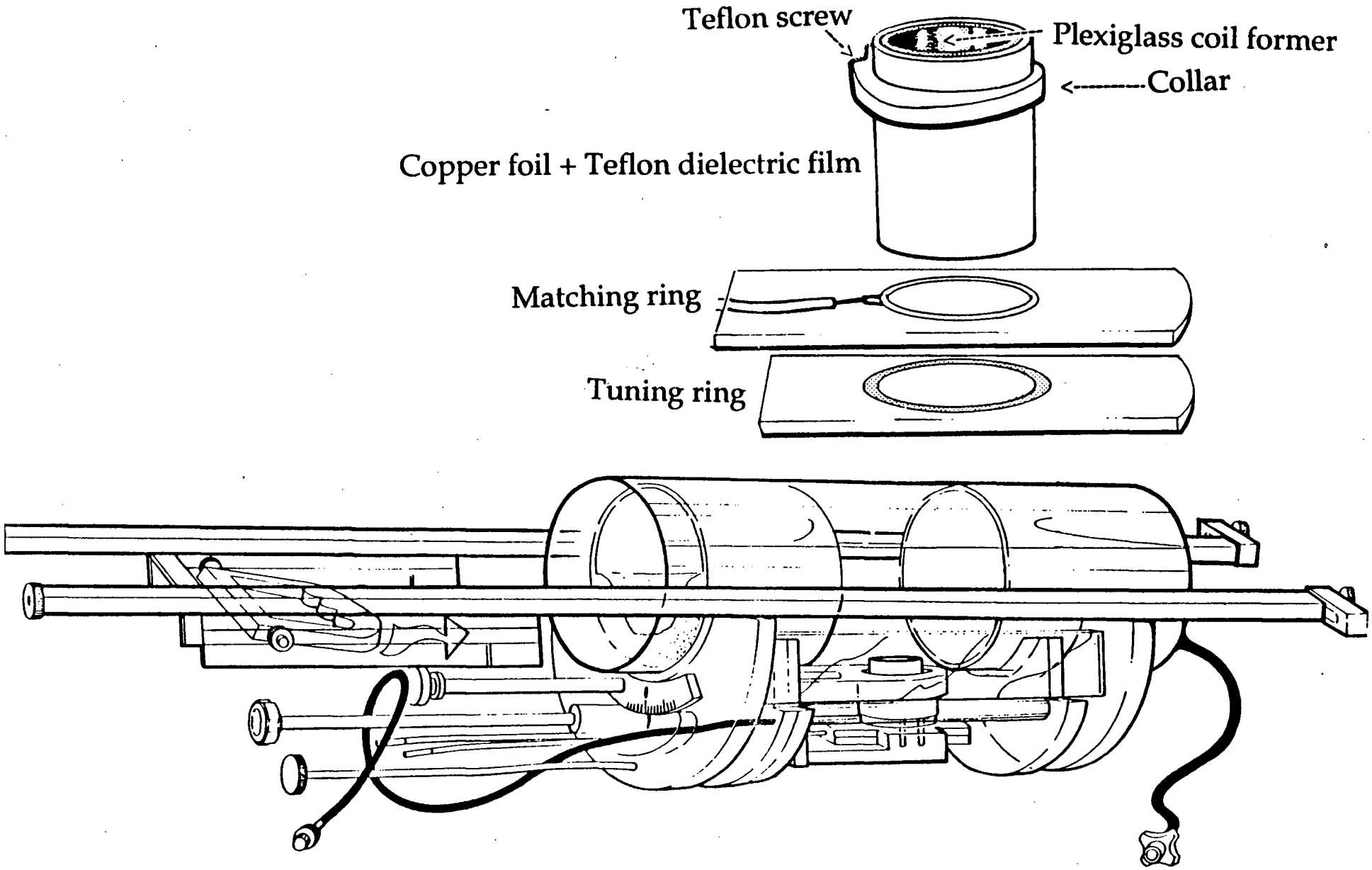

Figure 3-4 Schematic diagram (side view) of the NMR spiral resonator surface coil probe. The coil diameter is 4 cm., and the resonant frequency is 32.5 MHz. Copper foil (thickness:0.05 mm., length:32.5 cm., width:6 cm.) was wrapped around a Plexiglas coil former and then around itself; successive layers of copper foil were separated by teflon dielectric films (thickness:0.03 mm.). The RF transmitter/receiver is inductively coupled via a copper ring to the spiral resonator; coarse tuning of the coil can be made by adjusting the teflon screw located at the collar of the cylinder, and fine tuning is achieved by using a second unattached copper ring located on the same side of the coil.

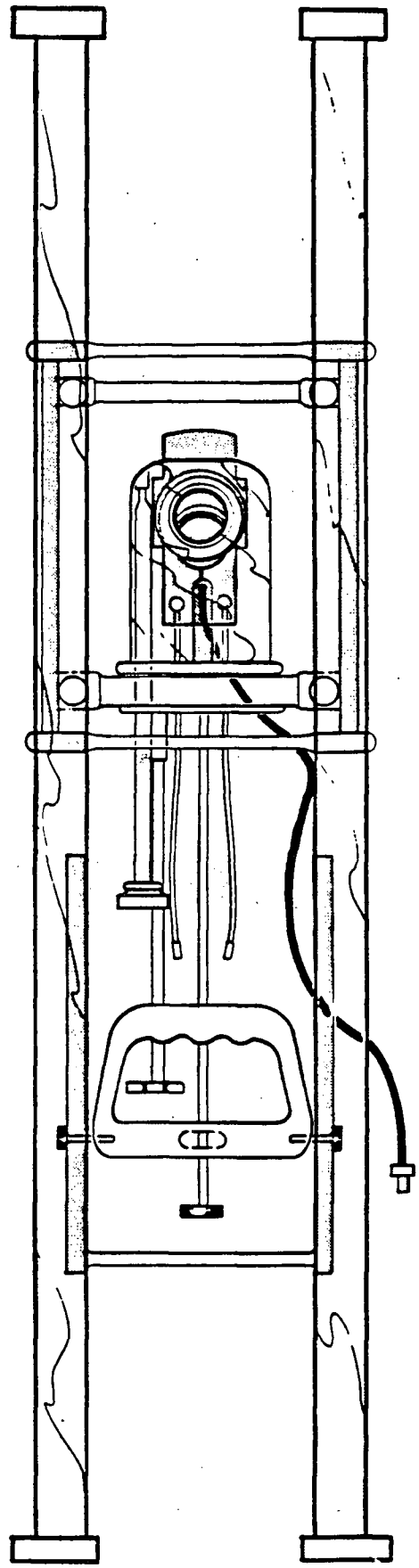

Figure 3-5 Schematic diagram (bird view) of the NMR spiral resonator surface coil probe.

search for the region of maximal biochemical involvement. Because of signal-to-noise constraint, we were limited to use a somewhat larger surface coil (4.0 cm in diameter) without the benefit of any localization techniques. However, the "roving" spiral resonator surface coil helped to alleviate some of our limitations. During a dynamic study of muscle fatigue, if we were sampling both the involved and uninvolved muscle fibers, the P*i* peak would tend to increase in width instead of height. The coil housed in the moving gantry could then be moved to sample at a different location without interfering with the patient's progress.

Tuning was initially performed with the coil at the anatomic region of interest of the first subject. Thereafter, the tuning was checked on each subject but was found to have changed so little when applied to the same region of a different subject that individual tuning proving unnecessary.

3.6 Experimental Evaluation of Surface Coil Probe Designs

Three P-31 NMR surface coil designs, the single turn circular copper tubing surface coil, the loop-gap resonator surface coil, and the spiral resonator surface coil were evaluated for their performance. All the designs were constructed with identical diameter (4.0 cm.) to enable direct comparison. The mechanical construction and electronic details of the surface coils were carried out by C. Neale and T. Markus, respectively, of the UBC Chemistry Department.

The surface coils constructed were experimentally evaluated by measuring several parameters which are directly related to the design of the probe. They are, the surface coil Q factor (both unloaded and loaded with a human arm), the effect of a human arm on the surface coil resonance frequency, the tuning range of the three designs. In addition, the signal-to-noise ratio and

the 90^0 pulse width for a 1.2 cm. in diameter spherical phantom filled with 85% concentrated phosphorous acid located at the top centre of surface coil were also determined.

The signal-to-noise ratios were determined using standard Nicolet software (41) assuming a true Lorentzian line shape. The surface coil Q factors, tuning ranges, and frequency shift upon introduction of a human arm were measured on the bench with the coil tuned and matched approximately to 32.5 MHz. The experimental setup (42) used was that available in the UBC Chemistry Department Electronic Shop. This included a signal generator (Wavetek 3001), a sweep generator (Wavetek 2002A), an RF reflexion bridge, an RF detector and an oscilloscope. The Q factors reported for each surface coil are the average values of several independent measurements, taken as the ratio of the resonance frequency to the full-width at half-power point (70% of the voltage maximum) of the surface coil resonance.

The experimental data obtained for the three surface coil designs are summarized in Table 3-2. The 90^0 pulse is almost the same among the three different designs; whereas the signal-to-noise ratio of the two resonator surface coils is twice that of the single turn circular copper tubing surface coil. On comparison of the Q values, the loop-gap resonator affords the highest loaded and unloaded Q. However, the inductively coupled spiral resonator surface coil also shows a significant improvement over the capacitively coupled single turn circular copper tubing surface coil. Presumably, because of the compactness of the spiral configuration, the spiral design has a higher coil resistance (R_{coil}), which results in slightly lower Q than its loop-gap resonator counterpart. The percentage reduction in Q upon loading is the highest in single turn circular copper tubing surface coil (77%), and the lowest in the spiral resonator surface coil (27%). Thus, the spiral design suffers the smallest inductive loss.

Table 3-2 Evalution of Different Coil Configurations (P-31 NMRS)

Coil diameter = 4.0 cm
Resonant frequency = 32.5 MHz

Coil Configuration	90^{o} pulse	S/N Ratio[a]	$Q_{unloaded}$	Q_{arm}	Tuning Range	Frequency Shift Upon Loading
Single turn circular copper tubing surface coil	18.8 µsec	12.2	325	76(77%↓)	+/- 1000 KHz	230 KHz
Loop-gap resonator surface coil	20 µsec	26.2	818	468(43%↓)	+/- 850 KHz	15 KHz
Spiral resonator surface coil	20 µsec	23.2	540	392(27%↓)	+/- 250 KHz	5 KHz

a. Measurements of S/N ratio and 90^{o} pulse were made with spherical phantom (1.2 cm in diameter) filled with 85% concentrated phosphorous acid located at the top centre of all surface coils used.

Since Δf_0 values are an indication of the dielectric losses, Table 3-2 shows that the maximum dielectric losses are associated with the single turn circular copper tubing surface coil. This is to be expected with a capacitively coupled coil configuration. Comparative Δf_0 values show the superior performance of the spiral resonator surface coil with regard to the dielectric losses. In fact, the tuning of the spiral design is sample independent (i.e. the tuning stays the same over weeks, and it does not need readjustment even if the sample is changed from a human arm to a nonconductive organic sample).

The above comparative results of different surface coils designs reveal the difficulty in optimizing all the desirable features with a single design. Thus compromises are essential. The spiral resonator surface coil, although it does not have the highest Q factor, experienced the smallest inductive and dielectric losses upon the introduction of biological samples, and provides the best overall performance.

3.7 Special Features of Spiral Resonator Surface Coil

Phantom studies were carried out to show the B_1 magnetic field gradient profile as well as to determine the contribution to the overall NMR signal from sample located at different distances away from the coil centre. The B_1 profile was obtained by placing a hollow rectangular PVC block (Figure 3-6a) filled with concentrated phosphoric acid on top of the resonator surface coil. Small plugs were inserted at regular intervals into the hollow PVC block to enable quantitative measurement of distance. The image (Figure 3-7) was produced using the 2-D spin warp imaging technique (43). The contribution study used a single vial of P*i*, PCr, and ATP mixture fitted into a rectangular Teflon block with drilled holes as pictured in Figure 3-6b.

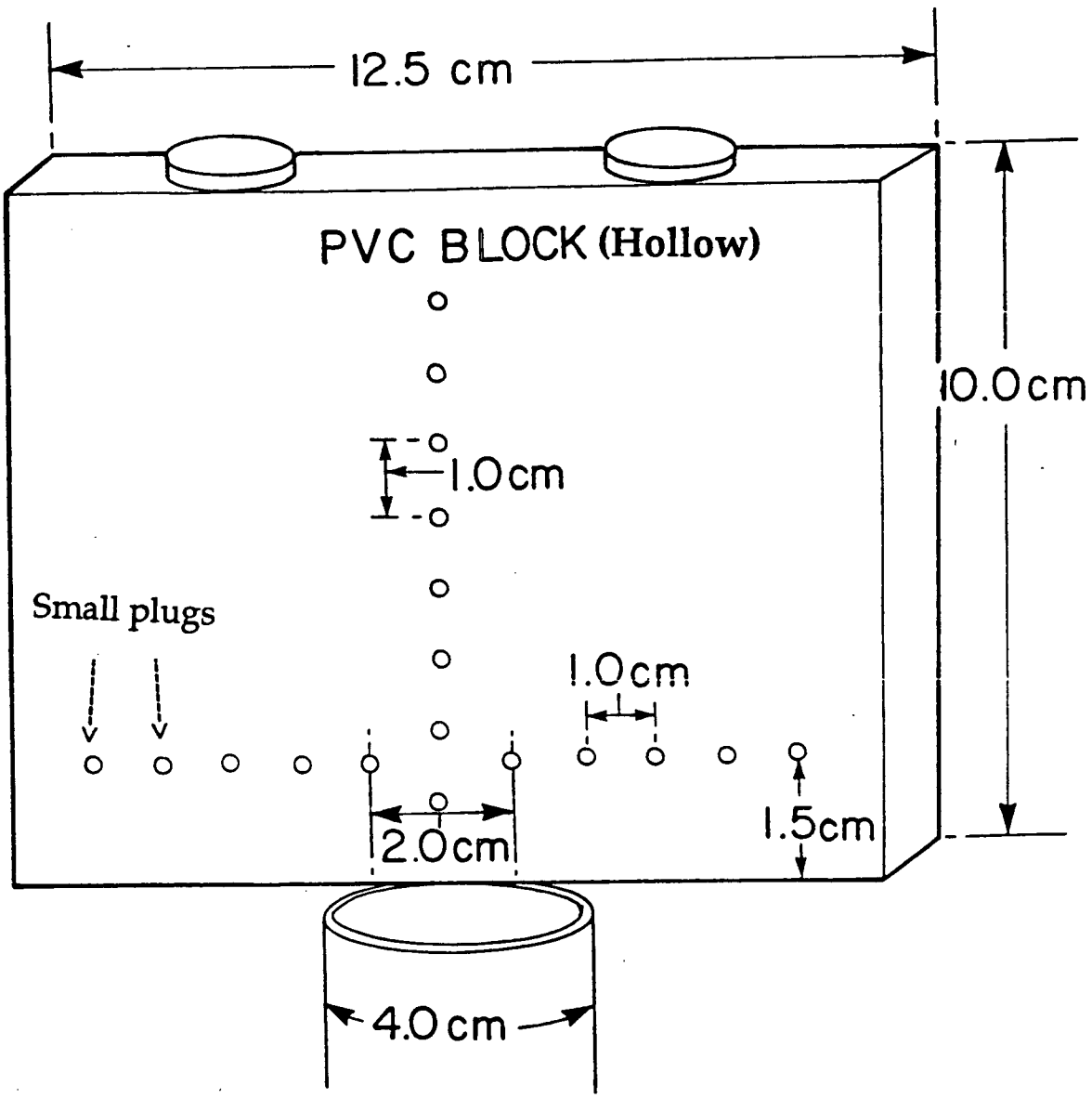

Figure 3-6a Schematic diagram of a hollow rectangular PVC block filled with 85% phosphoric acid placed on top of the spiral resonator surface coil. Small plugs were inserted at regular intervals to enable quantitative measurement of distance on its NMR image (Figure 3-7).

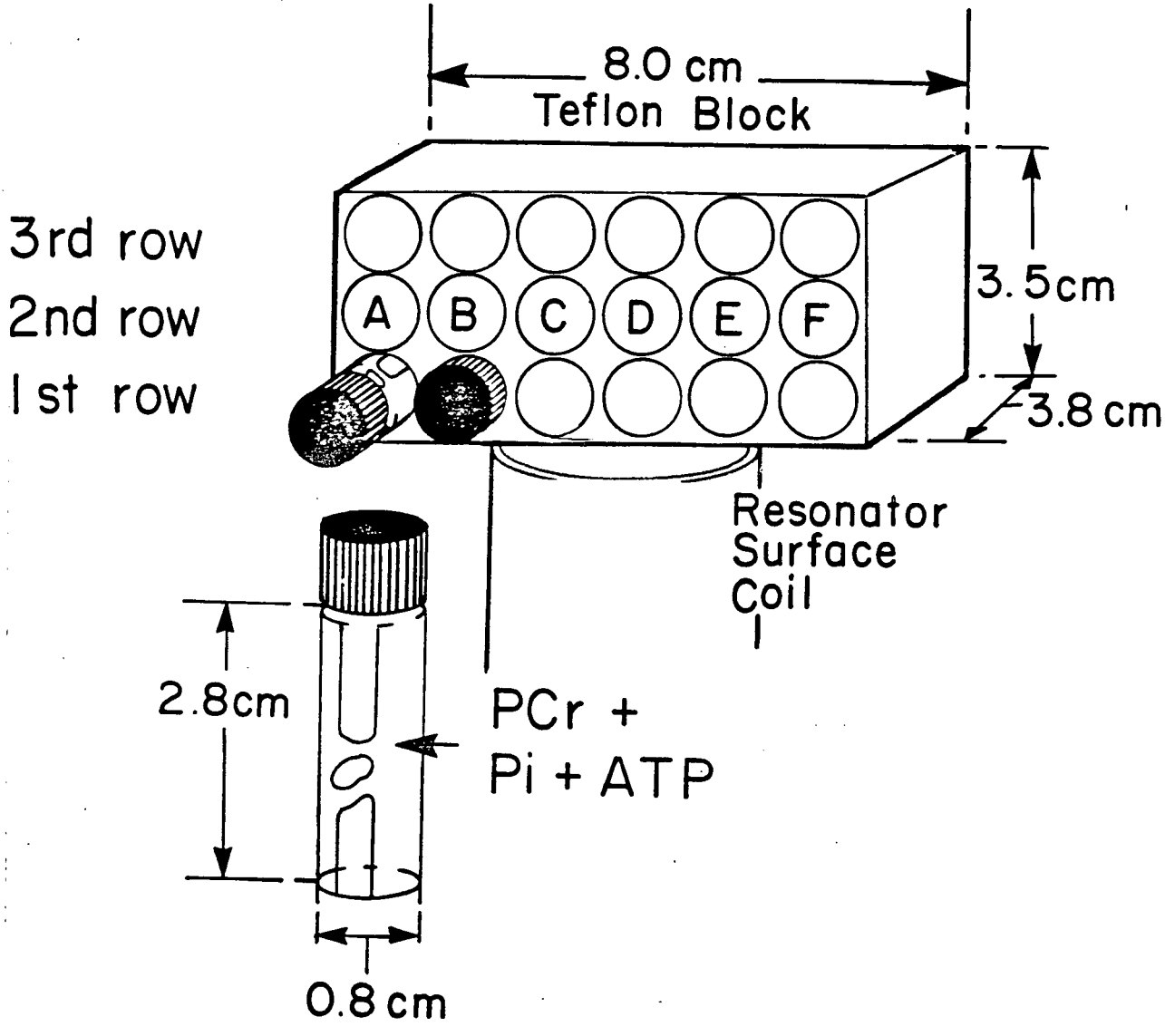

Figure 3-6b Schematic diagram of a single vial of PCr/Pi/ATP mixture fitted into the holes of a rectangular Teflon block placed on top of the spiral resonator surface coil.

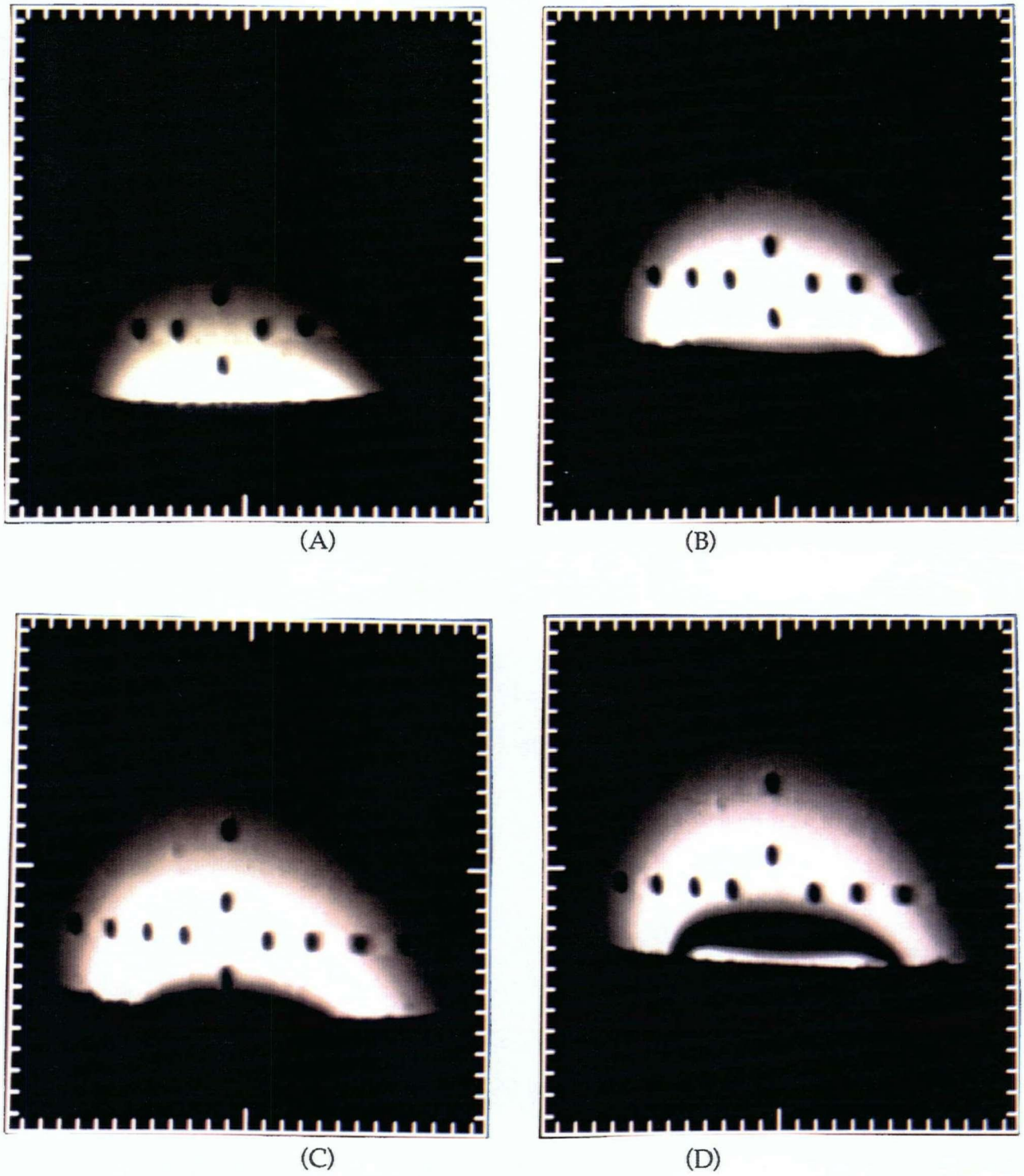

Figure 3-7 Series of B_1 profile showing the excitation pattern in the XY plane of the laboratory frame by the spiral resonator surface coil (4.0 cm. in diameter). The various flip angle at the coil center was (A) 90^0, (B) 180^0, (C) 270^0, and (D) 360^0.

Figure 3-7 shows the B_1 magnetic field gradient profile of the spiral resonator surface coil. It is evident that there is less variation in the intensity of B_{1x} than expected from that of an ordinary surface coil (i.e. flat, single turn, circular surface coil); and therefore, a more homogeneous B_{1x} distribution for the spiral resonator surface coil. In addition, as opposed to a conical shape sampled by the flat circular surface coil (38), the resonator boundaries of B_{1x} tend toward a cylindrical shape (i.e. for depth less than the radius of the resonator, the magnitude of B_{1x} shows little variation; whereas, for depth greater than the resonator radius, B_{1x} falls off more rapidly). Such characteristics are quite common among resonator surface coil designs (38).

As shown in Figure 3-8a, the further the sample is radially away from the resonator coil, the smaller the induced signal. However, surprisingly, the fact that P*i*/PCr ratio (Figure 3-8b) were only dependent on its axial position (i.e. not radially dependent) further validated its use as an index of biomechanical efficiency, as well as giving information about pathological conditions.

3.8 pH Calibration Curve at 1.89 Tesla

The significance of pH as an indicator of the intracellular environment is well established and P-31 NMR spectroscopy provides a non-invasive means of measuring intracellular pH (44-45). The chemical shift of P*i* is the weighted average of the chemical shift of $H_2PO_4^-$ and HPO_4^{2-}; the chemical shifts of these two species differ because of a different charge and a different set of resonant structures. Therefore, in a solution of rapidly exchanging phosphates, the average observed P-31 chemical shift of inorganic phosphate (δ_0) is given by:

$$\delta_0 = \{(\delta_{HPO4^{2-}}[HPO_4^{2-}])/[Pi]\}+\{(\delta_{H2PO4^-}[H_2PO_4^-])/[Pi]\} \qquad (3\text{-}14)$$

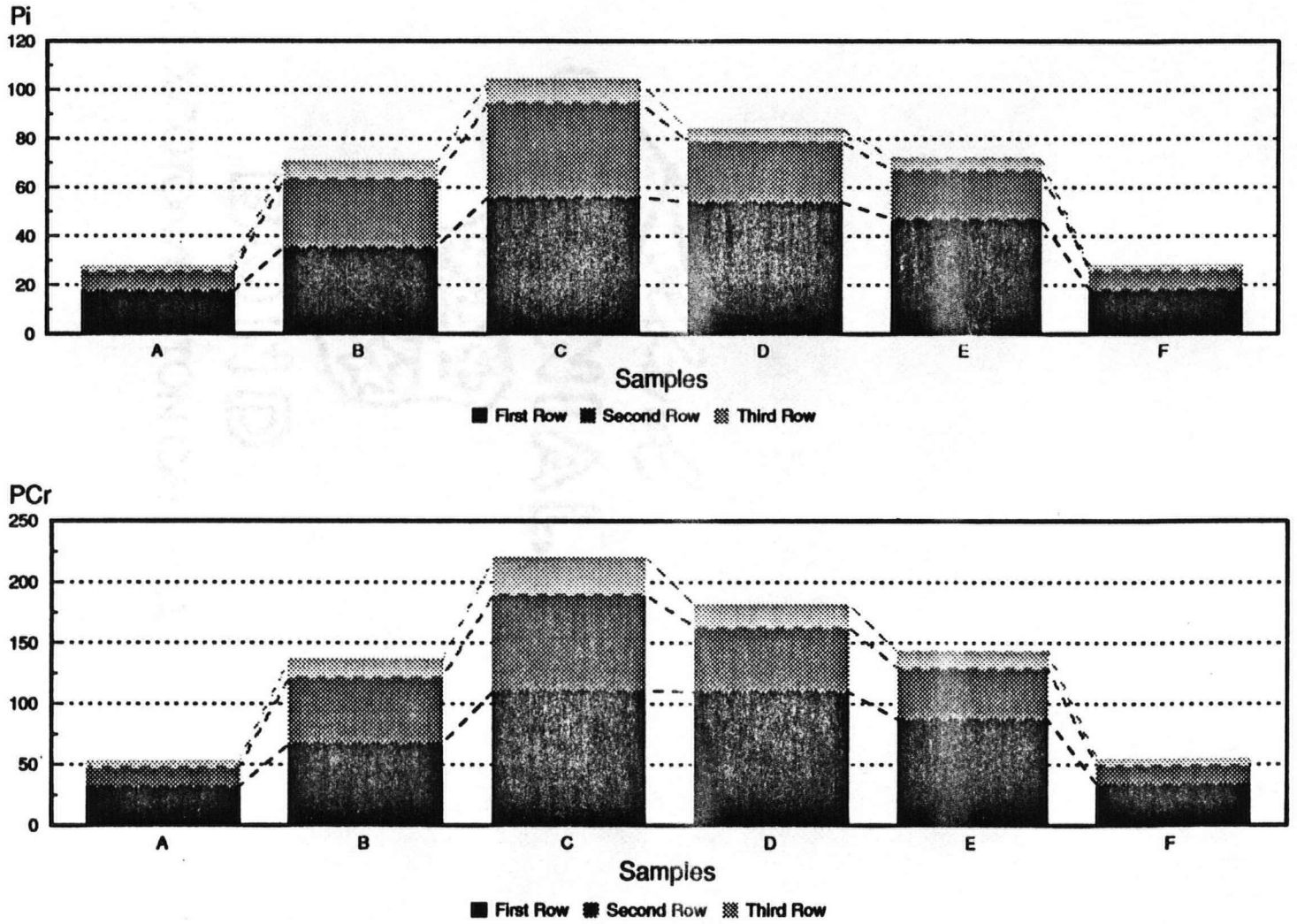

Figure 3-8a Signal Contribution (*Pi* and PCr) from samples, as pictured in Figure 3-6b, at different distances away from the centre of the spiral resonator surface coil (35 μsec pulse with repetition rate at 1 sec.).

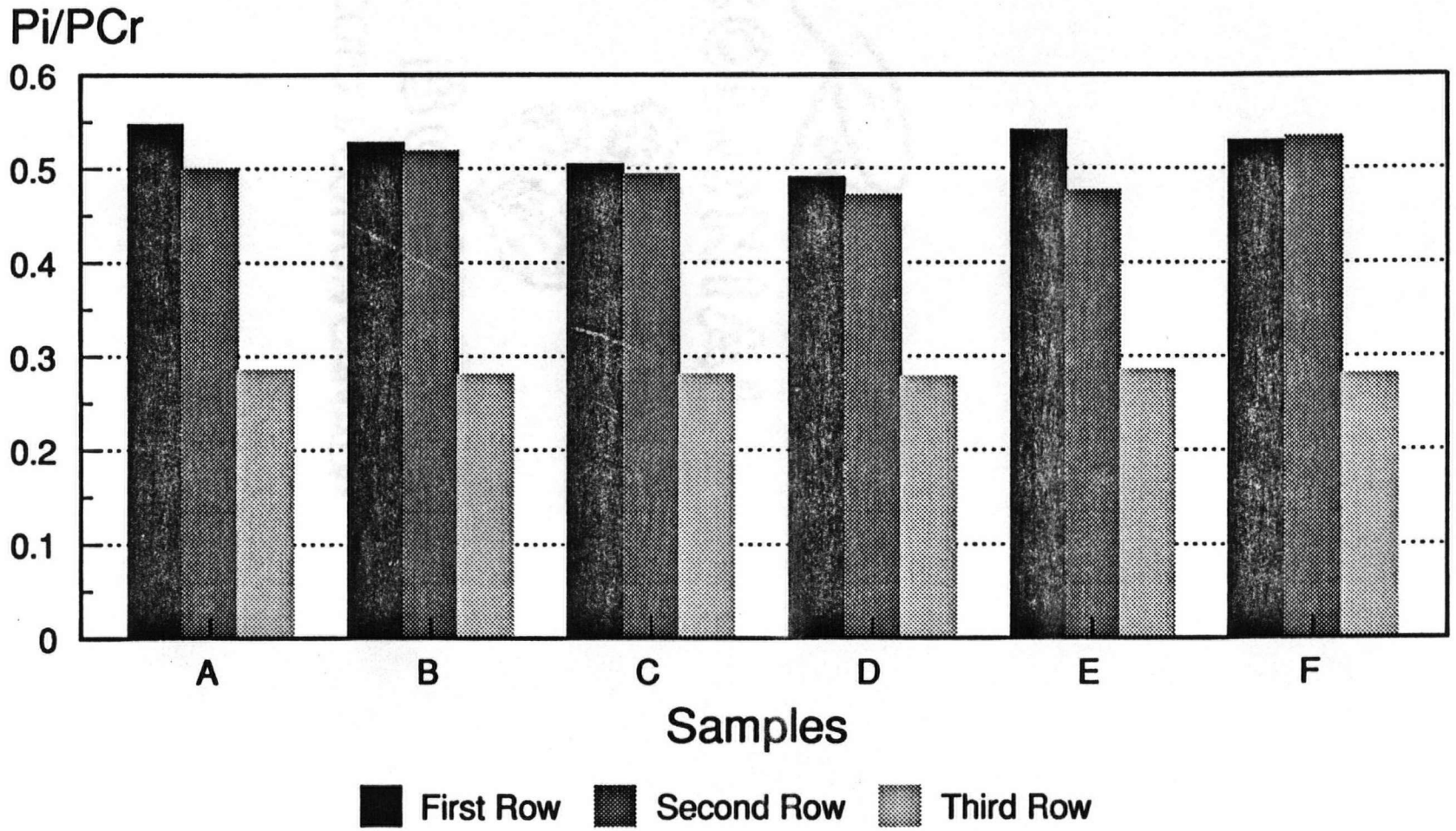

Figure 3-8b Signal Contribution (P*i*/PCr ratio) from samples, as pictured in Figure 3-6b, at different distances away from the centre of the spiral resonator surface coil (35 µsec pulse with repetition rate at 1 sec.).

In the absence of chemical exchange, $\delta_{HPO4^{2-}}$ and $\delta_{H2PO4^{-}}$ would be separated by about 2.35 ppm (46). Using the second acidic dissociation constant $K_a = ([H^+][HPO_4^{2-}])/[H_2PO_4^-]$ in terms of concentration, and $[Pi] = [HPO_4^{2-}] + [H_2PO_4^-]$, then

$$\delta_0 = \{(\delta_{HPO4^{2-}} K_a)/(K_a+[H^+])\}+\{(\delta_{H2PO4^-}[H^+])/(K_a+[H^+])\} \quad (3\text{-}15)$$

By rearranging using the traditional definitions of $pH = -\log[H^+]$ and pK_a, and equating activity with concentration, resulting in the familiar Henderson-Hasselbalch equation for a single equilibrium given in terms of chemical shift:

$$pH = pK_a + \log \{(\delta_0-\delta_A) /(\delta_B-\delta_0)\} \quad (3\text{-}16)$$

where δ_A and δ_B are the chemical shifts of the acid ($H_2PO_4^-$) and base (HPO_4^{2-}), respectively, in ppm. In this equation pK_a is the mid-point of the titration curve. Due to the presence of B_0 and B_1 inhomogeneity and local susceptibility effects, external standard is not suitable as they may lie in a different field to the buffer solution. Therefore, internal standards are preferred and PCr is conventionally used as reference standard with respect to which the chemical shift of P*i* is measured.

Methods The composition of the calibration solution was 10mM dipotassium phosphocreatine (K_2PCr), 10 mM K_2HPO_4, 10 mM Na_2HPO_4, and 10 mM $MgCl_2$. A series of buffer solutions was made, covering a pH range from 6.0 to 8.5 to encompass the physiological range. P-31 NMR spectra were acquired using the spiral resonance surface coil, the acquisition parameters were: frequency of 32.5 MHz, 2048 data acquisition points, 35 μsec. pulse width, and 1 sec. relaxation delay.

Result Figure 3-9 was the standard calibration curve obtained at physiological temperature (37 ^{0}C). Non-linear regression of data (R^2 = 97%) gave a pK_a value of 6.83, and δ_A and δ_B values of 3.24 and 5.71 respectively. Possible inaccuracies of such *in vitro* calibration curve with respect to *in vivo*

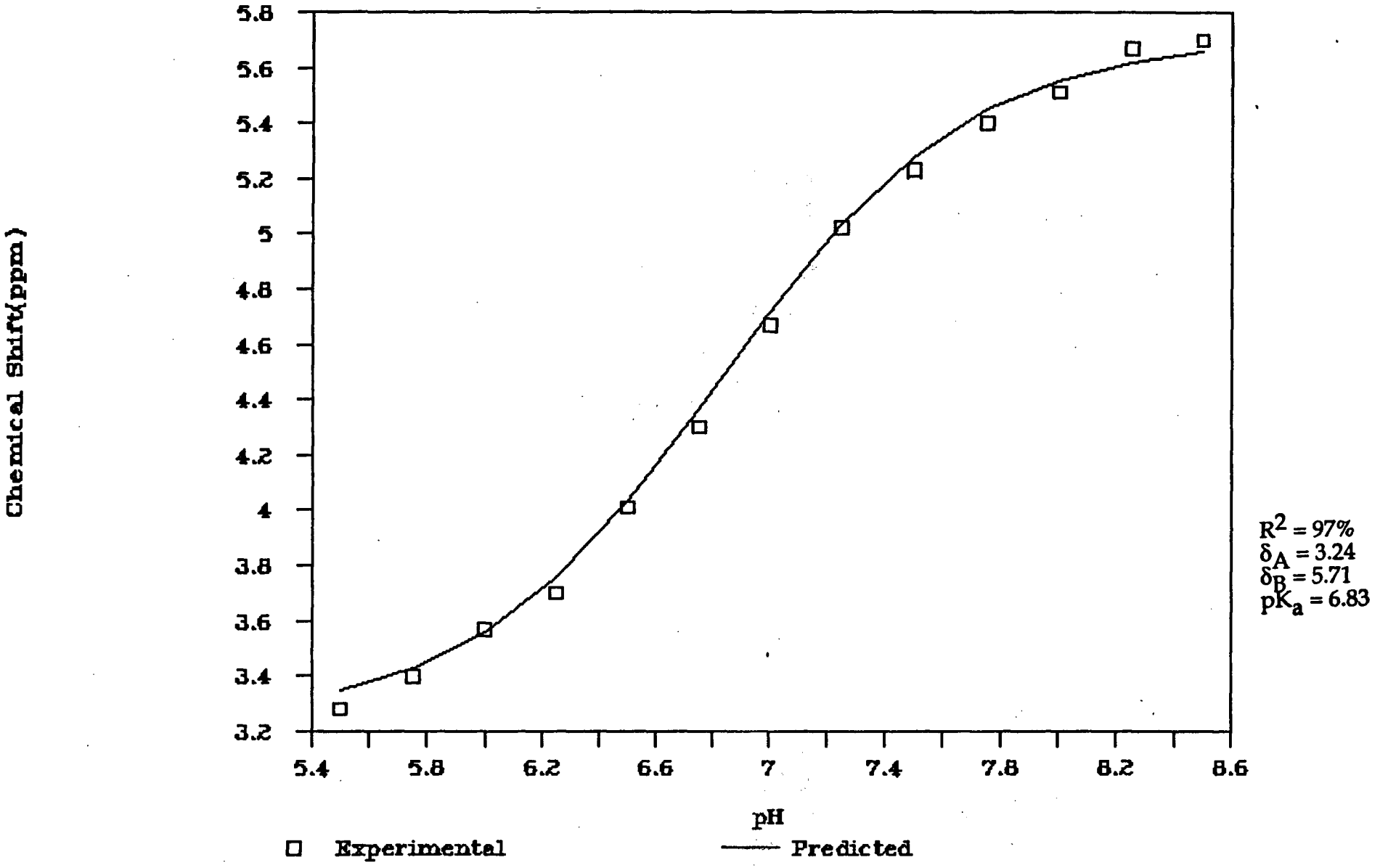

Figure 3-9 The standard calibration curve between pH and the NMR chemical shift of *Pi*.

physiological conditions may be due to the slightly different ionic strength, temperature, and the fluctuation of Mg^{2+} and Ca^{2+} concentration, as well as to the changes in intracellular conditions, other than pH, which affect P*i* chemical shift. These uncertainties should be bourne in mind when drawing clinical conclusions from *in vivo* measurements.

3.9 Repetition Time vs Signal-to-noise Optimization

The sensitivity and the size and location of the observed volume in surface coil NMR are dependent upon experimental conditions. Ideally, the repetition time should be chosen to be five times the longest T_1 of the peaks to be measured. In case of P-31 NMRS sampling high energy phosphate resonances in the human forearm, phosphocreatine has the longest T_1 (T_1 = 3.25 sec. at 1.89 Tesla). If it is not possible to wait $5T_1$, a saturation factor may be measured for each peak, and partially saturated spectra used, although this has the two following drawbacks. (a) If T_1 changes, then the measured saturation factors will be in error. (b) The saturation factor (SF) is given by:

$$SF = [1-\exp(-T_R/T_1)]/[1-\cos\ \theta\exp(-T_R/T_1)] \qquad (3\text{-}17)$$

where T_R is the repetitive time and θ is the nutation angle. This factor is dependent on θ, and therefore on position with respect to a surface transmitter coil. For $\theta = 90^0$, this reduces to the conventional expression $SF = 1-\exp(-T_R/T_1)$. For small θ (i.e. at positions distant from the coil), SF =1 and there is little signal reduction. Decreasing the repetition time (or increasing T_1) generally increases the saturation (i.e. reduces the signal) near the surface, while leaving the deeper tissues unaffected (47). Ackerman *et. al.* (48) showed that a gain in sensitivity of ~130% is provided by rapid repetition times ($T<<T_1$) in comparison with slow repetition times ($T\geq 5T_1$). In addition to greater sensitivity, the volume

observed extends further away from the coil in all directions, both lateral and perpendicular to the coil, and the sensitivity falls off more slowly as a function of spatial coordinates than it does for slow and intermediate ($T \approx T_1$) repetition times; thus a more uniform sensitivity is achieved over the observed volume. Although the B_1 (and therefore signal intensity) is weaker in the regions away from the coil, the total volume of those regions is greater than the regions near the coil. It is the contribution of signals from the regions further away from the coil which produce the relative gain in sensitivity with fast repetition times. If signal is desired only from a region adjacent to the coil, intermediate repetition times will minimize signal contribution from regions of the sample not adjacent to the coil and provide a substantial increase in S/N (~75%) over slow pulse repetition rates. If the sample is moved away from the coil (up to 0.4 radii), longer pulse widths will provide signal from regions extended in volume through the sample with minor loss in sensitivity (~20%).

In general, maximum S/N is of primary concern for metabolic studies; thus, rapid repetition times are most appropriate. Besides, due to the time constraint usually associated with clinical studies, long repetition times are not practical. However, reducing the repetition time can only be justified if its effect is determined not to unduly alter the P*i*/PCr ratio. Figure 3-10 shows that signal saturation in our studies produced about up to 60% peak attenuation, but, as signal intensity of both P*i* and PCr were similarly reduced if the repetition time was chosen not to be less than 1 second, their ratio was affected far less (<10% overestimate of the P*i*/PCr ratio) and this effect was constant between experiments and between individuals.

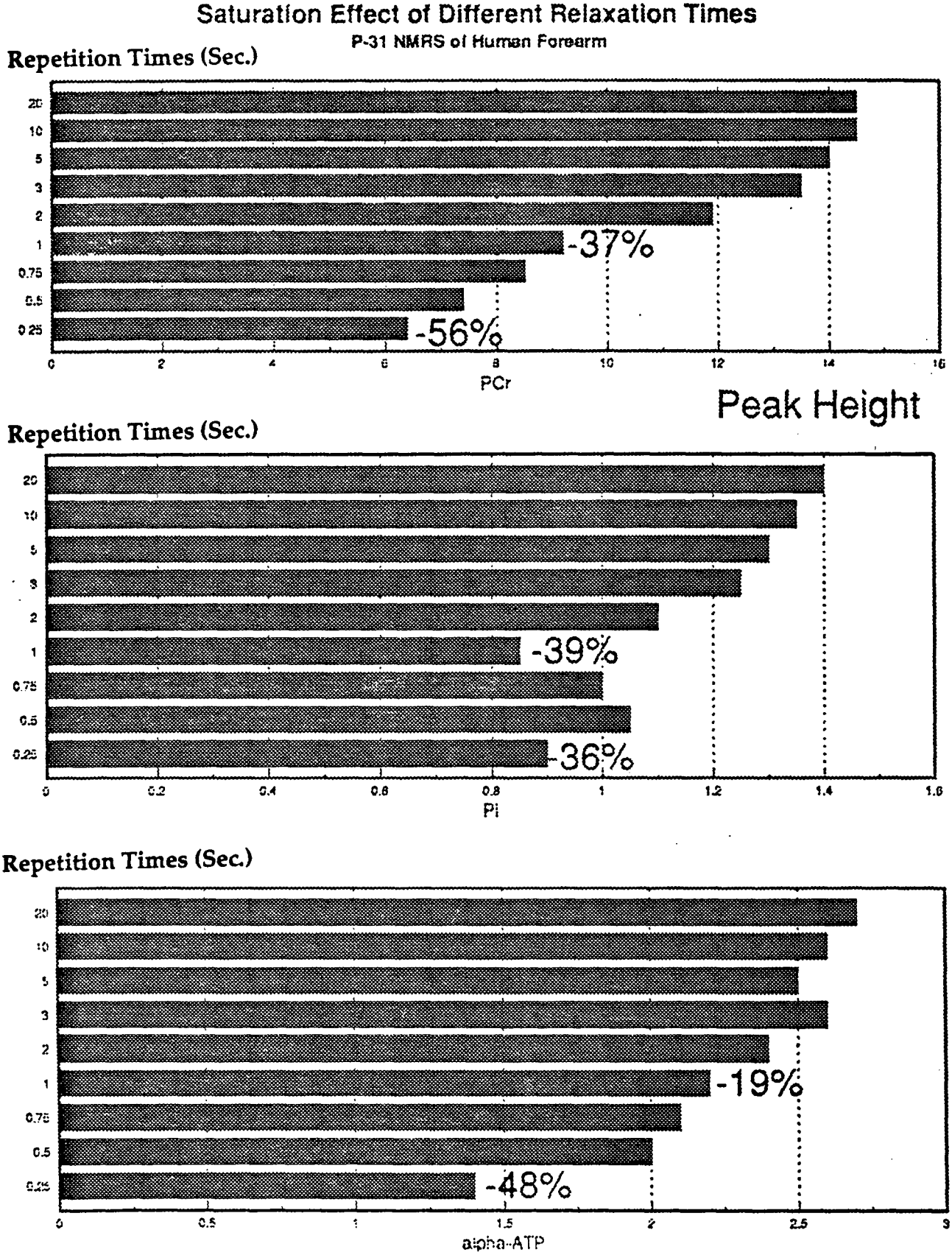

Figure 3-10a The saturation effect of different relaxation delays (or repetition rates) on the resonances of PCr, P*i*, and α-ATP of P-31 NMR spectra of human forearm.

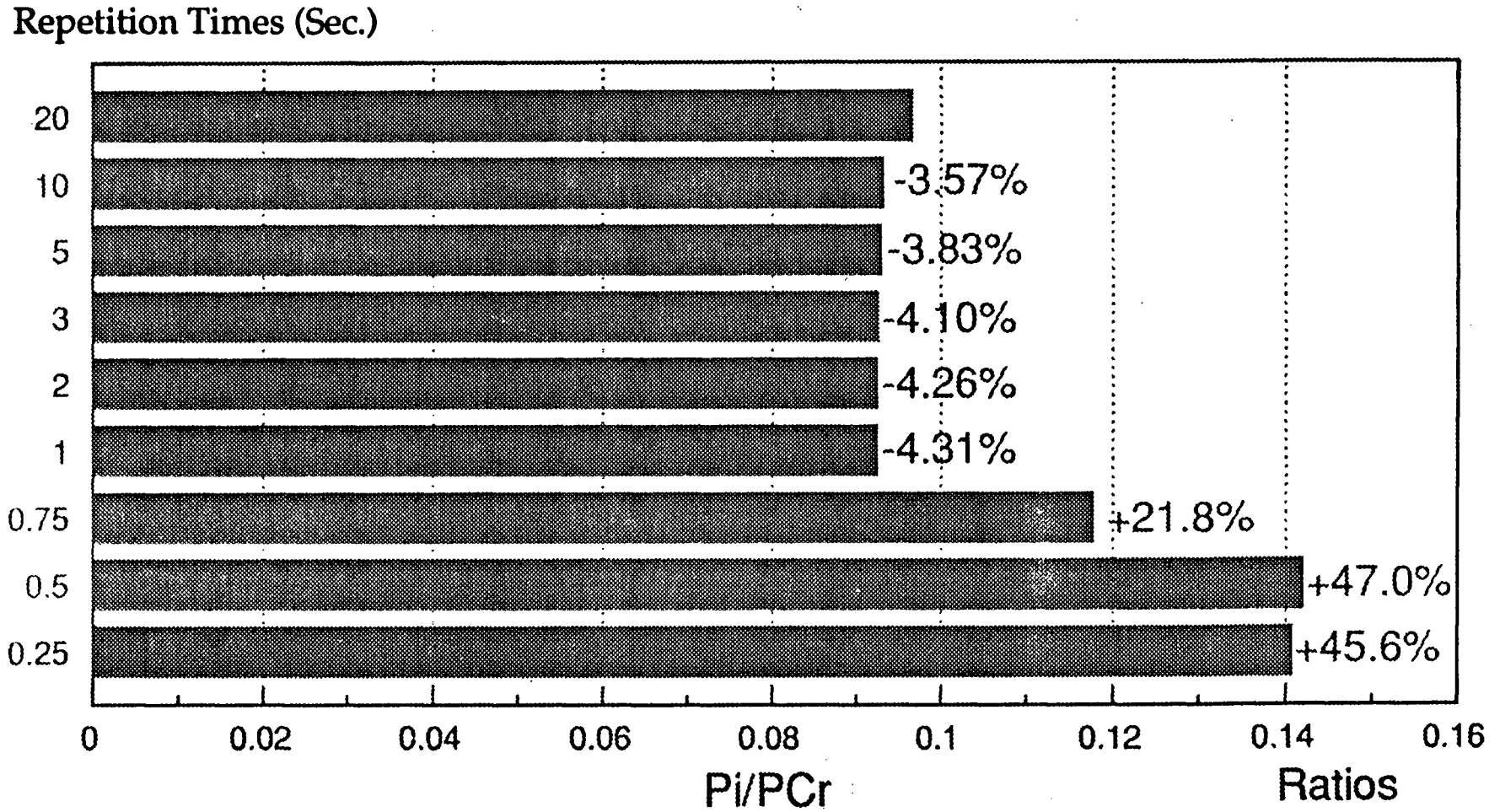

Figure 3-10b The saturation effect of different **relaxation** delays (or repetition rates) on the P*i*/PCr ratio of P-31 NMR spectra of human forearm.

3.10 Data Analysis

Spectra from *in vitro* samples usually have well separated peaks on a flat baseline, and present few problems. The integration procedure on the spectrometer will give peak areas. However, *in vivo* experiment is sensitive only to the most mobile of chemical entities in tissue-typically water, energy sources, and some amino acids. Other tissue components existing in relative bound states exhibit short spin-spin relaxation times ($T_2 \leq 1$ msec) and either do not appear in chemical shift spectra or contribute only a broad baseline hump. Possible origins of the broad component are bone, slow-moving macromolecular structures (e.g. nuclei acids and phospholipids), or metabolites from surrounding tissue broadened by magnetic field inhomogeneity. Therefore, *in vivo* spectra are nearly always more difficult to analyze because: (a) the peaks are broad (compared to *in vitro*) , and therefore often overlap; (b) in P-31 NMRS muscle spectra the additional broad phospholipid resonance, or hump, which underlines all the peaks, and represents an undetermined sloping (and curving) baseline. Most published spectra have been mathematically filtered to suppress both of these effects, using deconvolution (i.e., resolution enhancement) filters on the free induction decay before Fourier transformation. However, this usually alters the peak areas, and the ratio of their areas (49), and therefore is undesirable for quantification, unless these effects are known. A second method to eliminate the broad component is by saturation at a frequency which does not affect the intensities of the smaller phosphorus metabolite resonances (50). However, such technique may result in sample heating and may unnecessarily prolong the acquisition time.

Peak areas can be estimated by four means:

(a) **Peak Height.** The peak height is proportional to area, provided the line shape and width are constant. The height is easy to measure. Because it is a single measurement at the peak centre, it may be less susceptible to distortion by neighbouring peaks than integration (which uses the whole line width).

(b) **Triangulation.** Using a paper plot of the spectrum, straight lines are drawn through a peak, to fit it to a triangular shape. The area of the triangle is then calculated from its dimensions. This method involves considerable observer judgment.

(c) **Computer integration of the spectrum.** A 'gate' is defined around each peak, using two cursors on the computer screen, and the integral of the spectrum between these two points is computed. Peak overlap, if present, means that the integral line has no straight horizontal portion between peaks, so subjective judgement may be required to position the gate.

(d) **Computer fitting.** Two main approaches have been used, fitting of the spectrum, and fitting of the free induction decay. (i) *Fitting of the spectrum.* Least squares curve fitting methods have been applied to one peak of the spectrum at a time. The observer chooses the Gaussian/Lorentzian mix and the range of the fit; the linewidth, area and position are then fitted by the computer (51-52). The difficulties are that the actual line width is unknown, and rarely a simple sum of Gaussian and Lorentzian. Much of the area lies in the wings of the peak, which may lie under an adjoining peak. The least squares fitted area is likely to be very dependent on the initial processing (phase and baseline correction) applied to the spectrum. (ii) *Fitting of the free induction decay.* Using the time domain free induction decay (FID) data directly has several advantages over using the spectrum. The complete FID is the primary data produced by the spectrometer, and therefore its noise characteristics are well known; in particular, the noise at each point is equal, and uncorrelated. The first few points may be corrupted by

instrumental effects (e.g., transmitter pulse break through or receiver recovery), or by the presence of a broad, short-lived, lipid signal. The end of FID may be missing because data collection time was insufficient. By working in the time domain this missing data can simply be ignored in any fitting process; if a spectrum were calculated (by Fourier transformation) from this FID, the effect of truncation would be to produce curved baseline artifacts across the whole spectrum. In addition the noise in such a spectrum is correlated, and this may affect the validity of statistical methods applied to the spectrum. Finally, there are usually some observer-dependent parameters used in obtaining a Fourier transform spectrum (phase correction, line broadening, baseline correction), which are absent if the original FID is used. Observer-dependence, and therefore imprecision, are usually very low in time-domain methods, although accuracy may still not be good. Two approaches have been used in analyzing time-domain data. The linear prediction single value decomposition (LPSVD) technique has been used to calculated the area, position, width and phase of each peak (53-54). Its fundamental weakness is that Lorentzian lineshapes are assumed, which are clearly not realistic for many *in vivo* spectra. The maximum entropy method (MEM) has been successful in increasing peak visibility and suppressing baseline noise (55-56). The philosophical basis of the method is that it produces a maximum entropy (or disorder) solution, i.e. one containing minimum information. A peak is only produced at a particular chemical shift if there is good evidence for the existence of one. The method is therefore unlikely to produce false peaks, and no assumptions of lineshape are necessary; however, peak overlap remains a problem. More important, the method is non-quantitative because the lower signal-to-noise ratio peaks are biased towards zero (whereas the higher signal-to-noise ratio peaks are positively biased). Thus, peak ratios may be adversely affected.

None of the above fitting methods in either the frequency or time domain is entirely satisfactory because they produce some or all of the following errors. (a) Systematic bias. A particular peak may be consistently overestimated because of the underlying lipid hump, or adjacent lines; it may be underestimated because the wings are too far out to be included. (b) Variable contamination by neighbouring peaks. If a neighbouring peak increases, or moves closer, then the contribution of its wing to the peak of interest will increase. (c) Observer bias. Some of these methods are observer-dependent, in that subjective judgements must be made. If a different person performs the analysis, the peak area estimates are likely to be different. Even the same person will produce slightly different results from day to day.

Since all of the methods mentioned above are less than perfect, a compromise has to be made within the constraints limited by the clinical setting. Thus, the exercise protocol outlined in the next chapter takes about one and half hours for each patient; and since we would like at least to have a clear indication as to the energy efficiency of the patient before he or she leaves the laboratory, data processing should to keep to a minimum. Besides, since we would like to tailor our exercise protocol to the patient's capability, and to prescribe treatment or to arrange for further clinical studies, NMR spectral result should be ideally available during the experiment. Therefore, peak height is used throughout this Thesis for quantification, because it is easiest, less time consuming, and less susceptible to distortion by neighbouring peaks than integration.

In order to justify the above simplification, we measured both the area and peak height (normal and expanded) of each phosphate resonance during a typical P-31 NMRS study of human forearm, and compared the two ratios

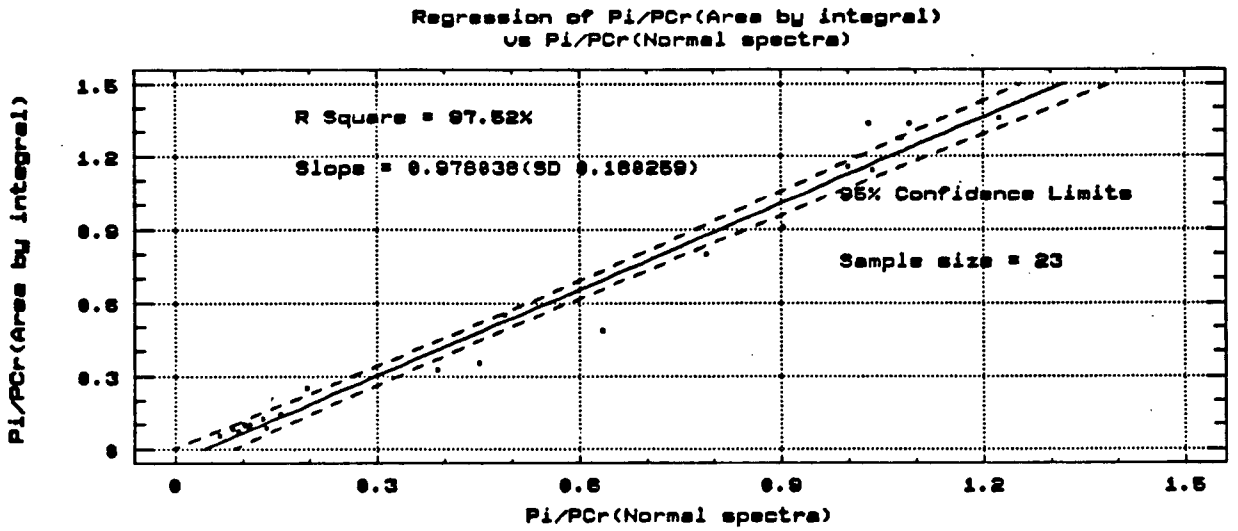

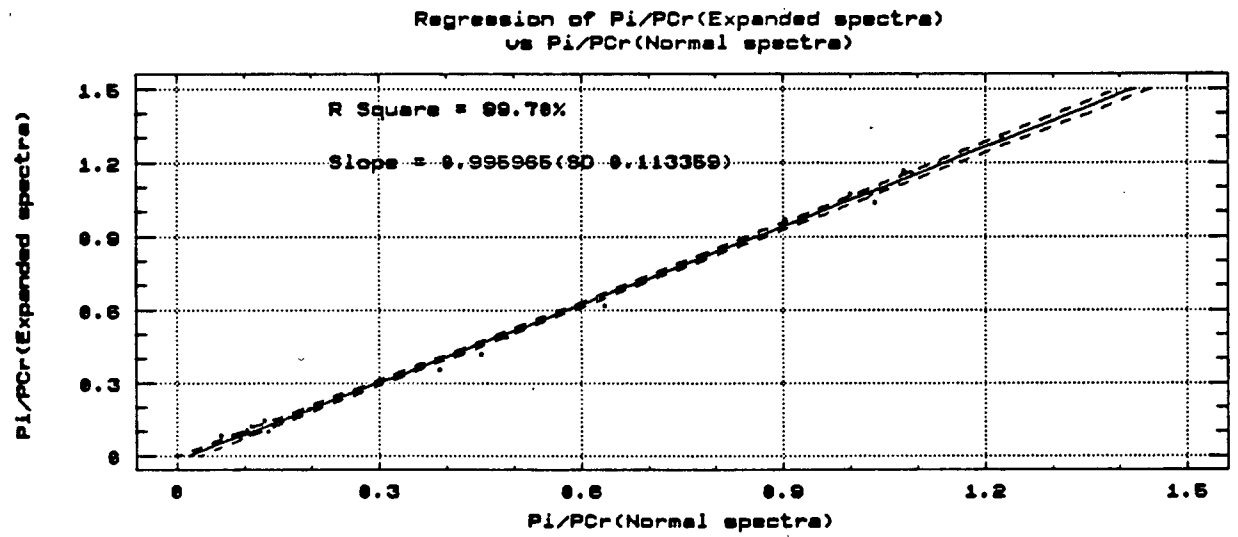

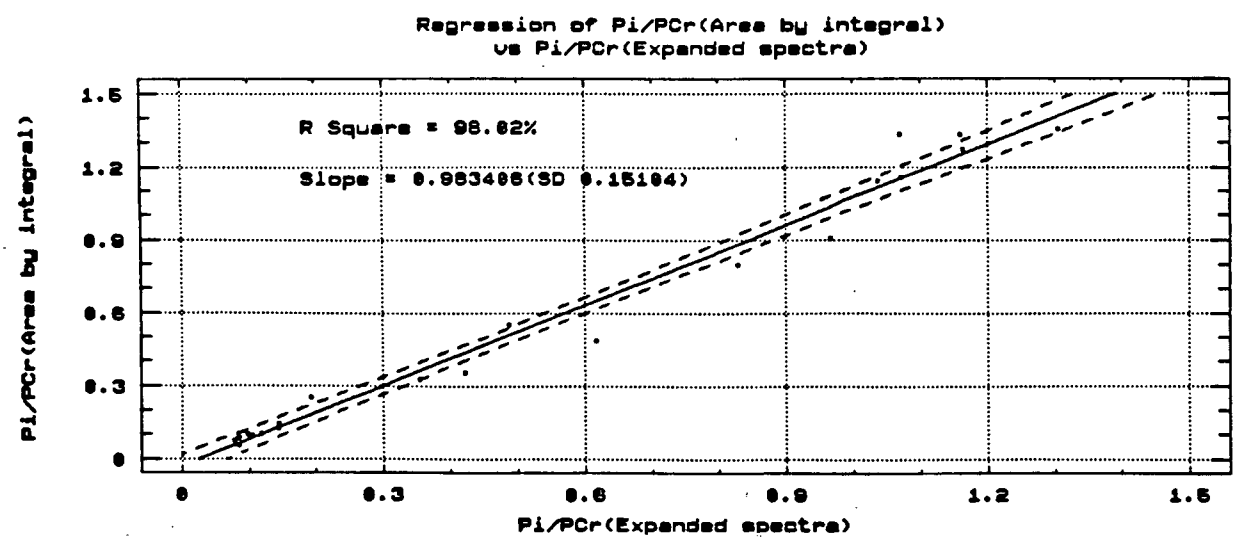

Figure 3-11a Regression analysis comparing the Pi/PCr ratios obtained, during a typical exercise sequence, via peak height measurement made with the normal spectra, the expanded spectra, and peak area measurement made by integrating area.

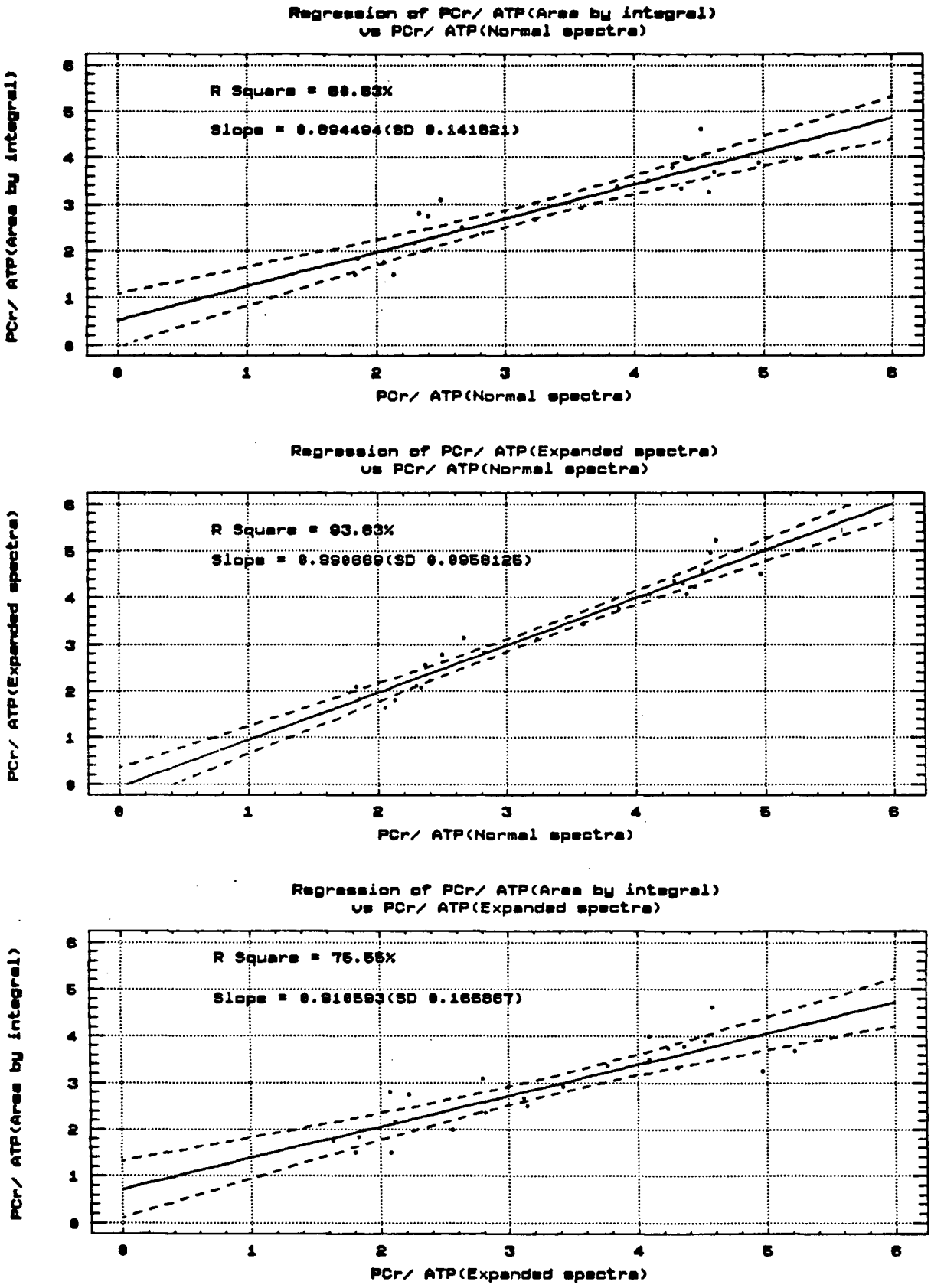

Figure 3-11b Regression analysis comparing the PCr/α-ATP ratios obtained, during a typical exercise sequence, via peak height measurement made with the normal spectra, the expanded spectra, and peak area measurement made by integrating area.

between *Pi* and PCr, and between PCr and α-ATP. Figure 3-11 showed remarkable and significant correlations ($R^2 > 97\%$ for *Pi*/PCr).

3.11 Conclusion

The spiral resonator surface coil evolved as a result of our continuous efforts to improve our instrumentation; this surface coil development paralleled an equally important effort to perfect a tractable clinical protocol to study muscle fatigue. Aside from offering improved S/N ratio, the spiral resonator surface coil is compact, stable, and best of all, very reliable. Before we further explore the flexibility and versatility of the spiral design, in the next two chapters we will concentrate on the clinical aspects of this project.

References

1. J. Schachter, M.Sc. Dissertation, Department of Chemistry, U.B.C., Canada, 1985.

2. S. L. Talagala, Ph.D. Dissertation, Department of Chemistry, U.B.C., Canada, 1986.

3. J. M. S. Hutchison, W. A. Steiner, Am. J. Roentgenol. 137:895, 1981.

4. D. I. Hoult, Rev. Sci. Instrum. 50:193, 1979.

5. R. E. Gordon, P. E. Hanley, D. Shaw, *et. al.*, Nature 287:367-368, 1980.

6. P. A. Bottomley, T. H. Foster, and R. D. Darrow, J. Magn. Reson. 59:338-342, 1984.

7. P. A. Bottomley, L. S. Smith, W. M. Leue, and C. Charles, J. Magn. Reson. 64:347, 1985.

8. P. A. Bottomley, and C. J. Hardy, J. Magn. Reson. 74:550-556, 1987.

9. W. P. Aue, S. Muller, T. A. Cross, and J. Seelig, J. Magn. Reson. 56:350, 1984.

10. P. R. Luyten, A. J. Marien, B. Sijtsma, and J. A. D. Hollander, J. Magn. Reson. 67:148-155, 1986.

11. D. M. Doddrell, J. M. Bulsing, G. J. Galloway, W. M. Brooks, J. Field, M. Irving, and H. Baddeley, J. Magn. Reson. 70:319-326, 1986.

12. D. M. Doddrell, J. M. Bulsing, G. J. Galloway, W. M. Brooks, J. Field, M. Irving, and H. Baddeley, J. Magn. Reson. 68:367-372, 1986.

13. S. Muller, W. P. Aue, and J. Seelig, J. Magn. Reson. 65:332, 1985.

14. R. J. Ordidge, A. Connelly, and J. A. B. Lohman, J. Magn. Reson. 66:283-294, 1986.

15. A. Connelly, C. Counsell, and J. A. B. Lohman, J. Magn. Reson. 78:519-525, 1988.

16. A. Haase, J. Frahm, W. Hanicke, and D. Matthaei, Phys. Med. Biol. 30:341, 1985.

17. L. D. Hall, S. Sukumar, and S. L. Talagala, J. Magn. Reson. 56:275, 1984.

18. A. A. Maudsley, S. K. Hilal, W. H. Perman, and H. E. Simon, J. Magn. Reson. 51:147, 1983.

19. H. W. Park, and Z. H. Cho, Magn. Reson. Med. 3:448, 1986.

20. A. Haase, and D. Matthaei, J. Magn. Reson. 71:550-553, 1987.

21. M. R. Bendall, and R. E. Gordon, J. Magn. Reson. 53:365, 1983.

22. M. R. Bendall, and W. P. Aue, J. Magn. Reson. 54:149, 1983.

23. M. R. Bendall, and D. T. Pegg, Magn. Reson. Med. 2:91, 1985.

24. M. Garwood, T. Schleich, G. B. Matson, and G. Acosta, J. Magn. Reson. 60:268, 1984.

25. M. Garwood, T. Schleich, B. D. Ross, G. B. Matson, and W. D. Winters, J. Magn. Reson. 65:239, 1985.

26. M. Garwood, T. Schleich, M. R. Bendall, and D. T. Pegg, J. Magn. Reson. 65:510, 1985.

27. M. Garwood, K. Ugurbil, T. Schleich, M. Petein, E. Sublett, A. H. L. From, and R. J. Bache, J. Magn. Reson. 69:576-581, 1986.

28. D. I. Hoult, J. Magn. Reson. 33:183, 1979.

29. J. J. H. Ackerman, T. H. Grove, G. G. Wong, D. G. Gadian, G. K. Radda, Nature 283:167-170, 1980.

30. W. R. Smythe, Static and Dynamic Electricity, 3rd ed. McGraw-Hill Publishing Co., New York, 1968.

31. D. I. Hoult, and R. E. Richards, J. Magn. Reson. 24:71-85, 1976.

32. A. Abragam, the Principles of Nuclear Magnetism, Clarendon Press, Oxford, 1961.

33. H. D. W. Hill, and R. E. Richards, J. Phys. E, Ser. 2 1:977, 1968.

34. D. I. Hoult, and P. C. Lauterbur, J. Magn. Reson. 34:425-433, 1979.

35. J. B. Hasted, Aqueous Dielectrics, Chapman & Hill Ltd., London, pp. 28-29, 1981.

36. F. E. Terman, Radio Engineer's Handbook, McGraw-Hill Phblishing Co., New York, pp. 73-90, 1943.

37. D. G. Gadian, and F. N. H. Robinson, J. Magn. Reson. 34:449, 1979.

38. T. M. Grist, and J. S. Hyde, J. Magn. Reson. 61:571-578, 1985.

39. W. Froncisz, and J. S. Hyde, J. Magn. Reson. 47:515, 1982.

40. J. S. Hyde, W. Froncisz, and A. Kusumi, Rev. Sci. Instrum. 53:1934, 1982.

41. NMC-1280 Software Manual, Nicolet Magnetics Corporation, California, December, 1982.

42. P. Daugaard, H. J. Jakobsen, A. R. Garber, and P. D. Ellis, J. Magn. Reson. 44:224, 1981.

43. W. A. Edelstein, J. M. S. Hutchinson, G. Johnson, and T. Redpath, Phys. Med. Biol. 25:751, 1980.

44. D. G. Gadian, G. K. Radda, R. E. Richards, and P. J. Seeley, in Biological Applications of Magnetic Resonance, ed. R. G. Shulman, Academic Press, New York, pp. 463-535, 1979.

45. R. N. Moon, and J. H. Richards, J. Biol. Chem. 248:7276-7278, 1973.

46. D. G. Gadian, Nuclear Magnetic Resonance and its Applications to Living Systems, Oxford University Press, Oxford, 1982.

47. P. S. Tofts, in Neonatal Physiological Measurements, ed. P. Rolfe, Butterworths Ltd., London, pp. 363-372, 1987.

48. J. L. Evelhoch, M. G. Crowley, and J. J. H. Ackerman, J. Magn. Reson. 56:110-124, 1984.

49. P. Tofts, and S. Wray, J. Physiol. 359:417-429, 1985.

50. R. Gonzalez-Mendez, L. Litt, A. P. Koretsky, J. V. Colditz, M. W. Weiner, and T. L. James, J. Magn. Reson. 57:526-533, 1984.

51. J. C. Haselgrove, R. Christen, V. H. Subramanian, S. Eleff, J. S. Leigh, and B. Chance, Soc. Magn. Reson. Med. 5th Annual Meeting, Montreal, pp. 503-504, 1986.

52. S. J. Nelson, and T. R. Brown, J. Magn. Reson. 75:229-243, 1987.

53. H. Barkhuijsen, R. de Beer, W. M. M. J. Bovee, and D. van Ormondt, J. Magn. Reson. 61:465-481, 1985.

54. W. M. M. J. Bovee, R. de Beer, A. A. de Graaf, J. Montizaan, and D. van Ormondt, Soc. Magn. Reson. Med. 6th Annual Meeting, New York, p. 383, 1987.

55. E. D. Laue, J. Skilling, J. Staunton, S. Sibisi, and R. G. Brereton, J. Magn. Reson. 62:437-452, 1985.

56. M. L. Waller, and P. S. Tofts, Magn. Reson. Med. 4:385-392, 1987.

Chapter 4

4. CLINICAL CONSIDERATIONS FOR STUDYING MUSCLE FATIGUE

4.1 Introduction

NMR spectroscopy has progressed from being novel, to become a more or less routine biological and clinical technique. Most of the studies performed attempt to measure metabolite levels in tissue; for example, under normal and pathological conditions or during rest and stimulation. P-31 NMR spectra are exceedingly simple; however, they can interrogate a well balanced metabolic machinery at work. In order to fully appreciate such a delicate system, I shall begin this chapter with some background information about exercising muscle.

Exercise performance is largely determined by one's capacity to generate energy. This capacity in turn, is intimately related to the food nutrients consumed in the diet and the metabolic and physiologic systems of energy delivery and energy utilization.

4.1.1 Nutrients

The carbohydrate, fat, and protein nutrients consumed daily provide the necessary energy to maintain body functions both at rest and during various forms of physical activity. Aside from their role as biologic fuel, these nutrients

also play an important part in maintaining the structural and functional integrity of the organism.

Carbohydrates serve as a major source of energy, provide a "protein sparing" effect, facilitate the metabolism of fat as metabolic primer, and supply the central nervous system with fuel; whereas, fats provide the largest nutrient store of potential energy to power biologic work, serve as a cushion for the protection of vital organs, provide insulation from the thermal stress of cold environments, as well as acting as the carrier of the fat-soluble vitamins, A, D, E, and K. The fuel mixture during exercise depends on the intensity and duration of effort, as well as the fitness and nutritional status of the subject (1-2).

Under most conditions, exercise brings about a marked increase in the production and release of glucose by the liver and its subsequent use by muscle (3). In the early minutes of intense exercise in which oxygen supply does not meet the demands for aerobic metabolism, stored muscle glycogen and blood-borne glucose are the prime contributors of energy. During continuous moderate exercise, such as marathon running, distance cycling, and swimming, energy is derived mainly from the breakdown of the body's stores of fat and carbohydrate. In the early stages of submaximal exercise, about 40 to 50% of the energy requirement is supplied by the glycogen stored in the liver and exercising muscle. As exercise continues and the glycogen stores become reduced, however, an increasingly greater percentage of energy (nearly 80%) is supplied through fat metabolism. Eventually, fatigue sets in and exercise must stop.

Proteins differ chemically from fats and carbohydrates in that they contain nitrogen. The protein in the nervous and connective tissue is essentially fixed; whereas, muscle and liver proteins, when the demand arises, can enter the process of energy metabolism (4-5). The amino acids alanine and glutamic acid play a key role in providing the equivalent of "carbohydrate" fuel for exercise,

especially prolonged, submaximal exercise. The alanine-glucose cycle (Fig. 4-1) may account for 40 to 50% of the total glucose released by the liver.

4.1.2 Energy for Physical Activity

The energy in food, in the form of chemical energy trapped within the bonds of carbohydrates, fats, and proteins, is extracted in small amounts as it is needed during complex, enzymatically controlled reactions with high efficiency. This "nutrient energy" is harvested and funnelled through the energy-rich compound adenosine triphosphate (ATP), which is considered as the cell's "energy currency". Only a small quantity of ATP is stored within the cell. This situation provides a sensitive mechanism for regulating energy metabolism in the cell.

The complete breakdown of 1 mole of carbohydrate at STP liberates 686 kcal of energy, of which about 263 kcal (38%) is conserved in the bonds of ATP. In the reactions of glycolysis in the cell cytoplasm, 2 ATP molecules are formed in the anaerobic process of substrate phosphorylation (Fig. 4-2). Continued release of anaerobic energy in glycolysis depends on the removal of lactic acid to the blood and liver via the Cori cycle (Fig. 4-3). However, this avenue for extra energy is only temporary because as the level of lactic acid in the blood and muscles increases, the regeneration of ATP will not be able to keep pace with its utilization.

In the second stage of carbohydrate breakdown in the presence of oxygen, pyruvic acid is converted to acetyl-CoA, which is then processed through the Krebs cycle. The hydrogen ions released during glucose breakdown are oxidized via the respiratory chain and the energy generated is coupled to phosphorylation. In the complete breakdown of carbohydrate in skeletal muscle a total of 36 ATP molecules are formed (Fig. 4-2).

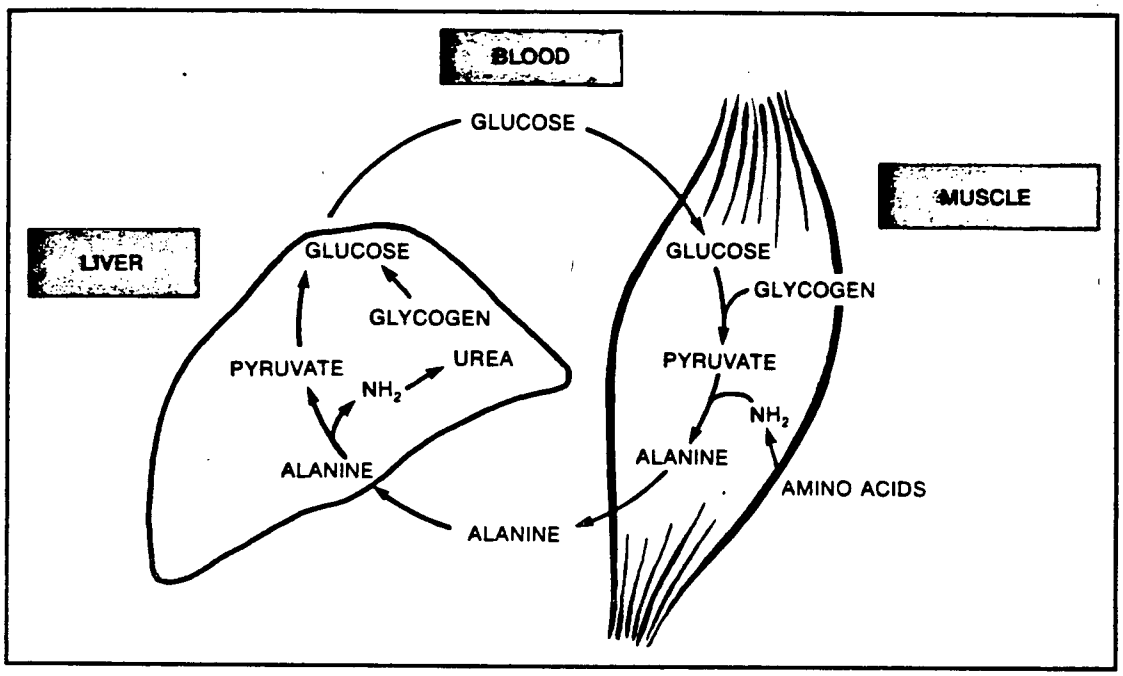

Figure 4-1 The alanine-glucose cycle in exercise.

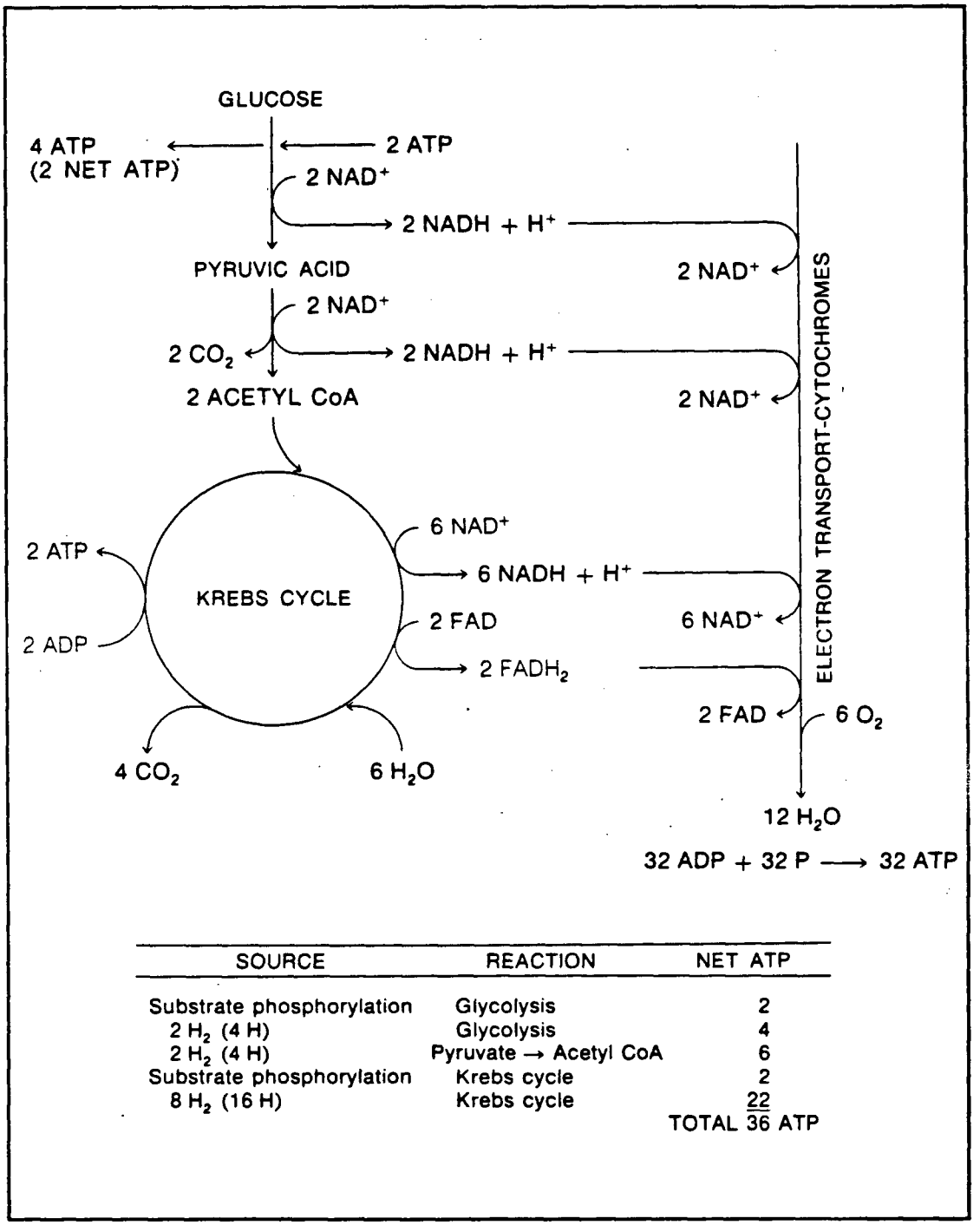

SOURCE	REACTION	NET ATP
Substrate phosphorylation	Glycolysis	2
2 H_2 (4 H)	Glycolysis	4
2 H_2 (4 H)	Pyruvate → Acetyl CoA	6
Substrate phosphorylation	Krebs cycle	2
8 H_2 (16 H)	Krebs cycle	22
		TOTAL 36 ATP

Figure 4-2 Adenosine triphosphate (ATP) yield from energy transfer during the complete oxidation of glucose.

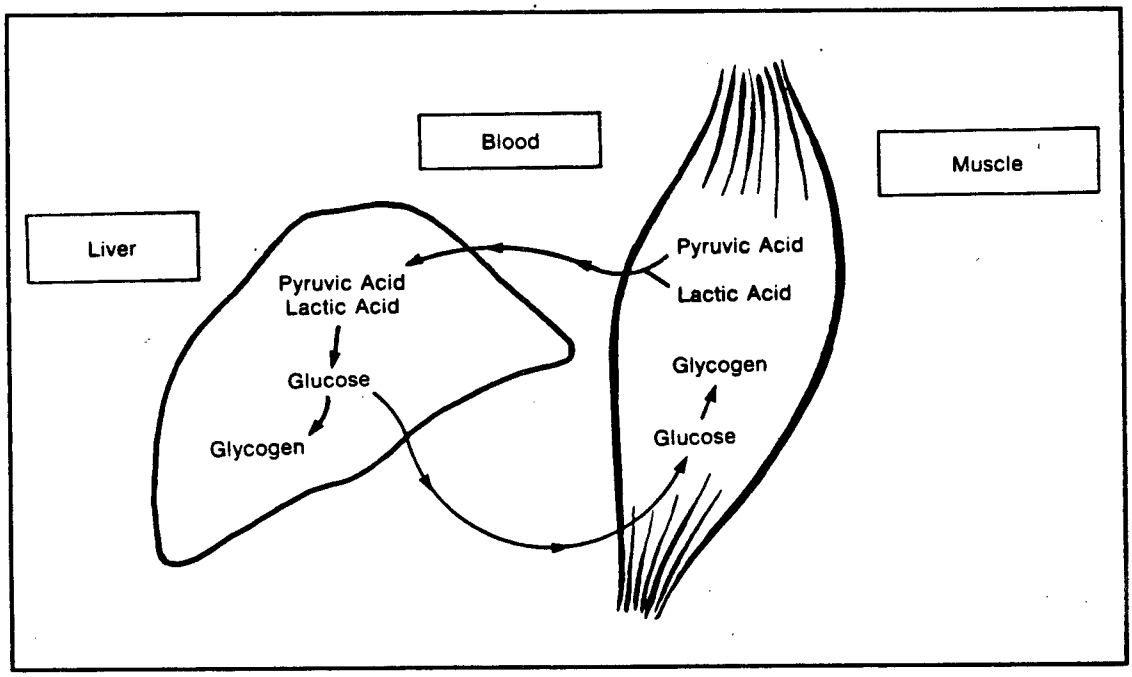

Figure 4-3 The Cori cycle provides for the removal of lactic acid formed in muscle with a resulting increase in available glucose.

Stored fat represents the body's greatest source of potential energy. The complete breakdown of a fat molecule yields 463 ATP molecules. Prior to energy release from fat, the triglyceride molecule is cleaved into glycerol and three fatty acid molecules. The mobilization of free fatty acids, or FFA, from adipose tissue is under hormonal control and the breakdown of fatty acids is directly associated with oxygen uptake. Oxygen must be available to accept hydrogen for the beta oxidation to proceed (Fig. 4-4).

Proteins can also serve as an important energy substrate. After nitrogen is removed from the amino acid molecule either in the liver or in the muscle, in the process of deamination, the remaining carbon skeleton can enter the Krebs cycle for the aerobic production of ATP.

Numerous interconversions are possible among the various food nutrients via the metabolic mill (Fig 4-5). For example, excess carbohydrates provide the glycerol and acetyl fragments for the synthesis of neutral fat. ; acetyl-CoA can also function as the precursor for the synthesis of cholesterol and many hormones. However, because the conversion of pyruvic acid to acetyl-CoA is not reversible, fatty acids cannot be used to synthesize glucose. Another interesting aspect of the metabolic mill is that the catabolism of fatty acids via the Krebs cycle depends on a continual supply of oxaloacetic acid, an intermediate furnished by glycolysis. To this extent, "fats burn in a carbohydrate flame".

The major means of ATP production differ depending on the intensity and duration of exercise. In intense exercise of short duration (100-yard dash, weight lifting), the energy is derived from the already present stores of intramuscular ATP and PCr. For intense exercise of longer duration (1-2 min), energy is generated mainly from the anaerobic reactions of glycolysis. As exercise progresses beyond several minutes, the aerobic system predominates and oxygen consumption becomes an important factor (Fig. 4-6).

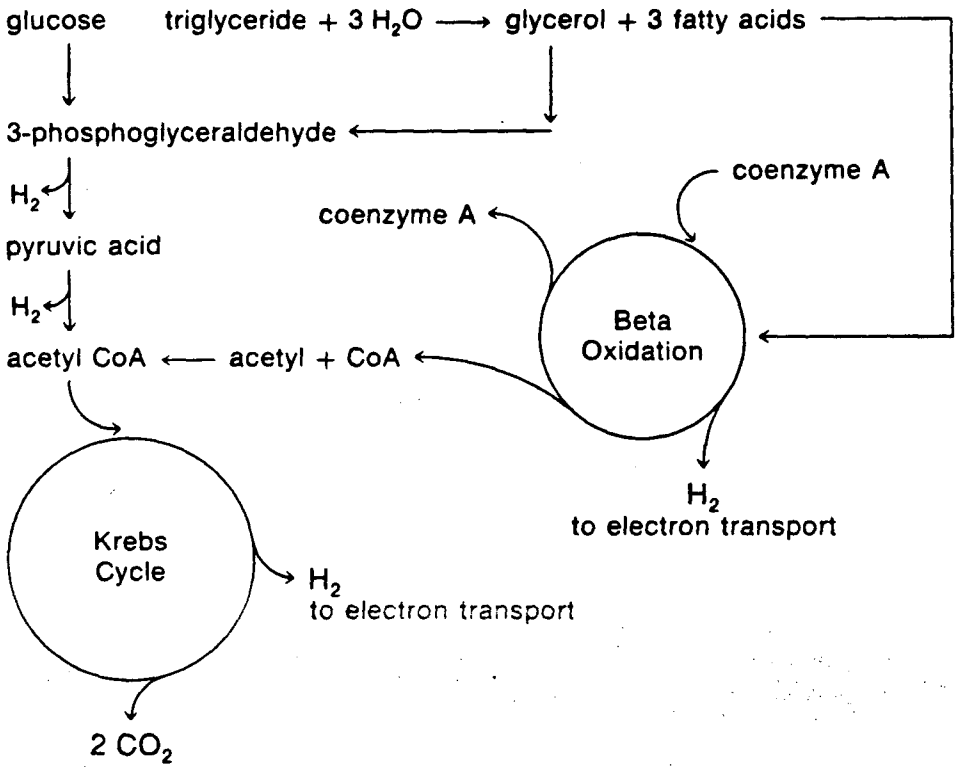

Source	Pathway	ATP Yield per molecule neutral fat
1 Molecule glycerol	Glycolysis + Krebs cycle	22
3 Molecules of 18-carbon fatty acid	Beta oxidation + Krebs cycle	441
		TOTAL 463

Figure 4-4 General scheme for the degradation of the glycerol and fatty acid fragments of neutral fat.

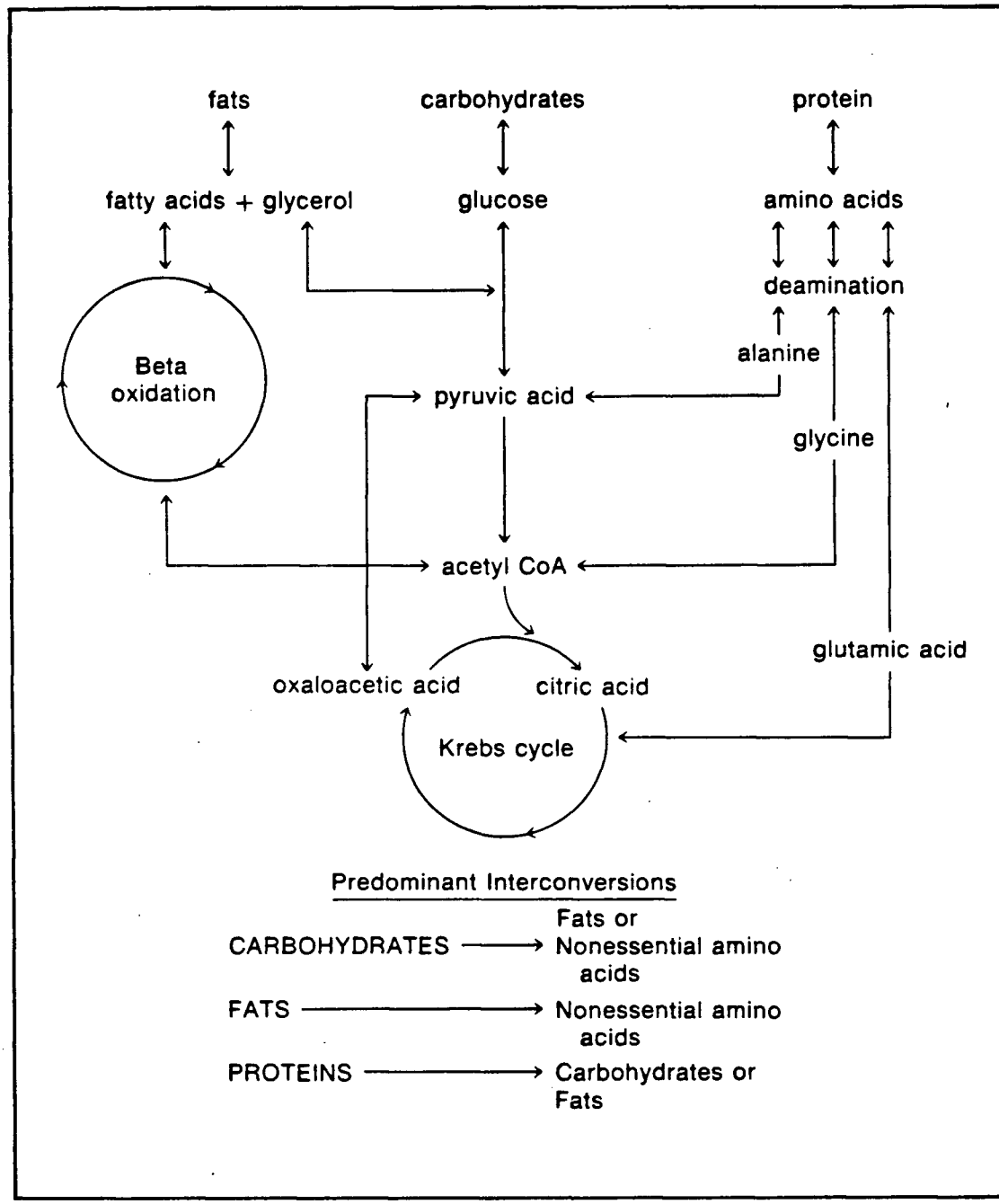

Figure 4-5 The metabolic mill: interconversions between carbohydrates, fats, and proteins.

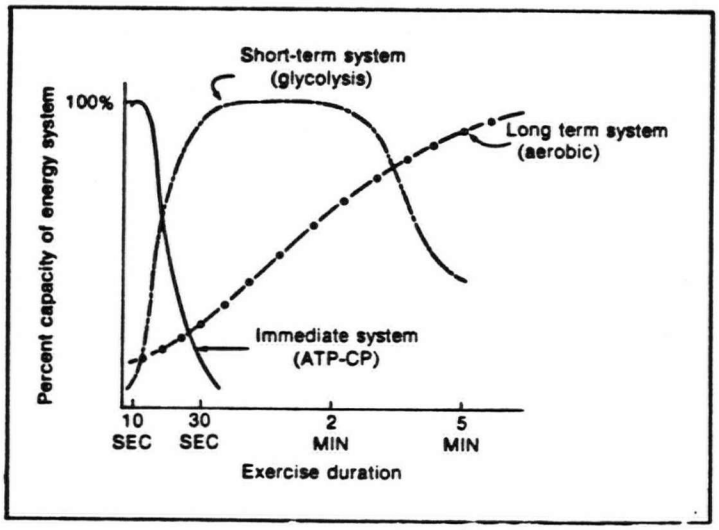

Figure 4-6a The various energy systems and their involvement during all-out exercise of different durations (after J. Appl. Physiol. 21:1662, 1966).

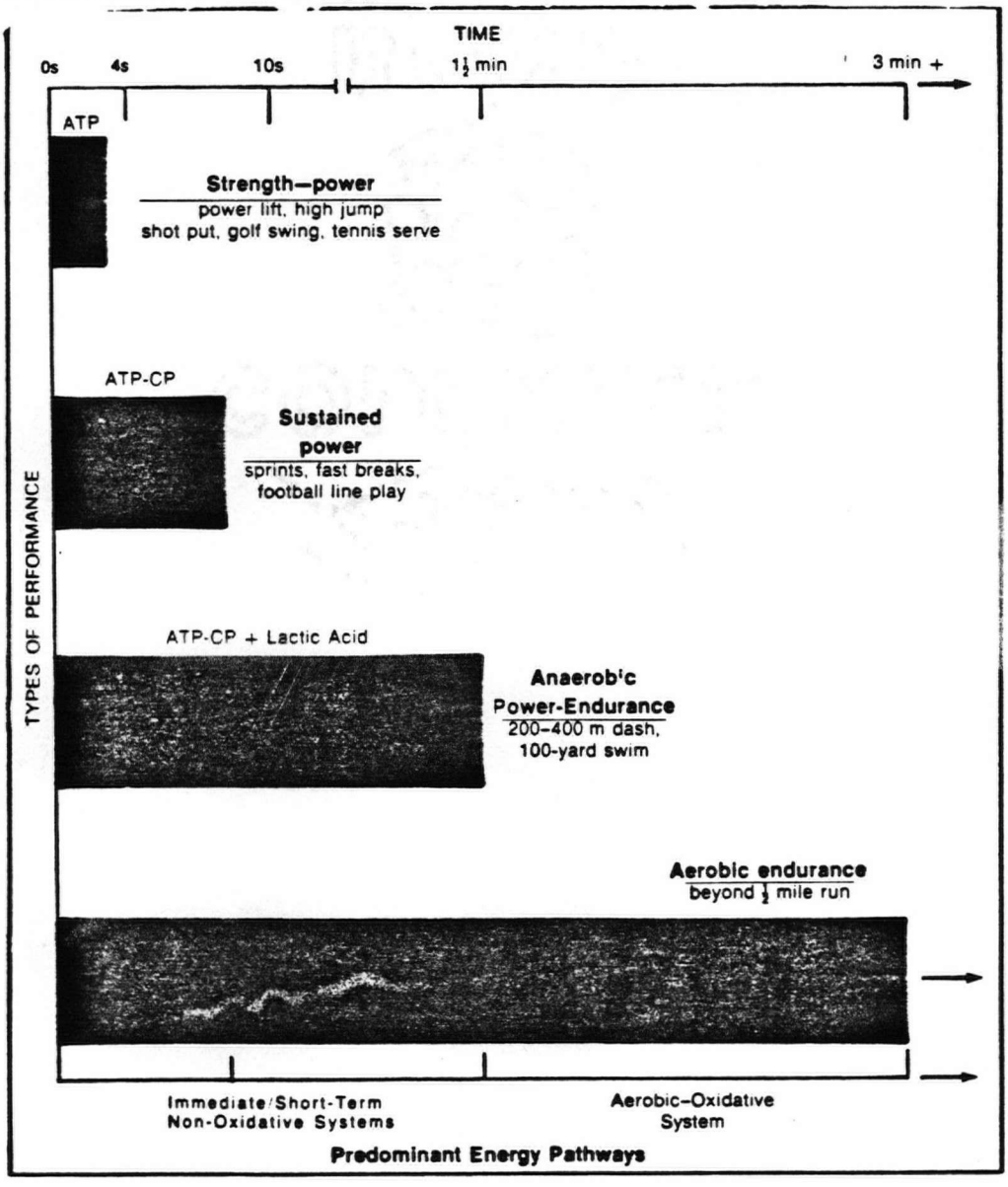

Figure 4-6b Classification of activities based on duration of performance and the predominant intracellular energy pathways (after J. Appl. Physiol. 38:151, 1975).

According to the "surface area law", energy metabolism required to maintain vital functions in the waking state (basal metabolic rate) is proportional to the surface area of the body. Figure 4-7 reveals that basal metabolic rate is influenced by age and is about 5 to 10% lower in women than in men. This is due to largely the fact that women generally possess more body fat than men of similar size, and fat is metabolically less active than muscle (6). Besides, environmental factors also influence resting metabolic rate. For example, the resting metabolism of people in a tropical climate is generally 5 to 20% higher than that of their counterparts living in a more temperate area. Different organs use different amounts of oxygen during rest and exercise. At rest, muscles require about 20% of the total oxygen uptake. During exercise, however, the oxygen uptake of skeletal muscle increases 100 times above rest; this represents close to 85% of the maximal oxygen uptake.

4.1.3 Skeletal Muscle(7-9)

Skeletal muscle is encased in various wrappings of connective tissue (Fig. 4-8). These eventually blend into and join the tendinous attachment to bone. This harness enables muscles to act on the bony levers to transform the chemical energy of ATP into mechanical energy and motion.

Surrounding each muscle fiber is the sarcolemma. The aqueous protoplasm or sarcoplasm of the muscle fiber contains the contractile proteins, enzymes, fat and glycogen particles, the nuclei, and various specialized cellular organelles. Embedded within the sarcoplasm is an extensive interconnecting network of tubular channels and vesicles known as the sarcoplasmic reticulum. Each muscle fiber is a single cell, multinucleated, long, and cylindrical in shape. The muscle fibers are made up of fibrils or myofibrils (approximately 1 micron in diameter), which are further divisible into individual filaments. The filaments are

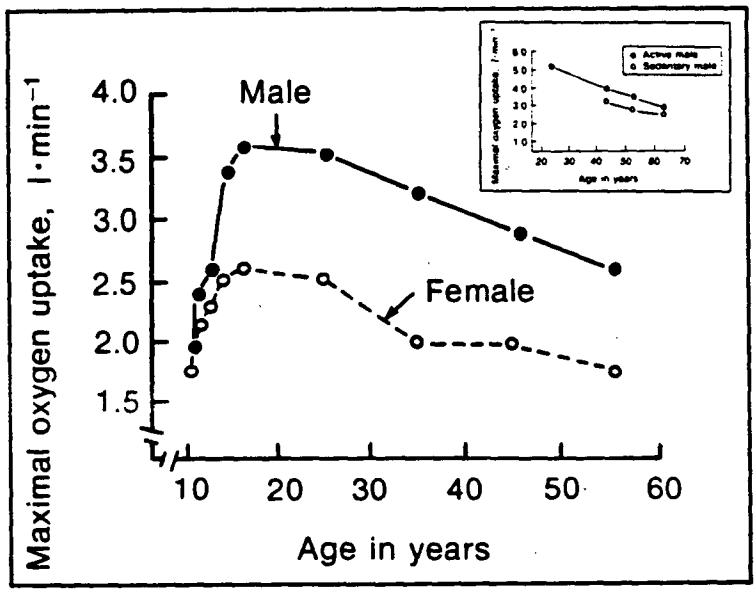

Figure 4-7 Maximal oxygen uptake as a function of age and level of activity in male and female subjects. (From L. Hermansen, Individual differences. In Fitness, Health, and Work Capacity. International Standards for Assessment. Edited by L.A. Larson, Macmillan Publishing Co., New York, 1974.) The insert graph was taken from P.O. Astrand, and K.R. Rodahl, Textbook of Work Physiology, McGraw-Hill Book Co., New York, 1970.

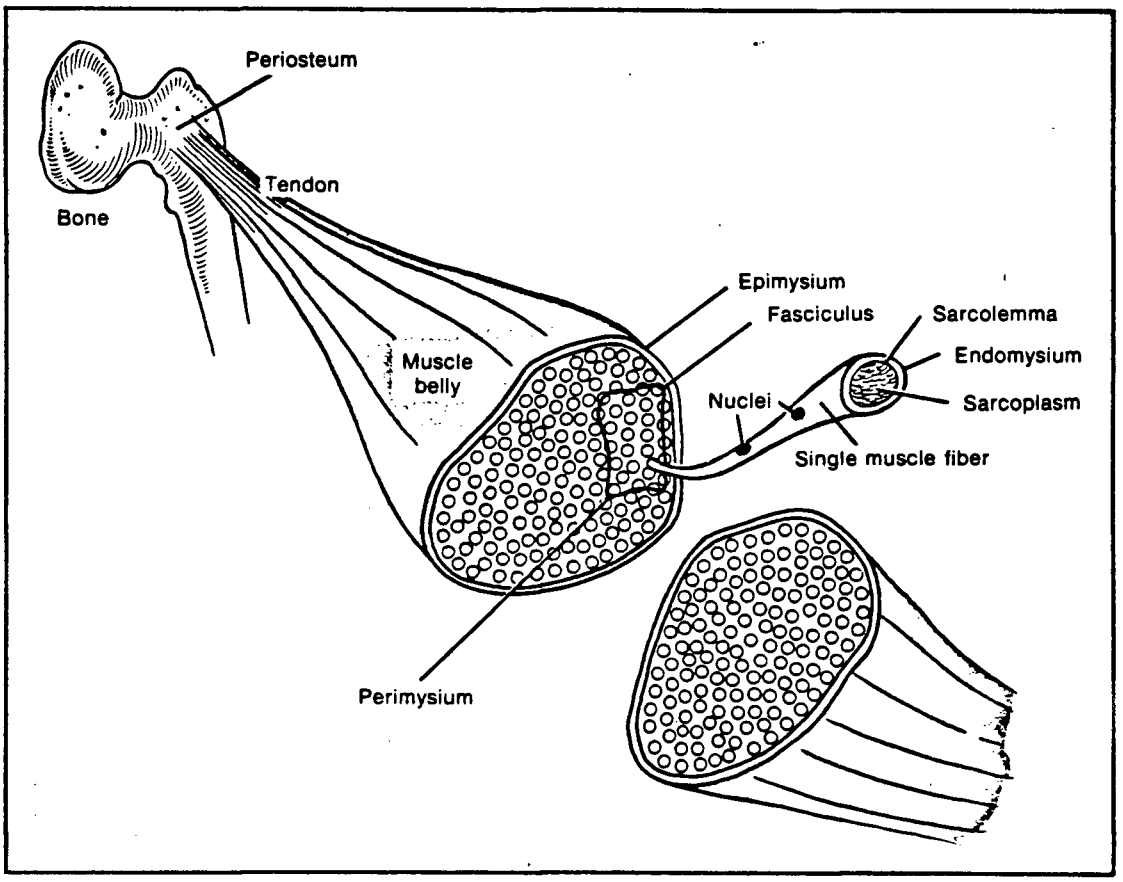

Figure 4-8 Cross section of a muscle and the arrangement of connective tissue wrappings. The individual fibers are covered by the endomysium. Groups of fibers called fasciculi are surrounded by the perimysium, and the entire muscle is wrapped in a fibrous sheath of connective tissue, the epimysium. The sarcolemma is a thin, elastic membrane that covers the surface of each muscle fiber.

made up mainly of two proteins, actin and myosin, that account for about 84% of the myofibrillar complex. Six other proteins, which have either a structural function or a significant effect on the interaction of protein filaments during contraction, are: tropomyosin (5%), troponin (3%), α-actinin (7%), β-actinin (1%), M protein (<1%), and C protein (<1%).

The cross-striations characteristic of skeletal muscle are due to differences in the refractive indexes of the various parts of the muscle fiber (Fig. 4-9). The lighter area is referred to as the I band, whereas the darker zone is known as the A band. The Z line bisects the I band and adheres to the sarcolemma to give stability to the entire structure. The sarcomere, the area between two adjacent Z lines, is the functional unit of the muscle cell. The thick filaments, which are about twice the diameter of the thin filaments, are made up of myosin; whereas, the thin filaments are made up of actin, tropomyosin, and troponin. The actin and myosin filaments within the sarcomere are primarily involved in the mechanical process of muscular contraction. The thick myosin filaments are lined up to form the A bands, while the array of thin actin filaments forms the less dense I bands. The center of the A band contains the H zone, a region of lower optical density due to the absence of actin filaments in this area. The central portion of the H zone is bisected by the M line, which consists of the transversely and longitudinally oriented protein structures that support the arrangement of the myosin filaments. If a transverse section through the A band is examined, each myosin filament is found to be surrounded by 6 actin filaments in a regular hexagonal pattern (Fig. 4-10).

Tropomyosin is distributed along the length of the actin filament in a groove formed by the double helix. Its function is to inhibit actin and myosin interaction or coupling and prevent them from permanent bonding. Troponin, which is embedded at fairly regular intervals along the actin strands, has a high

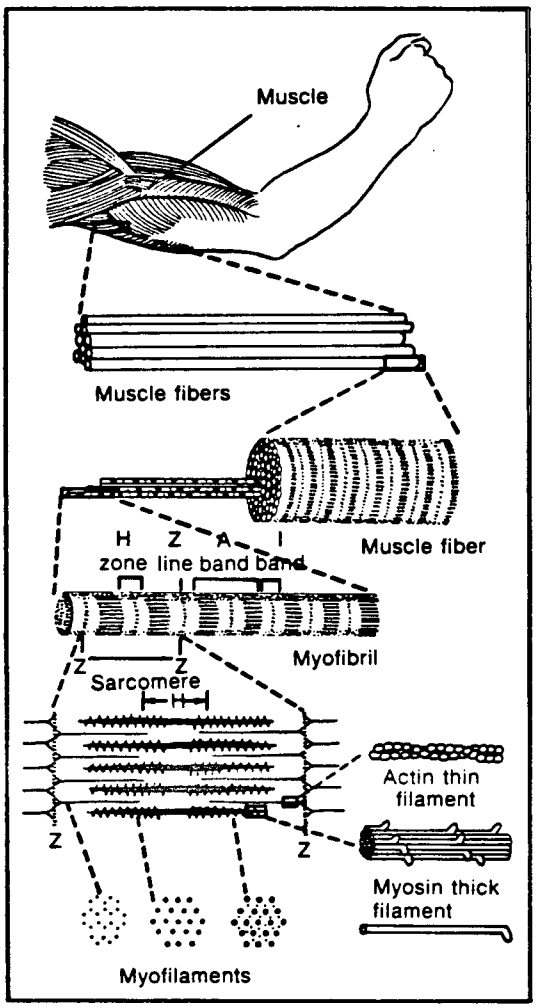

Figure 4-9a *Microscopic organization of skeletal muscle. The whole muscle is composed of fibers; these in turn are made up of myofibrils, of which the actin and myosin protein filaments are a part. If viewed under a microscope, magnification would be approximately 205,000 ×. (From Vander, A.J., Sherman, J.H., and Luciano, D.S.: Human Physiology, 2nd ed. New York, McGraw-Hill, © 1976.)*

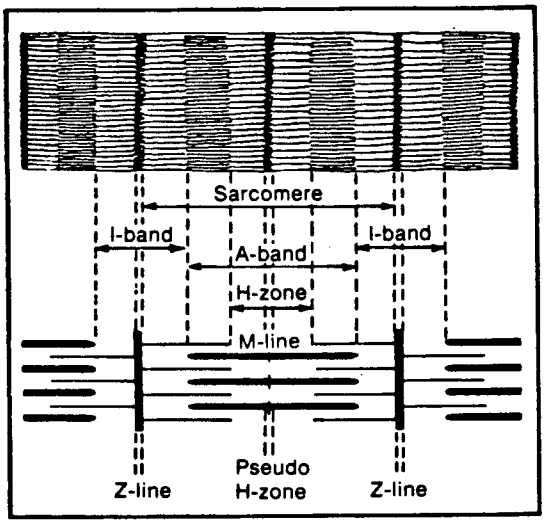

Figure 4-9b *Structural position of the myofilaments in a sarcomere. A sarcomere is bounded at both ends by the Z line. In a single muscle fiber consisting of 4500 sarcomeres, there are approximately 16 billion thick and 64 billion thin filaments. (From Huxley, H.E.: The Mechanism of Muscular Contraction. Copyright © 1965 by Scientific American, Inc.)*

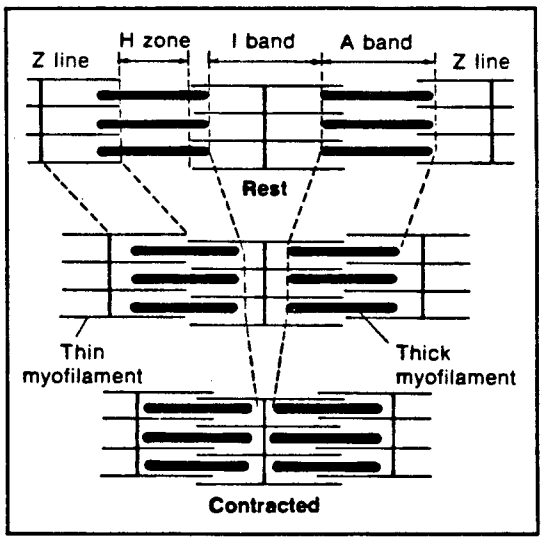

Figure 4-9c *Structural rearrangement of actin and myosin filaments at rest and during contraction.*

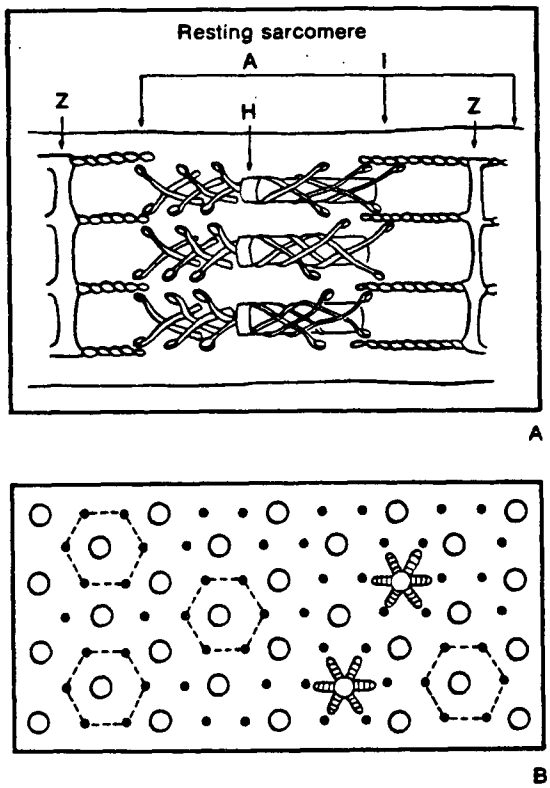

Figure 4-10a (A) Ultrastructure of actin-myosin orientation within a resting sacromere. (B) Representation of electron micrograph through a cross section of myofibrils in a single muscle fiber. Note the hexagonal orientation of the smaller actin and larger myosin filaments, as well as an example of the cross-bridges that extend from a thick to thin filament.

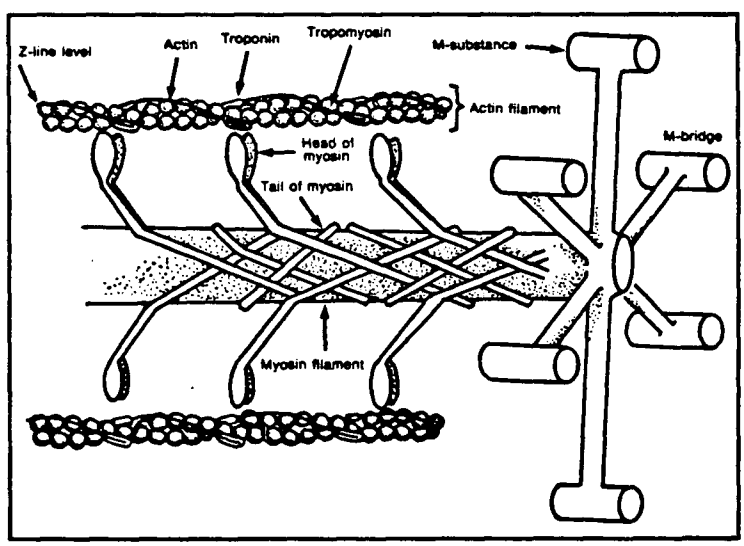

Figure 4-10b Details of the thick and thin protein filaments, including tropomyosin, troponin, and the M line. The myosin ATPase is located on the globular head of the myosin; this "active" head frees the energy from ATP to be used in muscle contraction. (From D.W. Edington, and V.R. Edgerton, The Biology of Physical Activity, Houghton Mifflin Company, New York, 1976)

affinity for calcium ions (Ca^{2+}). It is the action of Ca^{2+} and troponin that triggers the fibrils to interact and slide past each other. When the fiber is stimulated, the troponin molecules appear to undergo a conformational change that in some way "tugs" on the tropomyosin protein strand, moving it deeper into the groove between the two actin strands. This action "uncovers" the active sites of the actin and allows contraction to proceed.

An extensive network of interconnecting tubular channels, the sarcoplasmic reticulum, lies parallel to the fibrils. The lateral end of each tubule terminates in a saclike vesicle that stores Ca^{2+}. Another network of tubules known as the transverse tubule system or T-system runs perpendicular to the fibrils. The space between the 2 layers of the T-system is an extension of the extracellular space. The function of the T-system is the rapid transmission of the action potential from the cell membrane to all the fibrils in the muscle. The sarcoplasmic reticulum and the T-system come in contact at the junction of the A and I bands. At these junctions, the arrangement of the central T-system with sarcoplasmic reticulum on either side has led to the use of the term triads to describe the system, which appears to function as a microtransportation or plumbing network for spreading the action potential from the fiber's outer membrane inward to deep regions of the cell (Fig. 4-11).

According to the "sliding filament theory", a muscle fiber shortens or lengthens because the protein filaments slide past each other without changing their length. The muscular contraction and relaxation sequence (Fig. 4-12a) begins with the initiation of an action potential by the motor nerve. This impulse is then propagated over the entire surface of the muscle fiber as the cell membrane becomes depolarized: (a) the muscle action potential depolarizes the transverse tubules at the A-I junction of the sarcomere; (b) the depolarization of the transverse tubules causes Ca^{2+} to be released from the lateral sacs of the

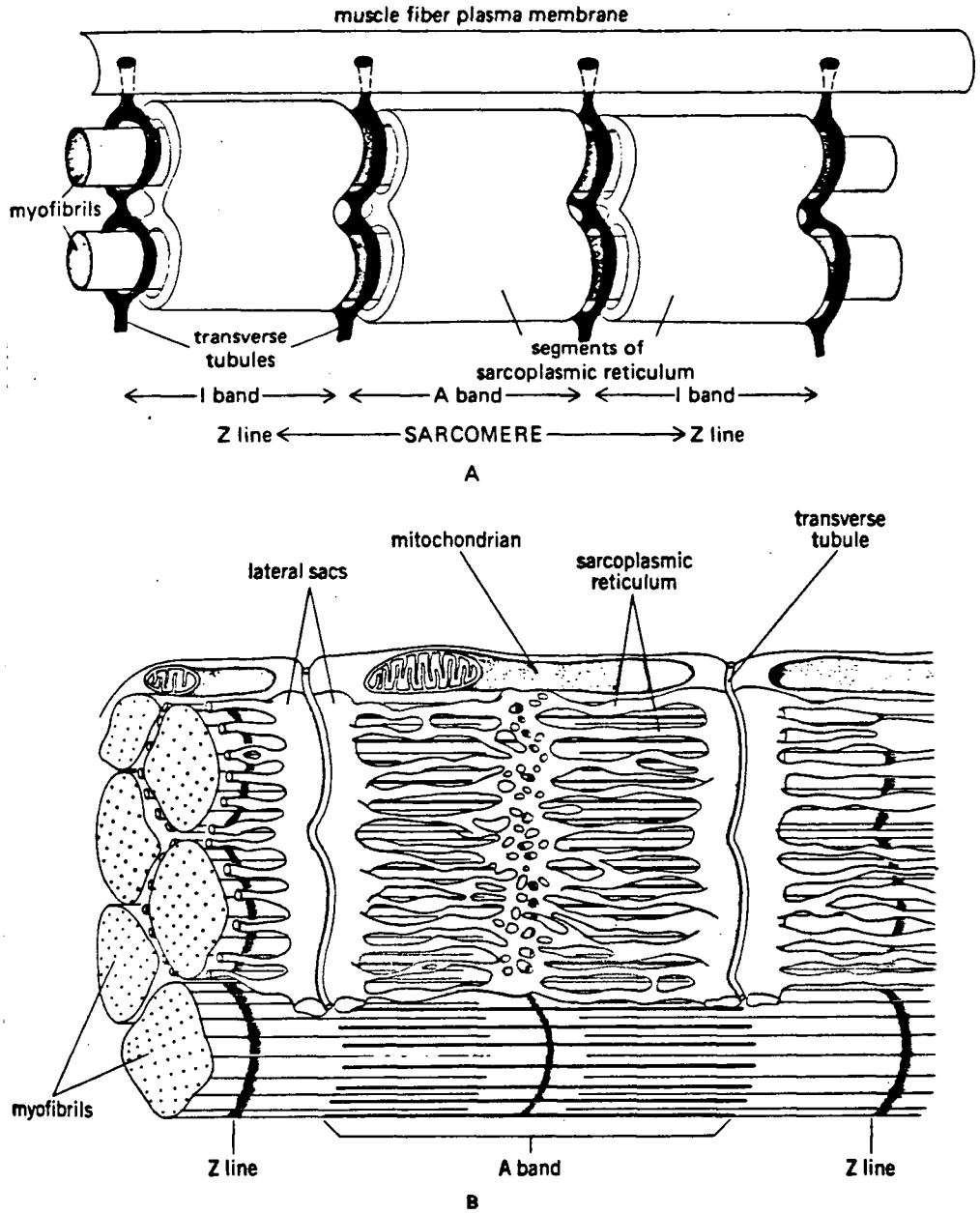

Figure 4-11 (A) Diagrammatic representation of the geometrical relationships between the membranes of the sarcoplasmic reticulum, the transverse tubules, and the myofibrils. (B) Three-dimensional view of transverse tubules and sarcoplasmic reticulum in human skeletal muscle.

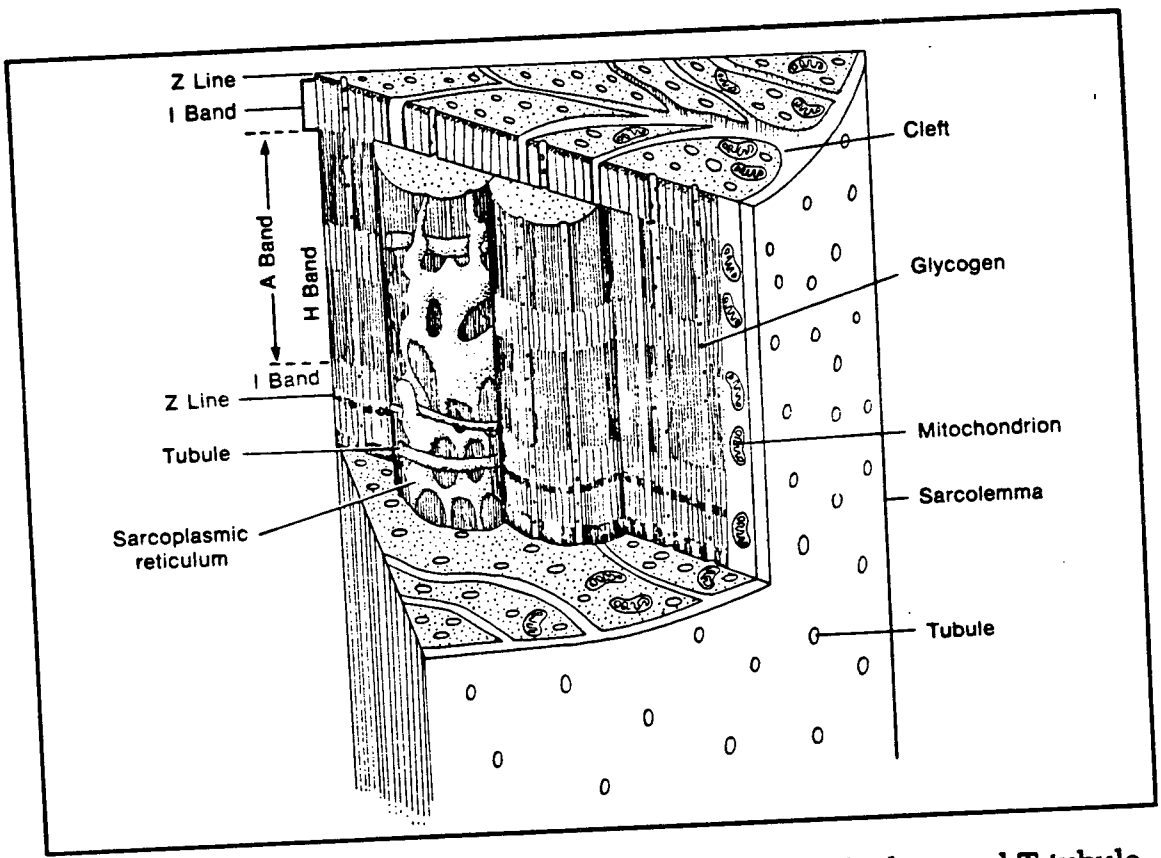

Figure 4-11 (C) Three-dimensional view of sarcoplasmic reticulum and T-tubule system within the muscle fiber. (From H. Graham, How is muscle turned on and off? Sci. Am. 222:84, 1970)

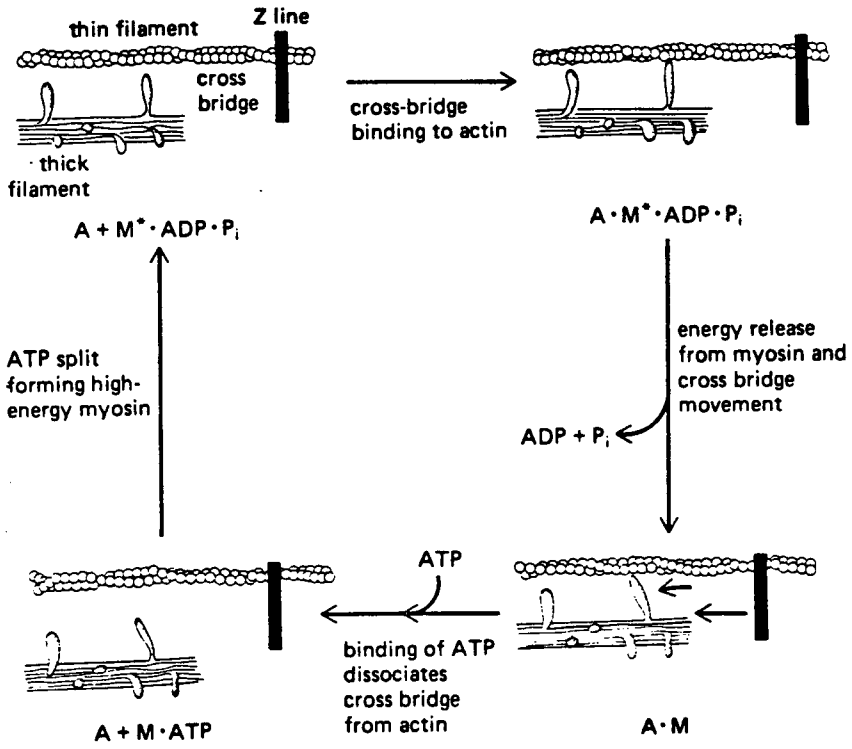

Figure 4-12a Chemical and mechanical changes during the stages of a single cross-bridge cycle. The cycle starts at the relaxed fiber in the upper left.

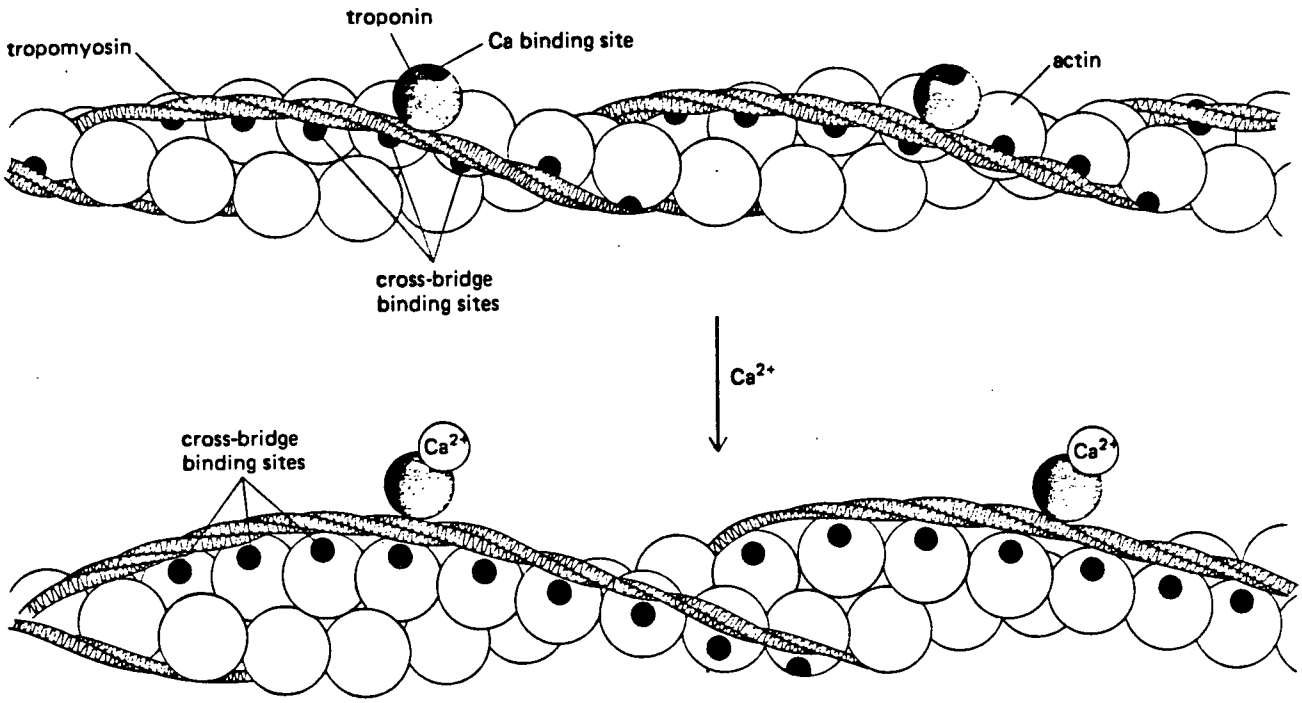

Figure 4-12b In the absence of calcium, tropomyosin blocks the cross-bridge sites on actin. Binding of calcium to troponin moves the tropomyosin to one side, exposing the binding sites and allowing cross bridges to bind to the thin filament.

sarcoplasmic reticulum; (c) Ca^{2+} ions bind to troponin-tropomyosin in the actin filaments, thus, releasing the inhibition that prevented actin from combining with myosin (Fig. 4-12b); (d) actin combines with myosin and activates the ATPase, which then splits ATP to provide the energy required to facilitate movement of the actin-myosin cross-bridge, as well as to create tension; (e) ATP breaks the actin-myosin bond by binding to the myosin bridge, and subsequently leads to a relative movement or sliding of the thick and thin filaments past each other and the muscle shortens; (f) cross-bridge activation continues as long as the concentration of Ca^{2+} remains high enough to inhibit the action of the troponin-tropomyosin system; (g) when the muscle is no longer stimulated, Ca^{2+} ions are actively pumped back into the lateral sacs of the sarcoplasmic reticulum; (h) the removal of Ca^{2+} ions restores the inhibitory action of troponin-tropomyosin, and actin and myosin remain in the dissociated, relaxed state.

4.1.4 Muscle Fibers

Muscle is an excellent tissue to work with because, compared with most internal organs, it is relatively homogeneous. However, muscle contains connective tissue, adipose tissue, and different fiber types, which complicates data interpretation.

Precise control of muscle force is essential for all movements, including normal daily activities and sport. This control is achieved through an extensive interaction between different input from several levels in the central nervous system. The force and speed of the contraction is determined by the number of motor units activated (recruitment) and by the firing rate of the motoneurones involved (often referred to as rate coding). By blending these two factors, optimal patterns of neural discharge permit a wide variety of graded contraction. According to the size principle, motor units are recruited in a fixed order: the

neurones with small, slowly conducting axons innervating slowly contracting, fatigue-resistant muscle fibers are recruited at low tension, and with increasing tension also the larger, rapidly conducting axons innervating rapidly contracting, fatigable muscle fibers are activated (10-14). In general, rapidly contracting muscle fibres in human have faster contraction/relaxation rates and higher actomyosin ATPase activities (15) which are approximately double those of slowly contracting muscle fibres. Many everyday activities are carried out with a low force of contraction in which the firing frequency of the motor neurons and muscle cells is likely to be 10-30 Hz (16-18). In maximal contractions the frequency may briefly rise to over 100 Hz (19) but after a second or two will settle down to 50-80 Hz.

Three fiber types in human skeletal muscle have been classified by staining methods for actomyosin ATPase (20-22) and by enzyme assays for lactate dehydrogenese and adenylate kinase in single fibers (23-24). By both types of methods, three major groups of muscle fibers have been identified:
(a) slow-twitch (type I) red fibers, rich in oxidative enzymes and poor in enzymes of glycolysis (i.e. low glycolytic capacity, and high oxidative capacity);
(b) intermediate fast-twitch (type IIA) fibers, with substantial amounts of both oxidative and glycolytic enzymes; and
(c) fast-twitch (type IIB) white fibers, rich in glycolytic enzymes and low in oxidative enzymes (i.e. high glycolytic capacity, and low oxidative capacity).
Type I and type IIA fibers provide the endurance capability for prolonged exercise; whereas type IIB glycolytic fibers supply ATP rapidly but are unable to maintain the ATP level and consequently fatigue readily.

Fast-twitch muscle fibers have a high capability for the electrochemical transmission of action potentials, a high activity level of actomyosin ATPase, and a rapid level of calcium release and uptake by the sarcoplasmic reticulum, all of

which relate to their ability to generate energy anaerobically for quick, forceful contractions. On the contrary, slow-twitch fibers generate energy for ATP resynthesis predominantly by means of the relatively long-term system of aerobic energy transfer. They are distinguished by a low activity level of actomyosin ATPase, a slow speed of contraction, and a less well developed glycolytic capacity. The slow-twitch fibers, however, contain relatively large and numerous mitochondria and myoglobin, which give their characteristic red pigmentation. Accompanying this enhanced metabolic machinery is a high concentration of mitochondrial enzymes required to sustain aerobic metabolism (15,25-27).

The recruitment of oxidative and glycolytic fibers has been studied (15,27-31). It was concluded that the oxidative muscle fibers type I and possibly some intermediate type IIA, are recruited first at low work loads (using 20% of maximum strength) (11,14,32-33); and the fast-twitch glycolytic fibers, type IIB, are predominantly recruited when the work load is raised to 40% of maximum strength (33-34).

The existence of various fiber types makes skeletal muscle an extremely heterogeneous tissue. Their combination in varying distributions creates conditions for a large diversity of muscles and helps to explain the ability of skeletal muscle to meet various functional demands. Thus, the overall properties of a given muscle depend primarily on its fiber composition. However, biochemical analyses of dissected single fibers have shown that these histochemically defined fiber types can no longer be envisaged as entities but a continuum. It has become evident that histochemical fiber type classification may delineate only gross categories because of the large spectrum of contractile and metabolic properties. The existence of a variety of myofibrillar protein isoforms

in various combinations in different fibers points to a much greater heterogeneity than previously imagined (35).

Edstrom and Kugelberg (36) found that fibers belonging to the same motor unit are metabolically uniform as judged by qualitative histochemistry. They also observed that the fatigability of the motor units was inversely correlated with their aerobic-oxidative capacity. Because it can be assumed that fibers of a given motor unit are uniformly activated, these results support the idea that phenotypic expression in muscle fibers is under neural control (35,37). The coexistence of metabolically different fibers in a given muscle, therefore, reflects differences in activity and recruitment of different motor units. Indeed, motor neuron firing patterns are of primary importance in determining expression of muscle fiber phenotypes (38).

It is tempting to speculate that the coexistence of metabolically different fibers reflects still another meaning, i.e. that of metabolic symbiosis. Thus, metabolically different fibers might be functionally linked by diffusible common metabolites. Among these, lactate might be an interesting candidate with regard to its different metabolic roles--end product in one fiber, substrate for terminal oxidation in a second, and glucogenic precursor in a third. The presence of a metabolic spectrum of fibers, therefore, greatly complicates metabolic studies of whole muscle. Obviously, each fiber represents a separate metabolic compartment, and it is not known whether interfiber communication exists.

4.1.5 Muscle Biochemistry and Control

The rationale for the biochemical/mechanical transfer function, the function that relates work to the concentration of the control chemicals, approach of Chance lies in the Michaelis-Menten relations:

$$V/V_{max} = 1/\{1+(K_m/[C])\} \qquad (4\text{-}1)$$

where V is the observed velocity or work (because the velocity of an enzymatic reaction is equal to work), V_m is the maximum velocity and varies with pH in a typical bell-shaped curve symmetrical about the physiological pH (39), K_m is the Michaelis-Menten constant, and C is the control chemical chemical regulating enzyme activity. According to Chance (40), the steady concentration of the control chemical must lie within the bounds of its K_m; while other non-controlling chemicals must lie above the K_m value. Empirical P-31 NMRS observation of undetectable ADP and readily detectable P*i* *in vivo* in human forearm (41), strengthens the support of ADP as the primary control of oxidative metabolism (42-43), even though control of metabolism by P*i* was long advocated (44-45). However, quantitative measurements *in vitro* have shown the concentration of P*i* is somewhat more than its K_m of 1 mM. On the contrary, the concentration of ADP is only a small fraction of its K_m. In functional activity, the ATPase produces equal amounts of ADP and P*i* from splitting ATP causing ADP to rise 50 times more in relation to its K_m than in the case of P*i*, thus ensuring that the primary control will be that exerted by ADP.

Two assumptions permit quantification of P-31 NMRS data and their use in predicting the metabolic fate of muscle: (a) a steady-state exists in the living systems whereby the generation of ATP equal to its consumption (40-41); (b) the creatine kinase system is in equilibrium. As long as these two conditions hold, the phosphorylation potential (the capability to do metabolic work), and the velocity of ATP generation in relation to the maximum velocity can be calculated (knowledge of V/V_{max} allows determination of the adequacy of ATP generation and the ability of the system to respond to additional metabolic demand):

$$PCr + ADP + H^+ \text{<------>} ATP + Cr \qquad (4\text{-}2)$$

$$[ADP] = \{[ATP]\,[Cr]\} \,/\, \{K_1\,[PCr]\,[H^+]\} \qquad (4\text{-}3)$$

for $[H^+]$ = constant, [ATP] ≈ constant, $[\Delta Cr] = [\Delta Pi]$, equation 4-3 becomes:

$$[ADP] = [Pi] / [PCr] \quad (4\text{-}4)$$

$$H^+ + ADP + Pi <------> ATP + H_2O \quad (4\text{-}5)$$

$$\text{phosphorylation potential} = [ATP] / \{[ADP]\,[Pi]\} \quad (4\text{-}6)$$

substitute the equations 4-4 into 4-6 gives:

$$\text{phosphorylation potential} = [PCr] / [Pi]^2 \quad (4\text{-}7)$$

The basic equation for oxidative phosphorylation of ATP is:

$$3ADP + 3Pi + NADH + H^+ + 1/2\,O_2 \text{ ------> } 3ATP + NAD^+ + 4H_2O \quad (4\text{-}8)$$

The relative V/V_{max} can be expressed by an extended steady state Michaelis-Menten equation for multiple noninteracting controls:

$$V/V_{max} = 1/\{1 + (K_1/ADP) + (K_2/Pi) + (K_3/O_2) + (K_4/NADH)\} \quad (4\text{-}9)$$

Under the conditions of oxygen deprivation, NADH will be in excess of K_4 and *Pi* will be in excess of K_2. Thus equation 4-9 can be rewritten as:

$$V/V_{max} = 1/\{1 + (K_1/ADP) + (K_3/O_2)\} \quad (4\text{-}10)$$

If, as stated above, creatine kinase is in equilibrium, the ADP can be estimated from PCr/*Pi*, so that resultant equation is:

$$V/V_{max} = 1/\{1 + K'_1 + ([PCr]/([Pi]) + (K_3/O_2)\} \quad (4\text{-}11)$$

Equation 4-11 clearly shows that under conditions of limited oxygen supply, *Pi*/PCr ratio increases. When V approaches V_{max} and metabolic controls become "quasi stable"; ATP homeostasis fails and ATP becomes depleted, resulting in a rapid irreversible loss of ATP to AMP and adenine, with the formation of hypoxanthine.

4.1.6 Muscle Fatigue

Fatigue is the loss of force consequent to muscular exercise, particularly during submaximal intermittent contraction. However, much evidence suggests that the physiologic events underlying fatigue commence very early, well before the loss of force. The site and mechanism of fatigue have remained a subject of controversy over the last century.

4.1.6.1 Site of Fatigue

Since the generation of a voluntary contraction involves the whole pathway from the brain to the contractile machinery, the various potential sites of fatigue (defined as failure to sustain force or power output) can be divided into three broad categories: (a) those which lie within the central nervous system (CNS), (b) those concerned with neural transmission from CNS to muscle, and (c) those within the individual muscle fibers.

4.1.6.2 Muscle Contractile Failure

Loss of contractile machinery of muscle due to destructive disease processes, as in the dystrophies, or disuse atrophy (without gross destruction) after immobilization of a limb after a fracture (46), or in metabolic myopathies due to steroids, hypo- or hyperthyroidism or vitamin D deficiency (47), is far more important than either of the other two mechanisms.

Skeletal muscle is analogous to an engine. It converts chemical energy to heat and work. Thus, when the energy supply cannot meet the energy demand, fatigue ensues. Slow muscle, which has a high oxidative potential, is less susceptible to developing fatigue than fast muscle (48-50). Thus, there is often obvious atrophy of the Type II muscle fibres. The substances directly involved in the transformation of chemical energy into mechanical work in skeletal muscle

are ATP, ADP, inorganic phosphate (P*i*), hydrogen ions (H^+), magnesium ions (Mg^{2+}), and phosphocreatine (PCr). Using nuclear magnetic resonance spectroscopy, Dawson *et al* (51) showed that PCr breaks down progressively; and creatine, ADP, and H^+ levels rise while ATP, the direct source of energy, is reduced by only 25%. The latter finding is consistent with the results obtained in normal subjects performing dynamic exercise until exhaustion (52). The increase in energy demands in excited muscles is provided mainly by the combustion of fats, blood glucose, and glycogen of the working muscles. The association of glycogen depletion with fatigue of the skeletal muscles (53) is well established. As the muscle fatigues, the concentration of ADP, P*i*, and H^+ increase considerably; and due to product accumulation, ATP breakdown is slowed, resulting in the decline of muscle force. In addition, perhaps, there is also a rate-limiting step in utilizing the blood-borne fuels.

Historically, lactic acid accumulation has received great attention as the culprit of fatigue in the skeletal muscles. The effect of lactic acid on force generation is believed to be mediated by lowering pH. At low pH, Ca^{2+} is sequestered in the sarcoplasmic reticulum (54), and a larger amount of Ca^{2+} is needed to produce a given tension. In addition, hydrogen ions exert a direct negative effect on the contractile process itself (55).

To summarize, glycogen depletion, lactic acid accumulation, inability to utilize blood-borne substances, and decrease in the rate of ATP hydrolysis are merged to explain the loss of force, but the exact interplay of all these factors is not yet identified in skeletal muscle.

4.1.6.3 Neuromuscular Transmission Failure

When a nerve muscle preparation is stimulated continuously, failure of propagation between nerve and muscle may occur presynaptically at nerve

terminal branches, postsynaptically from a decrease of end-plate excitability, or from excessive depletion of ATP in human muscle leading to rigor mortis (56-58). Conventional EMG techniques (59) are well suited to investigate these conditions and confirmation of a positive result can often be obtained by administration of an anticholinesterase, e.g. edrophonium.

4.1.6.4 Fatigue of CNS

It has always been recognized that much of the reduction in capacity to generate force or power output (which we call fatigue) may result from reduced neural drive (60). In addition, it is well established that fatigue is characterized not only by loss of force but also by slowing of the muscle contractile speed. For any muscle or motor unit the minimum excitation frequency required to generate force and tetanic fusion is proportional to its contractile speed. Thus, if during fatigue the degree of contractile slowing matches the decline in motoneuron firing rate, the latter does not result in any additional reduction in muscle force. Motoneuron firing rates may be inhibited by a reflex originating from the muscle in response to one of the many changes that fatigue induces, although the nature of such reflex is yet unknown. Such an adaptation would be rather beneficial; it would avoid the failure of electrical propagation associated with high-frequency fatigue as well as the complete depletion of vital chemicals within the muscle cell, which might otherwise occur if high firing rates were maintained.

4.1.6.5 Summary

As fatigue ensues, contractile slowing increases (61) and central discharge firing decreases, either as fatigue of the CNS (62) or adaptation to the altered chemistry and/or contractile characteristics of muscles, which may prevent their self-destruction by excessive activation. Thus fatigue may be caused by

inhibition of motoneurons and fatigue of the neuromuscular transmission and of the muscle fibres.

4.2 Clinical Results

There have been a number of reports of the use of Nuclear Magnetic Resonance Spectroscopy of muscle in the study of Mitochondrial Myopathy and Encephalomyopathy. These have described spectroscopic parameters of muscle at rest, as well as in exercise, and in subsequent recovery. Theoretically one might imagine that the most effective means of demonstrating subtle defects in energy metabolism would be to examine the system under duress. Such exercise studies however have been somewhat difficult to standardize and frequently possible in only a limited number of patients. Furthermore, patients tested generally appear to have had obvious muscle involvement and it is not clear how specific the abnormalities reported are when compared to other myopathies. Clinically it would be useful to diagnose more subtle changes such as in patients with CNS disease without apparent muscle involvement, in screening relatives of mitochondrial patients, in the work-up of fatigue patients, and in the assessment of new therapies. We present here modifications to previously described techniques which attempt to improve sensitivity by addressing the physiological and biochemical inhomogeneity of muscle through a more detailed analysis of the contractile output. At the same time the technique remains necessarily tractable enough for routine clinical use.

There are instances where a single, spectroscopic measurement will provide valuable clinical data, such as acquiring a resting spectrum, which measures the basal metabolic activity; these have been proven to be capable of distinguishing abnormalities in some patients. However, more conclusive result

can be obtained by measuring metabolic depletion rates in terms of P*i*/PCr ratio either directly, or more generally in response to some intervention, or stress test. More specifically, almost all the investigations on muscle metabolism and energetics in disease rely on the following changes in the concentration of high energy phosphates and in the pH values, in response to exercise (dynamic and isometric) and during the recovery phase after exercise.

4.2.1 Materials and Methods

Spectroscopy P-31 MRS measurements were made using a 1.9 Tesla Oxford Instruments magnet with a 30 cm. horizontal bore, and a console operating at 32.5 MHz. for P-31, adapted from a Nicolet NT-300 system and a Nicolet 1280 computer with a 293C pulse programmer. Spectra were collected as 2K data points using a sweep width of +/- 2000 Hz., a pulse width of 35 microseconds, and a relaxation delay of 1 sec; for resting studies 192 acquisitions were averaged, for dynamic studies 32. Peak heights were used for quantification; the rationale for this was given in Chapter 3 of this Thesis. Signal saturation with these parameters produced about 55-65% peak attenuation but, as P*i* and PCr were similarly affected, their ratio was affected far less (<10% overestimate of P*i*/PCr); because this effect was constant between experiments and between individuals we therefore did not correct for it.

Mechanical Analysis The technique used is a modification of that developed by Chance in which the rate of biochemical work involved in exercising muscle is related to the mechanical output of that muscle. As in Chance's analysis, the biochemical parameter is given by the ratio of the concentrations of inorganic phosphate to phosphocreatine (P*i*/PCr). Our mechanical parameter, however, is the "accelerating force" generated by the muscle, normalized to the cross-

sectional area of the forearm. We have found the "Accelerating Force" a more dependable parameter, probably because it accounts for some of the physiological variables not represented by a strict Newtonian analysis based on Work Rate (40,63). For example, in single-fibers energy efficiency drops with increasing twitch velocity. In whole muscle, Type II fiber recruitment increases with increasing contraction velocity, and efficiency again must suffer with this increase in glycolytic representation.

The experimental procedure involved use of the forearm finger-flexors to lift weights at a frequency of 1 Hz. via a pulley, with an in-line force transducer (Figure 4-13). Force output was displayed on an analogue plotter and also digitized and processed on an IBM AT computer. The IBM signal was filtered with a 3 Hz low-pass 3DB cut-off which reproduced the dynamic performance of the plotter. The "accelerating force" was taken as the mean of peak-to-peak excursions during each period of spectral acquisition. If the total tension recorded by the force transducer for a mass "m" is represented by:

$$T = mg + ma \qquad (4\text{-}12)$$

where" mg" equals the force due to gravity, and" ma" the force required to move that mass with an acceleration "a", then "ma" is the "accelerating force".

Spectra were acquired every minute using a 4 cm. diameter resonator surface coil located beneath the muscle bellies of the finger-flexors, until a "steady-state" was reached for that particular weight - usually 4 or 5 such spectral "acquisition periods" would make up a "weight run" which therefore typically would last 4 to 5 minutes. The criteria for steady state are described in the analytical methods below.

The coil was housed in a gantry which allowed it to be moved in 3 dimensions to provide an iteritive search for the region of maximal biochemical involvement as described in Chapter 3 of this Thesis; usually this would involve

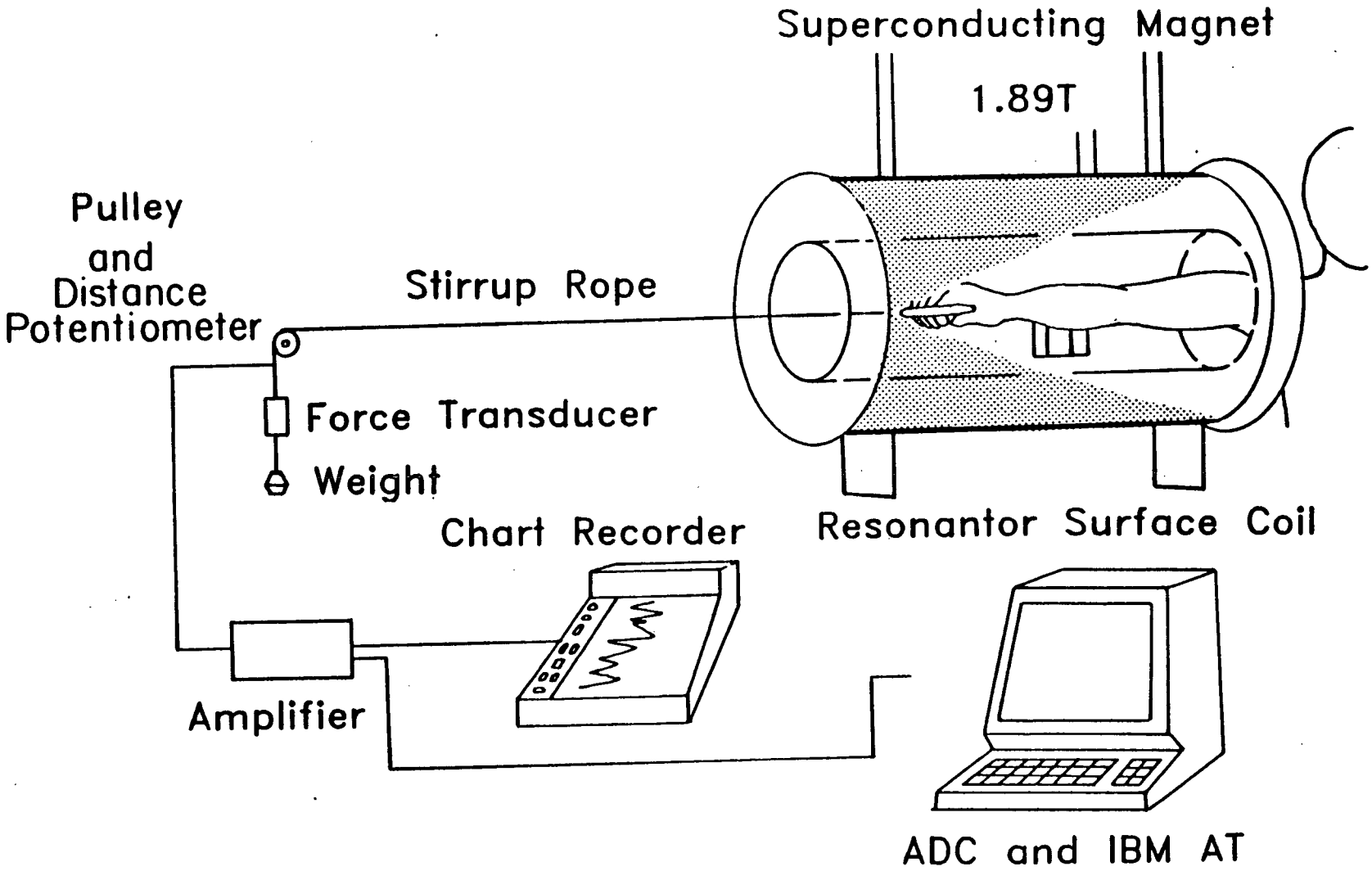

Figure 4-13 Mechanical aspects of the exercise experiment.

at least one weight run to confirm optimal coil positioning. A series of weight runs were conducted with each patient using increasingly heavy weights until Pi/PCr ratios greater than 1 were recorded. From this series of experiments a regression plot of Pi/PCr vs Force was constructed from which the force corresponding to a Pi/PCr ratio of 1 was interpolated. We refer to this point as the Isophosphate Force or the F1 value, which represents the accelerating force generated per unit area of muscle when Pi/PCr = 1.

Recovery sequences were also recorded for all patients starting immediately after the end of the last weight run, and with spectra collected every 45 seconds. Thus each sequence represents recovery from a standardized level of intracellular depletion as patients have completed the same protocol up to a Pi/PCr level of approximately 1.

Subjects 25 normal subjects were used with a mean age of 28 years and the age range was 16-70, and 23 patients with mitochondrial disease of different types were examined. 7 had muscle disease alone, 16 had mitochondrial encephalomyopathy. 10 have had full oxidative studies of their own muscle or that of an affected family member, performed by Dr. Nancy Kennaway *et. al.* of Portland Health Science Hospital (unpublished results). All patients had ragged red fibres on normal Gomori Trichrome staining and most had ultrastructural changes of mitochondria on electron microscopy.

Analytical Methods This study was designed prospectively to explore whether or not a formalized analysis of mechanical output using the accelerating force could provide reproducible and sensitive diagnostic criteria for mitochondrial disease while still remaining tractable enough for clinical use.

All data from the NMR and mechanical variables were processed on a PC together with the patient's arm circumference and grip strength. For each patient a linear regression of all Pi/PCr vs Normalized Force points which satisfy steady state criteria is constructed. "Steady-state" is calculated as those points within any weight run whose Pi/PCr ratio does not differ by more than $\pm$ 0.2 from a line of the same approximate slope as the regression line; this allows for parallel changes in force output with Pi/PCr during a weight run.

4.2.2 Results

Accelerating Force vs Work 3 studies were done in which the same weight was lifted once a second with different degrees of vigor. "Vigor" here means that the weight is lifted at a higher velocity for a shorter time The "Newtonian" work rate was calculated as the change in potential-energy of the system per second due to the lifting of the weight. This was obtained from the product of the mass and the mean distance travelled during the time of a spectra collection. The results show that the cellular energy state is very sensitive to the vigor (i.e. velocity of contraction). This is not reflected in the Newtonian work rate but is well represented by the Accelerating Force.

Normals vs Mitochondrial Myopathy The F1 values for 23 mitochondrial patients and 25 controls are shown in Fig 4-14a. The correlation coefficients for the linear regressions used to obtain these F1 values averaged 85%. The plot in Fig 4-14b is a box and whisker plot which demonstrates the distribution of values; each box represents the middle 50% of values, the whiskers representing the upper and lower quartiles, and the middle line the median. Although this is not a Gaussian distribution, there is excellent separation between groups and, using non-parametric statistics it can be shown that one may be 95% confident

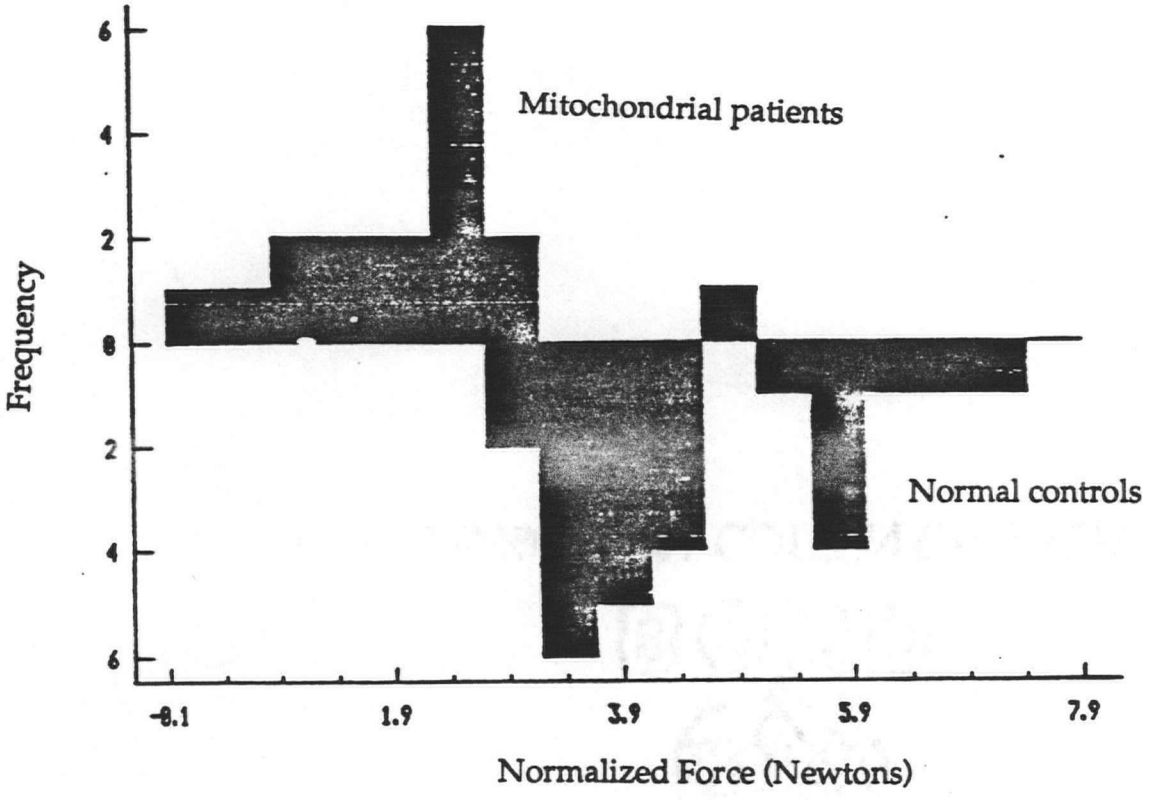

Figure 4-14a Frequency Histogram of F1 (Efficiency) of normal controls (lower) vs mitochondrial patients (upper).

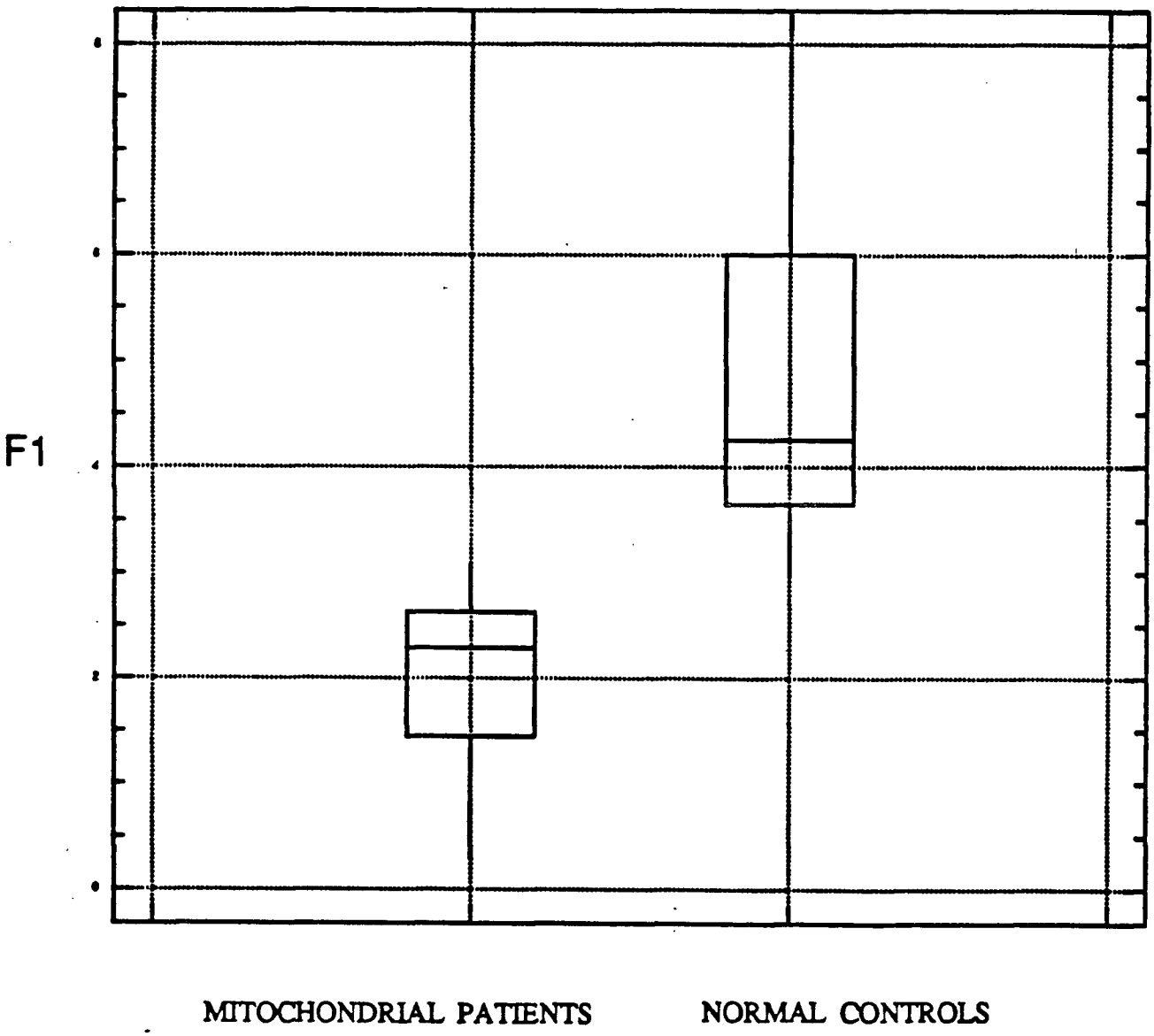

Figure 4-14b The Box and Whisker plot of F1 values depicts medians and quartiles and shows graphically the good seperation between normal controls and mitochondrial patients.

that 90% of normal values fall above the lowest normal value, which is 3. Using a break-point of 3 we examined the sensitivity and selectivity of the F1, and compared this to the sensitivity and selectivity of the resting P*i*/PCr for patients for whom both values were available:

Table 4-1 Sensitivity and Specificity of the F1 value and/or the resting Pi/PCr ratio for detecting abnormality among patients

	Sensitivity	**Specificity**
F1	87%	100%
Pi/PCr	73%	100%
Both	67%	100%
Either	100%	

If we compare the maximum grip strength of patients and controls with their F1 values, there is no significant correlation in either group. For a given grip strength, however, the mitochondrial patients have about half the F1 i.e. the F1 does not reflect weakness but, as hoped, an index of bioenergetic efficiency.

Concerning tractability, an F1 value was obtainable in 14 of 16 of the patients over the age of 13; failure occurred due to excessive dystonia in one patient, and a non-linear result in a another for whom a retest was never done. Testing was possible in only 3 of the 8 children who were large enough to fit in the machine; in general these children were severely affected and too demented to comply or too wasted to allow reasonable signal acquisition for dynamic studies. As a corollary of the more severe disease however they all also had very

abnormal resting Pi/PCr ratios. In another clinically normal child, on the other hand, who had two affected siblings, dynamic testing was straightforward and the abnormal F1 was in fact the first indication of disease which was subsequently proved on biopsy.

Therapy Monitoring Fig. 4-15 shows the Pi/PCr vs Force relation for a patient with mitochondrial encephalomyopathy which manifested in particular with episodes of stupor with transient neurological deficit. In the 18 months immediately prior to therapy she had been hospitalized 8 times. Following institution of high dose therapy with the cofactors riboflavin and nicotinamide she experienced a complete remission in these events, during which she had no relapse. After 18 months of treatment the therapy was withdrawn and a relapse occurred after 7 days; she recovered on reinstitution of therapy, then relapsed again 10 days after a second withdrawal. Her NMRS performance after both therapy withdrawals simultaneously decreased; the dotted lines represent the 95% confidence limits for the two regressions; the two lines are just separable at this level of significance.

Fig. 4-16 shows the same response for a patient with Mitochondrial Myopathy. Following an initial NMRS assessment 'OFF Rx' he began cofactor augmentation, and an 'ON Rx' response was recorded 60 hrs. later. He has continued to experience clinical improvement over the past 24 months, and this is also evident in his NMRS responses.

These observations cannot be generalized since clinical response varies from patient to patient and also depends on when these NMR examinations were conducted after the treatment. However, taking into account all of the information about a patient's treatment, it is possible to correlate NMR data to the therapeutic response. 6 other patients with various myopathies were

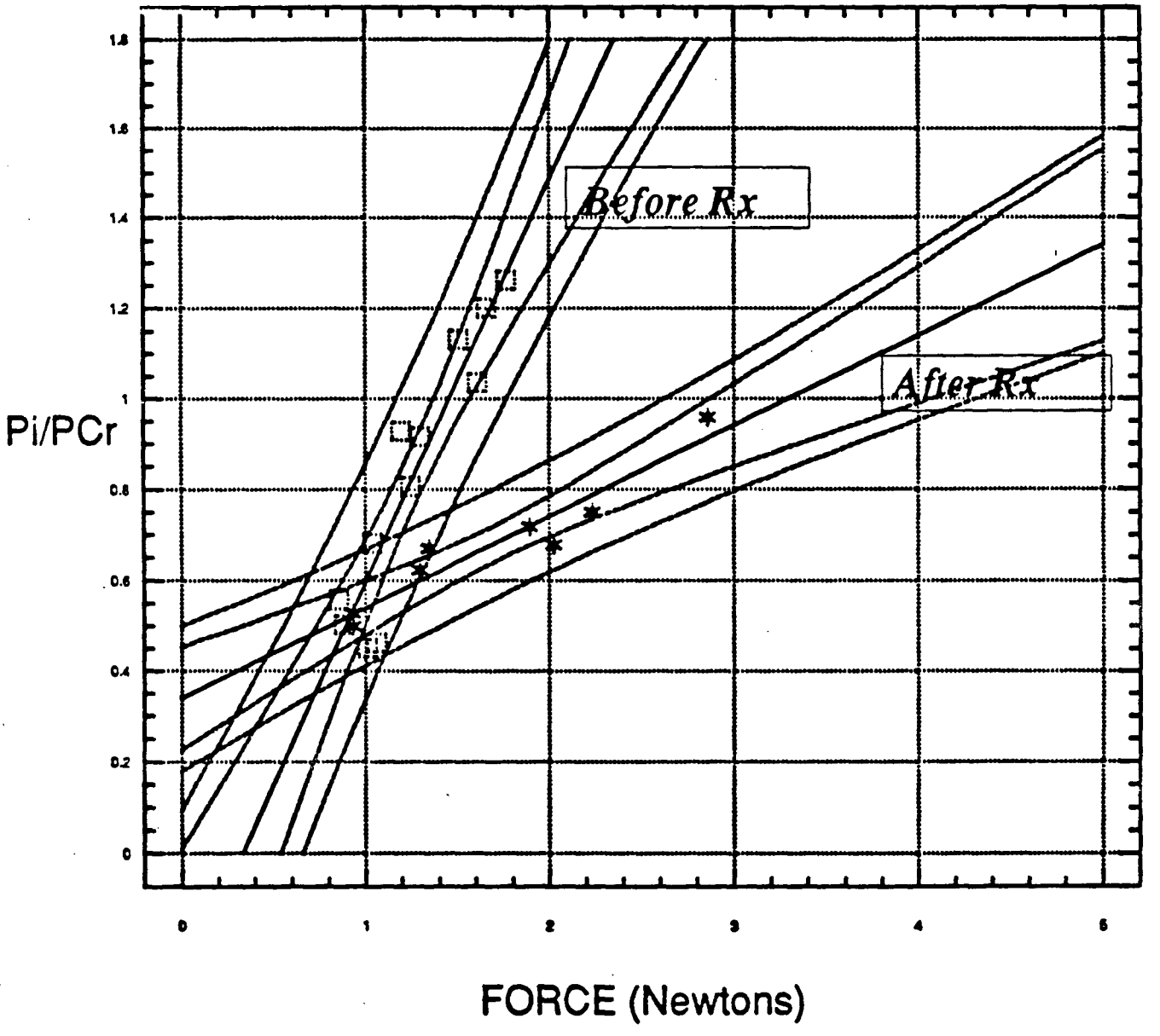

Figure 4-15 The Pi/PCr vs Normalized Force relation, before and after riboflavin/nicotinamide treatment for a patient with mitochondrial encephalomyopathy.

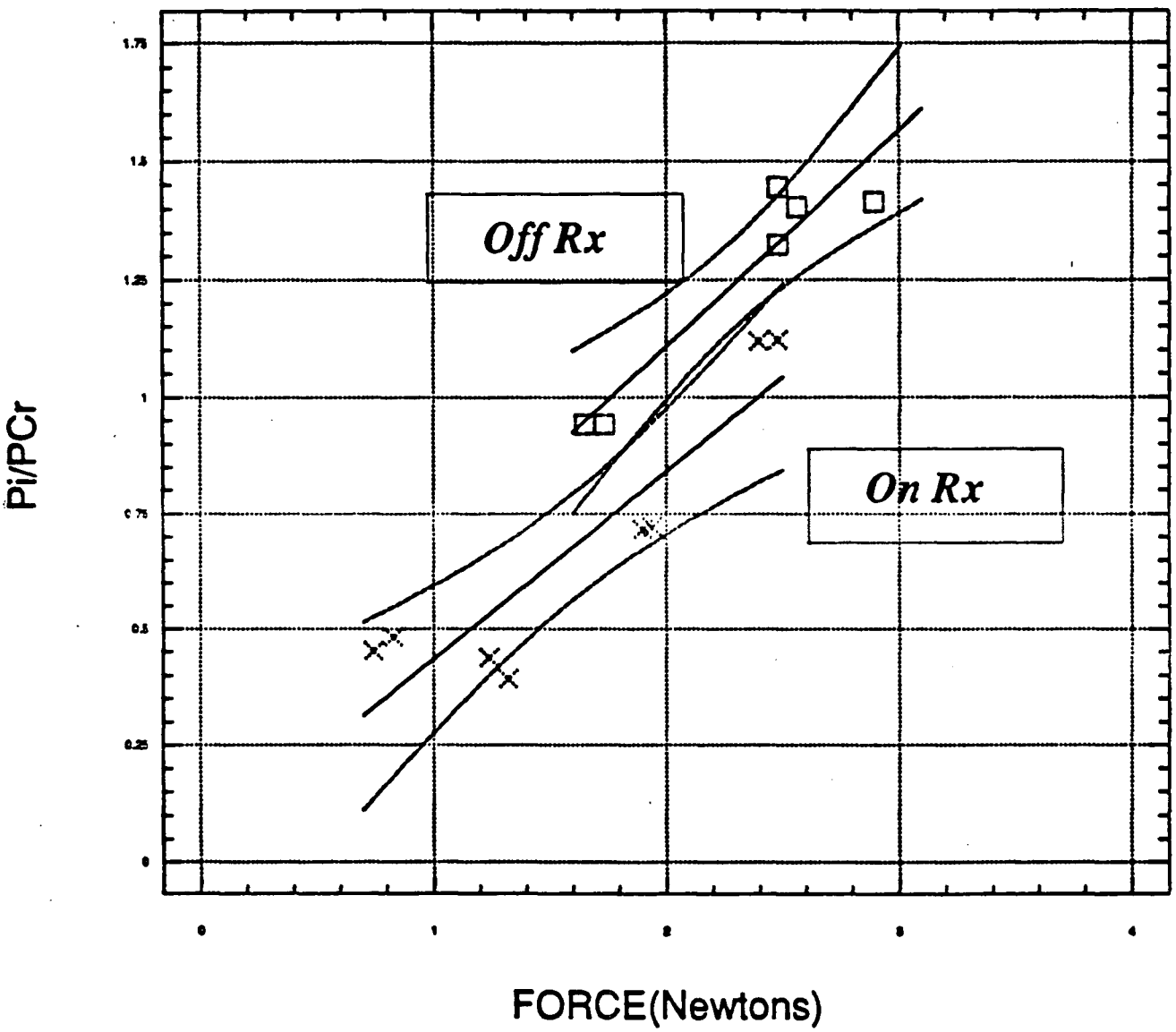

Figure 4-16 The Pi/PCr vs Normalized Force relation, before and after riboflavin/nicotinamide treatment for a patient with mitochondrial myopathy.

	Age	Clinical Features	Pi/PCr	F1	pHrest
1	43	Ex intol, cytochrome oxidase deficiency	0.20	1.45	7.06
		ON Rx: Improved subjectively.	0.21	3.29	7.06
2	31	Ex intol, encephalopathic spells, ocular pain.	0.14	1.75	6.96
		ON Rx: Marked improvement .	0.14	3.20	7.06
3	33	Ex intol, myoclonus, seizures,stroke-like spells.	0.16	1.55	7.01
		ON Rx: Cessation of spells and improved endurance.	0.20	2.73	7.00
4	47	Ex intol, short stature, involved son . Complex 1 deficiency?	0.26 +/-.035		6.98
		ON Rx: Improved endurance, weight gain	.199+/-.013		7.06
5	44	PEO,myopathy	0.19	3.07	6.92
		ON Rx: No convincing improvement.	0.15	4.86	6.98
6	19	PEO,RP,myopathy	0.19	2.29	7.00
		ON Rx: No convincing improvement.	0.21	2.38	7.00

Ex intol = Exercise Intolerance
PEO = Progressive External Opthalmoplegia
RP = Retinitis Pigmentosa

Figure 4-17 Clinical and spectroscopic responses to therapy.

monitored for their responses to riboflavin/nicotinamide therapy, all showed significant improvement in "F1" (Fig. 4-17).

4.2.3 Discussion

Peak heights were used for quantification in this study rather than peak areas. We have shown that this provides a reasonable estimate or correlate of the major phosphorous containing compounds as long as there is no inordinate peak broadening. It is more accurately estimated than peak area when working with the lower signal to noise ratios encountered in these short acquisition-time dynamic studies; it is also faster to measure which contributes to the tractability of the technique. There is no significant difference between our resting normative values (Fig. 4-18) and those in the literature (64) :

$$0.115 \pm 0.021 \quad \text{vs} \quad 0.117 \pm 0.031.$$

With dynamic studies, use of a "roving" coil minimizes peak broadening that may otherwise result from the superimposition of two different muscle bellies; restricting studies to the range of Pi/Pcr less than 1 has the same effect.

Like EMG, diagnostic criteria may be of no use if anatomic localization is wrong. Coil placement is an obvious priority for a reliable NMRS exercise exam. Readings from the wrong muscle will clearly underestimate the relative biochemical duress for the given output. This will overestimate the F1. The "roving coil" design largely overcomes this issue, however error will still occur and probably accounts for the occasional case in which no good linear response occurs. It will not produce an underestimate however. One can therefore miss a diagnosis but not make a false positive diagnosis because of it. This asymmetric bias may also explain the non-Gaussian distribution of the normal controls.

We have found the "accelerating force" to be a more dependable parameter than "work rate" probably because it accounts for some of the

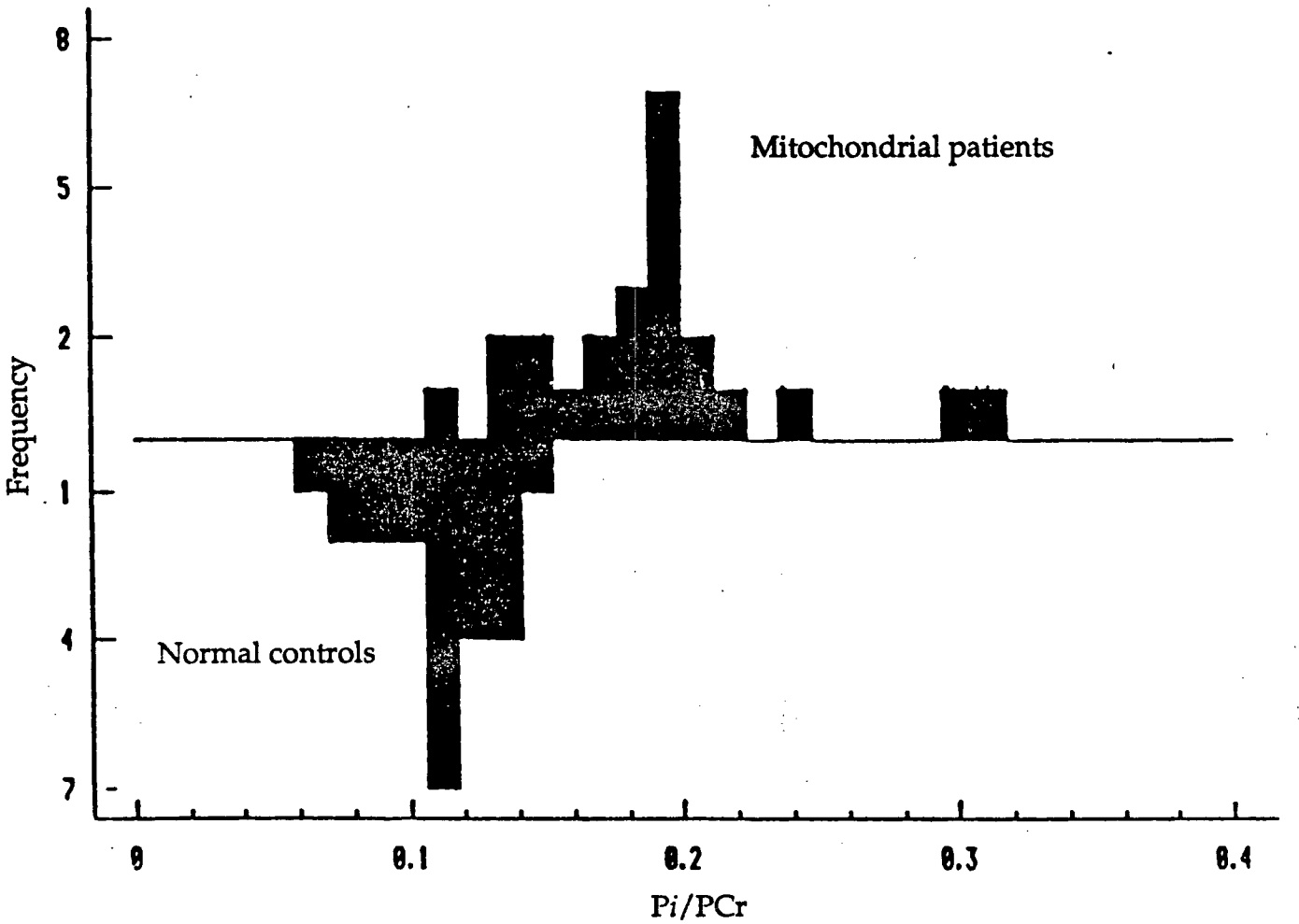

Figure 4-18 Frequency Histogram of resting Pi/PCr ratio for normal controls and mitochondrial patients

physiological variables not represented by a strict Newtonian analysis. Put more simply, in biological systems it matters not only how **much** work is done but also, **how** that work is done. This has been shown in single-fiber work where energy efficiency drops with increasing twitch velocity. Furthermore, it is well known that in whole muscle, Type II fibre recruitment increases with increasing contraction velocity and efficiency again must suffer with this increase in glycolytic representation. Though technically we are measuring the acceleration, the low-pass filtering used, partially integrates the signal weighting it towards velocity. Obviously this empiric analysis is only a first approximation. The true relationship between biochemical and mechanical work is a complex one with dependencies on excitation-contraction coupling, mechanical properties of the myofibril and musculo-skeletal apparatus, and the numerous bioenergetic reaction pathways, their substrate supply and metabolite egress. The next chapter will provide a model of this association more precisely based on the interrelated mechanical variables of acceleration, velocity and distance as well as inertial mass or isokinetic force. In the meantime the present representation provides a reliable and tractable first approximation.

The use of the *Pi*/PCr ratio related to Work stems from Chance's biochemical modelling of muscle contraction on the basis of Michelis-Menton kinetics. Though this is an elegant analysis it suffers from the problems of the heterogeneity of muscle. Our calculations were designed to give only some yardstick of the efficiency of muscle contraction per unit of cross-sectional area. Mitochondrial lesions affect primarily the economy of muscle contraction by shifting ATP generating mechanisms from the more economical aerobic pathways to the less economical but more robust anaerobic ones. This means more substrate must be consumed per mole of ATP produced and more lactate generated. Presumably as well to bring these anaerobic reactions into play the

various equilibria including the CPK and ATP reactions must be pushed farther to the right. This would then be observed as a higher than normal Pi/PCr ratio for a given output of ATP. ATP consumption is related to mechanical output and therefore presumably why we see higher Pi/PCr ratios for given mechanical outputs (i. e. lower efficiency curves) in mitochondrial disease. Theoretically however muscle could solve its reduced ATP generating dilemma merely by increasing the number of mitochondria. This is in fact known to occur in mitochondrial disease. This however would still only accentuate the problem of economy putting higher demands on substrate supply and metabolite generation. Once again this is observed in mitochondrial disease where increased stores of glycogen and lipid are seen histologically, and higher rates of lactate extrusion are suggested from spectroscopic and blood analysis. Nonetheless one might expect that our technique would not detect any change in efficiency of muscle contraction, in a situation in which small defects in ATP generating economy were rectified by increased numbers of mitochondria. A more sensitive index might be the absolute throughput of substrate. This too could be measured spectroscopically using saturation-transfer techniques or proton spectroscopy.

We had chosen to normalize the accelerating force to the cross-sectional area of the forearm. This decision was based on the knowledge that contractile force is proportional to the cross-sectional area of muscle. Though we could have used the maximum grip strength instead, such a variable is too dependent on patient effort, a particular problem with some fatigue patients and those with ataxia. The data bear this out as a comparison of F1 values normalized by grip strength separates normals from mitochondrial patients poorly.

In representing the dynamic performance of the muscle we have chosen to interpolate a single value from a regression curve which we call the F1 value. There are a number of practical reasons for choosing this parameter:

(a) A plot of Pi/PCr vs Force usually produces an inflection point at a Pi/PCr ratio of approximately 1, but below this point the relationship is reasonably linear.

(b) This region has the best precision in the assessment of Pi/PCr, since both these NMR resonances (and therefore their signal-to-noise ratios) are large.

(c) This procedure does not require driving the muscle to high output levels at which longer lasting fatigue mechanisms may set in, confounding subsequent testing. The total work period usually amounts to 5 consecutive five minute work periods interspersed with about the same duration of rest and at forces between 5% and 25% maximal contraction strength, though always in rhythmic non-sustained contraction.

(d) Though the suggestion by other groups of calculating a Vmax and Km has more biochemical appeal, it requires Michaelis-Menton kinetics from a rather complex system. Even if the biology complies to this extent, the patient may not with the increased experimental burden. In practice one may frequently make a decision on a patient's exercise performance at the time of testing; for example, if a normalized output force of 4 is being produced and the Pi/PCr still lies below 1 the test will be normal, i.e. the F1 value is sure to lie well above the lower limit of normal which with our data is 3.

We were able to obtain an F1 value in 88% of patients over the age of 13. In children between the age of 6 and 13, an F1 value was obtained in only 38% of cases. The usual corollary of a paediatric presentation is that of more severe disease, in which case it may not be as necessary to have the exercise study to augment the resting studies. For those patients below the age of 6 we use resting spectra alone and, when the arm is not big enough, we collect spectra from the calf muscle; a different normative range however applies to this muscle.

These results therefore suggest that this exercise technique can be used tractably in routine examination of patients with muscle complaints. When used in combination with resting spectra it may add considerable information to the clinical, EMG and pathological examination. We have found the F1 value more sensitive than the resting Pi/PCr in the diagnosis of mitochondrial disease, when compared to the normal population. There is no correlation between decreased strength and decreased bioenergetic efficiency as represented by the F1 value (i.e. it is not an merely an expensive way of detecting weakness!). Using both resting and exercise parameters together provides the most selective criteria, though less sensitive. However there is obviously difficulty in assessing the true sensitivity and selectivity of a technique when no absolute standard exists to compare it to. Morphological changes on biopsy are frequently lacking in cases that appear clinically and biochemically to be mitochondrial . *In-vitro* biochemical tests on the other hand, are very labour intensive and are still fought with technical problems especially in the diagnosis of Complex 1 deficiencies. New molecular biological techniques, as they improve, may clarify this issue but their complexity will probably preclude their use from more routine testing; neither has their utility in the approach to therapy yet been established.

In the investigation of patients with fatigue but without other clinical or EMG findings, spectroscopy may help with the decision on biopsy. In presentations of idiopathic myopathy, stroke in young patients, Ramsay-Hunt syndrome, myoclonic epilepsy or other syndromes in which a mitochondrial etiology is suspected, spectroscopy may help one decide how aggressively to pursue complex biochemical or molecular biological studies. There is indeed great potential in further exploring the higher sensitivity of the F1 in demonstrating therapeutic benefit in the treatment of mitochondrial disease and

other metabolic muscle disease, its use in diagnosing disease in family members, and in the approach to patients with fatigue.

4.2.4 Conclusion

The pathophysiological basis of human mitochondrial myopathy is poorly understood. High-energy phosphates have a central role in the bioenergetics of skeletal muscle. Before the development of large-bore magnets and P-31 NMRS *in vivo*, almost no information was available regarding the concentrations of high-energy phosphates and the metabolic response to exercise in patients with mitochondrial myopathy.

In our studies, we have found that P-31 NMRS of exercising muscle is a useful diagnostic technique. We believe that the specific exercise protocol used in this work improves both sensitivity and selectivity in that it allows diagnosis of mitochondrial disease, even when little or no muscle symptoms are present, but other organ-systems show involvement. Because the method is safe, it may be used to detect disease amongst asymptomatic relatives of patients. We have also demonstrated that it may be a useful technique for monitoring pharmaceutical intervention. We have used it longitudinally to substantiate the therapeutic benefit of riboflavin and nicotinamide administrated in high dose in the treatment of a sample case of mitochondrial encephalomyopathy. Although in this case there was a good clinical end-point, many chronic presentations of mitochondrial disease do not; hence an objective measure such as NMRS, which can be applied serially is a powerful adjunct to therapy. The 'Isophosphate Force', F1 value is a practical variable to use in the assessment of patients as it is reproducible, and tractable enough for routine clinical use.

The clinical application of *in vivo* human spectroscopy holds great potential. The unique capability exists to provide a fundamental link between

biochemistry and human disease. The ability to detect noninvasively the biochemistry aspects of abnormalities in the human body provides hope for early detection of disease and prediction of therapeutic response. With improved methodologies, it is expected that clinical NMR spectroscopy will provide quality results in clinical practice.

References

1. G. Ahlborg, *et. al.*, J. Clin. Invest. 53:1080, 1974.

2. E. Jansson, and L. Kaijser, Acta Physiol. Scand. 115:19, 1982.

3. M. Vranic, and M. Berger, Diabetes 28:147, 1979.

4. P. Felig, and J. Wahren, N. Engl. J. Med., 293:1078, 1975.

5. R. S. Goodhart, and M. E. Shils, Modern Nutrition in Health and Disease, 6th ed., Philadelphia, Lea & Febiger, 1980.

6. P. L. Altman, and D. S. Dittmer, Metabolism, Federation of American Societies for Experimental Biology, Bethesda, 1968.

7. W. F. Ganong, Review of Medical Physiology, 9th ed., Lange Medicine Publications, Los Altos, 1979.

8. T. C. Ruch, and H. D. Patton, Physiology and Biophysics, 19th ed., W. B. Saunders Co., Philadelphia, 1965.

9. A. J. Vander, J. H. Sherman, and D. S. Luciano, Human Physiology-the Mechanisms of Body Function, 3rd ed., McGraw-Hill Book, Co., Toronto, 1980.

10. P. D. Gollnick, K. Piehl, and B. Saltin, J. Physiol. (London) 241:45-57, 1974.

11. P. D. Gollnick, J. Karlsson, K. Piehl, and B. Saltin, J. Physiol. (London) 241:59-67, 1974.

12. V. Dubowitz, and M. Brooke, Muscle Biophy. A Modern Approach, W. B. Saunders, London, 1973.

13. R. I. Close, Physiol. Reviews, 52:129-197, 1972.

14. H. S. Milner-Brown, R. B. Stein, and R. Yemm, J. Physiol. (London), 230:359-370, 1973.

15. B. Essen, E. Jansson, J. Henriksson, A. W. Taylor, and B. Saltin, Acta Physiol. Scand. 95:153-165, 1975.

16. B. Bigland, and O. C. J. Lippold, J. Physiol. (London) 125:322-335, 1954.

17. U. Freyschuss, and E. Knutsson, Acta Physiol. Scand. 83:278A-379A, 1971.

18. G. Grimby, and J. Hannerz, J. Physiol. (London) 264:865-879, 1977.

19. C. D. Marsden, J. C. Meadows, and P. A. Merton, J. Physiol. (London) 217:12p-13p, 1971.

20. M. H. Brooke, and K. K. Kaiser, J. Histochem. Cytochem. 18:670-672, 1970.

21. L. Guth, and F. J. Samaha, Exp. Neurol, 25:138-163, 1969.

22. P. Nemeth, and D. Pette, J. Physiol. (London) 320:73-80, 1981.

23. C. V. Lowry, J.S. Kimmey, S. Felder, M. M. Y. Chi, K. K. Passonneau, J. N. Kirk, and O. H. Lowry, J. Biol. Chem. 253:8269-8277, 1978.

24. C. S. Hintz, E. F. Coyle, K. K. Kaiser, M. M. Y. Chi, and O. H. Lowry, J. Histochem. Cytochem. 32:655-660, 1984.

25. J. A. Faulkner, *et. al.*, Clin. Sci. 57:20, 1979.

26. P. D. Gollnick, J. Appl. Physiol. 34:107, 1973.

27. E. Jansson, and L. Kaijser, Acta Physiol. Scand. 100:315, 1977.

28. D. L. Costill, W. J. Fink, and M. L. Pollock, Med. Sci. Sports 8:96-100, 1976.

29. G. W. Heath, J. M. Hagberg, A. A. Ehsani, and J. D. Holloszy, J. Appl. Physiol. 51:634-640, 1981.

30. J. Hanricksson, and J. S. Reitman, Acta Physiol. Scand. 97:392-397, 1976.

31. M. M. Y. Chi, C. S. Hintz, E. F. Coyle, W. H. Martin, J. L. Ivy, P. M. Nemeth, J. O. Holloszy, and O. H. Lowry, Am. J. Physiol. 244:C276-C287, 1983.

32. F. Buchthal, and H. Schmolbruch, Acta Physiol. Scand. 80:378-382, 1970.

33. K. Piehl, Acta Physiol. Scand. 402:1-33, 1974.

34. P. Gollnick, R. G. Armstrong, G. W. Saubert, and W. L. Sembrowich, Pfluegers Arch. 344:1-12, 1973.

35. D. Pette, and G. Vrobova, Muscle and Nerve, 8:676-689, 1975.

36. L. Edstrom, and E. Kugelberg, J. Neuro. Neurosurg. Psychiatry 31:424-433, 1968.

37. F. Jolesz, and F. A. Sreter, Rev. Physiol. 43:531-552, 1981.

38. R. Hennig, and T. Lomo, Nature (London) 314:164-166, 1985.

39. B. Chance, and H. Conrad, J. Biol. Chem. 234:1568-1570, 1959.

40. B. Chance, J. S. Leigh Jr., B. J. Clark, J. Maris, J. Kent, S. Nioka, and D. Smith, Proc. Natl. Acad. Sci. U.S.A. 82:8384-8388, 1985.

41. B. Chance, S. Eleff, D. Sokolow, and A. Sapega, Proc. Natl. Acad. Sci. U.S.A. 78:6714-6718, 1981.

42. W. E. Jacobus, Annu. Rev. Physiol. 47:700-725, 1985.

43. B. Chance, G. Mauriello, and X. M. Aubert, in Muscle as a Tissue, eds. K. Rodahl, and S. M. Horvath, McGraw-Hill Publishing Co., New York, 128-145, 1962.

44. R. Wu, and E. Racker, J. Biol. Chem. 234:1036-1041, 1959.

45. F. Lynen, and R. Koenigsberger, Ann. Chem. 573:60-84, 1951.

46. A. J. Sargeant, C. T. M. Davies, R. H. T. Edwards, C. Maunder, and A. Young, Clin. Sci. and Molecular Med. 52:337-342, 1977.

47. V. Dubowitz, and M. Brooke, Muscle Biopsy. A Modern Approach, W. B. Saunders, London, 1973.

48. R. E. Burke, D. N. Levine, F. E. Zajac, P. Tsiris, and W. K. Engel, Science 174:709-712, 1971.

49. V. R. Edgerton, G. E. Gaslow, S. A. Rassmusen, and S. A. Spector, Nature 258:589-590, 1980.

50. K. Krnjevic, and R. Miledi, J. Physiol. (London) 140:440-461, 1958.

51. M. J. Dawson, D. G. Gardian, and D. R. Wilkie, Nature 274:861-866, 1978.

52. J. Hannerz, and L. Grimby, Muscle and Nerve 2:414-422, 1979.

53. J. Bergstrome, L. Hermansen, E. Hultman, and B. Saltin, Acta Physiol. Scand. 71:140-150, 1967.

54. Y. Naess, and A. Storm-Mathisen, Acta Physiol. Scand. 34:351-366, 1955.

55. A. Fabiato, and F. Fabiato, J. Physiol. (London) 276:233-255, 1978.

56. B. Bigland, D. A. Jones, and J. J. Woods, Exp. Neurol. 64:414-427, 1979.

57. J. Jardin, G. Farkas, C. Prefaut, D. Thomas, P. T. Macklem, and C. Roussos, Am. Rev. Respir. Dis. 124:274-279, 1981.

58. H. Monod, and J. Scherrer, Ergonomics 8:329-337, 1965.

59. A. J. McComas, Neuromuscular Function and Disorders, Butterworth Ltd., London, 1977.

60. C. Roussos, and P. T. Macklem, J. Appl. Physiol. 43:189-197, 1977.

61. S. A. Esau, F. Bellemare, A. Grassino, S. Permutt, C. Roussos, and R. L. Pardy, J. Appl. Physiol. 54:1353-1360, 1983.

62. F. Bellemare, and B. Bigland-Ritchie, J. Appl. Physiol. 62:1307-1316, 1987.

63. B. Chance, J. S. Leigh Jr., K. McCully, S. Nioka, B. J. Clark, J. M. Maris, and T. Graham, Proc. Natl. Acad. Sci. U.S.A. 83:9456-9462, 1986.

64. R. D. Griffiths, and R. H. T. Edwards, J. Inher. Metab. Dis. 10(Suppl. 1):147-158, 1987.

Chapter 5

5. FURTHER REFINEMENT OF CLINICAL PROTOCOL

5.1 Introduction

In the last chapter, we presented preliminary clinical results in monitoring muscle fatigue among patients. The dynamic exercise technique was proven to be very sensitive and selective to the diagnosis of bioenergetic defects. With the over 300 patient studies over the past five years, we have made the following observations:

(a) The technique is reproducible under most circumstances though there must be reasonable adherence to the exercise protocol.

(b) The technique reveals a clear separation, independent of muscle strength, between normal and mitochondrial patients. It is thus a sensitive and selective test.

(c) Applied to relatives of patients with mitochondrial disease, the technique has successfully diagnosed disease in asymptomatic individuals in whom resting spectra were normal.

(d) The technique is also sensitive enough to detect improvement following treatment. This has been demonstrated in the treatment of mitochondrial disease with Riboflavin, and in the treatment of hyperthyroid myopathy by normalization of thyroxin levels, as well as in the treatment of McArdles Disease

patients by instituting a high protein diet (results to be published, Dr. Andrew Penn, *et. al.*).

However, due to the considerable spread of experimental results, some of which are not the direct results of diversity among individual human subjects, we gradually realized that a more rigorous analysis of the mechanical variable is necessary, also that we should pay closer attention at each individual's exercise pre-conditions, such as increased buffer capacity and prior muscle injury. In addition, we also came to the understanding that work rate alone cannot be used fully to account for the occasional discrepancies even among control subjects. This latter observation merits further investigation and will form the basis of the first half of this chapter; whereas the second half of this chapter will concentrate on investigation of certain pre-conditions which may affect subsequent exercise performance.

5.2 Relative Metabolic Efficiency of Concentric and Eccentric Exercise

5.2.1 Introduction

It is important to know the metabolic cost of different activities both in research and in clinical practice. Because the nervous system, skeletal muscles and external loads interact in a very complex way to make the entire system very adaptive, natural movement such as ambulation at a self-selected cadence tend to be carried out in a manner which minimizes the rate of energy consumption (1). Thus when one is analyzing biomechanical observations in normal subjects, it is helpful to know the relative metabolic efficiency of alternative mechanisms for the task the subjects are performing. Similarly, when one is supervising a person who is exercizing at the upper limit of his or her physiologic capacity (whether an athlete or a person with a physical impairment), such knowledge is

a prerequisite to formulation of an exercise prescription or other intervention intended to maximize that person's functional capacity.

The 'metabolic cost' of an activity traditionally is estimated from the change in the rate of oxygen consumption by the body during the activity, relative to the baseline rate, via a calculation based on knowledge of the biochemistry involved (1-2). The amount of metabolic energy expended during concentric work (such as raising a weight a certain distance in a certain time) is greater than that expended during the same nominal amount of eccentric work (such as lowering the same weight through the same distance in the same time) (2-4). Because of this fact, it has been the usual practice, when one is trying to estimate the total mechanical power generated during a movement involving both concentric and eccentric contractions, to add only a portion of the "negative mechanical power" (eccentric) to the "positive mechanical power" (concentric) to estimate the total. This portion has been estimated to be as small as 15% and as large as 50% in experiments by different workers (4-5). This has led to a wide range of estimates of the relative metabolic efficiency of positive and negative work.

Previous studies of 'negative work' used whole-body measures of metabolic energy expenditure, such as oxygen consumption. However, the energy metabolism of a localized volume of skeletal muscle can now be monitored quantitatively in humans during exercise, painlessly and noninvasively, by means of P-31 nuclear magnetic resonance (NMRS) (6). In addition, previous studies used ergometer measurements to estimate the mechanical output while the subject performed a 'negative work' task, rather than while the subject performed a pure eccentric exercise.

In order to determine the relative metabolic efficiency of negative to positive muscular power (4), we used P-31 NMRS to monitor the cellular energy

metabolism of limb muscles in healthy humans during a mixed concentric-eccentric activity, and also during its concentric and eccentric components. The activity was very simple, and the mechanical output was amenable to accurate measurement. We also studied isometric contractions.

5.2.2 Methods

Subjects The subjects were 8 healthy men and women volunteers. Informed consent was obtained under the format approved by the responsible institution for this NMRS apparatus. The subjects were not on any medication. There was no neuromuscular disorder present according to a screening history, physical examination, and the observed performance during the exercise protocol. All were Caucasian and were physically active; a few were elite athletes. None was overweight. The range was 22-40 years.

Exercise Protocol The exercise consisted of raising and lowering a weight at a steady rate, during the flexing of the medial four fingers. The apparatus, shown in Figure 5-1, was arranged so that the vertical position of the weight was displayed to the subject in real time as the vertical position of a horizontal trace on a dual-beam oscilloscope. The vertical position of the second trace of the oscilloscope was controlled by a signal generator, and varied sinusoidally at a constant rate and amplitude. The pacing frequency was 0.5 Hz for these experiments, the excursion of the weight was approximately 3 cm., and the size of the weight was 0.25 to 12 kg.

The subject followed the pace and the amplitude set by the signal generator. The weight could be manipulated by one of the operators, so that extra weight could be added during either the concentric or the eccentric part of each cycle. Variations of the protocol were: (a) 'sinusoidal' exercise at constant

load at a frequency of 0.5 Hz; (b) "sinusoidal' exercise at 0.5 Hz but with the load taken by one of the operators during the eccentric portion of each cycle, so the subject would raise the full weight but then lower only the weight of the carriage (about 0.25 kg) (lower left panel of Fig. 5-1); (c) as for (b) but with the load taken by one of the operators during the concentric portion of each cycle (lower right panel of Fig. 5-1); (d) support of a constant load, with no raising or lowering (isometric exercise). The forearm was held by a flexible sleeve of 4 mm. thick neoprene with an aperture for the surface coil positioned over the appropriate musculature, as shown in Fig. 5-1.

Analysis of the Mechanical Output The mechanical output of the contractile apparatus of the muscle is only accessible at the joints, as active movement or as resistance to imposed movement. The subject's forearm was held in a fixed position relative to the surface coil, by means of the proximal limb musculature and the distal weight of the pulley system. The apparatus was designed to make it possible to monitor simultaneously the energy changes of the weight as it moved, and the metabolism of the muscles causing the weight to move, at various steady mechanical loads, while keeping the physical movements of the muscles and joints the same for each load. The surface coil was positioned over the finger flexors, and only the finger flexors should act on the test weight. Subjects were instructed and coached not to employ other movements such as wrist extension to accomplish the prescribed task.

The position of the weight as a function of time was recorded on a chart recorder, and the position potentiometer signal also was fed into a data acquisition program running on a personal computer with data acquisition at 20 Hz. In addition, the output of a force transducer through which the cable controlled by the subject was connected to the weight platform (Fig. 5-1) was

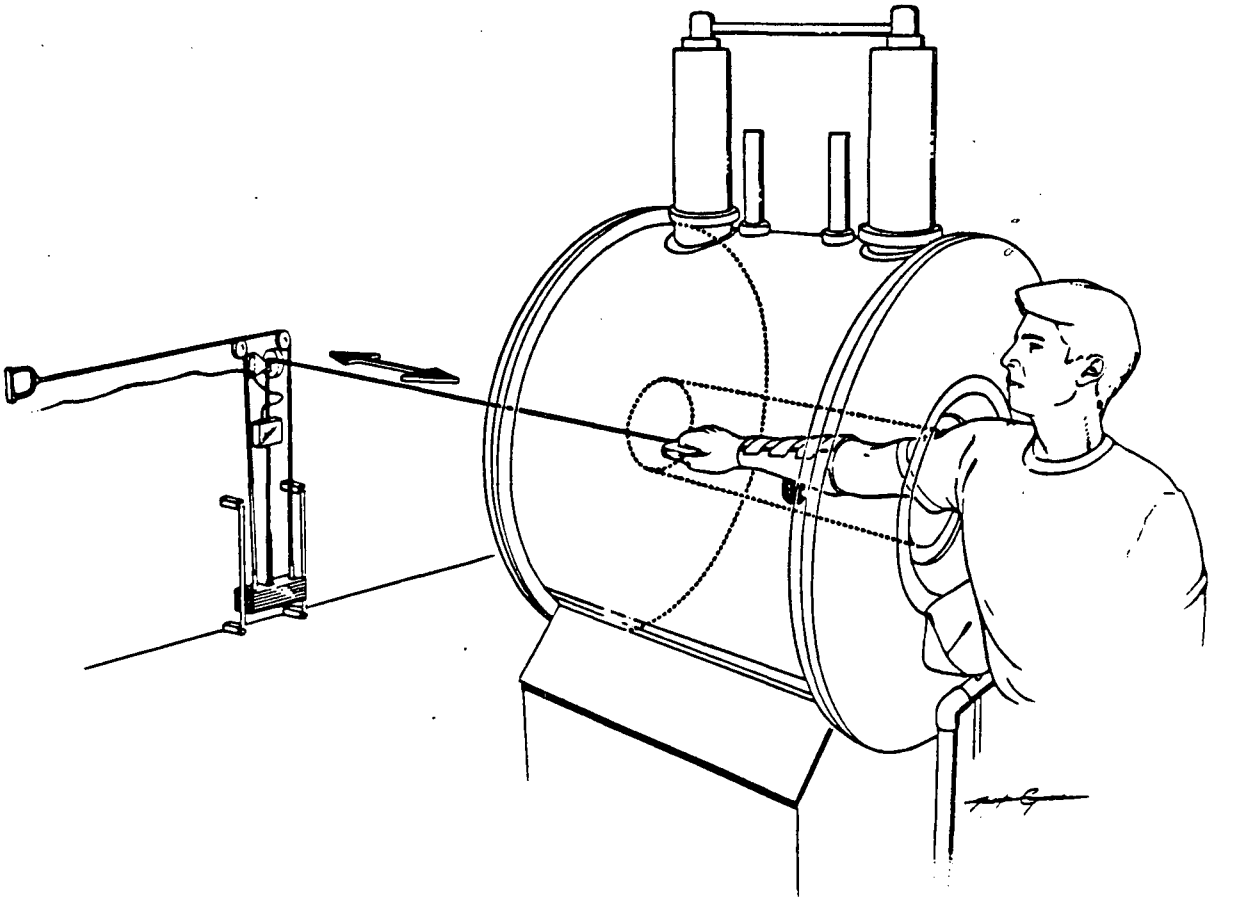

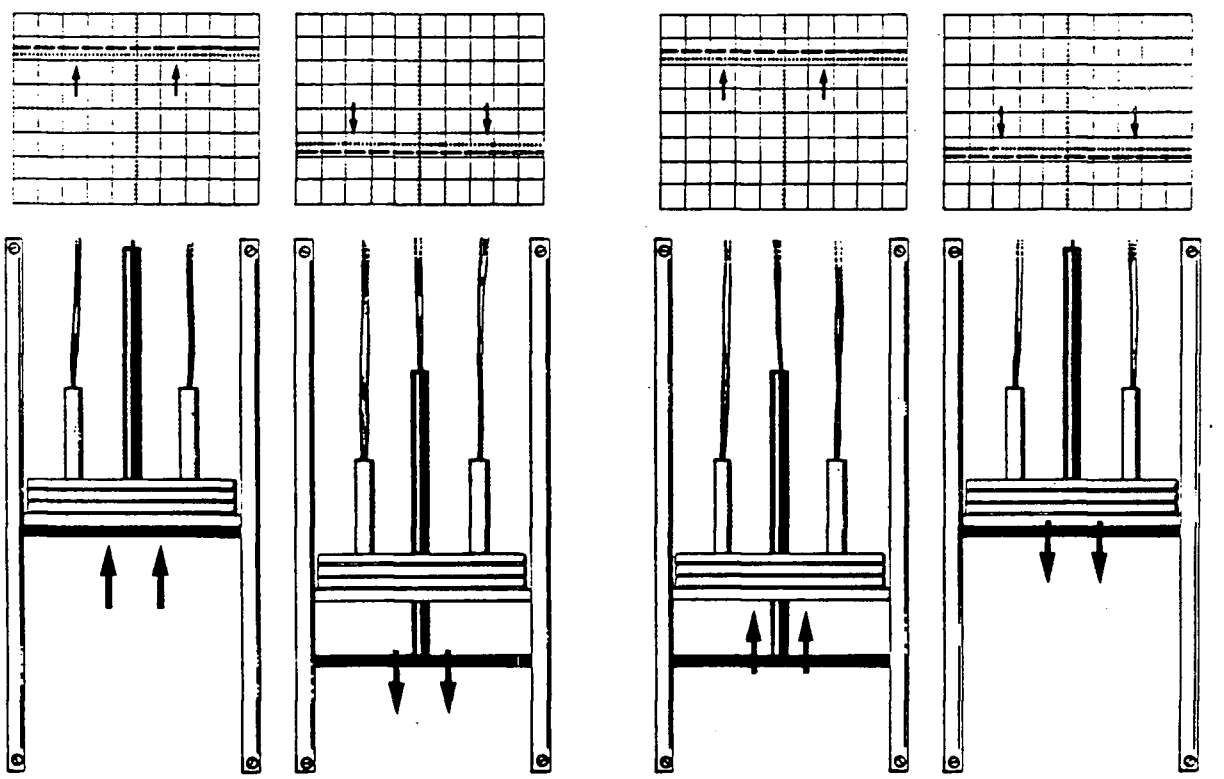

Figure 5-1 Configuration of the spectrometer and the exercise apparatus. A soft rubber cuff is position on the subject's forearm with an aperture over the site of interest. The field coil (small dark cylinder) fits into this aperture, so the subject can maintain the position of the field coil during exercise. A position transducer in the pulley apparatus provides visual feedback to the subject on the position of the test weight relative to a pacing signal, and position-time data to a computer. A force transducer measures the actual instataneous tension experienced by the flexing fingers. The lower panels show details of the weight carriages. The dark carriage is controlled by the subject, and the grey carriage is controlled by an operator. On the lower left, the pacing trace on the oscilloscope (darker line) moves up, and the subject lifts the weight to keep the weight position trace (lighter line) adjacent to it. The operator allows the full weight to rest on the subject's carriage during the ascent. Then the subject lowers his carriage, following the pacing signal, but the operator lowers the weight more slowly, so the subject's eccentric contraction is unweighted. Thus the work done by the subject is almost entirely concentric. On the lower right, the operator lifts the weight while the subject raises his carriage, but allows the weight to rest on the subject's carriage while the subject lowers it. Thus the work done by the subject is almost entirely eccentric.

recorded. The computer program calculated the instantaneous mechanical power and a running average of the mechanical power from the position-time data. Also calculated were the average mechanical power during the concentric (weight ascending) and eccentric (weight descending) portions of the exercise.

The performance of one subject, attempting to follow a sinusoidal pacing signal of frequency 0.5 Hz and amplitude 3 cm. is shown in Fig. 5-2. The position data closely approximate the pacing waveform. The velocity calculated from the position-time data is also sinusoidal with a frequency of 0.5 Hz but shifted in phase by 0.5 second (one quarter period) relative to the position. The erratic variations superimposed on the sinusoid are to some extent an artefact of the method of calculation (the raw signal was not smoothed prior to differentiation), but most of the variation reflects real velocity changes as the subject corrects his performance in response to visual feedback of the position of the weight relative to the pacing signal (Fig. 5-1).

Also shown in Fig. 5-2 is the raw data from the in-line force transducer. It clearly shows periodic variation around a baseline of about 1.5 newtons (a bias has been imposed; the actual weight used in this case was 2 kg), and the force variations as the subject attempts to match the pacing signal. Particularly prominent, however, is the intermittent pattern to the force during the eccentric phase. There are large excursions of the force, well above and below the baseline, corresponding to the small steps in the position-time trace, as if the weight were being lowered in an irregular succession of steps. This pattern is typical of eccentric contractions and can be sensed by the subject.

The mechanical power generated by the finger flexors which were being sampled by the surface coil was assumed to be directly proportional to the rate of change of the energy of the weight platform under these conditions. The latter energy (in joules) is:

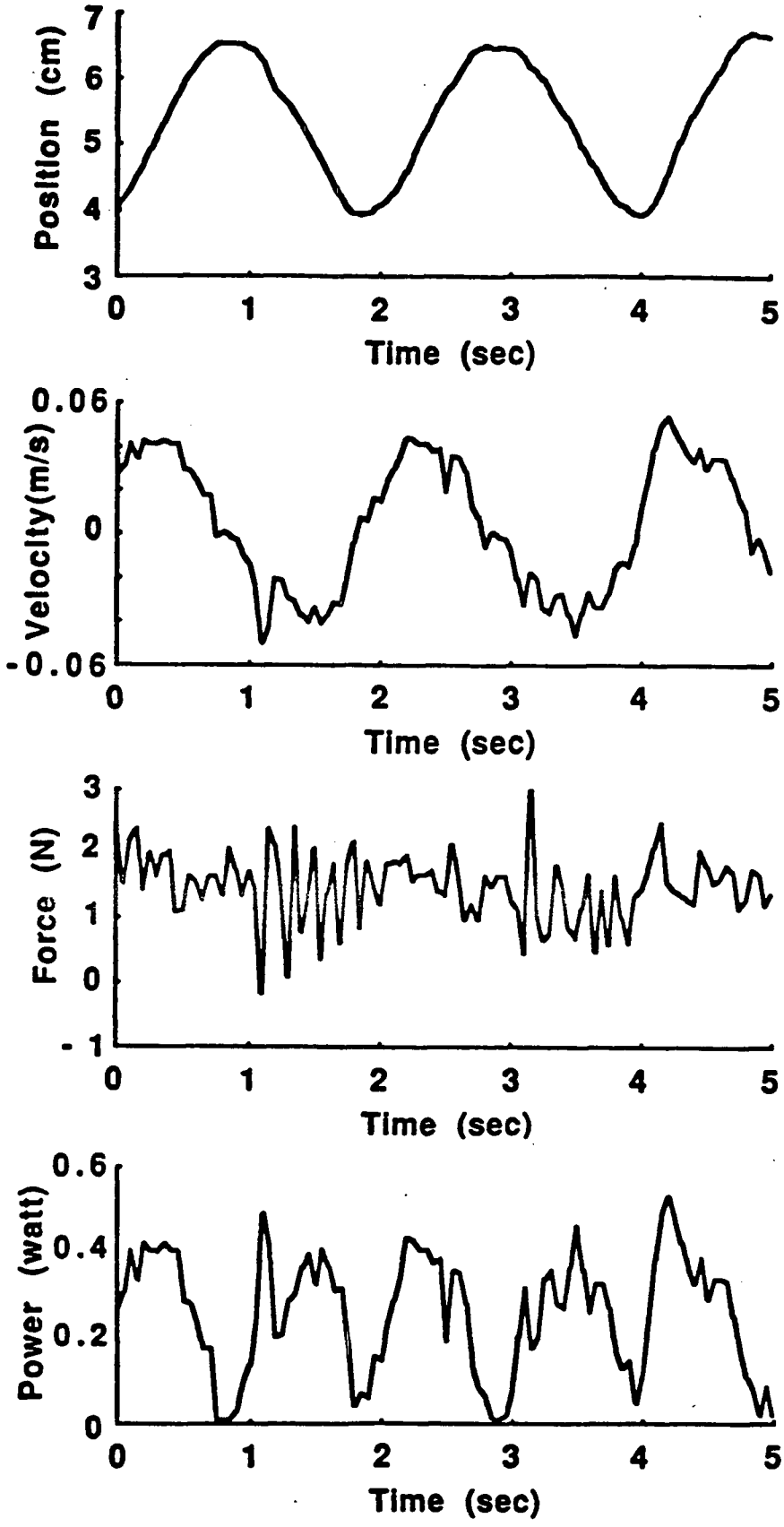

Figure 5-2 Performance of a subject attempting to follow a sinusoidal pacing signal at a frequency of 0.5 Hz and amplitude 3 cm. Position of the weight carriage is recorded from the position transducer in the pulley. Velocity is calculated from the raw position data. Force is recorded from the force transducer. Power is calculated from the magnitude of the velocity as described in the text.

$$E = Mgh + [(Mv^2)/2] \quad (5\text{-}1)$$

where M is the weight (kg), g is the acceleration due to gravity ($9.8 m/s^2$), h is the height of the weight above an arbitrary reference level, v=dh/dt is the velocity of the weight, and movement is positive in the direction of raising the weight against gravity.

It should perhaps be emphasized that the weight acquires the same amount of gravitational potential energy during a given concentric half-cycle no matter how the lift is executed. To accomplish the rising part of the oscillatory motion, the muscle is activated, develops tension, shortens, and raises the weight. The weight starts at rest, and finishes at rest at a greater height. In order to accomplish this, the muscle can either exert a small force throughout the entire concentric phase, so v is always small, or it can exert a large force only at the beginning of the phase, so v is large initially but gradually decreases. An important complication of the analysis is that although the change in energy of the weight is the same in both cases, and the power averaged over a complete cycle is the same, the peak power demanded from the muscle is much greater when v is larger. Further, the energy change in the muscle is different: muscle cells with different energy characteristics are recruited for movement of different types (7). Relatively low and slowly-varying tensions were studied here, in an attempt to minimize the confounding influence of motor unit recruitment.

The mechanical power P is equal to the rate of change of the energy dE/dt. The kinetic term averages to zero during each half-cycle (concentric or eccentric), and the average power (in watts) is:

$$P = Mgv \quad (5\text{-}2)$$

where v is the average velocity during the half-cycle. The average velocity is positive during the concentric phase (v>0), and the source of motive energy is the muscle. It is negative during the eccentric phase (v<0), and the motive force

is gravity: the muscle absorbs the gravitational potential energy, by resisting the descent of the weight and bringing it to rest at the lower limit of the range of travel. For analysis and for display, the instantaneous power (concentric, eccentric, or combined, as appropriate) was averaged over the period of simultaneous NMRS data acquisition (45 sec.).

Analysis of the NMR signal The P-31 NMRS measurements were collected using a 1.89 Tesla Oxford Instruments magnet with a 30 cm. horizontal bore, as described in Chapter 4 (p.134) of this thesis. The radiofrequency surface coil is of novel design, constructed specifically for these clinical measurements (8). Peak heights were used for quantification. Signal saturation produces less than 10%, yet consistent, overestimate of the P*i*/PCr ratio (6,8).

Source of the NMR Signal The radiofrequency surface coil receives significant signal only from the ca. 2 cm. diameter hemisphere of the forearm immediately adjacent to it. The site of the surface coil used was determined from dissections of cadaver forearms, and was chosen to maximize the contribution from the finger flexors actually used in the exercise. The phosphorus species which give significant signal are those which are mobile and present in concentrations in the millimolar range (6). In particular, PCr, P*i*, and ATP are prominent. The ATP signal remains constant in all but the most extreme situations. The PCr peak diminishes and the P*i* peak increases with increasing metabolic demand (such as during exercise) because the reaction mediated by creatine kinase rephosphorylates the ADP produced by the functional ATPases such as actomyosin. The creatine is in turn rephosphorylated at the mitochondria, at the expense of ATP produced there by oxidative phosphorylation (9). For a steady demand which does not exceed the maximum

oxidative capacity of the mitochondria, this network of reactions comes to a steady condition, and the ratio of the amount of P*i* to the amount of PCr (i.e. the quantity measured by the NMRS apparatus) is essentially proportional to the energy flow through the system. No significant signal is received from tissue other than muscle in the area of pickup, either because the content of PCr is relatively small compared to that in muscle (as in skin and connective tissue) or because the phosphate compounds are immobilized (as in bone).

5.2.3 Result

Variation of P*i*, PCr, and P*i*/PCr with Power A sequence of steady workloads of different levels was examined. The workload was varied by changing the mass while holding the amplitude and frequency of continuous 'sinusoidal exercise' constant. This was done because all aspects of the instantaneous mechanical power output are linearly proportional to the mass, while the frequency, amplitude, and 'profile' of the periodic exercise potentially are interdependent through velocity and acceleration. The results are shown in Fig. 5-3a. The resting level of P*i*/PCr is about 0.1. As the mass is increased, the ratio rises to a higher level, with a time constant of about 30 sec. when the mass subsequently is increased to a higher steady level, the ratio also rises to a higher steady level, and when the mass then is decreased, the ratio also decreases.

The composite plot of the steady level of P*i*/PCr versus Power is shown in Fig. 5-3b. In this low power range, the relationship is approximately linear, and shows no significant hysteresis. Significant deviations from linearity can be expected to occur as P*i*/PCr approaches unity (6), but the results reported here deliberately were confined to the 'linear' region where P*i*/PCr is less than unity.

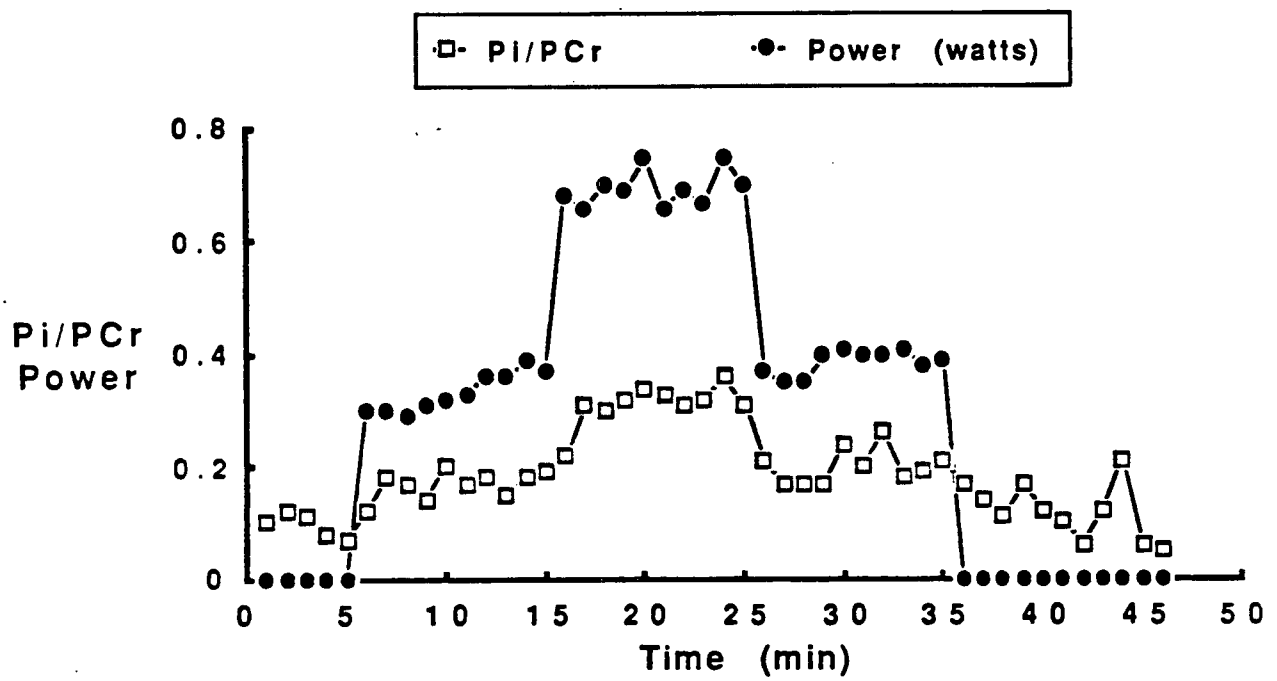

Pi/PCr acquired during first 45 sec of each minute.

Figure 5-3a Variation of the ratio Pi/PCr with time as the exercise load is incremented and decremented.

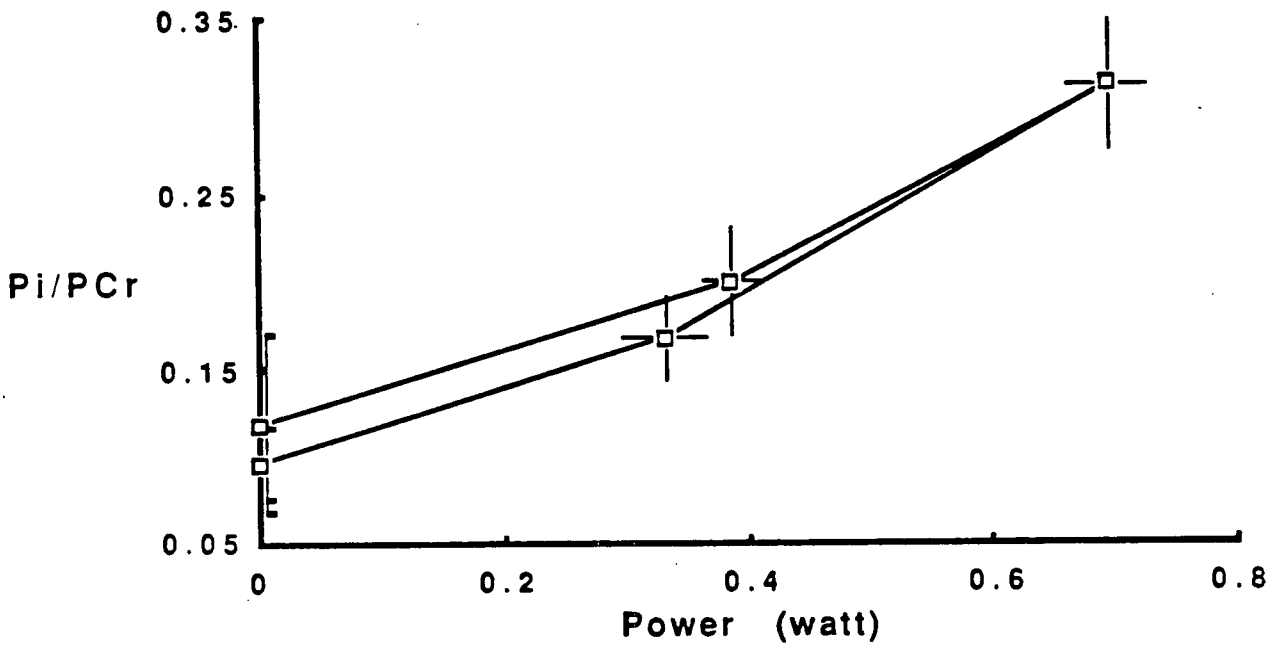

Bars indicate ± SD for 10 data points.

Figure 5-3b Summary plot of the steady value of P*i*/PCr during a period of steady exercise load, versus the mean mechanical power output. The symbol indicates the mean and the bars +/- SD for 10 data points from figure 5-3a.

Concentric, Eccentric, and Isometric Exercise Different types of exercise were examined by manipulation of the load during a particular portion of each cycle of continuous sinusoidal exercise. For concentric exercise, the subject lifted the full weight through the prescribed amplitude, but lowered only the carrier apparatus (about 250g; exercise with only 250g of weight and 'sinusoidal' profile at up to 1 Hz caused no detectable change in P*i*/PCr). For eccentric exercise, the subject lowered the full weight through the prescribed amplitude, but lifted only the carrier apparatus. For isometric exercise, the subject supported the full weight motionless at the middle of the prescribed amplitude. A problem arises in attempting to compare the metabolic cost of the different types of exercise if the P*i*/PCr is plotted versus power, as in Fig. 5-3b. For example, the nominal power is zero for all weight during isometric exercise. Therefore, the P*i*/PCr ratio was plotted versus the mass used, for each type of exercise.

The results are shown in Fig. 5-4. For concentric exercise, the relationship between P*i*/PCr and mass is not significantly different from that for mixed concentric and eccentric exercise. For eccentric exercise, the characteristic curve has a much lower slope. Examination of the records of power calculated from the displacement-time data and of the tension developed during different phases of the exercise as indicated by the output from the in-line force transducer (as in Fig. 5-2) suggests that contamination of the eccentric exercise with concentric exercise occurred at the higher loads. This is consistent with our clinical observations during the exercise. Overall, then, these results suggest that for 'pure' eccentric exercise there is a low energy cost, and further that this energy cost is almost independent of the apparent workload.

To test the likelihood that the variations in P*i*/PCr with weight during eccentric exercise were due to chance, an analysis of variance was calculated for the data at rest and the data during eccentric exercise, for each mass. The

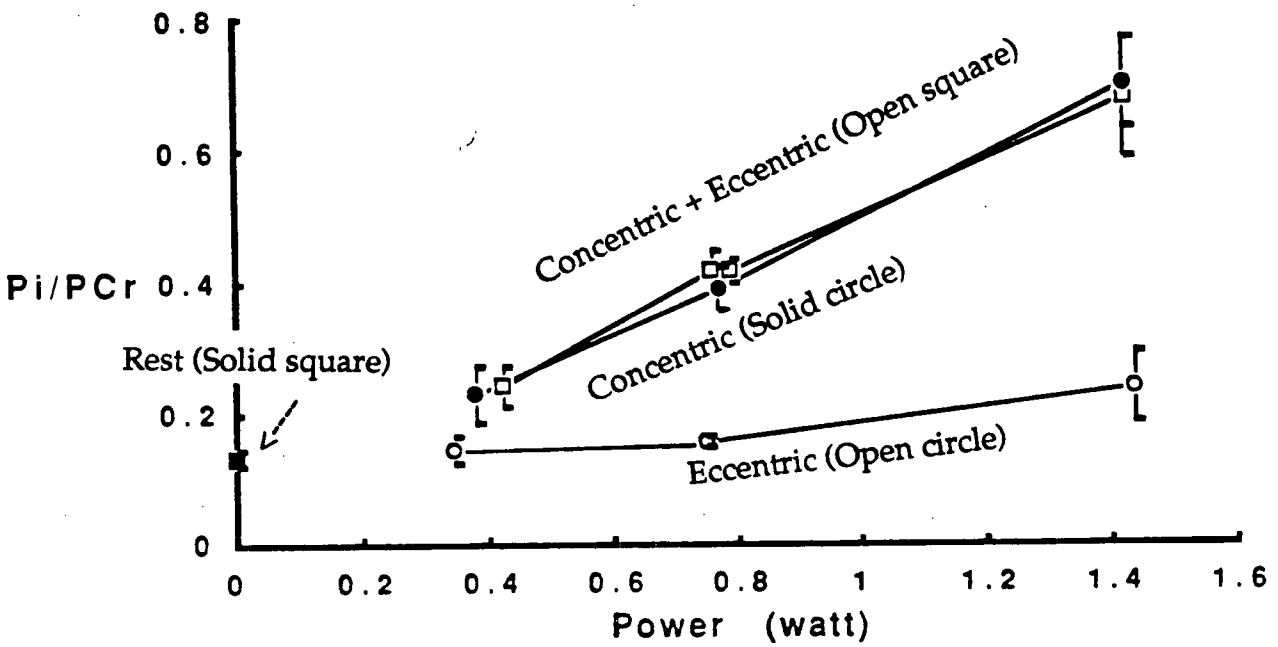

Figure 5-4a Effect on Pi/PCr of different types of exercise at the same nominal power output. The (concentric + eccentric) exercise consists of raising and lowering a particular weight. The (concentric) exercise consists of raising the weight only: the operator lowers the weight during the eccentric part of each cycle. The (eccentric) exercise consists of lowering the weight only: the operator raises the weight during the concentric part of each cycle. The dashed line shows the data for the (concentric + eccentric) exercise plotted versus only the 'positive' (concentric) power generated during that exercise.

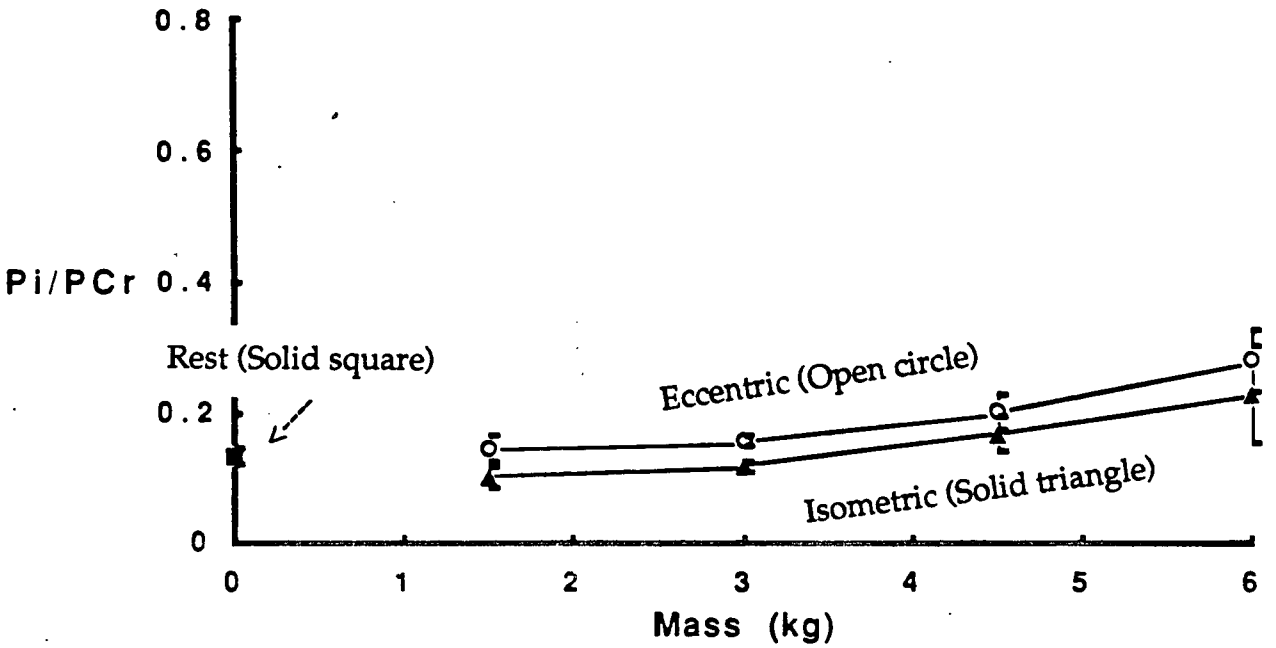

Figure 5-4b Isometric exercise consists of holding a given weight stationary for a period of 10 min. The steady value of *Pi*/PCr attained is plotted versus the size of the weight. For comparison, the data for eccentric exercise are replotted versus weight.

differences observed were not significant. That is, the value of Pi/PCr during eccentric exercise at these intensities is not significantly different from the value at rest.

Comparison of Different Subjects The data for 8 different subjects are shown in Fig. 5-5. The Pi/PCr ratio is plotted versus nominal power in order to compensate for the slight inter-subject variation in adherence to the pacing signal (that is, to compensate for variations in velocity). The measured values shown in Fig. 5a exhibit the same pattern for nominally concentric versus nominally eccentric exercise in each of the 8 subjects: for nominally concentric exercise, above a threshold, the ratio Pi/PCr increases in direct proportion to the mechanical power produced, while for nominally eccentric exercise, the variation of Pi/PCr with power is small.

A particular work load constitutes a different fraction of the maximal work capacity for subjects of different strength. Therefore in comparing different subjects, the energy flow through the muscle at a particular load should be corrected in some way for strength. The slope of the concentric data for each subject in Fig. 5-5a is approximately linear. When the slope of a linear regression of Pi/PCr on power is calculated for each subject, there is a strong correlation between that slope and the maximal grip strength of that subject (r^2=0.83, N=8 for linear regression of slope ($watt^{-1}$) on grip strength), as shown in Fig. 5-5b. Thus a substantial portion of the inter-subject variation in the slope of the data for concentric exercise probably is related to the variation in strength.

5.2.4 Discussion

It is well known that eccentric exercise, in comparison to concentric exercise, is associated with a lower metabolic cost for a given nominal amount of

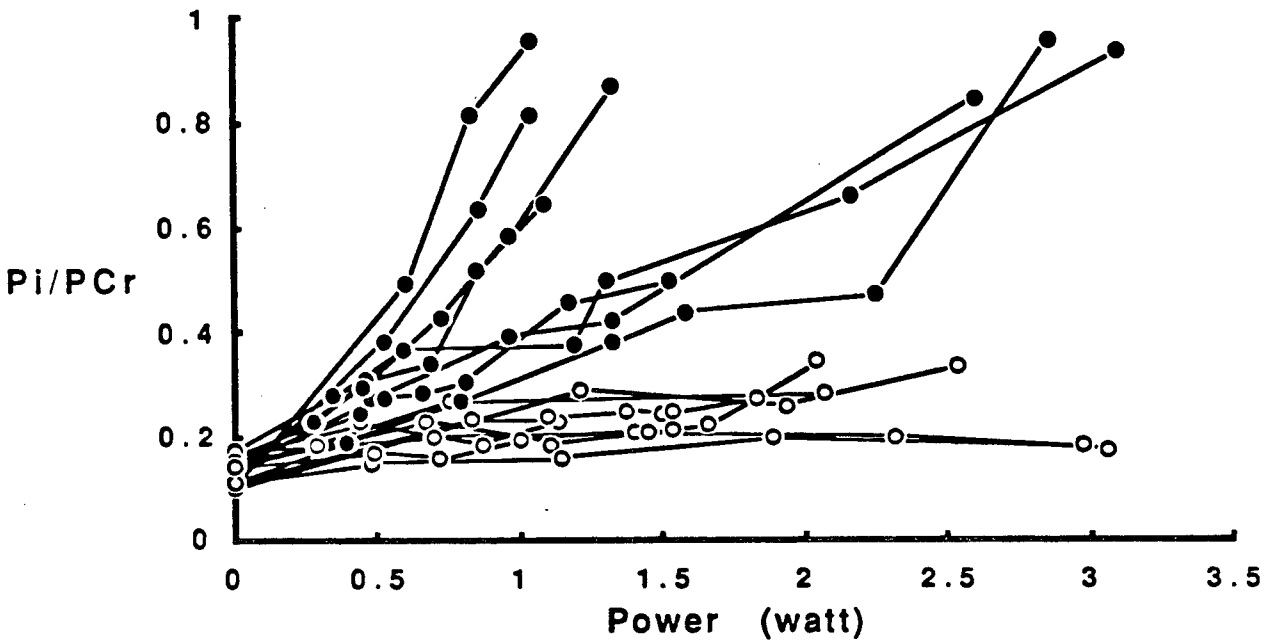

Open symbol = Eccentric. Closed symbol = Concentric.

Figure 5-5a Comparison of the response of Pi/PCr to concentric and eccentric exercise in a 8 different subjects. Plots comparable to figure 5-4 for each subject, but plotted versus power rather than mass (see text).

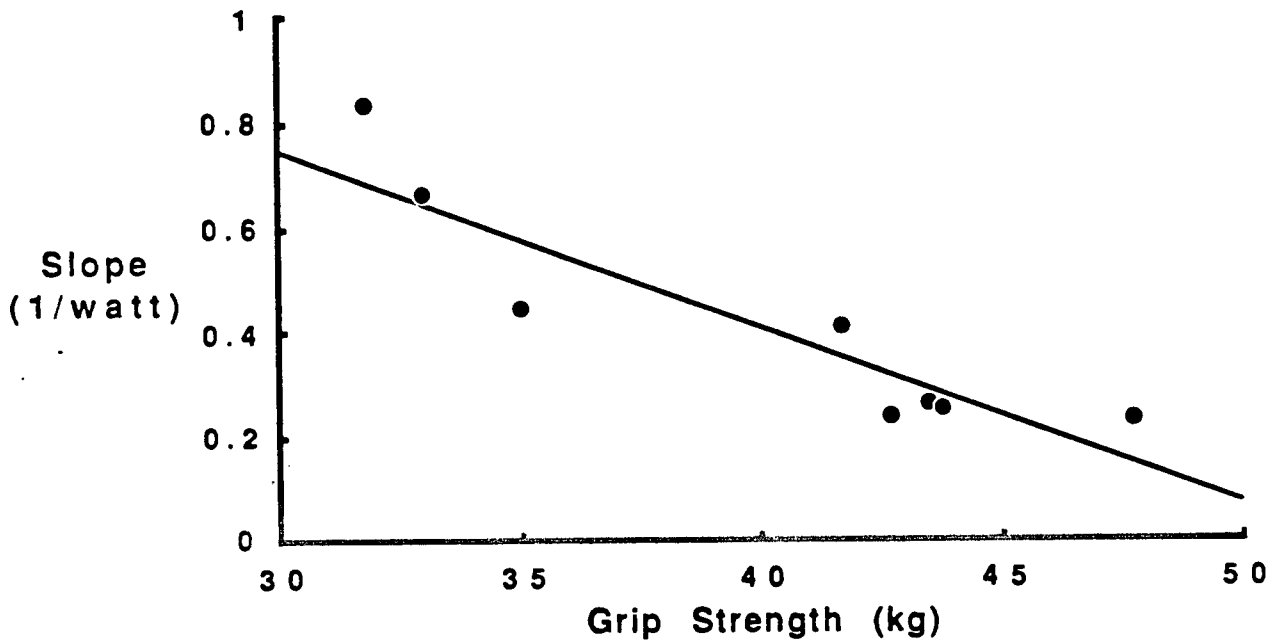

N=8, R2=0.83, a=1.7734, b=-0.0341

Figure 5-5b Comparison of the response of Pi/PCr to concentric and eccentric exercise in a 8 different subjects. Correlation of the slope of the concentric data for a subject with that subject's maximal grip strength, in Kg., measured with a hand ergometer.

mechanical work (4,10). The results of the present experiments show that if metabolic cost to the muscle cell is measured by Pi/PCr, then the metabolic cost of concentric work at relatively low intensity is proportional to the rate of doing work (power), while the metabolic cost of eccentric exercise is virtually independent of the apparent power. This result, together with the observation that most motor tasks compromise both concentric and eccentric contractions of various muscle masses, explains the wide range of estimates produced by previous investigators for the apparent relative metabolic efficiency of positive and negative work as derived from whole-body metabolic measurements (4,5): even a small concentric component in an apparently eccentric exercise will substantially increase the metabolic cost of that exercise; and even for pure concentric and pure eccentric exercise, the relative metabolic cost at a particular nominal workload is different at high versus low workloads, with a greater apparent relative metabolic efficiency of eccentric exercise at higher nominal workloads.

These results must be analyzed in the context of the events at the site of chemomechanical coupling, the actomyosin ATPase, as they currently are understood. The ATPase activity of the contractile apparatus is located in the crossbridges, and thus the active sites are fixed to the contractile myofilament apparatus at regular intervals of distance. The hydrolysis of ATP which occurs when the actin and myosin filaments are allowed to interact can proceed through the 'preferred' reaction sequence only if the filaments are allowed to slide relative to each other (11,12). When a muscle is able to shorten, and thus to do work in the usual sense of a force applied through a distance, the rate of ATP hydrolysis increases.

In an eccentric contraction, the activated muscle is stretched. This can only occur if the contractile filaments slide relative to one another in the direction

opposite to the 'preferred' direction. This prevents the actomyosin ATPase from proceeding through the 'preferred' reaction, and in fact it tends to drive it through a reaction sequence which is energetically very unfavorable. To do this, one must apply a tension greater than that which is developed as the muscle attempts to shorten, which is to say greater than the isometric tension. Dr. M.R. Menard *et. al.* previously have shown in isolated muscle that the activated muscle is stiffer (greater change in tension per unit change in length) when subjected to a small stretch than it is when it subjected to a small release, under conditions which reveal the ensemble mechanical properties of the crossbridges themselves (13).

If the contractile filaments are to remain intact when an activated muscle fiber is stretched, the crossbridges must detach without going through their preferred reaction sequence, and this will only occur if external energy is supplied. The muscle fibre remains activated, though, so the detached crossbridge is able to reattach to the next available binding site. However, if the filament is to remain intact, the crossbridge must detach again as the stretch continues, and this requires the input of more external energy. Further, since the crossbridges in a myofibril must act in concert due to restrictions imposed by their firm attachment to each other, the contractile apparatus is very prone to mechanical disruption during such a stretching process. Such disruption has been observed, and is the basis of the delayed muscle soreness seen after eccentric exercise (14).

In terms of the energy cost of an eccentric contraction to the muscle cell, the metabolic machinery need only supply enough energy to maintain the cell in an activated state. All of the energy which goes into stretching the contractile apparatus comes from an external source. Thus it is not surprising that the flow

of metabolic energy in the cell as reflected in the Pi/PCr ratio is not significantly different at rest and during an eccentric contraction.

The subjects in this study were normals, and the questions concerned normal physiology. However, these techniques can be used in the investigation of neuromuscular disease as a clinical tool complementary to electrodiagnostic studies. For the technique to be useful in this context, it must be possible to establish normal ranges for the quantities measured. In the present study, the same qualitative pattern in concentric versus eccentric exercise was seen in all subjects tested, but the qualitative parameters derived from the data showed a great deal of variation.

We suspect that the principal cause of this variation was the measurement of mechanical output. The mechanical output of the forearm flexors which is measured in our protocol is not identical to the tension in the cells of the muscle mass sampled by the field coil, because of pennate muscle cell configuration, and co-contraction of antagonists. In addition, what the body performs in our protocol is a task: it is not a pure contraction such as those studied in isolated muscle preparations. Recruitment of motor units in order to accomplish the task is modulated by a variety of central and peripheral factors. The body will use its assets to maintain the volitional task of the exercise protocol as best it can, so the details of the execution will change with load or with time of exercise. We attempted to optimize our measurement by stabilizing the limb, avoiding compromise of peripheral sensation, coaching the subjects, and positioning the field coil to sample the working muscle volume almost exclusively. However, different subjects have different strengths.

Quantitative comparison of different subjects cannot be done without normalization for the size (cross-sectional area) of the muscles being sampled by the spectrometer. The cross-sectional area of the forearm flexors cannot be

measured without some form of medical imaging, and the objective assessment of strength is a complex undertaking (15). However, the configuration of the muscles should be similar in all subjects, so the cross-section of the active muscles should be at least approximately proportional to the cross-sectional area of the forearm (assuming no specific training of one muscle group for bulk has occurred), and to the maximal grip strength (assuming no training for coordination of the finger flexors has occurred, which might increase strength with little change in bulk (10). We have found that with a protocol of exercise at higher velocities (up to 0.2 m/sec), and normalization by forearm cross-sectional area, there is satisfactory normalization to allow discrimination between normals and patients with various muscle diseases (16).

The role of eccentric contractions in a regimen of therapeutic exercise remains to be determined. The clearest advantage for eccentric exercise would appear to be when the goal involves hypertrophy of the muscle, where the key parameter is the tension in the muscle (17). The tension of a maximum isometric contraction is the most that actually can be produced by the muscle itself. A higher tension can be supported by the activated muscle as it lengthens, but only if the tension is imposed from an external source. Bodybuilders are skilled in imposing eccentric 'overload' during training, to stimulate an increase in muscle bulk (18).

The high apparent work output of a carefully executed eccentric exercise could yield the psychological benefit of an improved sense of self-efficacy in a weak or apprehensive patient. However, the hazard in applying such overloads is the possibility of causing disruption of the muscle or tendon. Even for loads less than the maximum isometric tension at a particular muscle length, eccentric exercise tends to cause disruption of the contractile apparatus and delayed muscle soreness (14). Concentric exercise causes neither. For the muscle in situ,

timely inactivation of motor units probably is more important than timely activation, in order to permit lengthening to occur without damaging loads developing in the contractile apparatus. Indeed, training reduces delayed muscle soreness (19).

In terms of the biomechanical analysis of muscle action, these results suggest that muscle be thought of as being capable of two different types of action. The familiar concentric contraction causes movement. The isometric and eccentric contractions represent the ability of the muscle to be positioned and then to be made very stiff, so that it can act as a passive, elastic element in response to an imposed load. The latter role is passive in the sense that the metabolic energy required is essentially just that to maintain the activated state, but precise neural control of the contraction is required if the mechanical integrity of the muscle is to be preserved.

In summary, a stretch-shortening cycle will always improve muscle efficiency since the force enhancement during stretching remains inexpensive in terms of chemical energy cost. We hypothesize that the high apparent relative metabolic efficiency of eccentric exercise observed in our experiments is due to the mechanism of enzyme which effects chemo-mechanical coupling, the actomyosin ATPase. The substrate for this enzyme is ATP, which is produced in the mitochondria and translocated to the myofibril by diffusion of phosphocreatine. The product of the process is tension, which can be produced without overall shortening of the contractile apparatus, at the cost of a small amount of metabolic energy. That is, activation of the muscle makes it stiff, and able to support high external loads. If the contractile apparatus is allowed to shorten, the ATPase cycles more rapidly and consumes more metabolic energy. Only in this circumstance does the muscle actually do work in the usual sense. To maintain the supply of metabolic energy at the contractile apparatus during a

concentric contraction, the rate of energy transduction from the mitochondria through the phosphocreatine shuttle increases, and changes occur in the relative abundance of phosphocreatine and inorganic phosphate. Under steady conditions, the latter can be measured quantitatively via P-31 NMRS. Overall, this means that the behavior of the oxidative metabolism of the mitochondria can be manipulated and measured in human muscle in situ, continuously and quantitatively, at rest and during exercise, painlessly and noninvasively, in health and in disease.

5.3 The Importance of Muscle Contraction Velocity

5.3.1 Introduction

Following seminal work in the laboratories of George Radda and Britton Chance there have been growing numbers of reports of the clinical applications of P-31 Nuclear Magnetic Resonance Spectroscopy to muscle disease (20-28). In most studies ratios of high energy phosphate compounds measured spectroscopically have been related to the mechanical state of the muscle. Three mechanical states have been used; resting, exercise and post-exercise recovery. Though spectroscopic considerations have usually been fairly rigorous, there has been less attention paid to the mechanical variables. At best, muscle has been treated as a Newtonian machine with output expressed as work rate (power). Our early observations of non-Newtonian characteristics of muscle (29) are supported by a body of literature extending back to the turn of the century (30-32). We therefore hypothesize that the relation between biochemical and mechanical work rates cannot be studied without accurate measurement or control of contraction velocity, and that increased clinical utility of NMRS will result from quantification of this joint relationship. We study the P*i*/PCr ratio in

human finger flexors in a steady state of rhythmic flexion-extension under several combinations of mechanical work rate and peak contraction velocity.

5.3.2 Experimental Methods

Exercise protocol The subject (AMWP) placed his right forearm in the magnet, and with 4 fingers, gripped a handle connected by a non-distensible fibre-glass belt and pulley to a 6 foot elastic cord system hung from the ceiling (Fig. 5-6). A force transducer was positioned in-line with the belt, and a distance transducer was incorporated into the pulley. The subject pulled the handle a fixed distance (2.2 cm) in and out once per second for 5 minutes for each run. To keep the mechanical kinetics as constant as possible throughout such a run, the subject watched the wave from the distance transducer on an oscilloscope screen and tracked his movements to a second waveform trace supplied by a signal generator. A series of 4 such waveforms runs were conducted (Fig. 5-7) at force F determined by the elastic cord. Mean mechanical work is the same for all 4 waveforms but the peak velocity attained in each contraction is not. The force was then increased by stretching the elastic cord further and the whole series repeated. Four such force series were done on separate days, using forces all less than 10% of the subject's maximal contraction strength (Fmax). In addition 2 further series were done. One incorporating a very low force F and maximal contraction velocities, and another in which the contraction velocity was kept the same at the lowest level but the elastic force was increased over successive runs. Reproducibility was assessed by examining the overlap of this last series with the previous ones and by repeating a series.

Mechanical monitoring Data from the 2 transducers was digitized at 20 Hz. through an analogue-to-digital convertor and fed to an IBM AT computer using

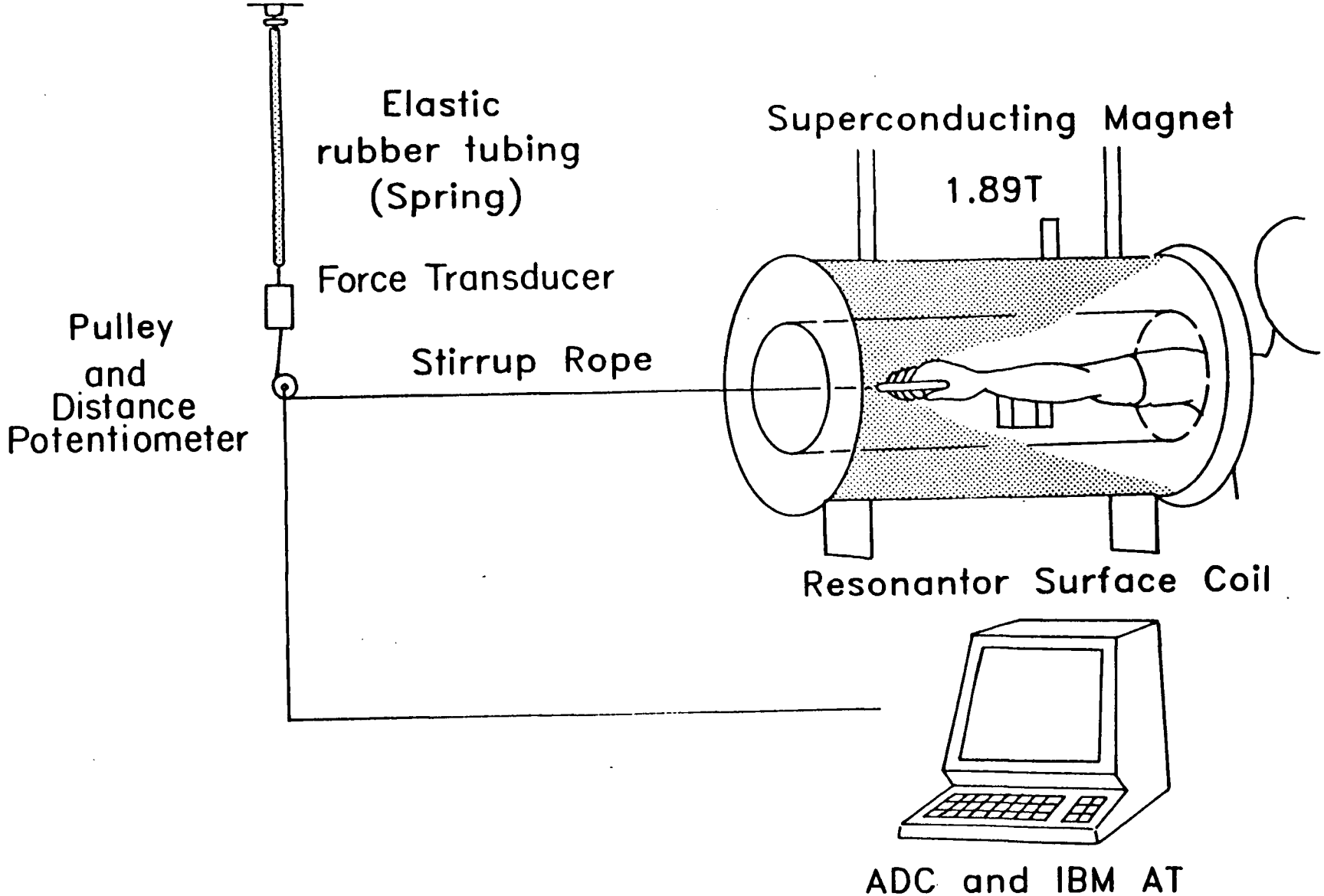

Figure 5-6 Experimental setup to examine the importance of muscle contraction velocity.

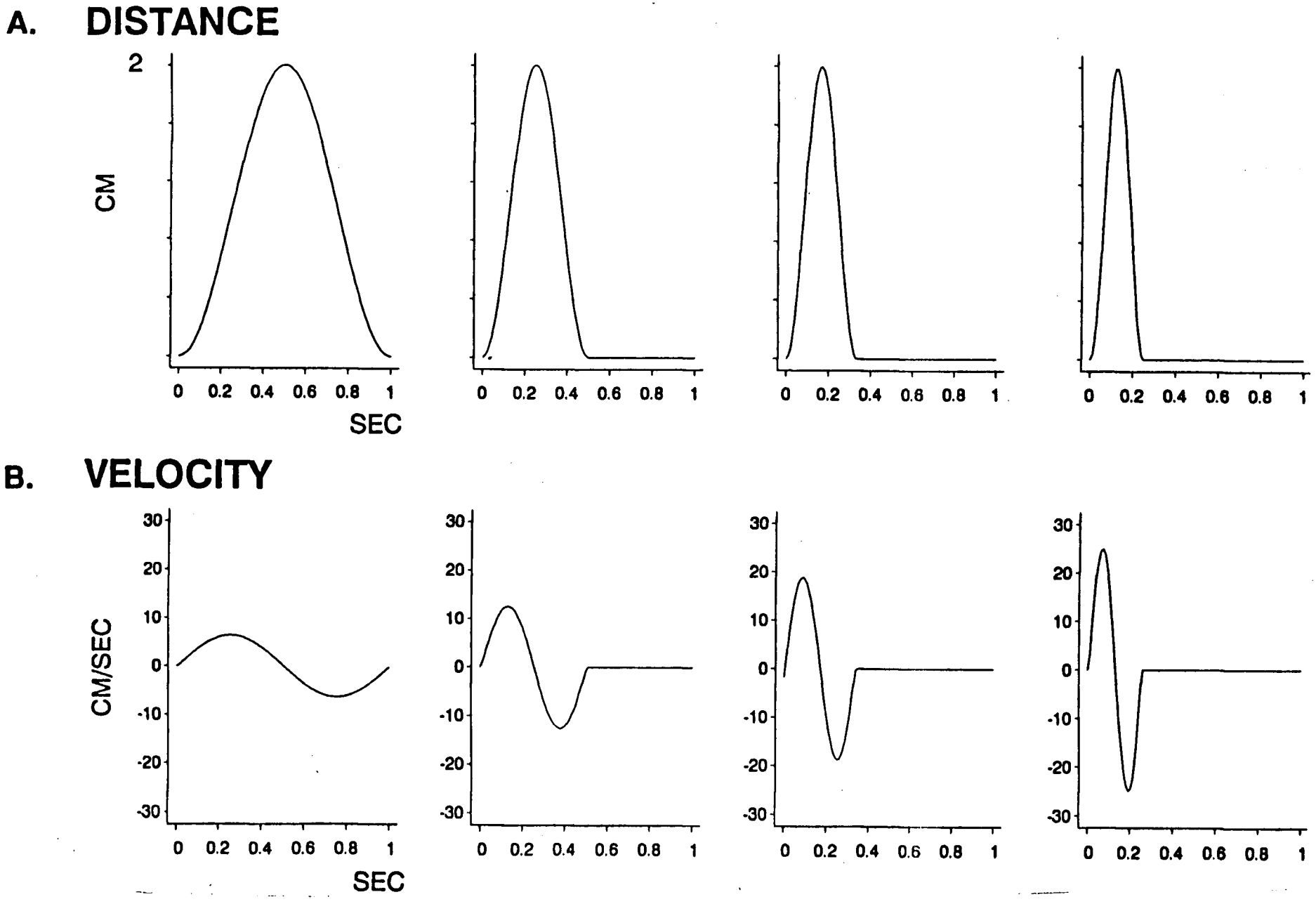

Figure 5-7 Contraction profiles. (A) The 4 waveforms tracked by the subject are depicted in these Distance vs Time plots. They are generated using one cycle of 1, 2, 3, or 4 Hz wave in each on second period. They peak to peak amplitude corresponds to an excusion of 2.2 cm. of the subjects fingers. (B) shows the first differential of the distance trace in plot (A) i.e. Velocity vs Time.

Labtech Notebook software (Wilmington, MA). Signal differentiation to obtain a velocity trace was performed using DADiSP Signal Processing software (Cambridge, MA) and positive velocity peaks extracted and averaged over periods corresponding to the NMR acquisition periods. We refer to this variable hereafter as peak concentric velocity, Vcp. The velocities attained in the maximum velocity run were used to determine Vcp_{max}. Velocities are expressed as a proportion of this value, V/Vmax.

Spectroscopy P-31 NMRS measurements were collected on a 1.9 Tesla Oxford Instruments spectrometer with a 30 cm. horizontal bore, as described in Chapter 4 of this thesis. The coil is a custom built resonating coil of 4 cm diameter. Peak heights were used for quantification but the P*i* peak width was minimized using a roving coil mechanism. This allows a topographical search of the muscle during steady state exercise for the area of maximal biochemical involvement and avoids P*i* broadening due to interrogation of different muscle bellies. Coil localization was determined initially in this subject and not changed thereafter. A low flip angle was used to limit the volume of interest. Studies using our protocol with a phosphocreatine/ATP/phosphate agar phantom suggest that significant contributions to the signal come from a depth of up to 2.5 cm for a pulse of 35 μsec., and that differential saturation with depth does not contribute significant error to the estimate of the P*i*/PCr ratio.

The spectroscopic indicator of biochemical work was the inorganic phosphate/phosophocreatine (P*i*/PCr) ratio. Gyulai *et. al.* have presented data of isolated rat heart mitochondrial suggesting an exponential relationship exists between P*i*/PCr measured by NMRS and the rate of ATPase activity (33). We have conducted time gated studies looking for variation in P*i*/PCr within the one second duty cycle when work rate varied dramatically during that cycle. We

observed no significant fluctuations within the range of outputs used in the present experiment and conclude that the Pi/PCr ratio can be taken to represent an averaged index of chemical power.

5.3.3 Results

We observed a strong, approximately exponential dependence of the Pi/PCr ratio on peak contraction velocity independent of mean mechanical work rate (Figure 5-8 and 5-9). The data are well summarized (R^2= 0.88) by the following equation:

$$\log_e (Pi/PCr) = 41.6\ FV + 2.2\ V + 314\ F^3 - 2.3 \qquad (5\text{-}3)$$

where V represents relative peak concentric velocity Vcp/Vmax and F represents relative force F/Fmax.

This equation defines a surface which shows the joint dependence of the Pi/PCr ratio on both force and peak velocity under the conditions of this experiment where the distance of contraction is kept constant (Fig. 5-10).

5.3.4 Discussion

If human muscle were thermodynamically linear for concentric contraction then each of the 4 displacement waveforms shown in Fig. 5-7 would have the same metabolic cost and the plots of Pi/PCr against peak velocity would be flat. Our data show clearly there were large differences in metabolic cost between fast and slow displacements. They refute the adequacy of average mechanical power output (work rate) as a sole parameter in muscle spectroscopy experiments.

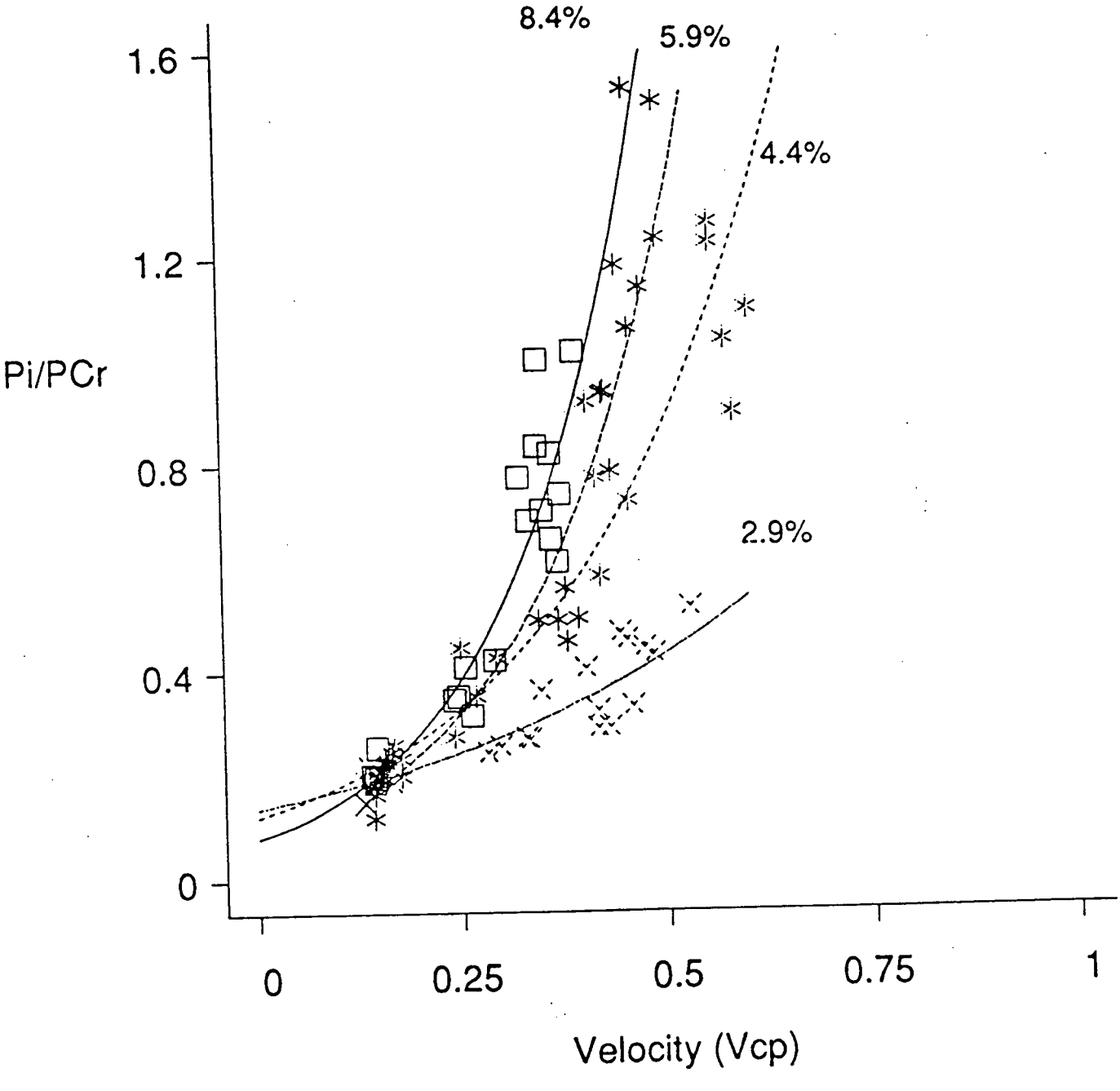

Figure 5-8 Exponential regression lines of velocity vs Pi/PCr for elastic force series corresponding to F/F_{max} of 8.4%, 5.9%, 4.4%, and 2.9%.

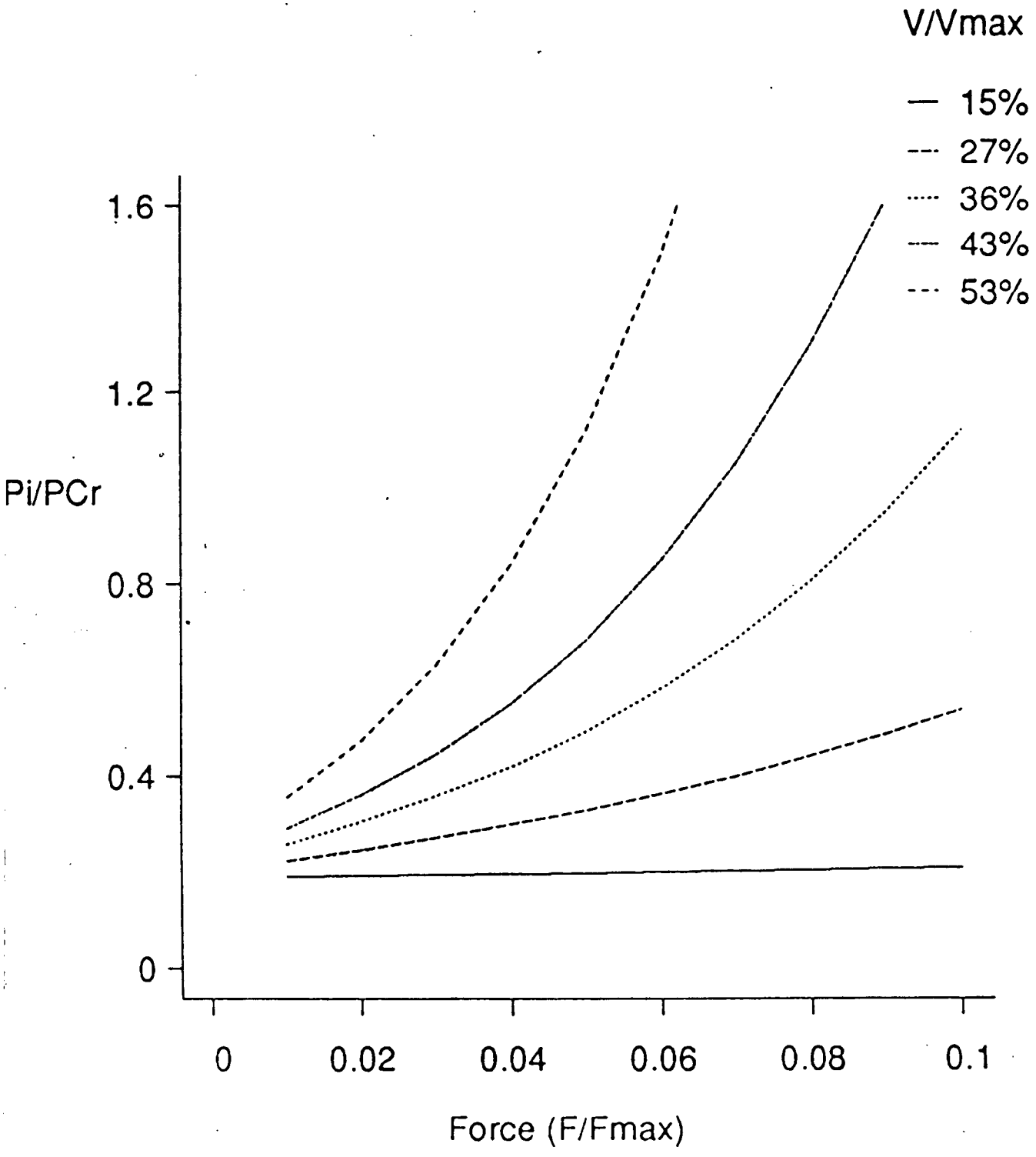

Figure 5-9 Exponential regression lines of force vs Pi/PCr for elastic force series corresponding to V/V_{max} of 15%, 27%, 36%, 43%, and 53%.

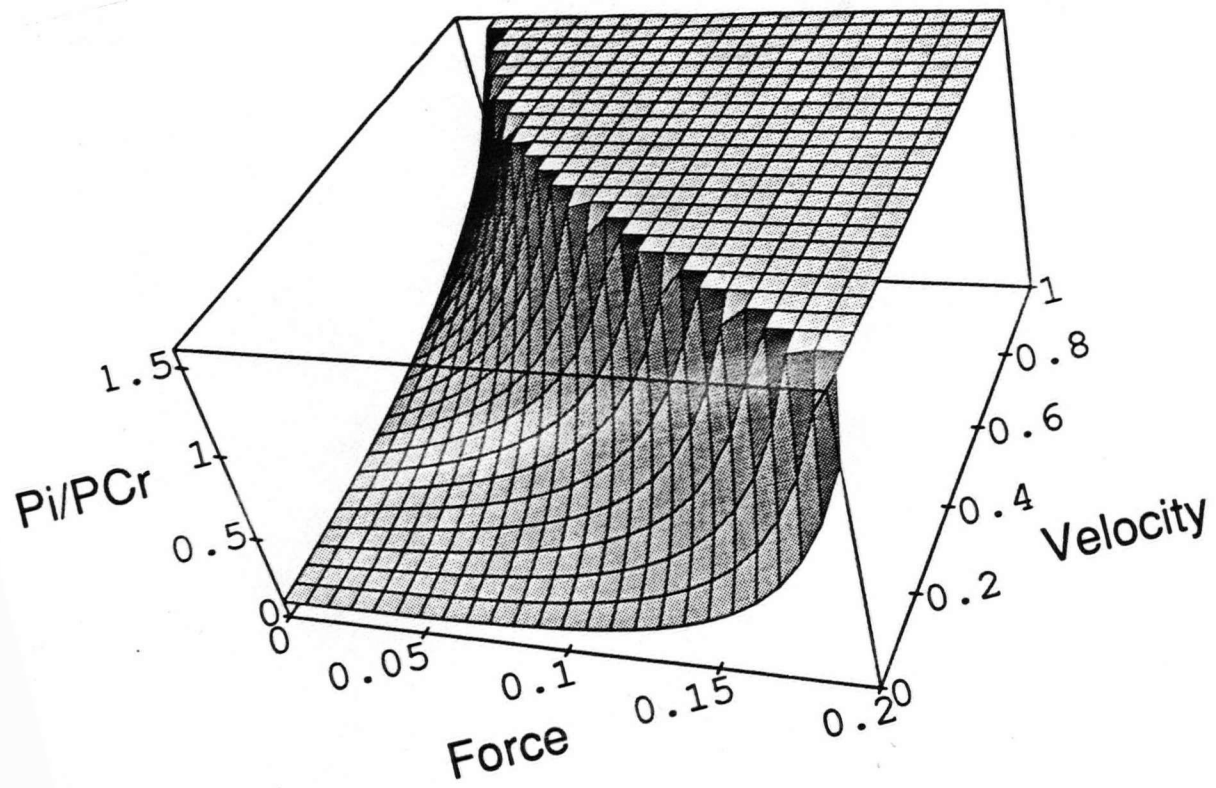

Figure 5-10 3-D surface derived from equation 5-3 representing the joint dependence of Pi/PCr on both force and peak velocity. These axes are also proportional to mean power and peak power respectively.

The dependence of chemical power consumption on contraction kinetics is not a new observation. Laulanie in 1905 described an inverse relationship of muscle efficiency (work/total energy) to contraction velocity but it was Fenn in 1935 and later A. V. Hill who established the more critical relationship between force and velocity (30-32). Though the biophysics underlying this phenomenon is still not fully illucidated, it would appear that the quantal contractile events in cross-bridge cycling may either store force or generate motion but to an extent these must be mutually exclusive. This reciprocity is embodied in the Hill equation:

$$V\,(F+a) = b\,(F_{max}-F) \qquad (5\text{-}4)$$

which can be rewritten:

$$VF + aV + bF = c \qquad (5\text{-}5)$$

Viewing the surface in Fig. 5-10 from above, a series of contour curves can be generated for constant Pi/PCr values (Fig 5-11). Solving Equation 5-3. for $Pi/PCr = 1$ gives us the equation describing this contour:

$$41.6\,VF + 2.2\,V + 313\,F^3 = 2.33 \qquad (5\text{-}6)$$

This has very similar form to the Hill equation except for a higher power dependence on F. The present data are not sufficient to create more than an empirical formulation with a number of solutions. These solutions however all share the basic framework of a reciprocal relationship of force and velocity. The present human study is novel in that contrary to previous experiments using tetanically stimulated muscle *in-vitro*, we are here able to examine the trade-off of force for velocity at sub-maximal levels of biochemical work. Furthermore, and most importantly, in our experiments it has been possible to normalize mechanical power so that velocity may be examined independently of it's contribution to mechanical power. The reciprocity of F and V could have been explained otherwise by their joint role in the determination of power (F x V) on a

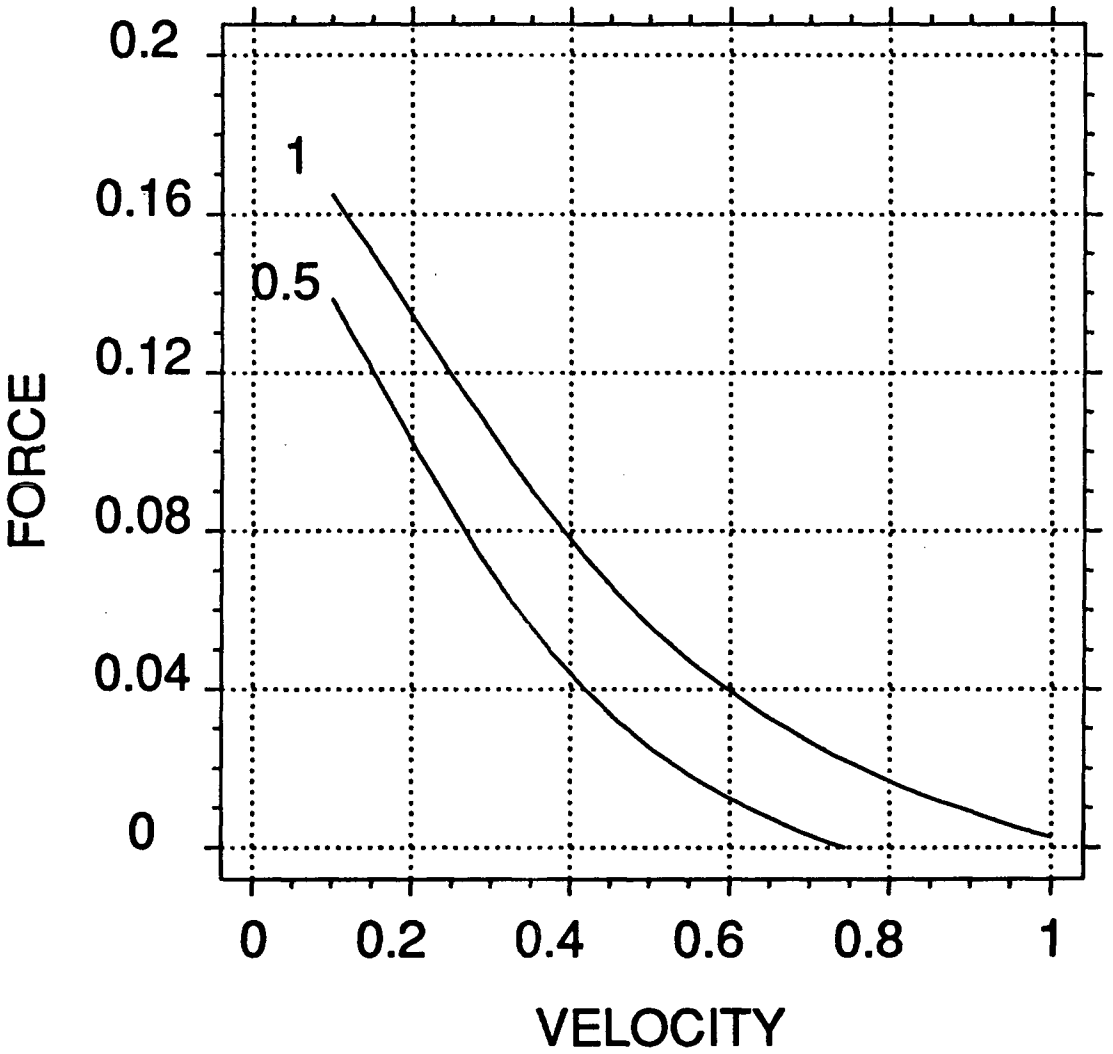

Figure 5-11a Contour lines from 3-D surface in figure 5-10 corresponding to P*i*/PCr values of 0.5 and 1.

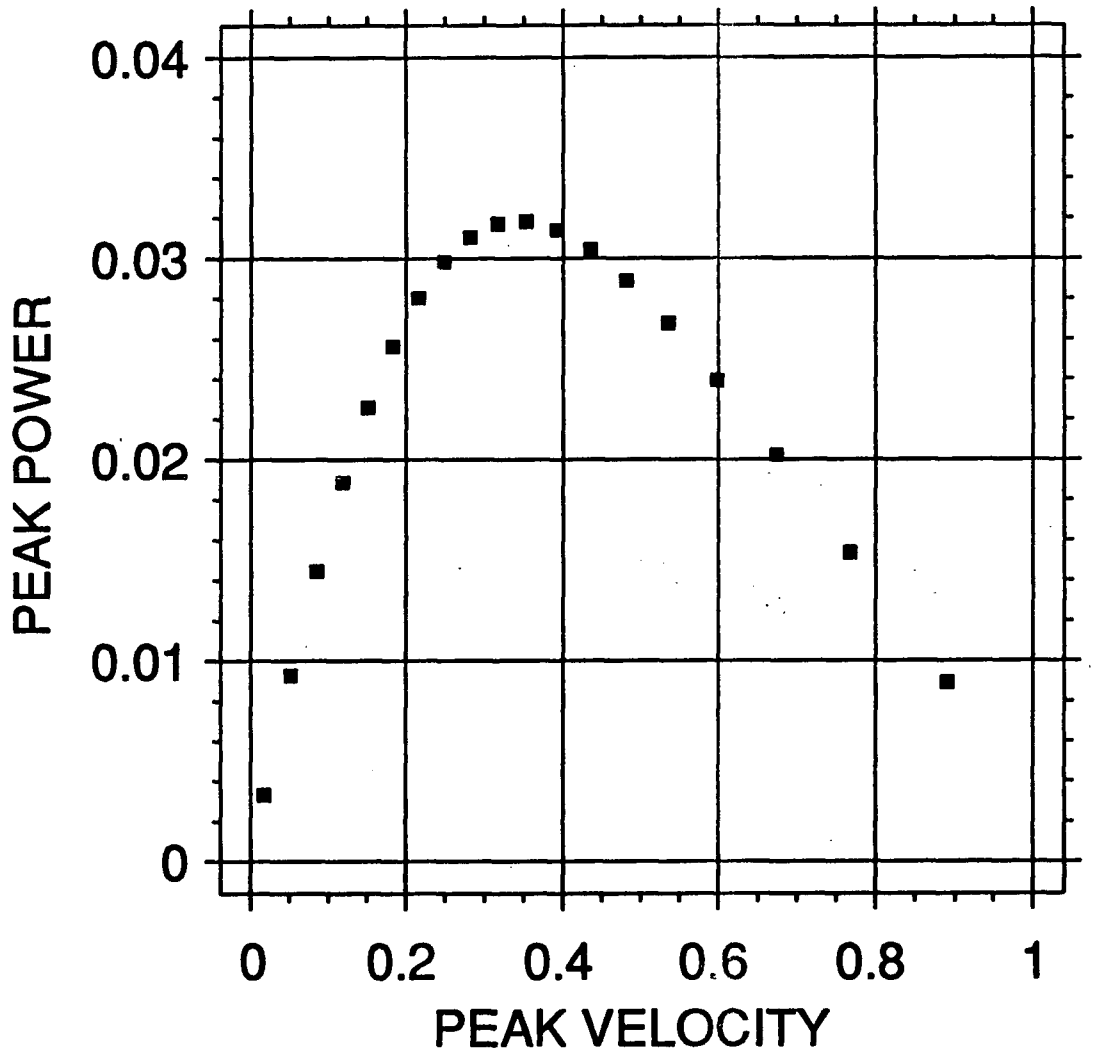

Figure 5-11b Efficiency curve at a given level of metabolic activity showing peak power output as a function of peak velocity at a Pi/PCr level of 1.

constant-total-power theory. This theory has also been refuted in *in-vitro* studies (31). We have not here varied force independently from it's contribution to mechanical power which may explain the better fit of our data to higher powers of F.

Another consequence of using voluntary muscle contraction rather than stimulated muscle is that the orderly recruitment of muscle fibre type is allowed to take place. As force or velocity of contraction increase, the representation of more glycolytic Type II fibres increases (34). Although the mechanical work obtained per ATP molecule may not be different in different fibre types contracting at the same rate, the biochemical derivation of that ATP is. Anaerobic production of ATP is less economic; it requires a higher substrate turnover rate per molecule of ATP produced. This would presumably be reflected spectroscopically as a higher P*i*/PCr ratio due to a right shift of the CPK and ATP equilibria. In summary, we would hypothesize that the shape of the surface in Fig. 5-10 is a manifestation of two physiological principles: the Fenn effect and differential recruitment of fibre types.

It is not possible to say what relative contribution these two components have. Indeed there is some contribution to the Fenn effect itself which may be due to pseudo-recruitment. That is although all muscle fibers are being stimulated, there may only be a proportion of the fastest twitch fibres that can keep up at higher velocities (32). It may be possible however to compare this human data roughly to in-vitro data by comparing the shape of efficiency curves. Using the data of Kushmerick and Davies, Wooledge has estimated the thermodynamic efficiency of contraction at different velocities in frog sartorius (efficiency = work/free energy) and suggested that it increases up to a V/Vmax of 35% then declines more or less linearly (35-36). We can construct a similar sort of efficiency curve with respect to velocity using the FV relation in Fig. 5-11.

Though we cannot measure ATP consumption these curves represent constant biochemical work rate as far as can be intimated by the Pi/PCr ratio (contours are shown for 0.5 and 1). The product of F and V plotted against V therefore gives the peak mechanical power output vs peak velocity for a given level of biochemical work. Figure 5-11a shows efficiency curves for 2 Pi/PCr levels. They have almost identical form to those shown by Wooledge with peak efficiency at a V/Vmax of 35%. Given the uncertainty of the relationship between Pi/PCr and ATP consumption, in the presence of fibre recruitment, this correlation with *in-vitro* work is somewhat surprising. It might suggest that the Fenn effect rather than physiological fibre recruitment is the major contributor to the relationship of biochemical efficiency to contractile velocity demonstrated here in normally contracting human skeletal muscle.

Unfortunately this relationship of peak power to peak velocity may not really be directly comparable to one of mean power to mean velocity. Our data does not give the latter because mean velocity is the same in all runs at 2.2 cm/sec. The maximum efficiency seen at V/Vmax of 35% signifies the peak velocity at which the maximum peak power can be obtained at Pi/PCr = 1 (Figure 5-11b). The peak velocity for which maximum mean power can be obtained is somewhat lower. It can be determined directly from the contour curves of Fig. 5-10 because mean velocity is constant at 2.2 cm/sec therefore mean power is proportional to Force. This curve has no maximum within our experimental range, however our range does not extend below a velocity of 12.5% (V/Vmax), due to the difficulties in obtaining accurately meaningful data at lower velocities.

If it is true that the Fenn effect contributes significantly to this observed velocity dependence, one ramification is that cardiac muscle, as it too exhibits the Fenn effect (31), should be approached with the same attention to contraction

kinetics in NMRS studies. Similarly with calf muscle studies, it is possible that the different curve shapes obtained by Chance and his colleagues may be a consequence of changes in contraction velocity. Pictorially this could be represented on the 3-Dimensional surface of Fig. 5-10 as a curve crossing onto successively lower velocity contours as power output increases. This is frequently observed in exercise studies as muscle output increases, lower velocities are subconsciously used to defer onset of fatigue. Though we have not covered the topic of pH in this study, this variable suffers from the added confounding effect of excretion kinetics. In our experience pH is even more susceptible than Pi/PCr to contraction kinetics and hence a less reliable clinical parameter. To improve it's utility however these same principles should apply.

Extrapolation of Chance's original concept of relating mechanical to biochemical power beseeches the question in general whether all P-31 MRS including brain should be interpreted in the light of cellular work rate. Though cellular work is easy to appreciate in terms of muscle contraction it has been shown that Ca^{+2} pumping accounts for 25% of ATP consumption in active muscle (37). Cellular work in brain is primarily ion pumping and there is a smaller range of work than in muscle; nevertheless, Pi/PCr ratios may well be quite variable within that range, underlining the need for a measurement of cellular work.

The present study describes only a single subject and does not address inter-subject variability. However, our results clearly outline a pattern which indicates the importance of velocity in affecting biochemical efficiency. Furthermore, we have experience with of over 300 clinical studies using a protocol that embodies the physiological principles described in the last chapter as well as effective localization and normalization techniques. This technique has proved to be reproducible with clinically useable normative ranges and sensitive

in the diagnosis of mitochondrial dysfunction and in the monitoring of new therapies (16,39-41).

In the next section, we will start investigating certain important pre-conditions which may affect endurance. However, before we present our own experimental results, let's review what we know about inter-subject variability from the literature.

5.4 Inter-subject Variability

Physical performance in general terms is determined by a combination of many different physiological and psychological factors. The relative importance of these factors vary with the type of exercise carried out. These can be summarized in three main ones, namely energy yield (aerobic and anaerobic power), neuromuscular function (coordination and muscle strength) and psychological factors. The physical performance can be negatively or positively modified by factors such as heat, cold, sickness and altitude; it can also be improved by physical training. By definition, maximal aerobic power is the highest oxygen uptake obtained during dynamic exercise with large muscle groups involved, performed at sea level. However, there is a limit which is determined by circulation, stroke volume, hemoglobin concentration, heredity, age, sex, level of health, etc.

The structural differences in muscle between individuals determine also their physical performance capacity (42). The maximum isometric force that can be generated by a muscle can be predicted with considerable accuracy based on the total physiological cross-sectional area of all muscle fibers. For example, the maximum isometric tension normalized to cross-sectional area (i.e. specific tension) for a variety of fast skeletal muscles appears to be about 23 N/cm^2;

whereas, slow motor units seem to have a lower specific tension, i.e. about 17 N/cm^2 (43-47). Besides, there is a strong environmental (e.g. training) influence. It appears that neural adaptations are the primary factors contribution to strength gains during the initial part of training (48-50).

Skeletal muscle is a very adaptable tissue which responds to an altered usage pattern by changing its structure to suit the new metabolic demands. There exists an interplay between structure and function such that signals which result from altered function feed back to modify structure. Although a number of stimuli have been identified which result in adaptive change, such as endurance training (51), chronic stimulation (52), vascular insufficiency (53), and altered thyroid state (54), the nature of the intracellular signals which trigger the process of adaptation is unknown.

Muscle Mass Strength and resistance training increase lean body or muscle mass (55-60). Muscle hypertrophy, as reflected by a greater muscle cross-sectional area, is primarily the result of enhanced size of individual muscle fibers, as indicated by the increase in myofibrillar volume (55-56, 61-63). In strength trained athletes, such as sprinters, synthesis of contractile proteins occurs in both fiber types, but seems to be greater in fast twitch than in slow twitch fibers. In addition, according to Staron *et al.* (64), it appears that the fast twitch hypertrophy is confined to the oxidative fast twitch, Type IIA fibers. Endurance athletes, such as bodybuilders, tend to display a relatively high percentage of slow twitch fibers (65-67).

Capillary Supply The capillary density and the mean muscle fiber in skeletal and heart muscle usually show an inverse relation (68). Since strength training is typically associated with increased individual muscle fiber size, one would

expect capillary density, assuming no capillary neoformation, to decrease in parallel with strength training-induced muscle hypertrophy. In concordance with this hypothesis high-caliber Olympic weight- and power-lifters displayed 30% lower capillary density than non-trained subjects (69). Endurance trained athletes, however, demonstrated somewhat greater number of capillaries per fiber and similar capillaries per unit area as non-athletes (65).

It therefore appears that heavy-resistance training, emphasizing high - load, low-repetition exercises, will not result in capillary proliferation. Instead, when pronounced hypertrophy of individual muscle fibers occurs, the capillary density decreases. A more intense training regimen, on the other hand, emphasizing moderately high load and a high number of repetitions , as performed by bodybuilders, may induce a certain capillary neoformation.

Mitochondrial Density Mitochondrial density is reduced in trained muscles (61,66,70). Thus, whereas mitochondrial volume remained unchanged, myofibrillar protein content increased. These findings are in contrast to earlier observations on lower mammals (71).

Enzyme Activity Six months of strength training performed either as heavy-resistance or explosive-strength training was not associated with any increased activities of enzymes reflecting phosphagen, glycolytic, or oxidative metabolism (70).

Muscle Substrate Levels Glycogen levels increase and increased capacity for intra-muscular lipid storage were confirmed in a group of bodybuilders (63,70); whereas, ATP, PCr, Cr, as well as glycogen levels were found to increase in individuals who were involved in resistance training (72). However, it is not

known if this response is due to hormonal stimulation, but it has been suggested that increased testosterone levels may enhance glycogen synthesis (73-74).

Lactate Removal Cellular adaptation with training would also enhance the rate of lactate clearance (75). It also suggests that lactate formed in one part of a working muscle can be oxidized by other fibers in the same muscle or by less active neighboring muscle tissue (76). Besides, some mitochondrial myopathy patients may have developed an adaptive mechanism for moving intracellular lactate into the bloodstream (77).

Work Capacity Strength training is known to increase both maximal force production and the rate of force production, expressed either in absolute terms or relative to muscle cross-sectional area. These effects are mainly brought about by increased muscle mass and/or neural phenomenon such as recruitment or frequency modulation (78).

Hormonal Response The testosterone/cortisol ratio increased progressively during the training period and decreased at cessation of training (79). This change was brought about by a significant decrease in cortisol and a concomitant elevation of testosterone concentration. A positive relationship was confirmed between the increase in maximum strength and the increase in the testosterone/cortisol ratio suggesting a hormonal influence on the adaptive response to strength training.

Heavy Resistance Training Despite the relatively low energy output, plasma levels of glucose, glycerol, FFA and lactate were elevated during exercise (80). Thus, heavy-resistance exercise of high intensity could mobilize all available

energy systems despite the relatively low energy output as reflected by oxygen consumption (48% of $V_{oxygen\ max}$) measured during exercise. This finding may imply that factors other than the relative exercise intensity per se dictates the substrate choice during prolonged exercise. It is known that weight-lifting activities are associated with increased blood pressure response (81), which in part is attributed to increased sympathetic activity. The increased sympathetic drive of heavy-resistance exercise is also reflected in the multifold increase in plasma catecholamines as compared to walking at the same energy expenditure (82). It therefore appears likely that the load per se, applied in heavy-resistance exercise, influences the acute metabolic and hormonal response and probably the subsequent long-term metabolic adaptation.

Conclusion In summary, long-term heavy-resistance training is associated with increased synthesis of myofibrillar proteins. The increased muscle cross-sectional area subsequent to training is brought about mainly by hypertrophy of fast twitch fibers with less of hypertrophy of slow twitch fibers. There are also reasons to believe that long-term training may produce a proliferation of muscle fibers. Along with the hypertrophic effect, mitochondrial volume density decreases. Since typically no capillary neoformation occurs during strength training the capillary density is reduced. Similarly, the activity of enzymes reflecting the 'aerobic energy machinery' decreases. This may reduce the aerobic endurance capacity. The rate of muscle glycogen synthesis is enhanced following strength training. However, many of the training improvements are lost within several months; even among highly trained athletes the beneficial effects of exercise training are transient and reversible (83-85).

5.5 The Effect of Metabolic Acidosis and Alkalosis

5.5.1 Introduction

Sprint-trained athletes demonstrate a remarkable ability to perform high-intensity, short-duration exercise which quickly results in fatigue. The energy requirement is being met principally by anaerobic glycolysis resulting in the rapid production of ATP, the energy source of muscular contraction, with an associated increase in muscle and blood lactate levels. However, the mechanism for these enhanced performance capabilities have not been fully elucidated. Elevation in glycolytic enzymes and increased fast-twitch fiber compositions which would result in an enhanced ability to produce ATP do not appear to be capable of accounting for the greatly enhanced performances (86-87). Associated with these performances are large accumulations of anaerobic end-products which produce decrements in intracellular pH. Because intracellular pH decrements of sufficient magnitude have been shown to inhibit athletic performances (88-89), it has been postulated that sprint-trained athletes have an enhanced proton-sequestering capability which would ultimately alter the rate of pH decrement. This would delay the inhibition of the enzymatic and contractile machinery resulting in enhanced performances. The intracellular buffers that are capable of contributing to this enhanced buffering capability were identified as inorganic phosphate, protein-bound histidine residues, the dipeptide carnosine, bicarbonate, and creatine phosphate. Thus, it has been suggested that increased buffer capacities within sprint-trained athletes may be a contributing factor to his/her enhanced anaerobic performance capacities.

The removal of lactate has generally been assumed to be a simple process of diffusion down the concentration gradients (90-92). It has become apparent recently that lactate transfer within a few tissue is carrier- mediated and that the

transfer process is pH-dependent. Lactate has many disposal sites: it can be stored within the producing muscle (93-94) or diluted in blood and other body fluids (90-92), and blood lactate may be taken up by liver, heart muscle, kidney, brain (95) and active and inactive skeletal muscle (96). Protons associated with lactate accumulate within muscle and are released to blood and extracellular fluids; it has been reported (92) that the rate of H^+ release was dependent upon external bicarbonate concentration

Evidence to support the theory that H^+ accumulation results in failure to maintain force during muscular contraction has been provided by studies which induced a state of alkalosis or acidosis in subjects prior to exercise. Sodium bicarbonate and sodium citrate ingestion have been shown to elevate preexercise blood pH and increase speed and endurance (97-98) while ingestion of ammonium chloride has resulted in a reduction in pre-exercise pH and a decrease in time to exhaustion (99-102). H^+ accumulation may impair muscle performance through its effect on glycolysis, on the contractile process itself, or on certain physiologically important equilibrium reactions. The present study was undertaken to compare the effects of a metabolic acidosis and a metabolic alkalosis on the high energy phosphate responses in man during exercise and to explore the utilities of P-31 NMR spectroscopy in monitoring such changes.

5.5.2 Materials and Methods

Six healthy male volunteers performed exercise at 5, and 10% of their maximum power output on three occasions, in random order. Each study was preceded by a 3-hours period in which capsules were taken by mouth, containing either $CaCO_3$ (control), NH_4Cl (acidosis), or $NaHCO_3$ (alkalosis) at a dose of 0.3 g/kg body weight. During the 3 hours in which the capsules were

taken the subject remained at rest and blood samples were obtained from a polyethylene catheter placed in a forearm vein.

The exercise consisted of raising and lowering a weight at a steady rate, using the finger-flexors. The subjects exercised for 5 minutes at a power output equivalent to 5% of their maximum grip strength, followed by one minute of brief resting, and then continued for 5 minutes at a power output at 10% of maximum grip strength.

P-31 NMR spectra were collected every minute during exercise as well as during the subsequent 10 minutes of recovery. The mechanical output of the contractile apparatus of the muscle was recorded by a position potentiometer and a force transducer. The signals were fed into a data acquisition program running on a personal computer. The computer program calculated the instantaneous mechanical power and velocity, as well as their running averages from the position-time data.

5.5.3 Results

Administration of $CaCO_3$, NH_4Cl, and $NaHCO_3$ resulted in a clear separation of pre-exercise blood pH among the three studies in each subject (Table 5-1). However, muscle pH (mean 7.0) at rest was not significantly affected despite an extracellular pH changes.

Table 5-1 Blood pH

Study	Blood pH
Control(Treatment A)	7.363+/-0.019
Acidosis(Treatment B)	7.235+/-0.027
Alkalosis(Treatment C)	7.422+/-0.009

The experimental design used in the present study ensured that each subject carried out identical exercise under three conditions of acid-base balance. Even though the mechanical power output as well as the exercise frequency were very much the same among different subjects and the three acid-base conditions; however, careful analysis of the mechanical data resulted in separation of the six subjects into two distinct groups: the first group of four subjects performing the exercise at a moderate velocity(0.2m/sec), and the second group of two subjects at relatively high velocity(0.45m/sec). The maximum velocity in our study was 0.55m/sec.

Our result showed that at moderate execise velocity, extracellular pH would not affect PCr utilization (Fig. 5-12). However, at high exercise velocity, significantly high percentages of PCr were used to fuel the immediate metabolic demands (Fig. 5-13). Since it is well documented that endurance time is prolonged under alkalosis (98), our result indicated that a slightly elevated intracellular concentration of either/or both P*i* and ADP might be necessary to trigger the increased recruitment of fast-twitch fibers as well as to enhance the body's proton-sequestering capability. Conversely, acidosis was associated with decreased buffering capability of bicarbonate, an inhibition of muscle glycolysis and lipolysis, and reduced endurance time (99-102); and our result showed that primarily PCr was used to meet the metabolic demand under acidosis condition.

5.5.4 Discussion

For many years it has been customary to consider the metabolic processes used in exercise in two categories- the aerobic oxidation of glycogen and fats, and the anaerobic metabolic of glycogen to lactate, these two processes being considered more or less separate. However, it has become clear that a dynamic

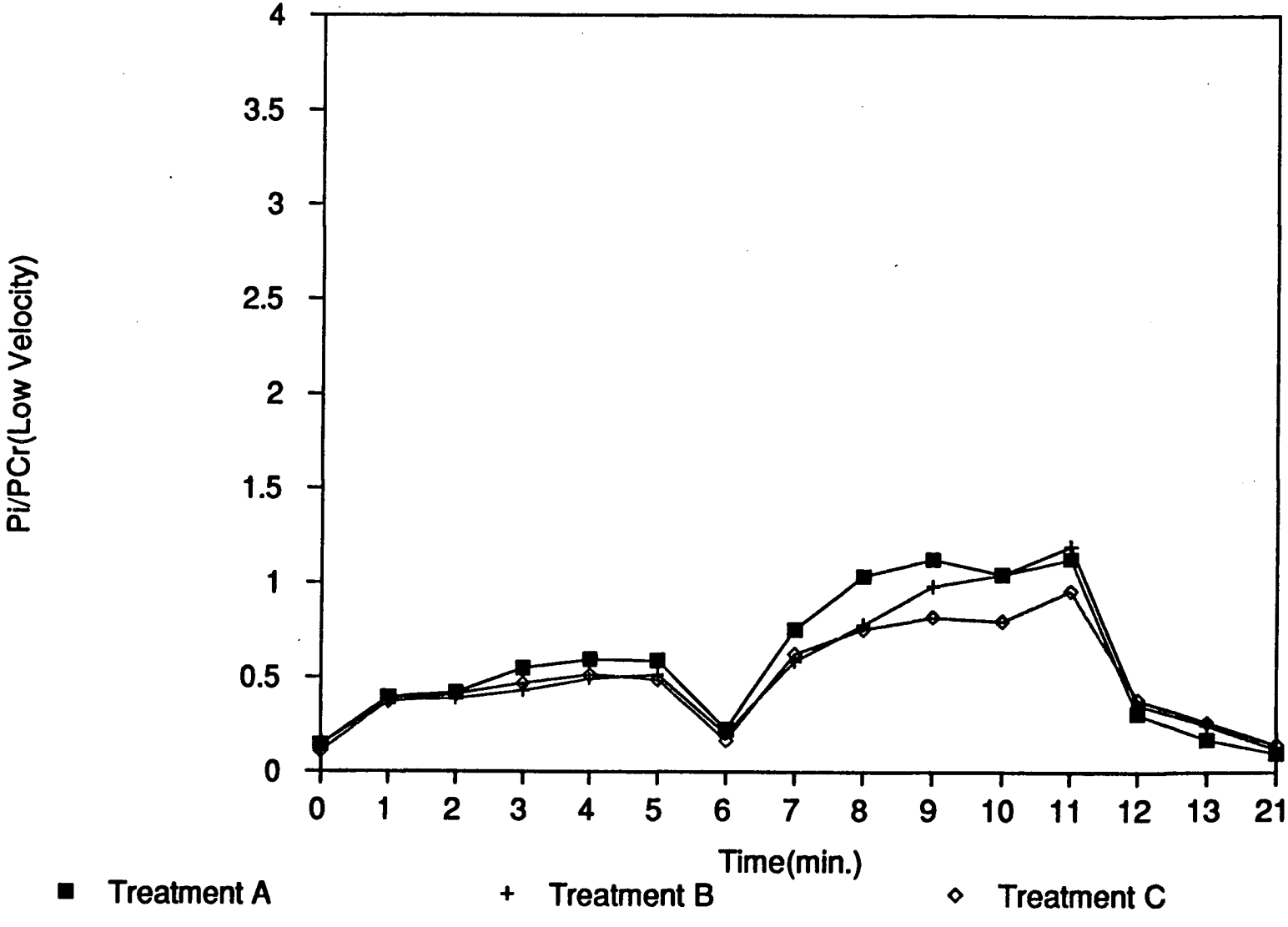

Figure 5-12 Effect of changing blood pH on muscle function at low to moderate exercise velocity.

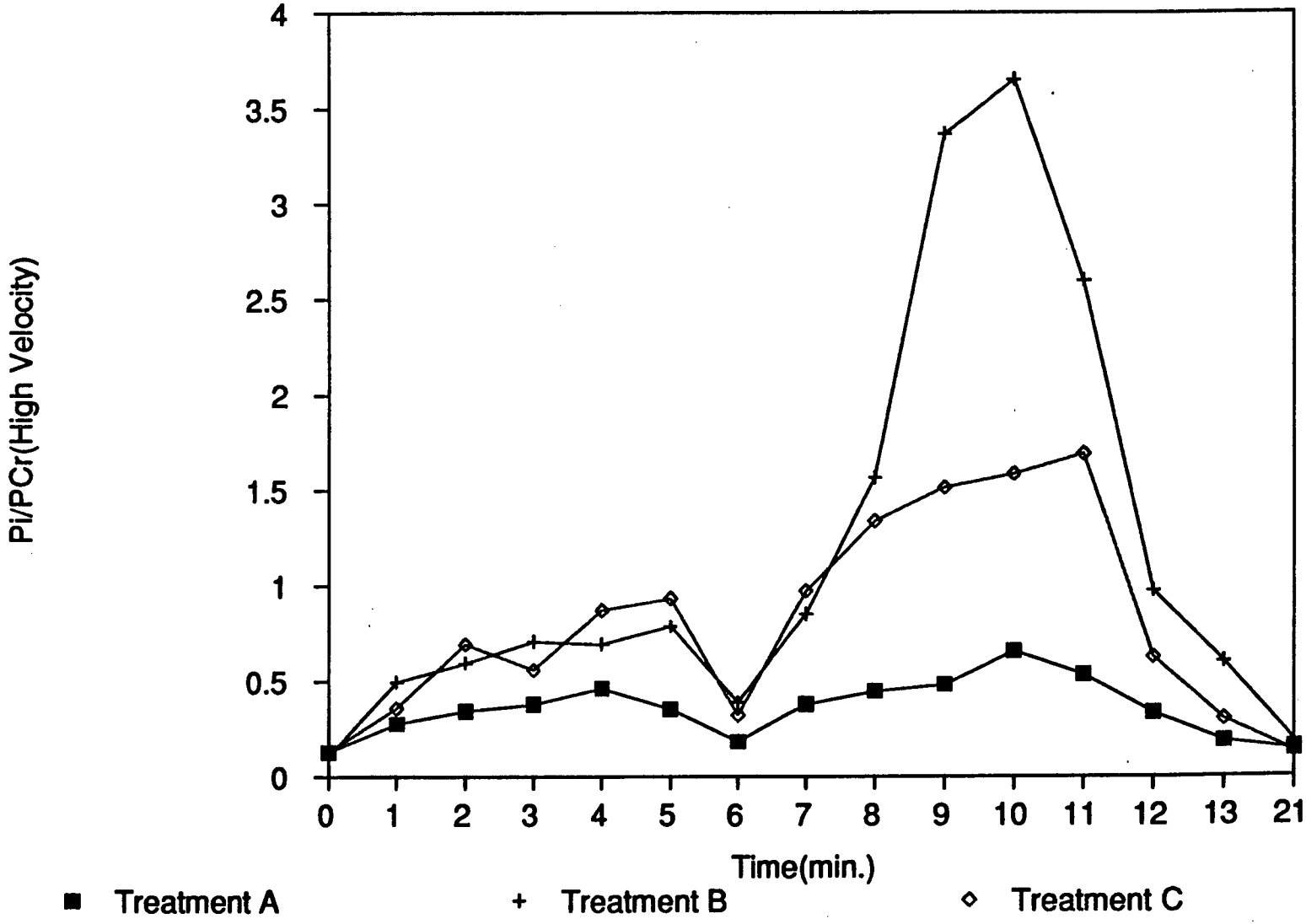

Figure 5-13 Effect of changing blood pH on muscle function at high exercise velocity.

relationship exists between these metabolic processes, in which each is capable of influencing the other in a variety of ways. The results of the present study may provide an explanation for the progressive reduction in endurance time when high levels of exercise are repeated, with only brief periods of rest between. This study also offers insight about variability even with the same individual depending on his physical and emotional conditions.

Extracellular pH decrease in the event of acidosis will place the muscle under enormous stress just to keep its internal environment isolated. Presumably, additional cellular energy in the form of ATP may be required just to keep H^+ ions outside, against a large proton gradient. Conversely, in the event of alkalosis, a portion of the lactate produced during glycolysis can be excreted via passive diffusion, thus conserving ATP for other metabolic functions.

Intracellular pH has many interactions with metabolic transformation. Decreased pH may affect membrane permeability to Na^+ and K^+ (103). As the pH is lowered, the sarcoplasmic reticulum binds more calcium, which may be essential for the activation of the phosphorylase in the glycolysis pathway. A reduced energy output via the anaerobic pathway will surely put a great strain on the creatine kinase system to produce ATP. Besides, a decreased active cross-bridge formation, due to proton competition with calcium for the actomyosin binding sites, may reduce exercise capability directly (104). An increased concentration of ADP could both slow down the cross-bridge detachment and reduce the activity of the Ca^{2+} pump ATPase of the sarcoplasmic reticulum membrane. With the reduced rate of ATP production when stimulation was continued, it was speculated that the decreased ATP/ADP ratio would fall below a level necessary for pumping calcium back into the sarcoplasmic reticulum at a normal rate (105) and therefore would slow down recovery.

The result from this section reiterates the importance of muscle contraction velocity, especially under unfavorable conditions. As the contraction velocity increases, progressively larger amount of PCr is used to fuel the contractile machinery. When glycolysis is slowed during acidosis, fatigue and pain set in to prevent further depletion of the PCr pool, thus avoiding the irreversible breakdown of ADP.

In the last section of this chapter, we will explore another aspect which may adversely influence the reproducibility of our exercise protocol. We will look at how muscle damage will affect subsequent exercise performance.

5.6 Exercise-induced Muscle Damage and Adaptation

5.6.1 Introduction

Exercise, especially unaccustomed strenuous activity, can result in damage to muscles. Many types of exercise have been shown to produce muscle damage, including isometric exercise(106-109), marathon running (110-113), and eccentric muscular activity (114-121). Evidence of damage includes morphological changes (114,122-127), temporary or delayed-onset muscle soreness and pain (108,115,121,128-130), performance decrements (131-137), and elevation of muscle protein levels in the blood, especially creatine kinase (107-108,115,118,138-141). Exercise-induced muscle damages is not permanent and tissues are repaired (113,123-125). Moreover, muscles adapt to stress of repeated exercise such that subsequent bouts of exercise result in little or no damage (107,115-116,120,142). Neither the precise cause of skeletal muscle damage induced by exercise nor the mechanism to explain the adaptation to training and repeat bouts of exercise are well understood.

Mechanisms Two basic mechanisms have been proposed to explain how exercise initiates damage. one mechanism describes a disturbance in metabolic function, and other addresses a mechanical disruption of the cell.

During prolonged submaximal exercise, metabolic events, such as ischaemia or hypoxia which result in altered ion concentrations, ATP deficiency and waste accumulation have been proposed to explain muscle damage (143-147). However, for eccentric muscle activity, if metabolic waste products were primarily responsible for exercise-induced muscle damage, then muscles which contract concentrically and fatigue more quickly would show more damage than muscles that develop active tension eccentrically; whereas, experimental results indicated just the opposite (114,132-133,148-154).

Many researchers base their arguments against metabolic hypotheses on the finding of greater damage following eccentric muscle actions (negative work) compared with concentric contractions (positive work). Muscles that develop active tension eccentrically require less energy but experience greater injury than muscles that contract concentrically, as indicated by morphological changes (114,127), delayed-onset soreness (119,136-137), performance changes (136-137), and increases in plasma proteins (114,118), especially creatine kinase (CK) which is found almost exclusively in muscle tissue, and is the most common plasma marker of muscle damage. EMG activity also is lower during negative work (maximal and submaximal) suggesting that relatively fewer fibers are recruited to produce large forces (155-156). Therefore, under comparable workloads, eccentric actions produce greater tension per cross-sectional area of active muscle than concentric contractions. In addition, eccentric muscle actions have been shown to produce more heat than concentric contractions at the same load (157-158). These elevated temperatures could damage structural and functional components within the cell. Electron micrographs have shown marked

broadening, streaming, and, in places, total disruption of Z-discs following eccentric exercise (117,122). In addition, structural changes include myofibrillar and sarcolemmal disorganization (114,123-124), widening of the A- and I-bands (114,124,127), displacement of organelles (124,127), increase in mitochondrial volume density (122,124), and cytoskeletal changes (125).

Repair Damage progresses in the postexercise period, but is not permanent (114,117,123-126). After eccentric exercise, there is an immediate decrease in maximal force production followed by a slow recovery (116,120,159). Strength may remain depressed for a week or longer (120).

Training A prior exercise may produce a rapid training response that could result in a protective effect. Training increases the number and size of mitochondria; subsequently, more ATP was available for maintenance of the cell membrane. Besides, any damage caused by the first bout of exercise might act as a stimulus for new collagen synthesis (120). In this way, the collagen structure would be strengthened and protected from further damage. In addition, stress-susceptible or degenerating fibres, which may develop through disuse or may represent a small percentage of ageing fibres, may embody a population of cells that are destroyed by an initial bout of exercise. Strong, health fibres that could withstand the effects of repeated bouts would survive.

Friden (117) has listed 3 possible mechanisms of structural myofibrillar adaptation that may result from eccentric training to limit damage. First, sarcomere length may be increased. However, this would be only a temporary solution for tension reduction because increased length would also result in non-optimal overlap between actin and myosin filaments. Second, sarcomereogenesis may result in an increase in the number of longitudinal sarcomeres, the

functional units of the contractile system. Third, an increase in synthesis of Z-band proteins or intermediate filaments may strengthen myofibrils.

Summary Extensive disruption of muscle fibres occurs after relatively short term eccentric exercise where high mechanical forces are generated. Biopsies taken after repetitive eccentric muscle actions have revealed broadening, streaming and, at time, total disruption of Z-discs. Muscles that develop active tension eccentrically also become sore, lose inherent force-producing capability, and show a marked release of muscle proteins into the circulation. Among the factors that may influence the damage and repair processes are calcium, lysosomes, connective tissue, free radicals energy sources, and cytoskeletal and myofibrillar proteins.

Damaged muscles adapt to exercise, and all indicators of damage are reduced following repeated bouts of exercise. Several hypotheses have been presented to explain muscle adaptation. Stress-susceptible fibres or susceptible areas within a fibre may be eliminated and then regenerated, or muscle fibres and/or connective tissue may be strengthened with an initial bout of exercise.

Thus, a previous bout of eccentric exercise up to a week earlier could cause muscle damage and affect subsequent exercise performance. In addition, the presence of stress-susceptible or degenerating muscle fibers, evolved through disuse or neuromuscular diseases, may also change the recruitment pattern. Therefore, having such knowledge of patient's exercise habit is essential to accurately assess his/her condition. Besides, detection of skeletal muscle injury is also important in order to determine the intensity of activity of exercise which is safe to prescribe to fatigue patients for therapeutic purposes.

5.6.2 Materials and Methods

Subjects The subjects were 6 healthy caucasian male volunteers. All were physically active and none was overweight. The age range was 23-42.

Exercise Protocol The subjects had been asked to performed for 40 minutes a stepping exercise known to cause mild injury to the right calf muscle of the leg (eccentrically exercised) but not to the left calf muscle (concentrically exercised). The actual exercise, involved stepping up and down of a stool, would cause similar injury as when the subjects run downhill or down a flight of stairs for the same period of time.

Biochemical and Spectroscopic Analyses Serial blood samples were taken with sterile disposable needles from a vein in the arm prior to exercise, immediately post exercise, and at 3, 6, 9, 12, 24, 48, 96, and 120 hours, and were assayed for creatine kinase (CK), CK isoforms, and myoglobin. Injury was localized by serial assessment of tenderness on a visual analogue scale at specified sites in the lower limb. The relative abundance of inorganic phosphate to phosphocreatine-ratio (P*i*/PCr) was measured serially in each calf muscle at rest by means of P-31 NMRS. The P-31 NMRS measurements were collected, as described in Chapter 4 of this thesis, from medial gastrocnemius, lateral gastrocnemius, and soleus of both legs prior to exercise, immediately after exercise, and at 6, 24, 48, and 120 hours.

5.6.3 Results

Serum CK rose from 108 IU/liter (Standard derivation 37.6 IU/liter) to a peak of 546.3 IU/liter (SD 451.8 IU/liter) at 12 hours, and returned to baseline after 120 hours in 4 of the 6 subjects (Fig. 5-14a); while two subjects showed late

increases (Fig. 5-14b). The ratio of CK MM3:MM1 isoforms climbed from 0.49 (SD 0.29) to a peak of 2.23 (SD 0.89) at 9 hours, and was still significantly above baseline at 24 hours (Fig. 5-15). Plasma myoglobin increased from 43.3 ng/ml (SD 16.8 ng/ml) to a peak of 147.2 ng/ml (SD 51.0 ng/ml) at 3 hours, and returned to baseline after 24 hours (Fig. 5-16). In all three cases, the changes from baseline to peak were highly statistically significant ($p<0.001$).

Clinical examination revealed that the left calf muscle did not become tender; whereas, the right calf muscle became maximally tender at 48 hours and was nontender after 120 hours. P-31 NMRS indicated an increase of Pi/PCr in the right calf muscle from 0.125 (SD 0.023) to a peak of 0.185 (SD 0.047) after 48 hours and a return to baseline after 120 hours; while the left calf muscle only registered a slight increase from 0.126 (SD 0.034) to 0.158 (SD 0.026) (Fig. 5-17).

The above results could be summarized in Fig. 5-18, which implied a significant correlation between the change in Pi/PCr with the subjective report of tenderness in the right calf muscle, as well as inferred linear relationships between the rise and fall of myoglobin and CK isoforms with respect to the total CK released due to injury.

5.6.4 Discussion

In this section, in order to study exercise-induced muscle damage and repair, we resorted to examination of the calf muscle of the leg, which by itself was in fact not a good choice even though its selection was based on the fact that it could very easily suffer injury resulting from eccentric exercise. However, since the pain and tenderness resulting from such exercise could last for over a week, it was not our intention to prevent our volunteer subjects from losing the use of their arms during this extended period. Therefore, we decided to exercise the leg instead. Over the years, most human calf muscle, which supported the

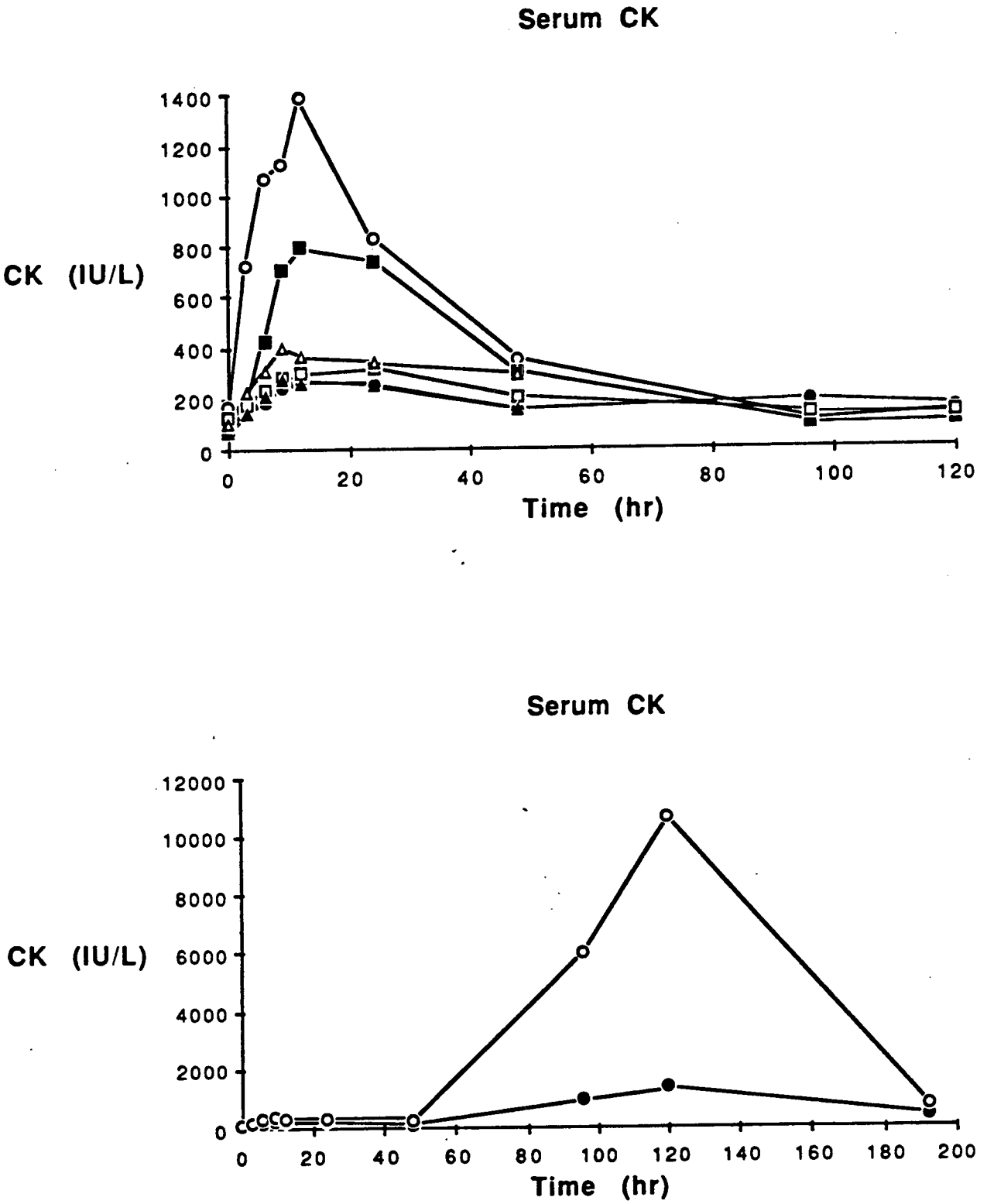

Figure 5-14 The serum creatine kinase profile after calf muscle injury following eccentric exercise.

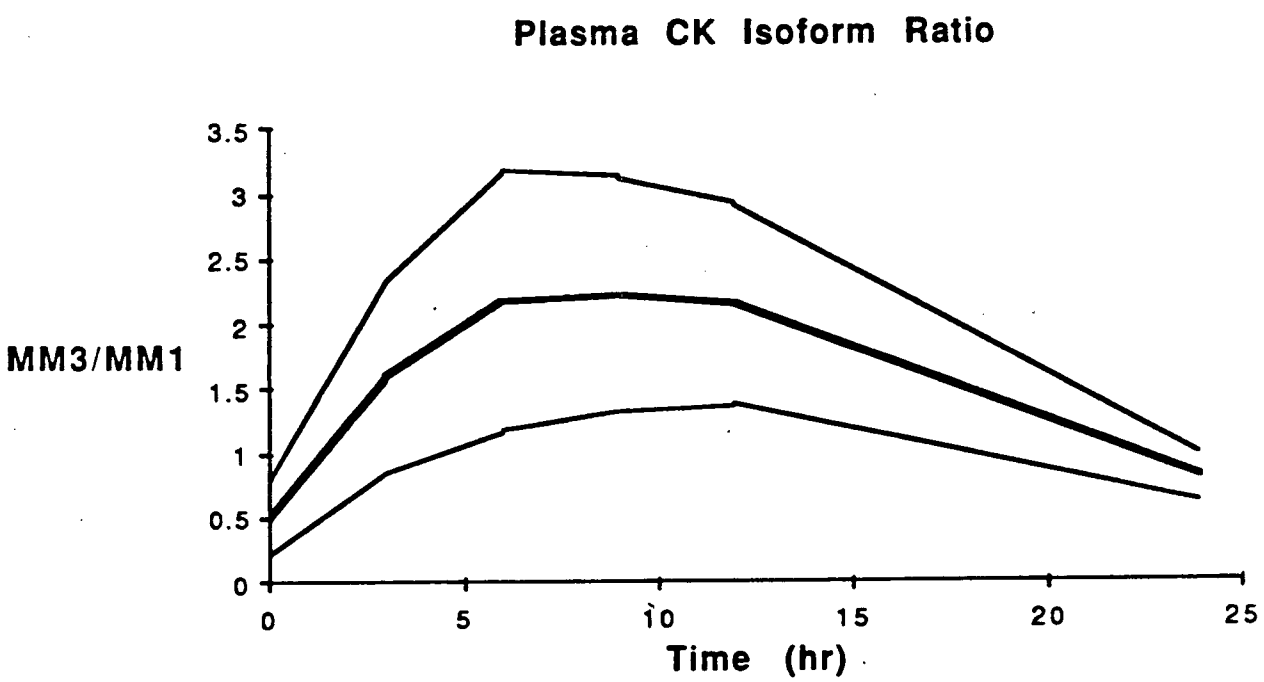

Figure 5-15 The profile of the ratio of CK MM3:MM1 isoforms after calf muscle injury following eccentric exercise.

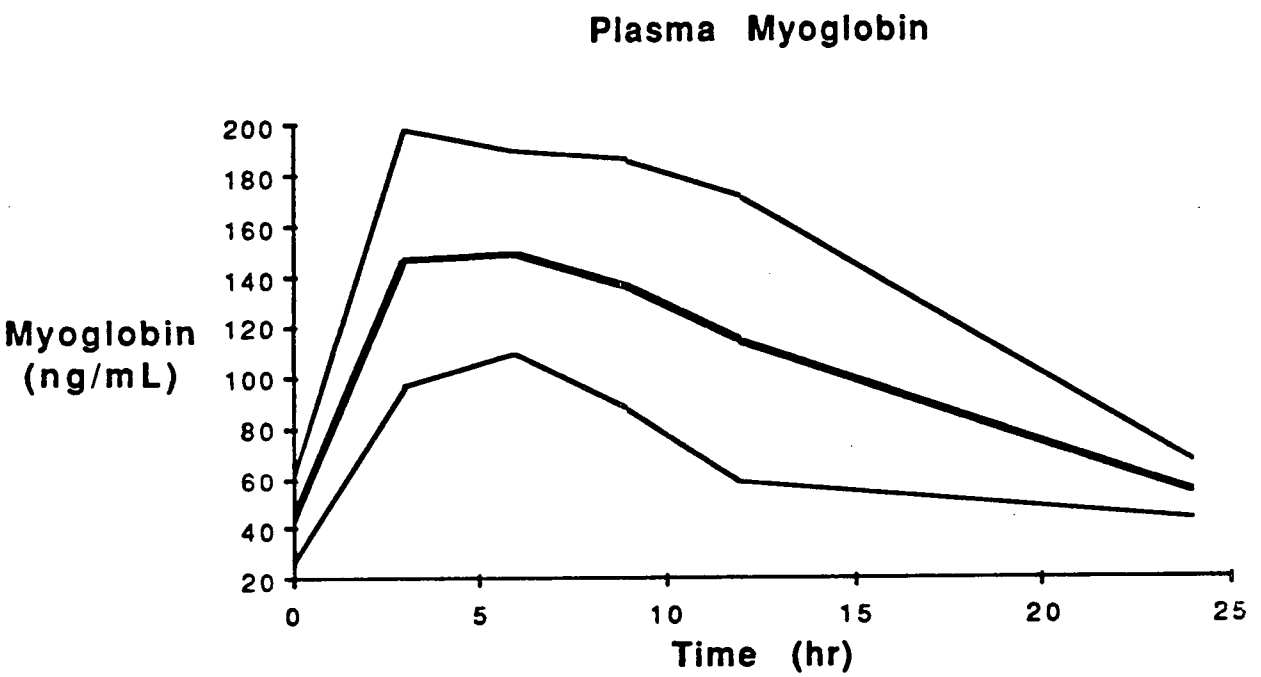

Figure 5-16 The profile of plasma myoglobin after calf muscle injury following eccentric exercise.

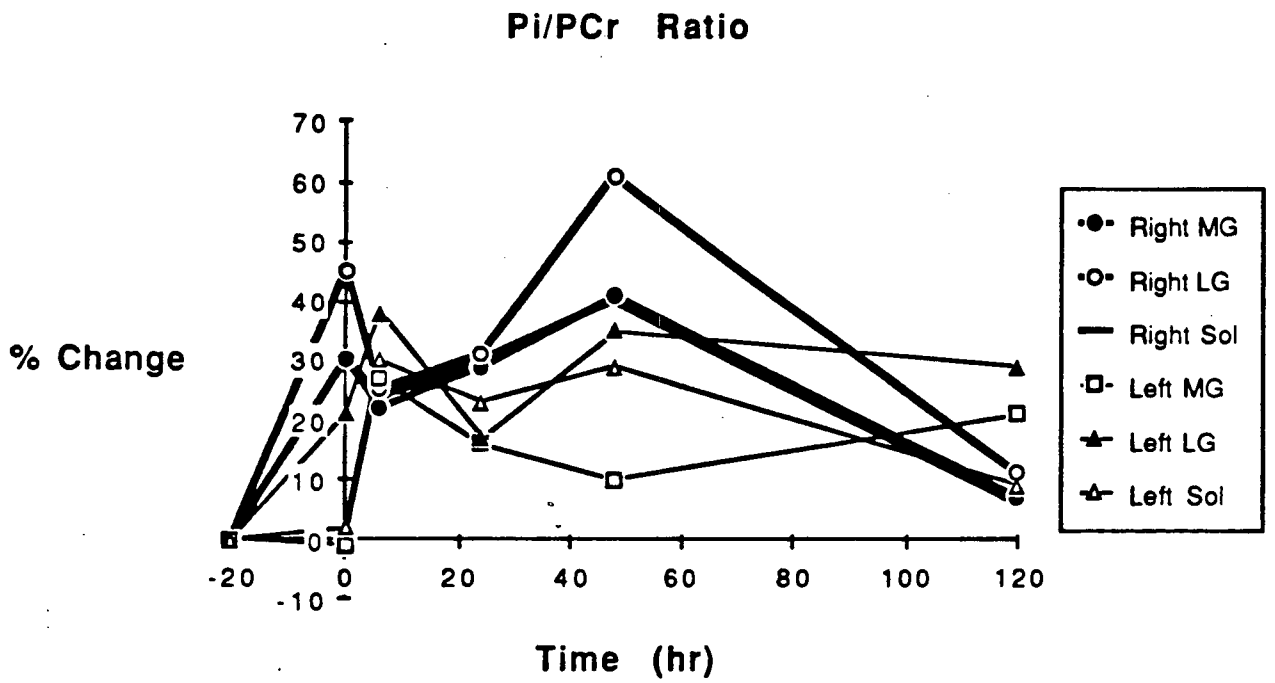

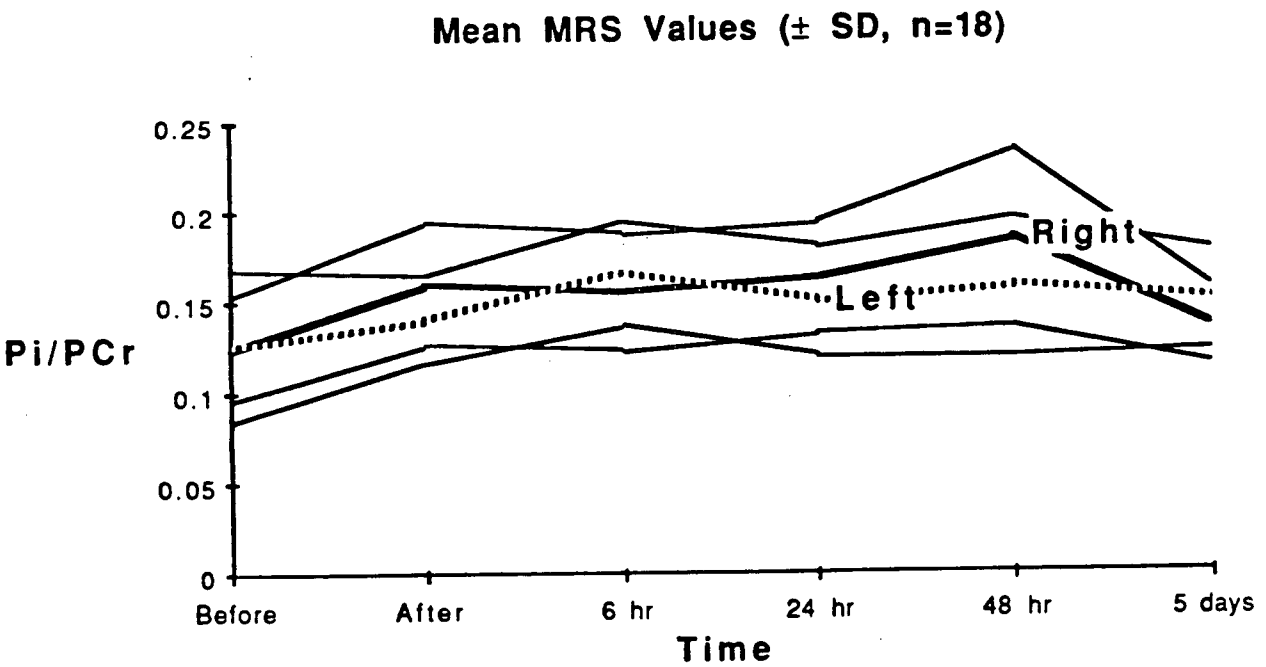

Figure 5-17 The profile of the ratio of Pi/PCr of calf muscle after injury following eccentric exercise.

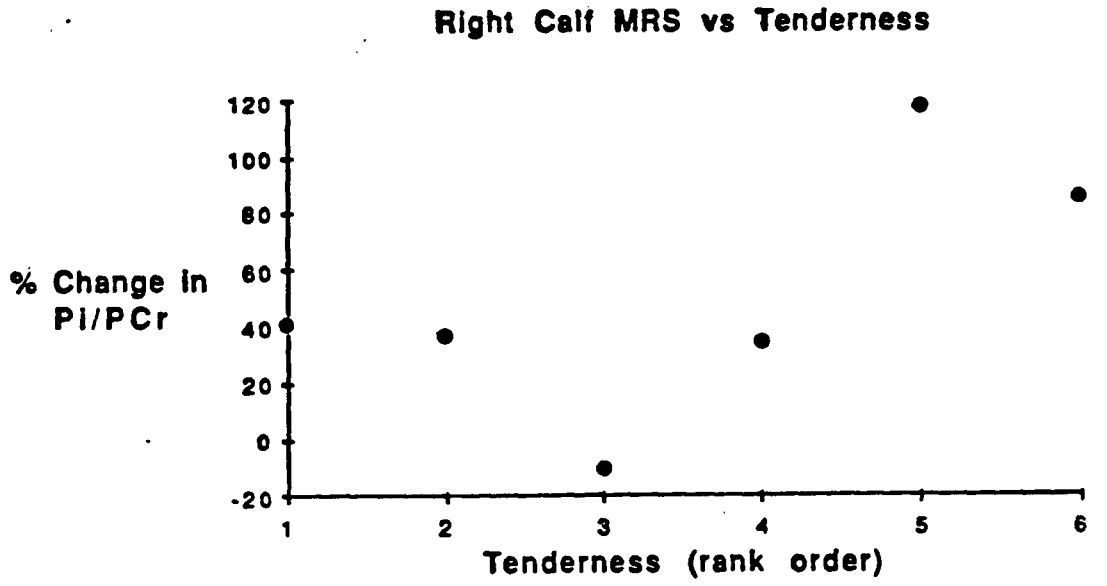

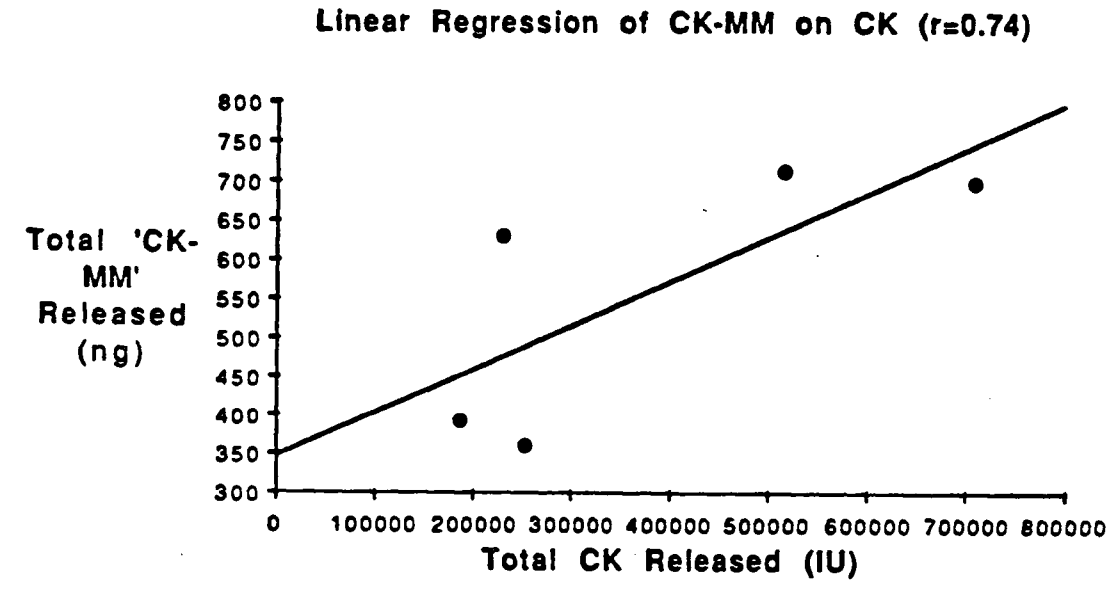

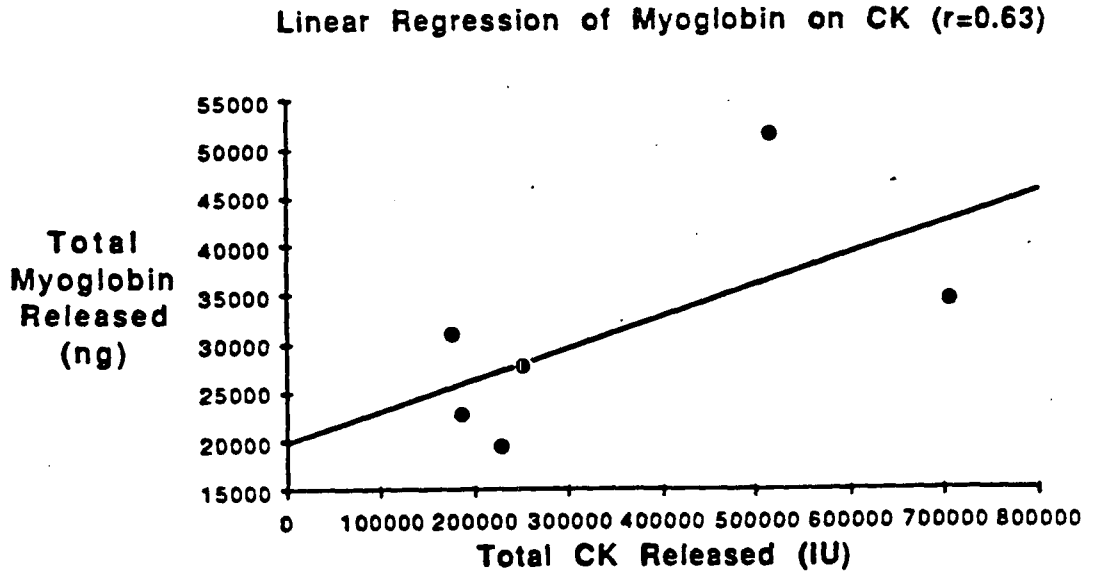

Figure 5-18 Summary results of the calf muscle injury study.

whole body weight, had experienced numerous damages and repairs (135), making it a very heterogeneous group of tissues. Thus, experimental results involving calf muscle were sometimes less well defined and occasionally extremely difficult to interpret.

For example, although the left calf muscle did not become tender, P-31 NMRS indicated a slight but significant increase in Pi/PCr ratio. This could be the adaptive measure that the body employed to shift the body weight from the injured right leg to the normal left leg, thus increasing its basal metabolism and as well as inducing minor damage in such compensatory manoeuvre.

The delayed rise of CK in two of the subjects probably was the result of re-injury. However, intersubject variability in CK response due to exercise is not a new problem, but in fact has been well documented (120,159-161). For example, Newham *et al.* reported in 1983 that in one study where subjects performed an eccentric exercise, some subjects showed increases of CK activity up to 34,500 IU/liter, while other subjects showed increases of less than 500 IU/liter (118). This variability is puzzling since in most cases it is unrelated to general fitness of subjects, physical characteristics of subjects, amount of soreness induced by exercise and amount of work done during exercise.

Kagen and Aram (162) reported that serum from certain patients with muscle disease contained a dialysable inhibitor of CK which resulted in a large underestimation of actual CK levels. It might be tempting to suggest that CK responses to exercise may have a genetic component; however, recent data from the laboratory of Ebbeling and Clarkson (163) showed that some subjects would be classified as high responders when exercising one arm and low responders when exercising the opposite arm. The higher CK response for one arm could not be accounted for by whether the subject performed the exercise with that arm first or second, arm dominance, amount of force exerted during the exercise, or

the degree of fatigue experienced during the exercise. At present there is no clear explanation for CK variability. Thus, CK is not a very good indicator of muscle damage after all.

Although in this study, we have not unequivocally established a relationship between muscle injury and Pi/PCr ratio, there is no doubt that exercise performance will be affected if the subject is involved in a previous bout of eccentric exercise within a week of precipitating in our exercise protocol outlined in the last chapter.

5.7 Conclusion

Our treatment, mostly qualitative and occasionally quantitative, of mechanical and physiological parameters, affecting subsequent exercise performance in this chapter, is by no means exhaustive. However, this Thesis evolved as we strided to make our exercise protocol more tractable and reproducible. This chapter represented our continuous effort to refine the whole technique.

Only recently, after the completion all experiments presented in this Thesis, did we realize that caffeine may be a factor affecting exercise performance. Our exercise protocol, carried out under informal setting in a research laboratory, usually lasts for one and a half hour. If the test starts early in the morning or during lunch time, many control subjects often prefer having a cup of coffee before or during the exercise protocol. Some individuals may elect to enjoy a cup of black coffee, while others may prefer to add cream and sugar.

The effect of caffeine at lower dose, yet unknown, may be minor, but Costill *et al*. had shown that consuming the amount of caffeine commonly found in 2.5 cups of regularly percolated coffee (330 mg) 60 minutes before

exercising significantly extended endurance in moderately strenuous exercise (164). Their study also showed that, even though heart rate and oxygen consumption were normal, the plasma glycerol and free fatty acid levels and the respiratory exchange ratio indicated a high level of fats metabolism and a corresponding reduced rate of carbohydrate oxidation. It is likely that this ergogenic effect of caffeine is due to the facilitated use of fat as a fuel for exercise. This would be of considerable benefit in prolonged exercise in which glycogen depletion is intimately related to diminished work capacity. Besides, the caffeine also made the work feel easier; this lessening of the subjective ratings of effort on neuronal excitability might be due to a lowering of the threshold for motor-unit recruitment and nerve transmission. The latter could be the effect of caffeine acting on the sarcoplasmic reticulum to increase its permeability to calcium, thus making it readily available for the contraction process.

Although some controversy exists as to the importance of ingesting sugar-rich drinks in long-term exercise (165-170), it appears that such drinks consumed at regular intervals during exercise benefit both moderate and relatively high intensity aerobic exercise (171-173). The benefits of ingesting glucose- or sucrose-rich drinks are observed only during the activity. Paradoxically, the muscle glycogen reserves become prematurely depleted at a more rapid rate when using pre-event sugar drinks in contrast to drinking plain water. In fact, drinking a strong sugary solution in the 30 to 60 minutes prior to exercise actually hinders one's endurance capability, due to an overshoot in the release of insulin from the pancreas (174-177). At the same time, insulin also inhibits the mobilization and utilization of fat for energy (175).

References

1. P. O. Astrand, and K. Rodahl, Textbook of Work Physiology. 3rd ed. McGraw-Hill Ltd., Toronto, 1968.

2. B. C. Abbott, B. Bigland, and J. M. Ritchie, J. Physiol. 117:380-390, 1952.

3. E. Asmussen, Acta Physiologica Scand. 28:364-382, 1952.

4. K. R. Williams, Med. Sci. Sports Exerc. 17:317-325, 1985.

5. H. Monod, and J. Scherrer, Medicine and Sport 8:Biomechanics III, 261-267, 1973

6. A. A. Sapega, D. P. Sokolow, T. J. Graham, and B. Chance, Med. Sci. Sports Exerc. 19:410-420, 1987.

7. T. A. McMahon, Princeton University Press, Princeton, 1984.

8. J. W. K. Lee, Chapter 3 of this Thesis/manuscript in preparation.

9. B. Chance, J. S. Leigh, B. J. Clark, J. Maris, J. Kent, S. Nioda, and D. Smith, Proc. Nat. Acad. Sci. (U.S.A.) 82:8384-8388, 1985.

10. B. J. Delateur, Therapeutic exercise to develop strength and endurance, in F. J. Kottke, G. K. Stillwell, and J. F. Lehmann, Krusen's Handbook of Physical Medicine and Rehabilitation, 3rd ed., W. B. Saunders Ltd., 427-464, 1982.

11. E. Homsher, Ann. Rev. Physiol. 49:673-690, 1987.

12. A. F. Huxley, Ann. Rev. Physiol. 50:1-16, 1988.

13. B. H. Bressler, L. A. Dusik, and M. R. Menard, J. Physiol. 397:631-641, 1988.

14. W. T. Stauber, Exercise and Sport Sciences Reviews 17:157-185, 1989.

15. H. S. Milner-Brown, M. Mellenthin, and R. G. Miller, Arch. Phys. Med. Rehab. 67:530-535, 1986.

16. A. M. W. Penn, A. A. Eisen, S. A. Hashimoto, J. W. K. Lee, and L. D. Hall, Neurology 37(Suppl. 1):135, 1987.

17. A. L. Goldberg, J. D. Etlinger, D. F. Goldspink, and C. Jablecki, Med. Sci. Sports 7:248-261, 1975.

18. A. Schwarzenegger, Arnold's Bodybuilding for Men. Simon & Schuster, New York, 1981.

19. R. Seaman, and C. D. Ianuzzo, Eur. J. Appl. Physiol. 58:257-261, 1988.

20. D. Gadian, G. Radda, B. Ross, J. Hockaday, P. Bore, D. Taylor, and P. Styles, Lancet 2(8250):774, 1981.

21. D. J. Taylor, P. J. Bore, P. Style, D. G. Gadian, and G. K. Radda, Molecular Biology Medicine 1(1):77-94, 1983.

22. B. Chance, Annals of the New York Academy of Science 428:318-32, 1984.

23. D. L. Arnold, D. J. Taylor, and G. K. Radda, Annals of Neurology 18(2):189-96, 1985.

24. Z. Argo, W.J. Bamk, J. Maris, J. S. Leigh Jr., and B. Chance, Annals of Neurology 22(1):46-51, 1987.

25. Z. Argov, W. J. Bank, J. Maris, P. Peterson, B. Chance, Neurology 37(2):257-62, 1987.

26. Z. Argov, W. J. Bank, J. Maris, and B. Chance, Neurology 37(11):1702-4, 1987.

27. P. E. Bollaert, L. Robin, B. Herbier, J. M. Escanye, P. Bauer, H. Lambert, J. Robert, and A. Larcan, Neurology 39(6):821-4, 1989.

28. D. Morvan, P. Jehenson, D. Duboc, A. Syrota, Magn. Reson. Med. 13:216-227, 1990.

29. L. D. Hall, J. W. K. Lee, A. M. W. Penn, V. P. Sweeney, and S. A. Hashimoto, Can. J. Neurol. Sci. 14(2):200, 1987.

30. Laulanie', Elements de Physiologie, 2nd ed., Paris, 1905.

31. W. O. Fenn, and B. S. Marsh, J. Physiol. 85:277-297, 1935.

32. A. V. Hill, First and Last Experiments in Muscle Mechanics, Cambridge University Press, 1970.

33. L. Gyulai, Z. Roth, J. S. Leigh, B. Chance, J. Biol. Chem. 260(7):3947-3954, 1985.

34. E. Henneman, G. Somjen, and D. O. Carpenter, J. Neurophysiol. 28:560-580, 1965.

35. M. J. Kushmerick, and R. E. Davies, Proc. Royal Society London, B, 174:315-353, 1969.

36. R. C. Wooledge, N. A. Curtin, and E. Homsher, Energetic Aspects of Muscle Contraction, Monograph of Physiological Society, 41:260-267, Academic Press, New York, 1985.

37. B. Chance, J. S. Leigh Jr., J. Kent, K. McCully, Federation Proceedings 45(13):2915-20, 1986.

38. E. H. Sonnenblick, Fed. Proc. 24(6):1936, 1965.

39. L. D. Hall, J. W. K. Lee, A. M. W. Penn, T. Perry, Soc. Magn. Reson. Medicine, 7th Annual Meeting, Book of Abstracts, 502, 1988.

40. K. R. Williams, Med. Sci. Sports Exerc. 17:317-325, 1985.

41. L. D. Hall, J. W. K. Lee, M. Menard, A. M. W. Penn, and L. A. Dusik, Arch. Phys. Med. and Rehab. (in press).

42. P. V. Komi, J. H. T. Viitasalo, M. Havu, B. Thorstensson, B. Sjodin, and J. Karlsson, Acta Physiol. Scand. 100:335-391, 1977.

43. V. R. Edgerton, S. C. Bodine, and R. R. Roy, Medicine Sport Sci. 26:12-23, 1987.

44. T. C. Cope, S. C. Bodine, M. Fournier, V. R. Edgerton, J. Neurophysiol. 55:1202-1220, 1986.

45. V. R. Edgerton, R. R. Roy, R. J. Gregor, and S. Rugg, in Jones, Human Muscle Power, Human Kinetics Publishers, Champaign, 43-64, 1986.

46. P. L. Powell, R. R. Roy, P. Kanim, M. A. Bello, and V. R. Edgerton, J. Appl. Physiol. 57:1715-1721, 1984.

47. S. A. Spector, P. F. Gardiner, R. F. Zernicke, R. R. Roy, and V. R. Edgerton, J. Neurophysiol. 44: 951-960, 1980.

48. T. Moritani, and H. DeVries, Am. J. Phys. Med. 58:115-130, 1979.

49. K. Hakkinen, and P. V. Komi, J. Hum. Mov. Stud. 7:33-44, 1981.

50. K. Hakkinen, M. Alen, and P. V. Komi, Acta Physiol. Scand. 125:573-585, 1985.

51. J. O. Holloszy, and F. W. Booth, Annu. Rev. Physiol. 38:273-291, 1976.

52. S. Salmons, and J. Henriksson, Muscle & Nerve 4:94-105, 1981.

53. A. C. Bylund, J. Hammarsten, J. Holm, and T. Schersten, Eur. J. Clin. Invest. 6:425-429, 1976.

54. R. H. Fitts, W. W. Winder, M. H. Brooke, K. K. Kaiser, and J. O. Holloszy, Am. J. Physiol. 238:C15-C20, 1980.

55. K. Hakkinen, P. V. Komi, and P. A. Tesch, Scand. J. Sports Sci. 3:50-58, 1981.

56. A. Thorstensson, B. Hulten, W. von Dobeln, and J. Karlsson, Acta Physiol. Scand. 96:392-398, 1976.

57. V. L. Katch, F. I. Katch, R. Moffatt, and M. Gittleson, Med. Sci. Sports Exerc. 12:340-344, 1980.

58. A. Young, M. Stokes, J. M. Round, and R. H. T. Edwards, Eur. J. Clin. Invest. 13:411-417, 1983.

59. T. Haggmark, E. Jansson, and B. Svane, Scand. J. Clin. Lab. Invest. 38:355-360, 1978.

60. B. Dons, K. Bollerup, F. Bonde-Petersen, and S. Hancke, Eur. J. Appl. Physiol. 40:95-106, 1979.

61. J. M. Luthi, H. Howald, H. Claassen, K. Rosler, H. Hoppeler, and P. Vock, Int. J. Sports Med. 7:123-127, 1986.

62. P. V. Komi, J. Karlsson, P. Tesch, H. Suominen, and E. Heikkinen, in Komi, Exercise and Sport Biology, International series on Sports Sciences, Human Kinetics Publishers, Champaign, 12:90-102, 1982.

63. P. A. Tesch, E. B. Colliander, and P. Kaiser, Eur. J. Appl. Physiol. 55:362-366, 1986.

64. R. S. Staron, R. S. Hikida, F. C. Hagerman, G. A. Dudley, and T. F. Murray, J. Histochem. Cytochem. 32:146-152, 1984.

65. P. Schantz, Acta Physiol. Scand. 114:635-637, 1982.

66. J. D. MacDougall, D. G. Sale, G. C. B. Elder, and J. R. Sutton, Eur. J. Appl. Physiol. 48:117-126, 1982.

67. P. A. Tesch, and L. Larsson, Eur. J. Appl. Physiol. 49:301-306, 1982.

68. O. Hudlicka, Circulation Res. 50:451-461, 1982.

69. P. A. Tesch, A. Thorsson, and P. Kaiser, J. Appl. Physiol. 56:35-38, 1984.

70. J. D. MacDougall, D. G. Sale, J. R. Moroz, G. C. B. Elder, J. R. Sutton, H. Howald, Med. Sci. Sports 11:164-166, 1979.

71. D. Seiden, Am. J. Anat. 145:459-468, 1976.

72. J. D. MacDougall, G. R. Ward, D. G. Sale, J. R. Sutton, J. Appl. Physiol. 43:700-703, 1977.

73. C. A. Gillespie, and V. R. Edgerton, Hormone Metabol. Res. 2:264-266, 1970.

74. C. Y. Guezennec, P. Ferre, B. Serrurier, D. Merino, and M. Aymonod, Eur. J. Appl. Physiol. 52:300-304, 1984.

75. C. M. Donovan, and G. A. Brooks, Am. J. Physiol. 244 (Endocrinol. Metab. 7):E83, 1983.

76. J. Karlsson, and I. Jacobs, Int. J. Sports Med. 3:190, 1982.

77. D. L. Arnold, D. J. Taylor, and G. K. Radda, Annals of Neurology 18(2): 189-196, 1985.

78. P. V. Komi, in Terjung, Exercise and Sport Science Reviews, the Collamore Press, Lexington, 12:81-121, 1984.

79. K. Hakkinen, A. Pakarinen, M. Alen, and P. V. Komi, Eur. J. Appl. Physiol. 53:287-293, 1985.

80. P. A. Tesch, Medicine Sport Sci. 26:67-89, 1987.

81. J. D. MacDougall, D. Tuxen, D. G. Sale, J. R. Moroz, and J. R. Sutton, J. Appl. Physiol. 58:785-790, 1985.

82. B. F. Hurley, D. R. Seals, A. A. Ehsani, L. -J. Cartier, G. P. Dalsky, J. M. Hagberg, and J. O. Holloszy, Med. Sci. Sports Exerc. 16:483-488, 1984.

83. M. Y. Chi, *et. al.* Am. J. Physiol. 244 (Cell Physiol. 13):276, 1983.

84. E. F. Coyle, *et. al.* J. Appl. Physiol. 57:1857, 1984.

85. Y. Murase, *et. al.* Med. Sci. Sports Exerc. 13:180, 1981.

86. D. L. Costill, J. Daniels, W. Evans, W. Fink, G. Krahenbuhl, and B. Saltin, J. Appl. Physiol. 40:149-154, 1976.

87. W. S. Parkhouse, and D. C. McKenzie, Med. and Sci. in Sports and Exerc. 16(4):328-338, 1984.

88. J. Karlsson, F. Bonde-Petersen, J. Henriksson, and H. G. Knuttgen, J. Appl. Physiol. 38:763-767, 1975.

89. K. Klausen, H. G. Knuttgen, and H. V. Forster, Scand. J. Clin. Lab. Invest. 30:415-419, 1972.

90. H. Hirche, U. Wacker, and H. D. Langhar, Int. Z. Angew. Physiol. 30:52-64, 1971.

91. L. Jorfeldt, A. Juhlin-Dannfelt, and J. Karlsson, J. Appl. Physiol. 44:350-352, 1978.

92. G. W. Mainwood, and P. Worsley-Brown, J. Physiol. (london) 250:1-22, 1975.

93. L. Jorfeldt, Acta Physiol. Scand. (Suppl):338, 1970.

94. J. Karlsson, Acta Physiol. Scand. (Suppl.) 358:1-72, 1971.

95. A. N. Belcastro, and A. Bonen, J. Appl. Physiol. 36:932-936, 1975.

96. J. Quershi, and T. Wood, Biochim. Biophys. Acta 60:190-192, 1962.

97. D. P. M. MacLaren, and G. D. Morgan, Proceedings of the Nutrition Society 44(1):26A, 1985.

98. N. L. Jones, J. R. Sutton, R. Taylor, C. J. Toews, J. Appl. Physiol. 43:959-964, 1977.

99. E. Hultman, and K. Sahlin, Exerc. and Sport Sci. Reviews 8:41-128, 1980.

100. A. Fabiato, and F. Fabiato, J. Physiol. 276:233-255, 1978.

101. S. K. B. Donaldson, and L. Hermansen, Pflugers Archiv. 376:55-65, 1978.

102. E. Hultman, S. D. Canale, and H. Sjoholm, Clin. Sci. 69:505-510, 1985.

103. J. Nocker, Can. J. Appl. Sports Sci. 1:43-48, 1976.

104. A. M. Katz, Physiol. Rev. 50:63-158, 1970.

105. E. Hultman, H. Sjoholm, K. Sahlin, and L. Edstrom, in Human Muscle Fatigue, Ciba Foundation Symposium, London, Ptiman, 82:19-40, 1981.

106. P. M. Clarkson, W. Kroll, J. Graves, W. A. Record, Int. J. Sports Med. 3:145-148, 1982.

107. P. M. Clarkson, P. Litchfield, J. Graves, J. Kirwan, W. C. Byrnes, Eur. J. Appl. Physiol. Occupat. Physiol. 53:368-371, 1985.

108. P. M. Clarkson, W. C. Byrnes, K. M. McCormick, L. P. Turcotte, J. S. White, Int. J. Sports Med. 7:152-155, 1986.

109. P. M. Clarkson, F. S. Apple, W. C. Byrnes, K. M. McCormick, and P. Triffletti, Muscle and Nerve 10:41-44, 1987.

110. F. S. Apple, M. A. Rogers, W. M. Sherman, and J. L. Ivy, Clinica Chimica Acta 138:111-118, 1984.

111. F. S. Apple, M. A. Rogers, D. C. Casal, L. Lewis, J. L. Ivy, *et. al.*, Eur. J. Appl. Physiol. Occupat. Physiol. 56:49-52, 1987.

112. A. J. Siegel, L. M. Silverman, and L. Holman, J. Am. Med. Assoc. 246:2049-2051, 1981.

113. M. J. Warhol, A. J. Siegel, W. J. Evans, and L. M. Silverman, Am. J. Pathol. 118:331-339, 1985.

114. R. B. Armstrong, R. W. Ogilvie, and J. A. Schwane, J. Appl. Physiol. 54:80-93, 1983.

115. W. C. Byrnes, P. M. Clarkson, J. S. White, S. S. Hsieh, P. N. Frykman, *et. al.*, J. Appl. Physiol. 59:710-715, 1985.

116. P. M. Clarkson, and I. Tremblay, J. Appl. Physiol. 65: 1-6, 1988.

117. J. Friden, Umea University Medical Dissertations New Series 105, 1983.

118. D. J. Newham, D. A. Jones, R. H. T. Edwards, Muscle and Nerve 6:380-385, 1983.

119. D. J. Newham, D. A. Jones, S. E. J. Tolfree, and R. H. T. Edwards, Eur. J. Appl. Physiol. Occupat. Physiol. 55:106-122, 1986.

120. D. J. Newham, D. A. Jones, and P. M. Clarkson, J. Appl. Physiol. 63:1381-1386, 1987.

121. J. A. Schwane, S. R. Johnson, C. B. Vandenakker, and R. B. Armstrong, Med. and Sci. in Sports and Exerc. 15:51-56, 1983.

122. J. Friden, Int. J. Sports Med. 5:57-66, 1984.

123. J. Friden, M. Sjostrom, and B. A. Ekblom, Experientia 37:506-507, 1981.

124. J. Friden, M. Sjostrom, B. Ekblom, Int. J. Sports Med. 4:170-176, 1983.

125. J. Friden, U. Kjorell, and L. E. Thornell, Int. J. Sports Med. 5:15-18, 1984.

126. D. A. Jones, D. J. Newham, J. M. Round, and S. E. J. Tolfree, J. Physiol. 375:435-448, 1986.

127. D. J. Newham, G. McPhail, K. R. Mills, and R. H. T. Edwards, J. Neurol. Sci. 61:109-122, 1983.

128. E. Asmussen, Acta Rheumatologica Scandinavica 2:109-116, 1956.

129. M. F. Bobbert, A. P. Hollander, and P. A. Huijing, Med. and Sci. in Sports and Exerc. 18:75-81, 1986.

130. R. H. T. Edwards, K. R. Mills, and D. J. Newham, J. Physiol. 317:1P-2P, 1981.

131. C. T. M. Davies, and M. J. White, Pflugers Archiv. 392:168-171, 1981.

132. J. N. Howell, A. G. Chila, G. Ford, D. David, and T. Gates, J. Appl. Physiol. 58:1713-1718, 1985.

133. D. A. Jones, D. J. Newham, and P. M. Clarkson, Pain 30:233-242, 1987.

134. P. V. Komi, and J. T. Viitasalo, Acta Physiologica Scandinavica 100:246-254, 1977.

135. K. K. McCully, and J. A. Faulkner, J. Appl. Physiol. 59:119-126, 1985.

136. D. J. Newham, K. R. Mills, B. M. Quigley, and R. H. T. Edwards, Clin. Sci. 64:55-62, 1983.

137. T. S. Talag, Res. Quarterly, 44:458-469, 1973.

138. W. J. Evans, C. N. Meredith, J. G. Cannon, C. A. Dinarello, W. R. Frontera, *et. al.*, J. Appl. Physiol. 61:1864-1868, 1986.

139. J. B. Hunter, and J. B. Critz, J. Appl. Physiol. 31:20-23, 1971.

140. F. Q. Nuttall, and B. Jones, J. Lab. Clin. Med. 71:847-854, 1968.

141. J. H. Ross, C. Attwood, G. E. Atkin, and R. N. Villar, Quarterly J. Med. 206:268-279, 1983.

142. P. M. Clarkson, W. C. Byrnes, E. Gillisson, and E. Harper, Clin. Sci. 73:383-386, 1987.

143. R. B. Armstrong, Med. and Sci. in Sports and Exerc. 16:529-538, 1984.

144. R. B. Armstrong, Sports Medicine 3:370-381, 1986.

145. W. C. Byrnes, and P. M. Clarkson, Clinics in Sports Medicine 5:605-614, 1986.

146. H. A. DeVries, Am J. Phys. Med. 45:119-134, 1966.

147. A. Irintchev, and A. Wernig, Cell and Tissue Research, 249:509-521, 1987.

148. J. A. Schwane, B. G. Waltrous, S. R. Johnson, and R. B. Armstrong, Physicians and Sportsmedicine 11:124-131, 1983.

149. H. Kuipers, J. Drukker, P. M. Frederik, P. Geurten, and G. V. Kranenburg, Int. J. Sports Med. 4:45-51, 1983.

150. L. Gordon, H. J. Buncke, and J. J. Townsend, Plastic and Reconstructive Surgery 61:576-580, 1978.

151. R. J. Stenger, D. Spiro, R. E. Scully, and J. M. Shannon, Am. J. Pathology, 40:1-20, 1962.

152. H. Hoppeler, Int. J. Sports Med. 7:187-204, 1986.

153. M. Sjostrom, J. Friden, and B. Ekblom, Acta Physiologica Scandinavica 130:513-520, 1987.

154. B. Walmsley, J. A. Hodgson, and R. E. Burke, J. Neurophysiology 41:1203-1216, 1978.

155. B. Bigland-Ritchie, and J. J. Woods, J. Physiol. 260:267-277, 1976.

156. K. L. Rogers, and R. A. Berger, Med. and Sci. in Sports 6:253-259, 1974.

157. C. T. M. Davies, and C. Barnes, Ergonomics 15:121-131, 1972.

158. E. R. Nadel, U. Bergh, and B. Saltin, J. Appl. Physiol. 33:553-558, 1972.

159. A. J. Sargeant, P. Dolan, Eur. J. Appl. Physiol. and Occupat. Physiol. 56:704-711, 1987.

160. T. D. Noakes, Sports Medicine 4:245-267, 1987.

161. J. B. Whitefield, and N. G. Martin, Acta Geneticae Medicae Gemellologie 35:23-33, 1986.

162. L. J. Kagen, and S. Aram, Arthritis and Rheumatism 30:213-217, 1987.

163. P. M. Clarkson, and C. B. Ebbeling, Clin. Sci. 75:257-261, 1988.

164. D. L. Costill, *et. al.* Med. Sci. Sports 10:155, 1978.

165. G. J. Bagby, *et. al.*, J. Appl. Physiol. 45:425, 1978.

166. E. H. Christenson, and O. Hansen, Skand. Arch. Physiol. 81:152, 1939.

167. P. Felig, *et. al.*, N. Eng. J. Med. 306:895, 1982.

168. R. A. Fielding, *et. al.*, Med. Sci. Sports Exerc. 17:472, 1985.

169. B. Krzentowski, *et. al.*, J. Appl. Physiol. 56:315, 1984.

170. P. J. Van Handel, *et. al.*, Int. J. Sports Med. 1:127, 1980.

171. D. L. Costill, and J. M. Miller, Int. J. Sports Med. 306:895, 1982.

172. E. F. Coyle, *et. al.*, J. Appl. Physiol. 55:230, 1983.

173. J. L. Ivy, Med. Sci. Sports Exerc. 15:466, 1983.

174. D. L. Costill, *et. al.*, J. Appl. Physiol. 43:695, 1977.

175. C. Foster, *et. al.*, Med. Sci. Sports 11:1, 1979.

176. K. Keller, and R. Schwarzkopf, Phys. Sportsmed. 12(4):89, 1984.

177. R. G. McMurray, *et. al.*, Res. Quart. Exerc. Sport 54:156, 1983.

Chapter 6

6. EXTENSIONS AND CONCLUSION

6.1 Extension of the Spiral Resonator Surface Coil Design

Since the P-31 spiral resonator can be removed from the gantry quite easily, it can be replaced by another spiral resonator tuned to observe a different nucleus, such as H-1, F-19, C-13, or Na-23; or it can be substituted by a longer spiral resonator which can act as a volume coil for a perfusion study of a small animal organ, such as a rabbit heart.

Preliminary results as shown in Figures 6-1 demonstrate the versatility offered by the spiral design housed in the gantry with revolving capability. Figure 6-1 is a C-13 NMR spectrum from a resting human forearm acquired without proton decoupling in less than 40 minutes. C-13 resonances can easily be assigned for the long chain alkyl groups, glycerol backbone, ester carbonyl and the double bond which arises from oleic acid. The complex alkyl portion is comprised of overlaid triplets which result from C-H coupling in the methylene groups (CH_2) of the chain. When experimental parameters are optimized, acquisition time can be further reduced, increasing the possibility of using C-13 NMRS to follow metabolic changes. The application of *in vivo* C-13 NMRS is in principle very broad and certainly very interesting when metabolic pathways and their regulation are to be studied. The large chemical shift range of the C-13

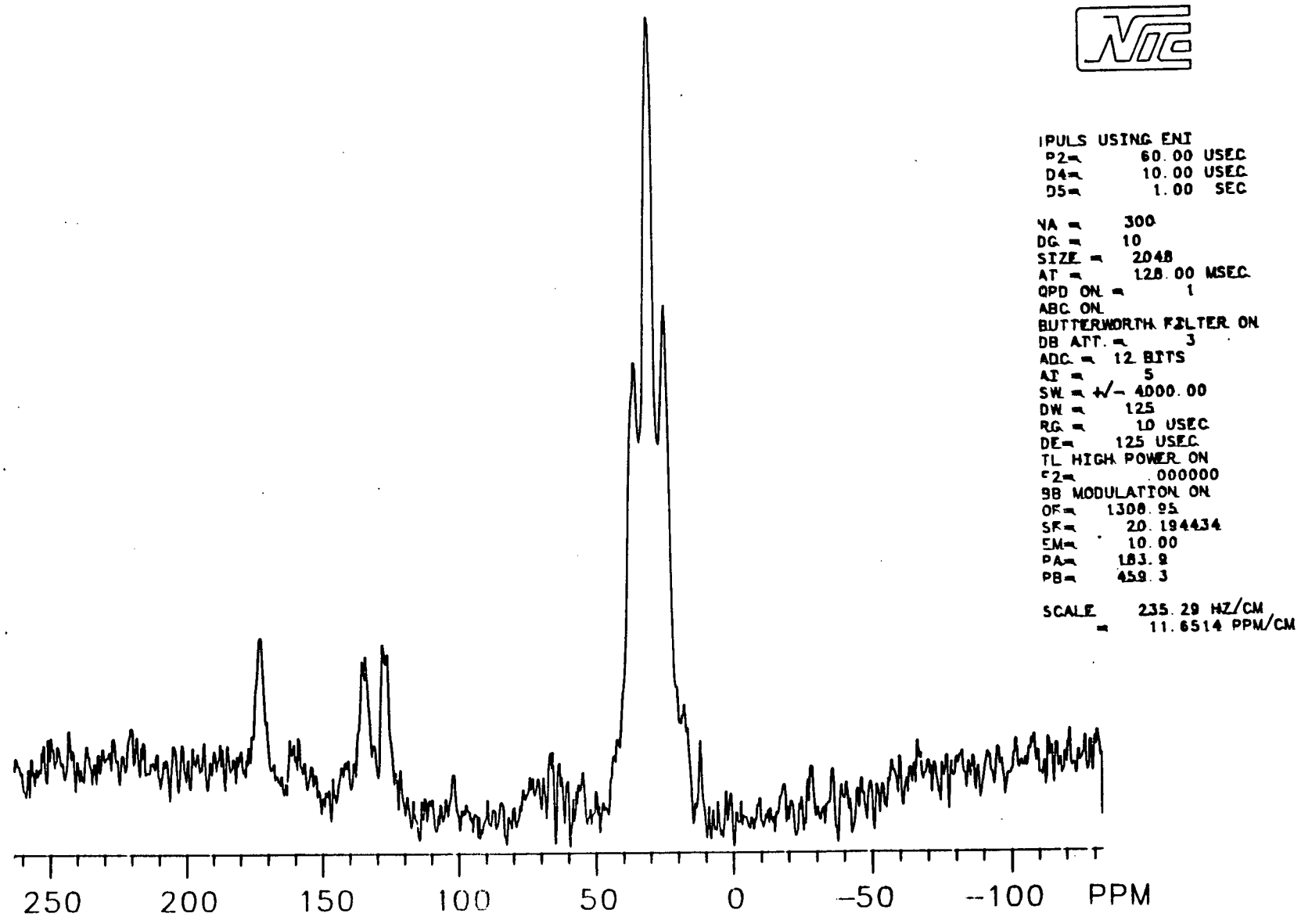

Figure 6-1 C-13 NMR resting spectrum of human forearm.

nucleus (≈ 200 ppm) allows the differentiation of many natural metabolites. Hence, after C-13-enriched substrates are injected into an organism, the compounds to which the C-13 label has migrated can be easily identified and even flux through different metabolic pathways can also be determined.

Figure 6-2 was obtained by placing an excised rabbit heart in a reperfusion chamber inside a long version of the spiral resonator (Figure 6-3). The latter was utilized to improve signal-to-noise ratio, as well as to place the sample in the center of the magnet, within the homogeneous field required for high resolution NMRS. The 1000 scan P-31 NMR spectrum was acquired in 20 minutes , and had already shown depletion of PCr with a concurrent increase in P*i*. If reperfusion started immediately after excision, a dramatic rise in the PCr peak coupled with a parallel decrease in the P*i* peak was observed (Figure 6-4). Subsequently, if reprefusion stopped, both the PCr and ATP reserves would gradually exhaust, leaving P*i* as the only observable signal. Because of the small size of a rabbit heart and the required time resolution, the P-31 NMR spectra shown in Figure 6-4 were very noisy. However, it is evident that this experimental setup can be used to study functional recovery of organs that have undergone ischaemia.

6.2 Prospective Role of P-31 NMRS in Monitoring HIV Disease and its Treatment

People with Human Immunodeficiency Virus (HIV) disease, especially those with Acquired Immune Deficiency Syndrome (AIDS) require a great deal of care, and so use many health care resources. The requirement for care is in large part equivalent to the ability to be independent in daily activities. This

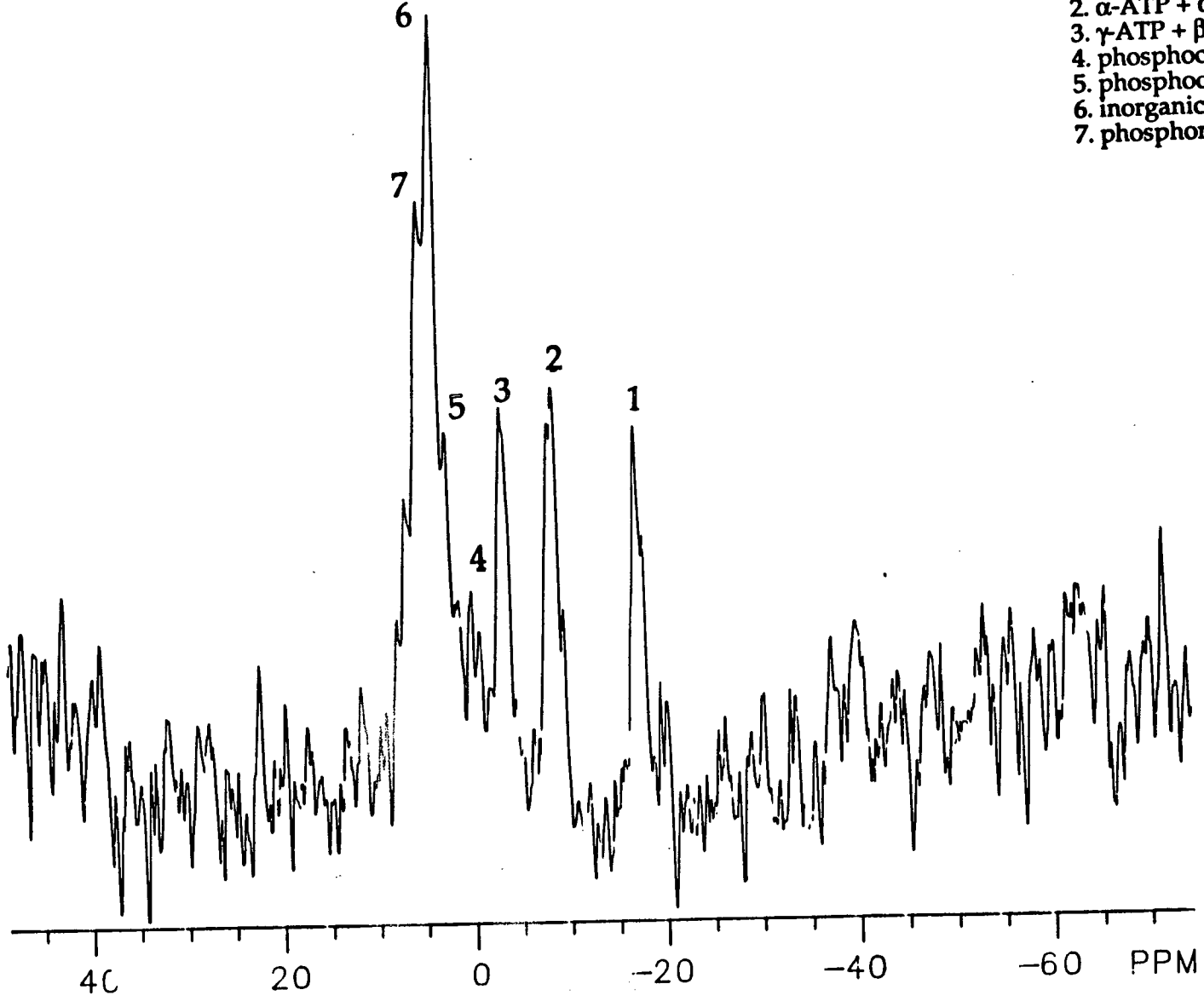

Figure 6-2 32.5 MHz P-31 NMR spectrum of the excised rabbit heart.

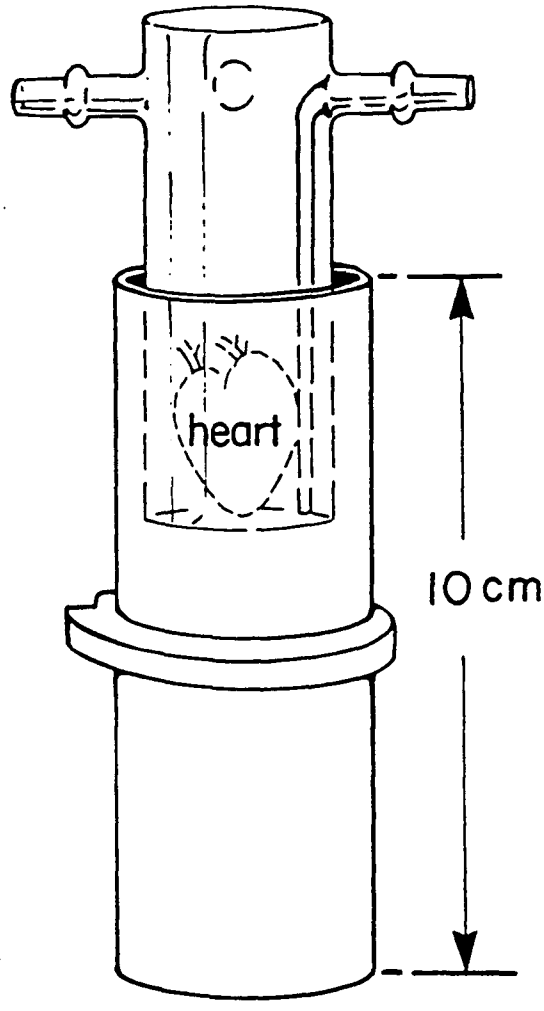

Figure 6-3 The longer version of the spiral resonator used to examine rabbit heart.

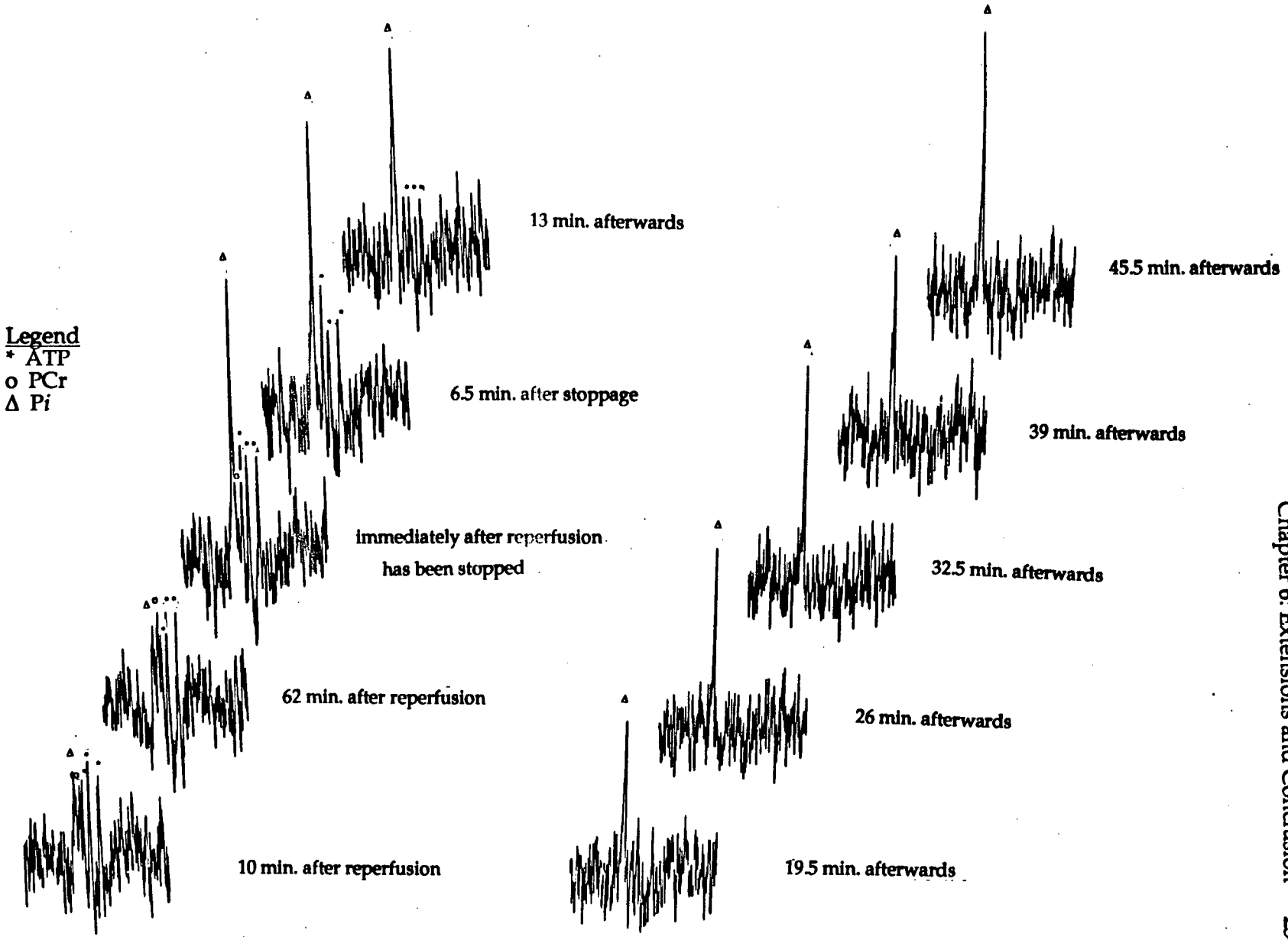

Figure 6-4 32.5 MHz P-31 NMR spectrum of the excised rabbit heart after reperfusion and subsequent stoppage of reperfusion.

independence relies on the use of muscle (motor performance). Muscle injury and fatigue are common in HIV disease and with some of the anti-HIV drugs.

A published report describes an incidence of clinical and subclinical neuromuscular disease in up to 50% of HIV-positive patients (1). This is manifest as decreased strength, decreased endurance, cramping, muscle tenderness, atrophy, and fatigue. Decreased motor performance in HIV disease thus can have a clear pathobiological basis. The most notable success in HIV therapeutics to date has been the antiviral drug AZT (Azidothymidine or Zidovudine). It initially was used only in limited trials, but now is considered to be appropriate even for asymptomatic seropositive people (2). Although its beneficial effects are undisputed, it has significant side effects (3). In particular, myopathy has been reported in 20% of recipients after 1 year of therapy. This is a mitochondrial myopathy, which coexists with the myopathy due to HIV itself (4). When a patient with HIV presents with decreased motor performance, the principal cause or causes must be determined before treatment can be given. Muscle biopsy used to be needed to make the diagnosis.

However, we hypothesized that P-31 NMRS could make the diagnosis noninvasively. In a nonspecific myopathy, the resting P*i*/PCr ratio is elevated but the exercise P*i*/PCr ratio pattern is normal. In mitochondrial myopathy, both are abnormal. Preliminary results from 10 patients with HIV and some degree of fatigue or myopathic symptoms, on AZT or on DDI (Dideoxyinosine) are so far consistent with the above hypothesis. For example, one patient who had been on AZT for 18 months developed severe myopathic symptoms. AZT was discontinued, and he improved rapidly. After two weeks, his creatine kinase (CK) had declined, but his resting and exercise P-31 NMRS were abnormal. After two months, he was much better clinically, the CK was nearing the upper limit of

normal, the exercise NMRS was in the normal range, the resting NMRS was nearing the upper limit of normal (Figure 6-5).

Establishing this differential diagnosis is important, because it is preferable not to discontinue AZT unless absolutely necessary. In future research, NMRS can be used serially in an attempt to detect subclinical myopathic changes as the problem develops. Since the myopathic symptoms are dose-related, it should be possible to adjust the dosage according to the NMRS values, to follow maintenance of effective antiviral coverage without significant clinical myopathy. In addition, the effect of other antiviral drugs, especially DDI, should also be determined.

6.3 Summary

The central theme of the work presented in this Thesis has involved the development, improvement, characterization, and experimental implementation of a novel design of surface coil, as well as the delineation, refinement, and clinical execution of a tractable protocol to study muscle fatigue. Assessment of the role of P-31 NMRS as a screening and diagnostic modality indicates that it can serve as an adjunctive tool. The P-31 NMR spectrum can provide information regarding the composition and level of the phosphate metabolites and thus can characterize cellular energetic state. It can also be used to determine the intracellular pH.

The specific exercise protocol outlined in chapter 4 of this Thesis improves both the sensitivity and the selectivity of the diagnosis of mitochondrial disease, even when little or no muscle symptoms are present. It is also a useful technique to monitor drug therapy. In chapter 5, we learn that several preconditions, such as muscle damage, training, and ingestion of drugs, glucose solution, and

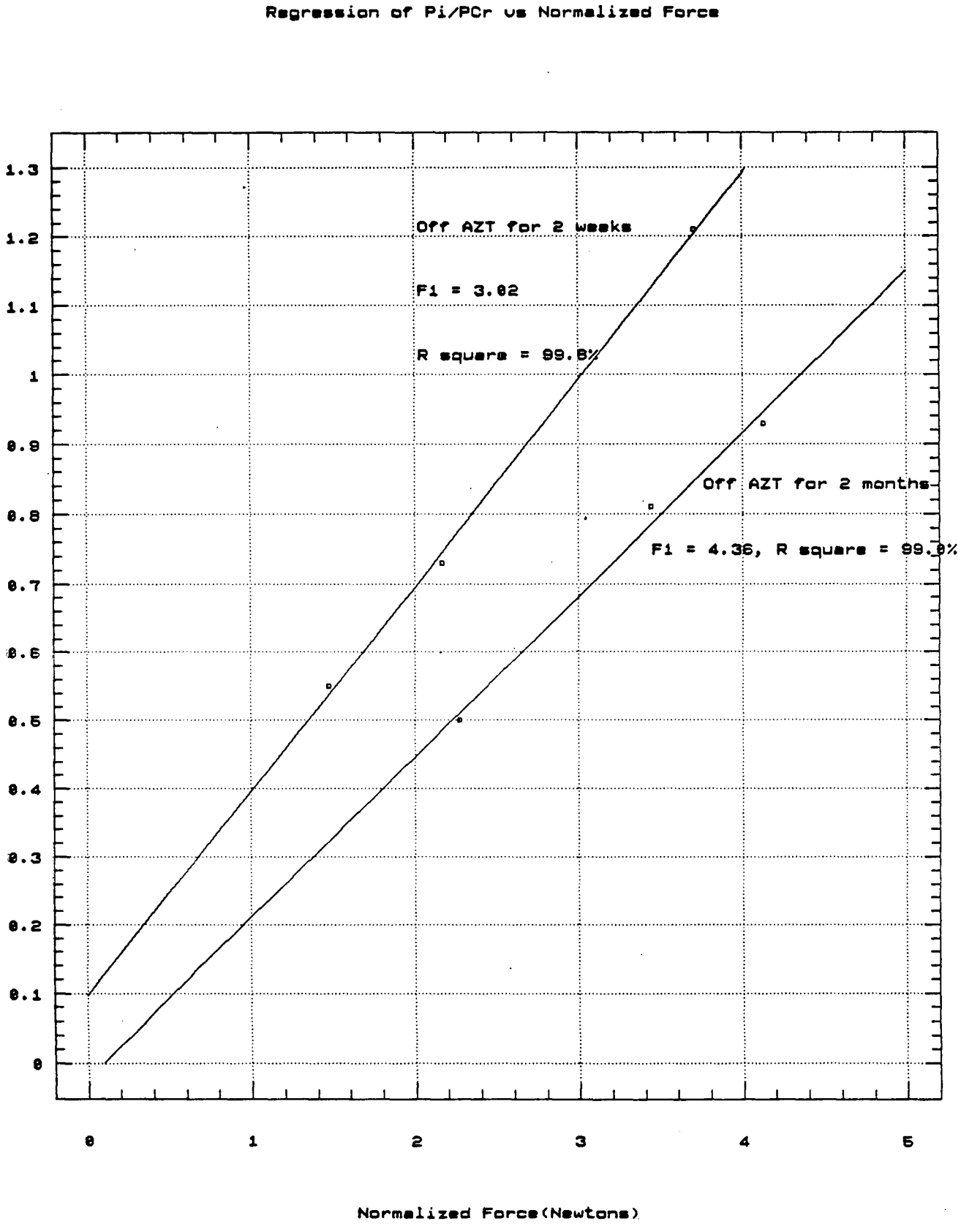

Figure 6-5 Improvement of muscular function after switching from AZT to DDI.

caffeine, etc. will alter subsequent exercise performance; therefore, careful attention must be paid if results are to be interpreted in a meaningful way.

One interesting development, which comes out of this work, is the use of an inductively coupled, spiral resonator surface coil housed in a gantry with revolving capability. The most important feature of this coil configuration is its flexibility with respect to the location where it can operate. Its stability and improved sensitivity are added advantages. At the beginning of this Chapter, we have already explored the versatility of such a design to function as a volume coil, as well as to observe C-13 resonances in human forearm.

6.4 Suggestions for Future Work

Over the past dozen years, nuclear magnetic resonance spectroscopy (NMRS) has opened unparalleled opportunities for noninvasive studies of function and metabolism in cell suspensions and isolated perfused tissues as well as in selected volumes within animals, normal human subjects, and patients. Spectroscopic studies using P-31, C-13, and H-1 are now being used to observe regional differences in chemical composition as well as variations in tissue metabolism and enzyme regulation. Other nuclei, such as Na-23, and K-39, are used to monitor ion transport and distribution within a number of organs.

However, many of the above mentioned techniques are by no means trivial, and implementation has never been automatic. Each research scientist has to face his own obstacles, and the author was humbled by the many challenges that this project provided. The work presented in this thesis advances the routine usage of P-31 NMRS to study muscle fatigue even in a laboratory with limited financial resources and manpower. During the past few years, we have made an effort to improve the technique to a stage where it is easy to implement in almost

any small research laboratory. Such technique has already proven to be tractable and credible with high sensitivity and selectivity.

Future work will probably involve the further refinement of the clinical protocol, by eliminating addition factors that may complicate the study, the extension of the spiral design to investigate other biochemical systems or even other nuclei. Nevertheless, although extra effort would be required to optimize each aspect, the present work provides a foundation for such research.

Finally, the spiral resonator surface coil housed in a moving gantry has not been tested with a whole body NMR spectrometer/imager in a hospital environment, equipped with efficient RF shielding. It has yet to be seen if such a design would improve the S/N ratio, as well as facilitate the *in vivo* study of metabolic diseases. Current efforts are being undertaken to transfer such technology to whole body NMRS's in the Walter Mackenzie Health Sciences Center, Edmonton, Alberta, Canada (under the direction of Dr. Andrew Penn), and in the Herchel Smith Laboratory for Medicinal Chemistry, Cambridge University Medical School, Cambridge, United Kingdom (under the leadership of Professor L. D. Hall).

References

1. M.C. Dalakas, and G.H. Pezeshkpour, Ann. Neurol. 23(suppl):S38-48, 1988.
2. P.A. Volberding, *et. al.*, New England J. Medicine 322:941-949, 1990..
3. A.R. Rachlis, Can. Med. Assoc. J. 143:1177-1185, 1990.
4. M.C. Dalakas, I. Illa, *et. al.*, New England J. Medicine 322:1098-1105, 1990..

Appendix A

A. GLOSSARY OF TERMS

Acetylcholine the acetic acid ester of the organic base choline: the neurotransmitter released at the synapses of parasympathetic nerves and at neuromuscular junctions. After relaying a nerve impulse, acetylcholine is rapidly broken down by the enzyme cholinesterase.

Acquisition time time required to carry out an NMR spectroscopic or imaging procedure comprising only the data acquisition time.

Action potential the brief regenerative electric potential that propagates along a single axon or muscle fiber membrane. The action potential is an all-or-none phenomenon; whenever the stimulus is at or above threshold, the action potential generated has a constant size and configuration.

Amplitude the maximum difference between two points, usually baseline to the most positive peak, baseline to the most negative peak, or the most negative peak to the most positive peak.

Analog-to-digital converter (ADC) part of the interface that converts ordinary (analog) voltages, such as the detected NMR signal, the position potentiometer signal, as well as the accelerating force signal from strain gauge, into digital number form, which can be read by the computer.

Angular frequency (ω) frequency of oscillation or rotation (measured, e.g., in radians/sec) commonly designated by the Greek letter ω: $\omega=2\pi f$ where f is the frequency (e.g., in Hz).

Antenna device to send or receive electromagnetic radiation.

Ataxia the shaky movements and unsteady gait that result from brain's failure to regulate the body's posture and the strength and direction of limb movements. It may be due to disease of the sensory nerves or the cerebellum. Friedreich's ataxia is an inherited disorder appearing first in adolescence. It has the features of cerebellar ataxia, together with spasticity of the limbs.

B_0 a conventional symbol for the constant magnetic (induction) field in an NMR system.

B_1 a conventional symbol for the radiofrequency magnetic induction field used in an NMR system.

Bloch equations phenomenological "classical" equations of motion for the macroscopic magnetization vector. They include the effects of precession about the magnetic field (static and RF) and the T_1 and T_2 relaxation times.

Boltzmann distribution if a system of particles which are able to exchange energy in collisions is in thermal equilibrium, then the relative number of particles, N_1 and N_2, in two particular energy states with corresponding energies, E_1 and E_2, is given by :

$$N_1/N_2 = \exp[-(E_1-E_2)/kT]$$

where k is the Boltzmann's constant and T is absolute temperature.

Carr-Purcell (CP) sequence sequence of a 90^0 RF pulse followed by repeated 180^0 RF pulses to produce a train of spin echoes; useful for measuring T_2.

Carr-Purcell-Meiboom-Gill (CPMG) sequence modification of Carr-Purcell RF pulse sequence with 90^0 phase shift in the rotating frame of reference between the 90^0 pulse and the subsequent 180^0 pulses to reduce accumulating effects of imperfections in the 180^0 pulses. Suppression of effects of pulse error accumulation can alternatively be achieved by alternating phases of the 180^0 pulses by 180^0.

Chemical shift (δ) the change in the Larmor frequency of a given nucleus when bound in different sites in a molecule, due to the magnetic shielding effects of the electron orbitals. Chemical shifts make possible the differentiation of different molecular compounds and different sites within the molecules in high-resolution NMR spectra. The amount of the shift is proportional to magnetic field strength and is usually specified in parts per million (ppm) of the resonance frequency relative to a standard.

Coherence maintenance of a constant phase relationship between rotating or oscillating waves or objects. Loss of phase coherence of the spins results in a decrease in transverse magnetization and hence a decrease in the NMR signal.

Chronic inflammatory neuropathy a disease of peripheral nerve, caused by reaction of the immune system against some component of the nerve; symptoms involve persistant pain, heat, redness, swelling, and loss of function of the nerves.

Coil single or multiple loops of wire (or other electric conductor, such as tubing, etc.) designed either to produce a magnetic field from current flowing through the wire or to detect a changing magnetic field by voltage induced in the wire.

Collagen-vascular neuropathy a peripheral nerve disease that is characterized by degenerative changes in collagen (the principal component of connective tissue), in which blood circulation is damaged.

Concentric needle electrode recording electrode that measures an electric potential difference between the bare tip of an insulated wire, usually stainless steel, silver or platinum, and the bare shaft of a steel cannula through which it is inserted. The bare tip of the central wire (exploring electrode) is flush with the level of the cannula (reference electrode).

Conduction velocity speed of propagation of an action potential along a nerve or muscle fiber. The nerve fibers studied (motor, sensory, autonomic, or mixed) should be specified. For a nerve trunk, the maximum conduction velocity is calculated from the latency of the evoked potential (muscle or nerve) at maximal or supramaximal intensity of stimulation at two different points. The distance between the two points (conduction distance) is divided by the different between the corresponding latencies (conduction time). The calculated velocity represents the conduction velocity of the fastest fibers and is expressed as meters per second (m/s). As commonly used, the term conduction velocity refers to the maximum conduction velocity. By specialized techniques, the conduction velocity of other fibers can be determined as well and should be specified, e.g., minimum conduction velocity.

Congenital myopathies myopathies that are recognized at birth or that are believed to have been present since birth. They are either inherited, or caused by exposure to an envirnmental factor before birth.

Continuous wave NMR (cw) a technique for studing NMR by continuously applying RF radiation to the sample and slowly sweeping either the radiofrequency or the magnetic field through the resonance values; now largely superceded by pulse NMR technique.

Contraction a voluntary or involuntary reversible muscle shortening that may or may not be accompanied by action potentials from muscle. This term is to be contrasted with the term contracture, which refers to a fixed muscle shortening.

Contracture the term is used to refer to immobility of a joint due to fixed muscle shortening. The term has also been used to refer to an electrically silent, involuntary state of maintained muscle contraction, as seen in phosphorylase deficiency, for which the preferred term is muscle cramp.

Crossed-coil coil pair arranged with their magnetic fields at right angles to each other in such a way as to minimize their mutual electromagnetic interaction

Cryostat an apparatus for maintaining a constant low temperature (as by means of liquid helium). Requires vacuum chambers to help with thermal isolation.

Degenerative disease a disease involes the deterioration and loss of specialized function of the cells of a tissue or organ.

Detector portion of the receiver that demodulates the RF NMR signal and converts it to a lower frequency signal. Most detectors now used are phase sensitive (e.g., quadrature demodulator/detector), and will also give phase information about the RF signal.

Diamagnetic a substance that will slightly decrease a magnetic field when placed within it (its magnetization is oppositely directed to the magnetic field, i.e., with a small negative magnetic susceptibility).

Duchenne dystrophy see **muscular dystrophy.**

Dystrophy a disorder of an organ or tissue, usually muscle, due to impaired nourishment of the affected part.

Eddy currents electric currents induced in a conductor by a changing magnetic field or by motion of the conductor through a magnetic field. One of the sources of concern about potential hazard to subjects in very high magnetic fields or rapidly varying gradient or main magnetic fields.

Electrode a conduction device used to record an electric potential (recording electrode) or to apply an electric current (stimulating electrode). In addition to the ground electrode used in clinical recordings, two electrodes are always required either to record an electric potential or to apply an electric current. Depending on the relative size and location of the electrodes, however, the stimulating or recording condition may be referred to as monopolar or unipolar.

Electrodiagnosis (EDX) the recording and analysis of responses of nerves and muscles to electric stimulation and the identification of patterns of insertion, spontaneous, involuntary and voluntary action potentials in muscle and nerve tissue.

Electrodiagnostic medicine a specific area of medicine practice in which a physician uses information from the clinical history, observations from the physical examination, and the techniques of electrodiagnosis to diagnose and treat neuromuscular disorders.

Electromyelography the recording and study of electric activity from the spinal cord and/or from associated nerve roots.

Electromyogram the record obtained by electromyography.

Electromyograph equipment used to activate, record, process and display nerve and muscle action potentials for the purpose of evaluating nerve and muscle function.

Electromyography (EMG) strictly defined, the recording and study of insertion, spontaneous, and voluntary electric activity of muscle.

Electron transport defects defects in one or more of a series of enzymes and proteins in the living cells through which electrons are transferred, via a series of oxidation-reduction reactions.

Electroneurography (ENG) the recording and study of the action potentials of peripheral nerves.

Electroneuromyography (ENMG) the combined studies of EMG and ENG.

Encephalopathy any of the various diseases that affect the functioning of the brain.

Excitation putting energy into the spin system; if a net transverse magnetization is produced, an NMR signal can be observed.

Facilitation improvement of neuromuscular transmission which results from the activation of previously inactive motor units.

Faraday shield electrical conductor interposed between transmitter and/or receiver coil and patient to block out electric fields.

Fat a substance that contains one or more fatty acids in the form of triglycerides and is the principal form in which energy is stored by the body in adipose tissue. It also serves as an insulating material beneath the skin in the subcutaneous tissue and around certain organs. Fat is one of the three main constituents of food; it is necessary in the diet to provide an adequate supply of essential fatty acids and for the efficient absorption of fat-soluble vitamins from the intestine.

Fatigue generally, a state of depressed responsiveness resulting from protracted activity and requiring an appreciable recovery time. Muscle fatigue is a reduction in the force of contraction of muscle fibers and follows repeated voluntary contraction or direct electric stimulation of the muscle.

Filling factor a measure of the geometrical relationship of the RF coil and the sample. It affects the efficiency of irradiation the sample and detecting NMR signals, thereby affecting the signal-to-noise ratio and, ultimately, spectral quality. Achieving a high filling factor requires fitting the coil closely to the region of interest, thus potentially decreasing patient comfort.

Firing pattern qualitative and quantitative descriptions of the sequence of discharge of potential waveforms recorded from muscle or nerve.

Firing rate frequency of repetition of a potential. The relationship of the frequency to the occurrence of other potentials and the force of muscle contraction may be descibed.

Flip angle amount of rotation of the macroscopic magnetization vector produced by an RF pulse, with respect to the direction of the static magnetic field.

Fourier transform (FT) a mathematical procedure to separate out the frequency components of a signal from its amplitudes as a function of time, or vice versa. The Fourier transform is used to generate the spectrum from the FID in pulse NMR techniques and is essential to mose spectral techniques.

Free induction decay (FID) if transverse magnetization of the spins is produced, e.g., by a 90^0 pulse, a transient NMR signal will result that will decay toward zero with a characteristic time constant T_2 (or T_2^*); this decaying signal is FID .In practice, the first part of the FID is not observable due to residual effects of the powerful exciting RF pulse on the electronics of the receiver.

Frequency (*f*) the number of repetition of a periodic process per unit time.

Gauss (G) a unit of magnetic flux density in the older (CGS) system. The earth's magnetic field is approximately one-half gauss to one gauss, depending on location. The currently preferred (SI) unit is the tesla (1 T = 10,000 G).

Glycogen a carbohydrate consisting of branched chains of glucose units. Glycogen is the principal form in which carbohydrate is stored in the body; it is stored in the liver and muscles and may be readily broken down to glucose.

Gradient the amount and direction of the rate of change in space of some quantity, such as magnetic field strength.

Gradient coils current-carrying coils designed to produced a desired gradient magnetic field (so that the magnetic field will be stronger in some locations than others). Proper design of the size and configuration of the coils is necessary to produce a controlled and uniform gradient.

Guillain-Barre syndrome a disease of the peripheral nerves and nerve roots in which there is numbness and weakness in the limbs. It usually develops 10-20 days after a respiratory infection that provokes an allergic response in the peripheral nerves. A rapidly progressive form of the disease is called Landry's paralysis.

Gyromagnetic ratio (γ) the ratio of the magnetic moment to the angular momentum of a particle. This is a constant for a given nucleus.

Hereditary sensorimotor neuropathy an inherited peripheral nerve disease involving both the sensory and motor nerves.

Homogeneity uniformity. In NMR, the homogeneity of the static magnetic field is an important criterion of the quality of the magnetic. Homogeneity requirements for NMR imaging are generally lower than the homogeneity requirements for NMR spectroscopy, but for most imaging techniques must be maintained over a larger region.

Inductance measure of the magnetic coupling between two current-carrying loops (mutual) (reflecting their spatial relationship) or of a loop (such as a coil) with itself (self). One of the principal determinants of the resonance frequency of an RF circuit.

Inhomogeneity degree of lack of homogeneity, for example, the fractional derviation of the local magnetic field from the average value of the field.

Inversion recovery (IR) two-pulse sequence in which the magnetization is first inverted by a 180^0 inversion pulse and subsequently detected by a 90^0 detection pulse.

Inversion time time between inversion and subsequent 90^0 pulse to elicit NMR signal in inversion recovery experiment.

Larmor equation states that the frequency of precession of the nuclear magnetic moment is proportional to the magnetic field.

$$\omega_0 = -\gamma B_0 \qquad \text{(radians/sec)}$$

or

$$f_0 = -\gamma B_0 / 2\pi \qquad \text{(Hz)}$$

where ω_0 or f_0 is the frequency, γ is the gyromagnetic ratio, and B_0 is the magnetic induction field. The negative sign indicates the direction of the rotation.

Larmor frequency (ω_0 or f_0) the frequency at which magnetic resonance can be excited; given by the Larmor equation. By varying the magnetic field across the sample with a gradient magnetic field, the corresponding variation of the Larmor frequency can be used to encode position. For protons (hydrogen nuclei), the Larmor frequency is 42.58 MHz/T; whereas for phosphorus, the Larmor frequency is 17.24 MHz/T.

Linewidth width of line in spectrum; related to the reciprocal of the transverse relaxation time (T_2^* in practical systems). Measured in unites of frequency, generally at the half-maximum points.

Localized nuclear magnetic resonance (LNMR) a particular technique for obtaining NMR spectra, for example, of phosphorus, from a limited region by creating a sensitive volume with inhomogeneous applied gradient magnetic fields, which may be enhanced with the use of surface coils.

Longitudinal magnetization (M_z) component of the macroscopic magnetization vector along the static magnetic field. Following excitation by RF pulse, M_z will approach its equilibrium value M_0, with a characteristic time constant T_1.

Longitudinal relaxation return of longitudinal magnetization to its equilibrium value after excitation; requires exchange of energy between the nuclear spins and the lattice.

Longitudinal relaxation time see T_1.

Lorentzian line usual shape of the lines in an NMR spectrum, characterized by a central peak with long tails; proportional to $1/[(1/T_2)^2 + (\omega - \omega_0)^2]$, where ω is the frequency and ω_0 is the frequency of the peak (i.e. central resonance frequency).

M conventional symbol for macroscopic magnetization vector.

M_{xy} see **Transverse magnetization.**

M_z see **Longitudinal magnetization.**

M_0 equilibrium value of the magnetization; directed along the direction of the static magnetic field. Proportional to spin density, N.

Macroelectromyography (Macro-EMG) general term referring to the technique and conditions that approximate recording of all muscle fiber action potentials arising from the same motor unit.

Macroscopic magnetic moment see **Macroscopic magnetization vector.**

Macroscopic magnetization vector net magnetization moment per unit volume (a vector quantity) of a sample in a given region, considered as the integrated effect of all the individual microscopic nuclear magnetic moments. Most NMR experiments actually deal with this.

Magnetic dipole north and south magnetic poles separated by a finite distance. An electric current loop, including the effective current of a spinning nucleon or nucleus, can create an equivalent magnetic dipole.

Magnetic field (H) the region surrounding a magnet (or current-carrying conductor) is endowed with certain properties. One is that a small magnet in such a region experiences a torque that tends to align it in a given direction. Magnetic field is a vector quantity; the direction of the field is defined as the direction that the north pole of the small magnet points when in equilibrium. A magnetic field produces a magnetizing force on a body within it. Although the dangers of large magnetic fields are largely hypothetical, this is an area of potential concern for safety limits. Formally, the forces experienced by moving charged particles, current-carrying wires, and small magnets in the vicinity of a magnet are due to magnetic induction (B), which includes the effect of magnetization, while the magnet field (H) is defined so as to include magnetization. However, both B and H are often loosely used to denote magnetic fields.

Magnetic field gradient a magnetic field which changes in strength in a certain given direction. Such fields are used in NMR spectroscopy or imaging with selective excitation to select a region of interest and also to encode the location of NMR signals received from the sample. Measured in teslas/meter (T/m).

Magnetic induction (B) also called magnetic flux density. The net magnetic effect from an externally applied magnetic field and the resulting magnetization. B is proportional to H ($B=\mu H$), with the SI unit being the tesla (T).

Magnetic moment a measure of net magnetic properties of an object or particle. A nucleus with an intrinsic spin will have an associated magnetic dipole moment, so that it will interact with a magnetic field (as if it were a tiny bar magnet).

Magnetic resonance see **Nuclear Magnetic resonance (NMR)**.

Magnetic susceptibility measure of the ability of a substance to become magnetized.

Magnetization see also **Macroscopic magnetization vector**. The magnetic polarization of a material produced by a magnetic field (magnetic moment per unit volume).

Magnetogyric ratio see **Gyromagnetic ratio**.

Malignant hyperthermia a life-threatening disorder of high body temperature.

Megahertz (MHz) unit of frequency, equal to $1x10^6$ Hz.

Muscle cramp an involuntary, painful muscle contraction associated with electric activity. Muscle cramps may be accompanied by other types of repetitive discharges, and in some metabolic myopathies (McArdle's disease) the painful, contracted muscle may show electric silence.

Muscle fiber action potential action potential recorded from a single muscle fiber.

Muscle fiber conduction velocity the speed of propagation of a single muscle fiber action potential in the muscle cell membrane, usually expressed as meters per second. The muscle fiber conduction velocity is usually less than most nerve conduction velocities, varies with rate of discharge of the muscle fiber, and requires special techniques for measurement.

Myasthenia gravis a chronic disease marked by abnormal fatiguability and weakness of selected muscles, which is relieved by rest or anticholinesterase drugs. The degree of fatigue can be so extreme that these muscles are temporarily paralyzed. The cause is impaired ability of the neurotransmitter acetylcholine to induce muscular contraction because of blockage of the acetylcholine receptors by antibodies..

Myopathy any disease of the muscles. The myopathies are usually subdivided into those that are inherited and those that are acquired. All are typified by weakness and wasting of the muscles which usually is more severe in the upper parts of the arms and legs.

Myositis any of a group of muscle diseases in which inflammation and degenerative changes occur. Myositis may be found in relation to systemic collagen disorders and a minority are caused by bacterial or parasitic infections.

Myotonia the clinical observation of delayed relaxation of muscle after voluntary contraction or percussion. The delayed relaxation may be electrically silent, or accompanied by propagated electric activity.

Myotonia congenita a benign disorder, present since birth, of the muscle fibers that results in abnormally prolonged contractions.

Myotonic dystrophy the commonest type of muscular dystrophy in which the muscle weakness and wasting is accompanied by an unnatural prolongation of the muscular contraction after any voluntary effort.

Nerve action potential strictly defined, refers to an action potential recorded from a single nerve fiber. The term is commonly used to refer to the compound nerve action potential, recorded from the whole nerve.

Nerve conduction studies (NCS) recording and analysis of electric waveforms of biologic origin elicited in response to electric or physiologic stimuli. Generally NCS refer to studies of waveforms generated in the peripheral nervous system, whereas evoked potential studies refer to studies of waveforms generated in both the peripheral and central nervous system. The waveforms recorded in NCS are compound sensory nerve action potentials and compound muscle action potentials. The compound sensory nerve action potentials are generally referred to as sensory nerve action potentials. The compound muscle action potentials are generally referred to by letters which have historical origins: M wave, F wave, H wave, T wave, A wave, R1 wave, R2 wave. It is possible under standardized conditions to establish normal ranges of amplitude, duration, and latencies of these evoked potentials and to calculated the maximum conduction velocity of sensory and motor nerve.

Nerve conduction velocity loosely used to refer to the maximum nerve conduction velocity.

Nerve fiber action potential action potential recorded from a single nerve fiber.

Neurapraxia failure of nerve conduction, usually reversible, due to metabolic or micro-structural abnormalities without disruption of the axon.

Neuromyotonia clinical syndrome of continuous muscle fiber activity manifested as continuous muscle rippling and stiffness. The accompanying electric activity may be intermittent or continuous.

Nicotinamide a B vitamin: the amide of nicotinic acid. It is an active component of the coenzymes NAD (nicotinamide adenine dinucleotide) and NADP, its phosphate. It is important for energy metabolism, especially in the mitochondria.

NMR signal electromagnetic signal in the radiofrequency range produced by the precession of the transverse magnetization of the spins. The rotation of the transverse magnetization induces a voltage in a coil, which is amplified and demodulated by the receiver; the signal may refer only to this induced voltage.

Nuclear magnetic resonance (NMR) the absorption or emission of electromagnetic energy by nuclei in a static magnetic field, after excitation by a suitable RF magnetic field. The peak resonance frequency is proportional to the magnetic field, and is given by the Larmor equation. Only nuclei with a nonzero spin exhibit NMR.

Nuclear spin see also **Spin**. An intrinsic property of certain nuclei that gives them an associated characteristic angular momentum and magnetic moment.

Nuclear spin quantum number (I) property of all nuclei related to the largest measurable component of the nuclear angular momentum. Nonzero values of nuclear angular momentum are quantized (fixed) as integral or half-integral multiples of $(h/2\pi)$, where h is Planck's constant. The number of possible energy states for a given nucleus in a fixed magnetic field is equal to $2I+1$.

Nucleon generic term for a neutron or proton.

Nutation a displacement of the axis of a spinning body away from the simple cone-shaped figure which would be traced by the axis during precession. In the rotating frame of reference, the nutation caused by an RF pulse appears as a simple precession, although the motion is more complex in the stationary frame of reference.

Off Rx after the withdrawal of prescription drugs.

On Rx on prescription drugs

Ophthalmoplegia paralysis of the muscles of the eye.

Paramagnetic a substance with a small but positive magnetic susceptibility (magnetizability). The addition of a small amount of paramagnetic substance may greatly reduce the relaxation times of water. Typical paramagnetic substances usually posses an unpaired electron and include atoms or ions of transition elements, rare earth elements, some metals, and some molecules including molecular oxygen and free radicals. Paramagnetic substances are considered promising for use as contrast agents in NMR imaging.

Partial saturation excitation technique applying repeated RF pulses in times on the order of or shorter than T_1 so as to increase signal-to-noise ratio, as well as image contrast, within the time constraint permitted under a certain clinical setting.

Periodic paralysis occasional muscle impairment or loss of muscle function that varies in its extent, its severity, and the degree of spasticity or flaccidity according to the nature of the underlying disease and its distribution in the brain, spinal cord, peripheral nerves, or muscles.

Permeability (μ) tendency of a substance to concentrate magnetic field, $\mu=B/H$.

Phantom an artificial object of known dimensions and proporties used to test aspects of a RF coil.

Phase in a periodic function (such as rotational or sinusoidal motion), the position relative to a particular part of the cycle.

Polarization as used in neurophysiology, the presence of an electric potential difference across an excitable cell membrane. The potential across the membrane of a cell when it is not excited by an input or spontaneously active is termed the resting potential; it is at a stationary nonequilibrium state with regard to the electric potential difference across the membrane. Depolarization decribes a reduction in the magnitude of the polarization toward the zero potential while hyperpolarization refers to an increase in the magnitude of the polarization relative to the resting potential. Repolarization describes an increase in polarization from the depolarized state toward, but not above, the normal resting potential.

Precession comparatively slow gyration of the axis of a spinning body so as to trace out a cone; caused by the application of a torque tending to change the direction of the rotation axis, and continuously directed at right angles to the plane of the torque. The magnetic moment of a nucleus with spin will experience such a torque when inclined at an angle to the magnetic field, resulting in precession at the Larmor frequency. A familiar example is the effect of gravity on the motion of a spinning top or gyroscope.

Pressional frequency see **Larmor frequency.**

Probe the portion of an NMR spectrometer comprising the sample container and the RF coils, with some associated electronics. The RF coils may consist of separate receiver and transmitter coils in a crossed-coil configuration, or, alternatively, a single coil to perform both functions.

Pulse, 90° ($\pi/2$ pulse) RF pulse designed to rotate the macroscopic magnetization vector 90° in space as referred to the rotating frame of reference, usually about an axis at right angles to the main magnetic field. If the spins are initially aligned with the magnetic field, this pulse will produce transverse magnetization and an FID.

Pulse, 180° (π pulse) RF pulse designed to rotate the macroscopic magnetization vector 180^0 in space as referred to the rotating frame of reference, usually about an axis at right angles to the main magnetic field. If the spins are initially aligned with the magnetic field, this pulse will produce inversion.

Pulse length (width) time duration of a pulse. For an RF pulse near the Larmor frequency, the longer the pulse length, the greater the angle of rotation of the macroscopic magnetization vector will be (greater than 180° can bring it back toward its original orientation).

Pulse NMR NMR techniques that use RF pulse and Fourier transformation of the NMR signal; have largely replaced the older continuous wave techniques.

Pulse programmer part of the spectrometer or interface that controls the timing, duration, and amplitude of the pulses (RF or gradient).

Pulse sequence set of RF(and/or gradient) magnetic field pulses and time spacings between these pulses; used in conjunction with gradient magnetic fields and NMR signal (reception to produce NMR images).

Q see **Quality factor.**

Quadrature detector a phase sensitive detector or demodulator that detects the components of the signal in phase with a reference oscillator and 90^0 out of phase with the reference oscillator.

Quality factor (Q) applies to any electric circuit component; most often the coil Q is limiting. Inversely related to the fraction of energy in an oscillating system lost in one oscillation cycle. Q is inversely related to the range of frequency over which the system will exhibit resonance. It affects the signal-to-noise ratio, because the detected signal increases proportionally to Q while the noise is proportional to the square root of Q. The Q of a coil will depend on whether it is unloaded (no patient) or loaded (patient).

Quantum mechanics physics of the microcosmos based on the concept that all physical quantities can exist as discrete quanta only.

Radian (rad) dimensionless unit of angular measure; $360^0=2\pi$ rad.

Radiofrequency (RF) wave frequency intermediate between auditory and infrared. The RF used in NMR studies is commonly in the megahertz (MHz) range. The principal effect of RF magnetic fields on the body is power deposition in the form of heating, mainly at the surface; this is a principal area of concern for safety limits.

Receiver portion of the NMR apparatus that detects and amplifies RF signals picked up by the receiving coil. includes a preamplifier, amplifier, and demodulator.

Receiver coil coil of the RF receiver; "pick up" the NMR signal.

Recruitment the successive activation of the same and additional motor units with increasing strength of voluntary muscle contraction.

Recruitment frequency firing rate of a motor unit action potential (MUAP) when a different MUAP first appears with gradually increasing strength of voluntary muscle contraction. This parameter is essential to assessment of recruitment pattern.

Recruitment interval the interdischarge interval between two consecutive discharges of a motor unit action potential (MUAP) when a different MUAP first appears with gradually increasing strength of voluntary muscle contraction. The reciprocal of the recruitment interval is the recruitment frequency.

Recruitment pattern a qualitative and/or quantitative description of the sequence of appearance of motor unit action potentials with increasing strength of voluntary muscle contraction.

Relaxation rates reciprocals of the relaxation times.

Relaxation times after excitation, the spins will tend to return to their equilibrium distribution, in which there is no transverse magnetization and the longitudinal magnetization is at its maximum value and oriented in the direction of the static magnetic field. It is observed that in the absence of applied RF, the transverse magnetization decays towards zero with a characteristic time constant T_2, and the longitudinal magnetization returns toward the equilibrium value M_0 with a characteristic time constant T_1.

Retinitis pigmentosa a noninflammatory hereditary condition involving progressive degeneration of the retina.

Repetition time (T_R) The period of time between the beginning of a pulse sequence and the beginning of the succeeding (essentially identical) pulse sequence.

Resonance a large amplitude vibration in a mechanical or electric system caused by a relatively small periodic stimulus with a frequency at or close to a natural frequency of the system; in nmr apparatus, resonance can refer to the NMR itself or to the tuning of the RF circuitry.

Resonant frequency frequency at which the resonance phenomenon occurs; given by the Larmor equation for NMR; determined by inductance and capacitance for RF circuits.

Resting membrane potential voltage across the membrane of an excitable cell at rest.

RF coil used for transmitting RF pulses and/or receiving NMR signals.

RF pulse brief burst of RF magnetic field delivered to object by RF transmitter. For RF frequency near the Larmor frequency, it will result in rotation of the macroscopic magnetization vector in the rotating frame of reference (or a more complicated nutational motion in the stationary frame of reference). The amount of rotation will depend on the strength and duration of the RF pulse; commonly used examples are 90^0 and 180^0 pulses.

Riboflavin (vitamin B_2) a vitamin of the B complex that is a constituent of the coenzymes FAD (flavine adenine dinucleotide) and FMN (flavine mononucleotide). Riboflavin is therefore important in tissue respiration.

Rotating frame of reference a frame of reference (with corresponding corrdinate systems) that is rotating about the axis of the static magnetic field B_0 (with respect to a stationary ("laboratory") frame of reference) at a frequency equal to that of the applied RF magnetic field, B_1. Although B_1 is a rotating vector, it appears stationary in the rotating frame, leading to simpler mathematical formulations.

Saturation a nonequilibrium state in NMR, in which equal numbers of spins are aligned against and with the magnetic field, so that there is no net magnetization. Can be produced by repeated supplying RF pulses at the Larmor frequency with interpulse times short compared to T_1.

Scanning EMG a technique by which an electromyographic electrode is advanced in defined steps through muscle while a separate single fiber EMG electrode is used to trigger both the oscilloscope-sweep and the advancement device. This recording technique provides temporal and spatial information about the motor unit. Distinct maxima in the recorded activity are considered to be generated by muscle fibers innervated by a common branch of the axon. These groups of fibers form a motor unit fraction.

Selective excitation controlling the frequency spectrum of an irradiating RF pulse (via tailoring) while imposing a gradient magnetic field on spins, such that only a desired region will have a suitable resonant frequency to be excited. Originally used to excite all but a desired region; now more commonly used to select only a desired region, such as a plane, for excitation.

Shim coils coils carrying a relatively small current that are used to provide auxiliary magnetic fields in order to compensate for inhomogeneities in the main magnetic field of an NMR system.

Shimming correction of inhomogeneity of the magnetic field produced by the main magnet of an NMR system due to imperfections in the magnet or to the presence of external ferromagnetic objects. May involve changing the configuration of the magnet or the addition of shim coils or small pieces of steel.

SI (International System of Units) the preferred international standard system of physical units and measures.

Signal-to-noise ratio (SNR or S/N) used to describe the relative contributions to a detected signal of the true signal and random superimposed signals ("noise"). One common method to improve (increase) the SNR is to average several measurements of the signal on the expectation that random contributions will tend to cancel out. The SNR can also be improved by sampling larger volumes (with a corresponding loss of spatial resolution) or, within limits, by increasing the strength of the magnetic field used. S/N will depend on the electrical properties of the sample or patient being studied.

Skin depth time-dependent electromagnetic fields are significantly attenuated by conducting media (including the human body); the skin depth gives a measure of the average depth of penetration of the RF field. It may be limited factor in NMR at high frequencies (high magnetic fields). The skin depth also affects the Q of the coils.

Solenoid coil a coil of wire wound in the form of a long cylinder. When a current is passed through the coil, the magnetic field within the coil is relatively uniform. Solenoid RF coils are commonly used when the static magnetic field is perpendicular to the long axis of the body.

Spectrometer the portions of the NMR apparatus that actually produce the NMR phenomenon and acquire the signals, including the magnet, the probe, the RF circuitry, etc. The spectrometer is controlled by the computer via the interface under the direction of the software.

Spectrum an array of the frequency components of the NMR signal according to frequency. Nuclei with different resonant frequencies will show up as peaks at different corresponding frequencies in the spectrum, or "lines".

Spin the intrinsic angular momentum of an elementary particle, or system of particles such as a nucleus, that is also responsible for the magnetic moment; or, a particule or nucleus possessing such a spin. The spins of nuclei have characteristic fixed values. Pairs of neutrons and protons align to cancel out their spins, so that nuclei with an odd number of neutrons and/or protons will have a net nonzero rotational component characterized by an integer quantum "nuclear spin number" (I).

Spin density (N) the density of resonating spins in a given region; one of the principal determinants of the strength of the NMR signal from the region. The SI units would be mole/m^3. For water, there are about $1.1x10^5$ moles of hydrogen/m^3, or 0.11 mole of hydrogen/cm^3. True spin density cannot be obtained directly, but must be calculated from signals received with different interpulse times.

Spin echo reappearance of an NMR signal after the FID has died away, as a result of the effective reversal of the dephasing of the spins ("refocusing") by such techniques as reversal of a gradient magnetic field (often referred to as a form of "time reversal"), or by specific RF pulse sequences such as the Carr-Purcell sequence (applied in a time shorter than or on the order of T_2). Multiple spin echoes or a series of spin echoes at different times can be used to determine T_2 without contamination by effects of the inhomogeneity of the magnetic field.

Spin-lattice relaxation time see T_1.

Spin-spin relaxation time see T_2.

Spin warp imaging a form of Fourier transform imaging in which phase encoding gradient pulses are applied for a constant duration but with varying amplitude. This is distinct from the original FT imaging methods in which phase encoding is performed by applying gradient pulses of constant amplitude but varying duration. The spin warp method, as other Fourier imaging techniques, is relatively tolerant of nonuniformities (inhomogeneities) in the static or gradient magnetic fields.

Stimulus any external agent, state, or change that is capable of influencing the activity of a cell, tissue, or organism. In clinical nerve conduction studies, an electric stimulus is generally applied to a nerve or a muscle. The electric stimulus may be described in absolute terms or with respect to the evoked potential of the nerve or muscle. In absolute terms, the electric stimulus is defined by a duration (ms), a waveform (square, exponential, linear, etc.) and a strength for intensity measured in voltage (V) or current (mA). With respect to the evoked potential, the stimulus may be graded as subthreshold, threshold, submaximal, maximal, or supramaximal. A threshold stimulus is that stimulus just sufficient to produce a detectable response. Stimuli less than the threshold stimulus are termed subthreshold. The maximal stimulus is the stimulus intensity after which a further increase in the stimulus intensity causes no increase in the amplitude of the evoked potential. Stimuli of intensity below this level but above threshold are submaximal. Stimuli of intensity greater than the maximal stimulus are termed supramaximal. Ordinarily, supramaximal stimuli are used for nerve conduction studies. By convention, an electric stimulus of approximately 20% greater voltage/current than required for the maximal stimulus may be used for supramaximal stimulation. The frequency, number, and duration of a series of stimuli should be specified.

Superconducting magnet a magnet which magnetic field originates from current flowing through a superconductor. Such a magnet must be enclosed in a cryostat.

Superconductor a substance which electrical resistance essentially disappears at temperatures near absolute zero. A commonly used superconductor in NMR imaging system magnets is niobium-titanium, embedded in a copper maxtrix to help protect the superconductor from quenching.

Surface coil NMR a simple flat RF receiver coil placed over a region of interest will have an effective selectivity for a volume approximately subtended by the coil circumference and one radius deep from the coil center. Such a coil can used for simple localization of sites for measurement of chemical-shift spectra, especially of phosphorus, and blood flow studies. Some additional spatial selectivity can be achieved with gradient magnetic fields.

T see **Tesla**.

T_1 **("T-one")** spin-lattice or longitudinal relaxation time; the characteristic time constant for spins to tend to align themselves with the external magnetic field. Starting from zero magnetization in the Z direction, the Z magnetization will grow to 63% of its final maximum value in a time T_1.

T_2 **("T-two")** spin-spin or transverse relaxation time; the characteristic time constant for loss of phase coherence among spins oriented at an angle to the static perfectly uniform magnetic field, due to interactions between the spins, with resulting loss of transverse magnetization and NMR signal. Starting from a nonzero value of the magnetization in the xy plane, the xy magnetization will decay so that it loses 63% of its initial value in a time T_2.

T_2^* **("T-two-star")** the characteristic time constant for loss of phase coherence among spins oriented at an angle to the static magnetic field due to a combination of magnetic field inhomogeneities, ΔB, and spin-spin transverse relaxation with resultant more rapid loss in transverse magnetization and NMR signal. NMR signal can still be recovered as a spin echo in times less than or on the order of T_2. $1/T_2^* = 1/T_2 + \Delta\omega/2$; $\Delta\omega = \gamma\Delta B$ (i.e. $T_2^* < T_2$).

Tetanic contraction the contraction produced in a muscle through repetitive maximal direct or indirect stimulation at a sufficient high frequency to produce a smooth summation of successive maximum twitches. The term may also be applied to maximum voluntary contractions in which the firing frequencies of most or all of the component motor units are sufficiently high that successive twitches of individual motor units fuse smoothly. Their tensions all combine to produce a steady, smooth maximum contraction of the whole muscle.

Tetanus the continuous contraction of muscle caused by repetitive stimulation or discharge of nerve or muscle.

Tetany a clinical syndrome manifested by muscle twitching, cramps, and carpal and pedal spasm. These clinical signs are manifestations of peripheral and central nervous system nerve irritability from several causes. In these conditions, repetitive discharges occur frequently with voluntary activation of motor unit action potentials or may appear as spontaneous activity and are enhanced by systemic alkalosis or local ischemia.

Tesla (T) the preferred (SI) unit of magnetic flux density. One tesla is equal to 10,000 gauss (G), the older (cgs) unit.

Thermal Equilibrium a state in which all parts of a system are at the same effective temperature, in particular where the relative alignment of the spins with the magnetic field is determined solely by the thermal energy of the system (in which case the relative numbers of spins with different alignments will be given by the Boltzmann distribution).

T_I inversion time. Time after middle of inverting RF pulse to middle of 90° pulse to detect amount of longitudinal magnetization.

Threshold the level at which a clear and abrupt transition occurs from one state to another. The term is generally used to refer to the voltage level at which an action potential is initiated in a single axon or a group of axons. It is also operationally defined as the intensity that produced a response in about 50% of equivalent trials.

Topical NMR in-vivo NMR spectroscopic technique using gradient fields to localize a volume for excitation.

Torque the effectiveness of a force in setting a body into rotation. It is a vector quantity given by the vector product of the force and the position vector where the force is applied; for a rotating body, the torque is the product of the moment of inertia and the resulting angular acceleration.

T_R repetition time. The period of time between the beginning of a pulse sequence and the beginning of the succeeding (essentially identical) pulse sequence.

Transmitter portion of the NMR apparatus that produces RF current and delivers it to the transmitting coil.

Transmitter coil coil of RF transmitter.

Transverse magnetization (M_{xy}) component of the macroscopic magnetization vector at right angles to the static magnetic field (B_0). Precession of the transverse magnetization at the Larmor frequency is responsible for the detectable NMR signal. In the absence of externally applied RF energy, the transverse magnetization will decay to zero with a characteristic time constant of T_2 or T_2^*.

Tuning process of adjusting the resonant frequency, e.g., of the RF circuit, to a desired value, e.g., the Larmor frequency. More general, the process of adjusting the components of the spectrometer for optimal NMR signal strength.

Vector a quantity having both magnitude and direction, frequently represented by an arrow whose length is proportional to the magnitude and with an arrowhead at one end to indicate the direction.

The motor unit with the more common disorders and relevant diagnostic tests are shown

Anterior Horn Cell	Peripheral Nerve	Neuromuscular Junction	Muscle
Diagnostic Tests:			
	Nerve Conduction Test	Electromyography(EMG)	Muscle Biopsy(invasive)
			P-31 NMRS(non-invasive)
Disorders:			
Spinal muscular atrophy	Guillain-Barre syndrome	Myasthenia gravis	Congenital myopathies
	Chronic inflammatory neuropathy	Defective acetylcholine synthesis or mobilization	Myotonic dystrophy
	Collagen-vascular neuropathy	End-plate acetylcholin-esterase deficiency	Myotonia congenita
	Toxic/metabolic neuropathy	Slow-channel syndrome	Periodic paralysis
	Hereditary sensorimotor neuropathy	Acetylcholine receptor deficiency	Duchenne dystrophy
	Degenerative diseases		Malignant hyperthermia
			Facioscapulohumeral dystrophy
			Myositis
			Glycogen storage diseases
			Fat myopathies
			Electron transport defects